BIOPHYSICAL MECHANISMS OF AMYLOID NUCLEATION IN POLYGLUTAMINE CONTAINING HTT FRAGMENTS

by

Rakesh Mishra

Bachelor of Technology, Anna University, 2007

Submitted to the Graduate Faculty of

School of Medicine in partial fulfillment

of the requirements for the degree of

Doctor of Philosophy

UNIVERSITY OF PITTSBURGH

School of Medicine

This dissertation was presented

by

RAKESH MISHRA

It was defended on

May 23, 2012

and approved by

Ivet Bahar, Ph.D., Department of Computational Biology

Patrick H. Thibodeau, Ph.D., Department of Cell biology and Physiology

Judith Klein-Seetharaman, Ph.D., Department of Structural Biology

Patrick van der Wel, Ph.D., Department of Structural Biology

Dissertation Advisor: Ronald B. Wetzel, Ph.D., Department of Structural Biology

Biophysical mechanisms of amyloid nucleation in polyglutamine containing huntingtin fragments

Rakesh Mishra

University of Pittsburgh, 2012

ABSTRACT

Huntington's disease, one of nine CAG repeat diseases, is triggered by an expansion of a polyglutamine (polyQ) tract in the huntingtin (htt) protein. The aggregation of the first exon of htt (and fragments thereof) is believed to be intricately tied to the pathology of Huntington's disease. Recent work in the field has identified a crucial role for the first seventeen residues of huntingtin (htt^{NT}), implicated in a wide range of cellular processes, in modulating the aggregation of htt both *in vitro* and *in vivo*. The focus of this work has been to identify the biophysical mechanisms underlying htt^{NT} mediated aggregation. Using a combination of experimental and computational techniques, we demonstrate the crucial role of the amphipathic helical propensity of htt^{NT} in mediating initial oligomerization of htt fragments and by extension, the aggregation of polyQ containing htt fragments. We also assess the effect of post-translational modifications (PTMs) within the htt^{NT} sequence on the aggregation of htt fragments, providing a biophysical perspective to the role that these PTMs might play in HD pathology. Finally, in addition to the role of htt^{NT} in directing the initial oligomerization of htt fragments, we also provide evidence for a role of polyQ expansion in stabilizing htt fragment oligomers. Overall, the results of these studies not only add to our understanding of htt exon-1 aggregation but also provide additional clues for the ultimate role that aggregation plays in HD pathology.

TABLE OF CONTENTS

LIST OF TABLES

LIST OF FIGURES

ABBREVIATIONS

HD	Huntington's disease
Htt	Huntingtin
NT	N-terminal
polyQ	polyglutamine
fl-htt	Full-length huntingtin
CD	Circular dichroism
PPII	Polyproline helix type-II
SAXS	Small-angle x-ray scattering
FRET	Förster Resonance Energy transfer
FTIR	Fourier-transform infra-red spectroscopy
ss NMR	Solid state nuclear magnetic resonance
TFA	2, 2, 2-Trifluoroacetic acid
HFIP	1, 1,1,3,3,3-Hexafluoro-2-propanol
RP-HPLC	Reverse-phase High performance liquid chromatography
UV	Ultraviolet
EM	Electron microscopy
DLS	Dynamic light scattering
EPR	Electron paramagnetic resonance

DEER	Double electron electron resonance
MD	Molecular dynamics

CONTRIBUTOR NAMES

A.K.T	Ashwani Kumar Thakur
B.S	Bankanidhi Sahoo
T.F	Tim Fulham
B.R	Bartholomew P. Roland
R.K	Ravindra Kodali
E.L	Elizabeth Landrum
I.B	Inja Byeon
J.S	Jessica Sarver

ACKNOWLEDGEMENTS

At the outset, I would like to express my gratitude to Prof. Ronald B. Wetzel, my thesis advisor and the best mentor that any graduate student could ask for. Over the years, I have stretched the limits of Ron's "open-door" policy, barging in with ideas that at the time seemed great but more often than not were outlandish. Ron has patiently listened to, and discussed the inconsistencies in, each one of these ideas while guiding me towards the ones that eventually did work. Aside from guiding my research, Ron has also always taken an active interest and supported me in my career goals. It has indeed been an honor to work with Ron over the past several years.

Over the years, I have had the opportunity to collaborate extensively and each of these collaborations has added to my growth as a researcher. I must thank Cody Hoop for her help with ssNMR experiments and Prof. Patrick Van der Wel for all the discussions that we have had on different aspects of the project. Also, Jessica Sarver and Sunil Saxena for their help with EPR experiments; InJa Byeon for her help with solution NMR experiments and William Yang (UCLA).

I must also acknowledge the contributions of other members of the lab who I have worked with: Murali, Kar, Elizabeth, Saketh, Yuhai, Tim, Kenneth and Bart. In particular; I would like to thank - Ravi for his help with the EM and also for all the conversations that we have had, inside and outside of the building; Banka, who at every step has been there to guide me

in my experiments and is undoubtedly “Mr. Troubleshooter” in the lab; Irene not only for her technical expertise but also for patiently listening to my graduate school woes, and Ashwani for epitomizing the qualities of a good mentor.

I would also like to acknowledge the contributions of my committee, students of MBSB and the Department of structural biology over the past five-years. A special note of gratitude is also due to Jennifer Walker for her help and support over the past five years. Thank you, Jen.

Finally, I would be remiss in my responsibilities if I were to not express my gratitude to my family (Baba, Mama and Rajesh) and my friends for their support over these years. Particularly- Grant for being a great classmate, a patient friend and an unwitting mentor whom I have always looked up to; Harshad, for his patience and support over the past eight years and for constantly teaching me new things; Siva, undoubtedly the nicest guy I have known and a great friend; and John, for all our fiery conversations. It has been an honor knowing each of you.

PUBLICATIONS

Mishra R, Hoop C.L, Kodali R, Sahoo B, Van der Wel P, Wetzel R. "Serine phosphorylation suppresses huntingtin amyloid accumulation by altering protein aggregation properties" *(manuscript submitted).*

Mishra R, Kodali R and Wetzel R. "Mutational analysis reveals a critical role for α-helical oligomer formation in the nucleation kinetics of amyloid formation by huntingtin N-terminal fragments" *(manuscript in preparation).*

Mishra R, Kodali R and Wetzel R. "Helix propensity of scrambled N-terminal sequences controls huntingtin amyloid nucleation mechanism" *(manuscript in preparation).*

Mishra R, and Wetzel R. "The Structural Biology of Huntington's disease." *(manuscript in preparation).*

Jayaraman M, *Mishra R*, Kodali R, Thakur AK, Koharudin LM, Gronenborn AM, *et al*. Kinetically competing huntingtin aggregation pathways control amyloid polymorphism and properties. Biochemistry. 2012;51(13):2706-16

Mishra R, Jayaraman M, Roland BP, Landrum E, Fullam T, Kodali R, *et al*. "Inhibiting the Nucleation of Amyloid Structure in a Huntingtin Fragment by Targeting alpha-Helix-Rich Oligomeric Intermediates". J Mol Biol. 2011; 415 (5):900-17

Jayaraman M, Kodali R, Sahoo B, Thakur AK, Mayasundari A, *Mishra R*, *et al*. "Slow Amyloid Nucleation via alpha-Helix-Rich Oligomeric Intermediates in Short Polyglutamine-Containing Huntingtin Fragments". J Mol Biol. 2011; 415 (5):881-99

Thakur AK, Jayaraman M, *Mishra R*, Thakur M, Chellgren VM, Byeon IJ, *et al*. "Polyglutamine disruption of the huntingtin exon 1 N terminus triggers a complex aggregation mechanism". Nat Struct Mol Biol. 2009;16(4):380-9.

Gu X, Greiner ER, *Mishra R*, Kodali R, Osmand A, Finkbeiner S, *et al*. "Serines 13 and 16 are critical determinants of full-length human mutant huntingtin induced disease pathogenesis in HD mice". Neuron. 2009;64(6):828-40.

1.0 INTRODUCTION (I): STRUCTURAL BIOLOGY OF HUNTINGTON'S DISEASE.

1.1 INTRODUCTION.

With the identification of the IT15 gene in chromosome 4 that harbors the CAG repeats implicated in Huntington's disease (HD) (1), the study of the disease shifted from the clinical setting into the cellular milieu. Since then, a lot of the progress made towards our current understanding of HD comes from studies that have aimed to investigate disease pathology from a structural biology perspective. The discovery of intra-nuclear inclusions in post-mortem HD brains that were enriched in aggregates of the protein huntingtin (htt) (2), the translation product of the IT15 gene, underscored for the first time the importance of adding a structural perspective to HD research. Over the past decade there has been a substantial increase in the application of structural and biophysical techniques to the study of different aspects of HD, not just limited to protein aggregation. While the study of htt aggregation and its relevance to HD pathology remains a major focus, biophysical approaches to HD research have added a whole new dimension to our understanding of a wide-range of cellular processes ranging from cellular localization to protein-protein interactions.

The CAG repeat expansion at the DNA level translates to a stretch of polyglutamine (polyQ) residues in the first exon of the protein huntingtin (htt). The exact function of the

huntingtin protein is still unclear though it has been implicated in several cellular processes based on its interactions with other proteins (Table 1-1). Most structural biology textbooks emphasize the hierarchy of structure, from the primary sequence level, to secondary and tertiary structural elements to quaternary structures. In the case of htt, there are substantial complexities at each of these levels. At the primary sequence level, this is manifested through the diverse sequence architecture and post-translational processing of the protein. The secondary and tertiary structures of htt are intricately tied to not only sequence context but also cellular roles. Similarly, in recent years there has been some evidence for a quaternary structure of htt that might underlie its binding and/or aggregation properties. Each of these levels can directly modulate the cellular fate of htt and, by extension, the pathology of HD. This chapter aims to review our current knowledge of these different levels of htt structure and their possible roles in HD pathology.

Structural biology of HD at the nucleic acid level: The study of HD from a structural biology perspective has almost exclusively focused on htt, the *prima culpie* in HD. Due to constraints of space, this focus on htt is also maintained in this chapter. Yet, as is now becoming apparent, there are some interesting structural aspects to HD at the nucleic acid level as well. CAG repeats in the huntingtin gene in chromosome 4 have been extensively studied in terms of their ability to promote replication instability which in the majority of cases leads to CAG expansion, a trigger for HD (1). CAG repeats, selectively enriched in exons in human DNA (3), have been observed to form unusual structures that are held together by Watson-Crick base pairing and through mismatched base-pairs, structures that can substantially modulate fundamental processes of DNA replication and repair (4). At the RNA level too, CAG repeats have been known to form stable hairpins and several recent studies have focused on exploring the possibility of a toxic

gain-of-function at the RNA level (5). The finding that RNA transcripts of expanded CAG repeats do not require a starting ATG for translation, possibly because of their propensities to form hairpins (6) underscores the importance of exploring the structural effects of CAG repeats. The reader is referred to these reviews (4, 7) for a detailed report of the current state of research relating to the structural biology of CAG repeats.

1.2 HUNTINGTIN SEQUENCE: STRINGING TOGETHER COMPLEX BUILDING BLOCKS.

Huntingtin is a 3144 amino acid protein (based on a normal polyQ repeat of 23) that is believed to be crucial to normal functioning of the basal ganglia (8) though the exact function is still unclear. This 350KDa protein is also characterized by a diverse sequence architecture which might explain its putative role as a cellular hub of protein-protein interactions (9). This section highlights some of the important components of the diverse htt sequence and their evolutionary and functional significance.

1.2.1 PolyQ stretch.

The polyQ stretch in htt, the fundamental disease locus in HD, is located in the N–terminal segment. The length of the polyQ tract varies between individuals with 17 glutamine residues the most common in non-disease patients and 40 residues being fully-penetrant amongst HD patients (10, 11). Phylogenetic analysis show that the polyQ stretch is an ancient acquisition in htt, dating back to a four residue NHQQ sequence in the sea-urchin (12) which gradually expanded into the polymorphic stretch that it has become in humans. The exact biological

significance of this polyQ stretch remains unknown, and in fact some suggest that it is not essential for huntingtin function (13). Nevertheless, despite its relatively monotonous appearance, the polyQ stretch seems to modulate a plethora of interaction and functional roles in htt, as described later.

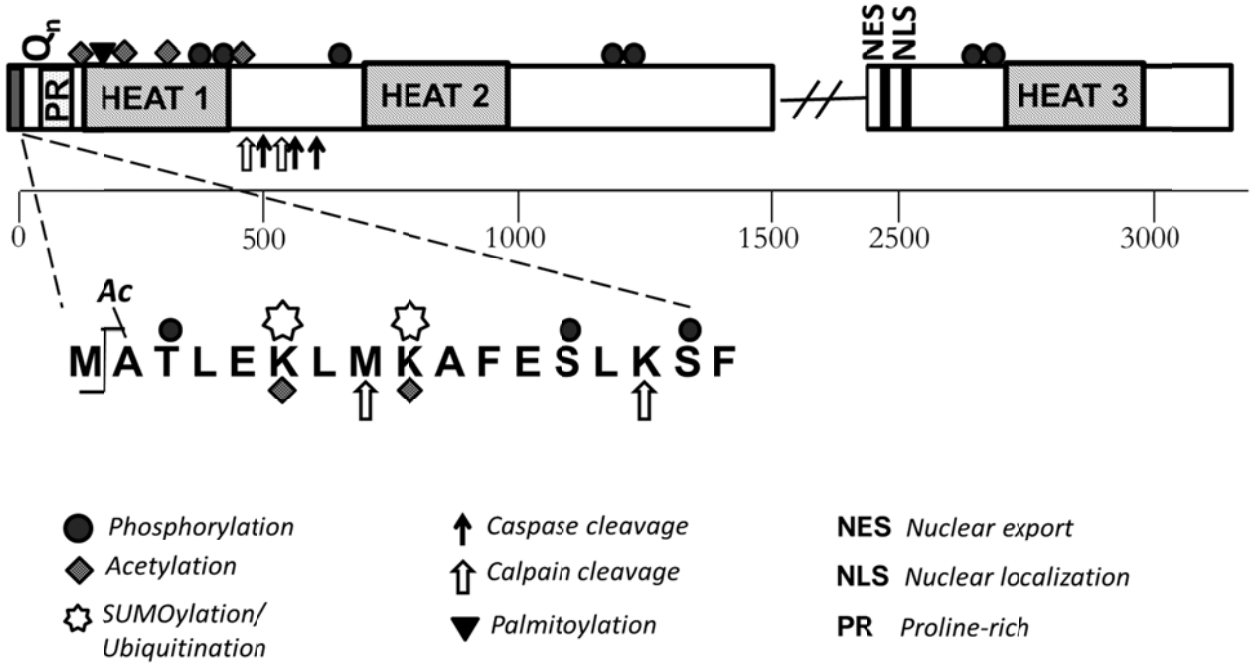

Figure 1-1: Sequence architecture of huntingtin. Shown are the major features of htt's sequence architecture. The numbering is based on a glutamine repeat length (Q_n) of 23. The first seventeen residues of huntingtin, htt^{NT} are shown in detail along with the major post-translational events that localize to this sequence. The three HEAT repeat clusters are highlighted. Also shown are some of the functionally significant post-translational events such as phosphorylation (14-17), acetylation (17, 18), SUMOylation/ubiquitination (19), palmitoylation (20) and proteolytic cleavage (21-26). Adapted from (27).

1.2.2 Sequence domains flanking polyQ.

The polyQ stretch in htt is flanked by two disparate and yet interesting sequence regions. N-terminal to the polyQ stretch lie the first seventeen residues of htt (htt^{NT}) which are highly conserved. This sequence, characterized by a mix of hydrophilic and hydrophobic residues, seems to modulate htt's partitioning between intra- and extra-nuclear compartments (28-30) and its propensity to form aggregates (28, 31). Following the polyQ stretch in htt, is the C-terminal region of htt exon-1 which is characterized by a preponderance of proline residues. Interestingly, this stretch of proline residues seems to have been acquired following the evolutionary expansion of the polyQ stretch thereby supporting the hypothesis that these proline residues serve to down-regulate the deleterious effects of polyQ expansion (19, 32).

1.2.3 HEAT repeats.

The huntingtin sequence is characterized by a series of 37-43 residues called HEAT repeats (33) (named after the proteins they were first identified in: huntingtin, elongation factor 3, subunit A of protein phosphatase 2A and TOR). The HEAT repeats, which typically occur in tandem, have assumed particular relevance because of their role in protein-protein interactions (see below). Though there is some debate about the number and organization of these HEAT repeats (12, 34), it is believed that there are at least three conserved clusters of such repeats (27).

1.2.4 Post-translational modifications in huntingtin.

The large size of the htt protein makes it an ideal candidate for several post-translational modifications (PTMs) that are increasingly believed to be crucially tied to htt's functional roles and its link to HD pathology. Both ubiquitination (2, 35) and SUMOylation (19) in htt have been described and are believed to compete for the same lysine residues in htt^{NT} (Fig 1-1) and regulate htt's stability, localization and effects on HD pathology. Additionally, full-length (fl) htt has 539 potential phosphorylation sites (14) and thus far, at least eleven phosphorylation sites have been characterized. Phosphorylation at some of these sites is believed to be tied to crucial pathological processes. For instance phosphorylation at serine 434 has been shown to reduce caspase cleavage at residue 513 and protects against toxicity (36) while phosphorylation at serine 536 reduces cleavage by calpains at this site (14). Similarly, phosphorylation at threonine 3 was shown to reduce neurodegeneration in a fly model of HD (17). More dramatically, transgenic (tg) mice expressing fl-htt with a S13D/S16D mutation to mimic the observed phosphorylation at these residues (37) did not develop the disease and lacked typical pathology seen in HD mice (16). Some of the other PTMs in htt that have been linked to HD pathology include palmitoylation at cysteine 214 that is linked to aggregation and toxicity (20) and acetylation at lysine 444 (amongst others) which has been shown to promote autophagosomal degradation (38). Taken together these observations highlight a crucial role for PTMs in modulating pathology possibly by altering the biophysical properties of htt.

1.2.5 Proteolytic processing of huntingtin.

Fl-htt purified from mammalian cells has been observed to be susceptible to significant proteolysis (39). Proteolytic processing of htt has been implicated as a trigger for HD pathology, forming smaller fragments which have a higher tendency to aggregate and which are the major components of neuronal intranuclear inclusions in post-mortem HD brains (2). Further support for such a "toxic fragment" hypothesis (40) comes from the finding that mice expressing truncated versions of htt exhibit a shorter life-span than do those expressing fl-htt (41) and the observation that inhibiting the cleavage of htt protects against aggregation and toxicity (24). Both wt and expanded htt are cleaved by caspases 2, 3, 6 and 7 at residues 513, 552 and 586 (22-24, 42). Interestingly, wt-htt can itself interact with caspase-3 when over-expressed thereby potentially allowing for an up-regulation of caspase activation under conditions of htt depletion (25). In addition to caspases, htt has also been found to be cleaved by other proteolytic enzymes like the calpains (21) and aspartyl endopeptidases (43). The cleavage sites for calpain 1 and 2 had earlier been mapped to the residues 469 and 536 (21) though more recent work suggests that calpain 1 can also cleave at positions 8 and 15 in htt^{NT}, an event that might be crucial for htt clearance (26). On the other hand, residues between 104 and 114 have been identified as the site of cleavage by aspartyl-endopeptidases releasing two fragments that differentially build up in cytoplasmic and nuclear inclusions (43). In addition to the ones mentioned above, new sites of proteolytic cleavage (and new proteases) are continuously being identified which might play a significant role in HD pathology (44-46). In any case, a direct effect of the proteolytic processing of htt observed *in vivo* is that it has allowed structural biologists to focus on these shorter fragments of htt which are more amenable to experiments and which might be the more relevant protein motifs in HD.

1.3 HUNTINGTIN: A HUB OF PROTEIN INTERACTIONS.

1.3.1 Huntingtin as an interaction scaffold.

Several *in vitro* and *in vivo* studies have ascribed a crucial role for htt as a hub of protein-protein interactions, interactions that influence a host of cellular processes (Table 1-1). The identification of diverse interacting partners strengthens the case for a multi-functional role for htt in the cell. This has led to the hypothesis that at the center of this multi-functionality lies the ability of htt to act as a molecular scaffold for protein interactions, facilitating the transfer of information across the cell. (47). However, htt's susceptibility to proteolysis (39) and its propensity to aggregate do raise questions about htt's ability to mediate such a scaffolding role.

The interactions of htt with transcription factors is of particular interest given the preponderance of polyQ sequences in transcriptional factors and the hypothesis that aggregate sequestration of polyQ rich transcription factors might be responsible for transcriptional dysregulation observed in HD (48). However, the ability of htt to interact with a wide –range of transcription-related proteins (49) without a polyQ tract points to a role for htt in transcriptional regulation that is distinct from one based on polyQ annealing. One such role could be htt's ability to act as a critical scaffold that brings together essential components of the transcription machinery (47). The binding of htt to Sp1 and its co-activator TAFII130 (50) has also been cited as an example in support of this hypothesis (47). Furthermore, htt has been implicated in at least one other protein complex involved in transcriptional repression (51).

Binding Partner	Function	Htt binding site	polyQ effect on binding
Transcription:			
CA 150 [52]	Transcription activator	Unknown	No.
CBP(53)	Transcription activator	NT(1-588)	Yes (↑)
CtBP(54)	Transcription repressor	Unknown	Yes (↓)
HYP-A,B(55)	RNA splicing	NT(polypro)	Yes (↑)
HYB-C(55)	Transcription factor	NT(polypro)	Yes (↑)
NCOR(51)	Transcription repressor	NT(1-171)	Yes (↑)
NF-κB(34)	Transcription factor	HEAT repeats	Unknown
SP1(50, 56)	Transcription activator	NT(1-171)	Yes (↑)
TAFII130(50)	Transcription activator	NT(1-480)	No
TBP[57]	Transcription factor	Unknown	Unknown
P53(53)	Transcription factor	NT(polypro)	No
REST-NRSE(58)	Transcription suppressor	NT(1-550)	Yes (↓)
Sin3a(53)	Transcription repressor	NT(1-171)	Yes (↑)
Trafficking/Endocytosis:			
HYP-J[55]	Endocytosis	NT(1-550)	Yes (↓)
HIP 1[59]	Endocytosis/pro-apoptotic	NT(1-550)	Yes (↓)
HIP 14[60]	Trafficking/endocytosis	NT(1-550)	Yes (↓)
PACSIN 1[61]	endocytosis	NT(polypro)	Yes (↑)
SH3GL3[62]	endocytosis/vesicle recycling	NT(polypro)	Yes (↑)
HAP1[63]	Trafficking/endocytosis	NT(1-230)	Yes (↑)
PSD-95[64]	Synaptic scaffold	Unknown	Yes (↓)
Signaling:			
Calmodulin[65]	Ca+ regulation	Unknown	Yes (↑)
CIP-4[66]	Cdc42 signaling	NT(1-152)	Yes (↑)
FIP2[55]	GTPase Rab8 interactor	NT(1-550)	Unknown
GRb2[67]	Growth factor signaling	NT(polypro)	Unknown
$IP_3$1[68]	Calcium signaling	NT(1-158)	Yes (↑)
RasGAP[67]	Ras GTPase	NT(polypro)	Unknown
TRAF6[69]	E3 ubiquitin ligase	NT(1-171)	No
MLK-2[70]	Mixed-lineage kinase	NT(polypro)	Yes (↓)
Other:			
Cystathione β-synthase[71]	Cys generation	NT(1-171)	No
GADPH[72]	Glycolytic enzyme	NT(polypro)	Yes (↑)
HIP2[35]	Ubiquitin conjugase	NT(1-540)	No
Rhes[73]	SUMO-E3 ligase	NT(1-171)	Yes (↑)
Gp78[74]	Ubiquitin ligase	HEAT 2/3	Yes (↑)
TpR [75]	Nuclear Export	NT(1-17)	Yes (↓)
TRiC[76]	Chaperonin	NT(1-17)	No

Table 1-1: Reported interaction partners of htt.

1.3.2 Structural loci of huntingtin interactions.

The majority of htt's interactions are localized to the N–terminal region of htt comprising residues 1-588, probably because of the fact that most of the yeast two-hybrid experiments have used this fragment as the "bait". Nevertheless, this particular sequence stretch in huntingtin is particularly attractive because of the presence of the polyQ stretch, and the proline rich sequence C terminal to it, and the first HEAT repeat cluster in this region.

1.3.2.1 HEAT repeats.

The ability to form super-helical structures (Fig 1-2.A) that can promote protein-protein interactions and their presence in eukaryotic proteins implicated in several crucial cellular processes, make the HEAT repeats in htt excellent candidates for putative interaction sites. Not surprisingly therefore, several of htt's interacting partners have been observed to bind in the region containing HEAT repeats (Table 1-1).

1.3.2.2 Proline-rich sequence.

The proline-rich sequence adjacent to the polyQ stretch in htt exon-1 has been implicated as the major locus of htt interactions based primarily on its ability to interact with proteins that contain SH3 (Src homology) or WW domains that bind proline-rich motifs in the target ligands (77). Interestingly, in almost all of the interactions that are mediated by this proline-rich sequence, the strength of association is modulated by the length of the adjacent polyQ repeat region, leading to the hypothesis that polyQ expansion is linked to conformational changes in the adjacent proline-rich region which can directly impact htt's interactions with its binding partners (61, 62, 70). However, the ability of polyQ expansion to promote aggregation, thereby

complicating interpretation of protein interactions (discussed below), presents a caveat to such a conformational re-arrangement hypothesis.

1.3.2.3 PolyQ sequence.

In addition to being the site of the expansion that is the primary trigger for HD, the polyQ sequence in htt is also crucial to htt's interactions with its binding partners. While polyQ expansion has been suggested to modulate interactions of htt with other proteins (Table 1-1), the polyQ stretch has itself been implicated as the binding site of only one other protein, GADPH (72). One explanation for this might be that self-association of polyQ in htt impairs its ability to bind other proteins. Yet, a role (albeit indirect) of polyQ in mediating protein interactions cannot be discounted. For instance, fusing a polyQ tract to a DNA binding domain was seen to activate transcription (78). A recent study by Schaefer *et al* (79) found that polyQ containing proteins interact with more partners than proteins lacking polyQ. Furthermore, they posit a structural role for polyQ in mediating protein-protein interactions in terms of its ability to adopt and extend a coiled-coil conformation in adjacent sequence domains in the bound state.

1.3.2.4 The seventeen residue htt^{NT} sequence.

The highly conserved N-terminal seventeen residues in htt have been the subject of considerable study in recent years because of their ability to modulate aggregation of htt exon-1 *in vitro (31)* and *in vivo* (28) as well as their ability to directly influence htt localization by binding membranes (29). Furthermore, the designation of this region as a MoRF (molecular recognition feature) (31) as well as its ability to adopt helical structures in complexes (80) make it an attractive candidate for mediating protein interactions. Thus far, the htt^{NT} sequence has been implicated in interactions with Tpr (nuclear pore protein translocated protein region) (75)

as well as the eukaryotic chaperonin TRiC (76). One possible explanation for the inability to identify more htt interaction partners binding to this sequence might be the reported sequestration of this region in htt exon-1 aggregates (31) which might be present in several of the methods used to identify interaction partners.

1.3.3 Relevance of htt association states to protein-protein interactions.

Most of htt's interaction partners have been identified either by yeast-two hybrid screening or by employing biochemical approaches such as affinity purification, GST pull-down assays and/or co-immunoprecipitation. The results of such assays can easily be influenced by the aggregation states of htt. In fact, enrichment of aggregates in samples could provide an alternative explanation to the role of polyQ expansions in mediating htt interactions. Similarly, one could rationalize the observation that several interaction partners of htt bind shorter fragments more efficiently than they do fl-htt (56, 75, 81) by invoking the greater propensity of such fragments to aggregate. In fact, a recent study by Davranche *et al* (82), demonstrated that polyQ aggregation can strongly bias the results of pull-down assays and that aggregate free preparation of htt N-terminal samples do not display any dependence on polyQ expansion in binding other proteins. They then proceed to argue that htt aggregates can selectively sequester binding epitopes thereby modulating htt's interactions with its partners. Interestingly, an earlier study showed that N-terminal fragments of htt bind post-synaptic membranes in R6/2 mice in an oligomeric state (83) underscoring the importance of accounting for aggregation in analyzing htt's interactions.

1.4 SOLUTION STRUCTURE OF HUNTINGTIN.

The large size of the fl-htt molecule has made it inaccessible to high-resolution structure determination methods. Furthermore, the high propensity of htt fragments to aggregate make it challenging to determine the structure of the monomeric form in solution, if such a form even exists. Thus, most of the efforts geared towards determining the solution structure of huntingtin have adopted a reductionist approach by looking at the structure of smaller sequence domains in isolation. In this section, we review some of the work that has been done in elucidating the structural properties of huntingtin in solution.

1.4.1 HEAT repeats.

The identification of HEAT sequences in htt and the prediction of such sequences forming helical structures painted a structural picture of htt for the first time (33). We now know that tandem HEAT repeats in proteins adopt helical structures that are believed to be the structural determinants to the multitude of interactions that such proteins participate in. A crystal structure of 15 tandem HEAT repeats in the PR65/A subunit of protein phosphatase 2A (84) shows that this molecule forms an extended, curved structure (Fig 1-2A) comprised entirely of helices connected by loops, akin to a molecular hook. Each HEAT motif has two anti-parallel helices that are stacked parallel to the adjacent repeat thereby forming a double-layer of helices across the entire length of the molecule (Fig 1-2.A, inset). Using molecular modeling techniques, Li *et al* showed that HEAT repeats in fl-htt adopt an extended conformation (39). The presence of exposed hydrophobic residues within intra-repeat turns that might become buried upon binding provides a structural basis to the implication that HEAT repeats serve to mediate protein-

protein interactions (33). More recently, Navarro and group (85) have found three clusters of α-rods (3-D arrangements of elongated anti-parallel helices) matching the locations of the three HEAT clusters. Interestingly, they were able to show that these α-rods mediate intra- and inter-molecular interactions suggesting that these structural clusters might be important determinants of fl-htt's tertiary and/or quarternary structure (Fig 1-2.B). The presence of such a folded structure in fl-htt is also borne by results that indicate that fl-htt remains associated non-covalently despite proteolytic cleavage (39).

1.4.2 Structural studies on htt fragments.

1.4.2.1 PolyQ structure.

Studies of the solution conformation of polyQ sequences assume particular significance in the light of the toxic monomer hypothesis which suggests that expanded polyQ is associated with a conformational transition within the monomer which represents the toxic species (see discussion below and Fig 1-3). Thus, a multitude of computational and biophysical methods have been applied to investigating structural aspects of polyQ sequences. Fluorescence correlation spectroscopy studies of polyQ peptides showed that these sequences are inherently insoluble in water (a poor solvent for polyQ) adopting compact conformations across both short and long repeat lengths (86). Evidence for compact non β-sheet conformations across different polyQ repeat lengths was also observed in atomic force microscopy studies of polyQ sequences flanked by folded proteins which also ascribed substantial mechanical resilience to such conformations (87).

Despite the inherent challenges posed by the insolubility of polyQ sequences, a multitude of structural tools have been applied to the study of polyQ structure. Circular dichroism studies

of synthetic polyQ peptides, of both pathological and non-pathological lengths, first showed that the polyQ sequences lack any stable secondary structural elements and exist predominantly as random-coils (88) in solution though there are hints of some helical propensities especially at lower temperatures (89). Since the CD spectra of random coil and PPII helical conformations are similar, it is possible that seemingly disordered proteins can adopt PPII helical conformations. In fact, PPII helical conformations have been observed in polyQ peptides, especially at lower repeat lengths (90, 91) though there are hints of a transition to β-sheet conformations (91) at higher polyQ repeat lengths. While it is possible that polyQ sequences can sample PPII helical conformations locally, studies using high resolution structural techniques like X-ray diffraction and NMR suggest that in solution polyQ sequences lack any stable structure though they might transiently sample secondary structural elements (80, 92). This view is also supported by computational studies which indicate that polyQ sequences might adopt a mixture of random-coil, helical and β rich structures in solution (93, 94) with the caveat that results of simulations seem to depend on the choice of parameters (95).

An additional level of complexity to the study of polyQ conformations arises from the protein context. In other words, the presence of flanking domains can influence the conformational preferences of polyQ. Using X-ray diffraction, Kim *et al* showed that the polyQ sequence in a maltose binding protein-htt exon 1 construct adopts conformations ranging, from α-helical or random coil in residues proximal to htt^{NT}, to extended in residues adjacent to the polyproline stretch (80). Other studies have demonstrated the ability of the polyproline sequence to induce PPII helical structures within polyQ (91). Such a change in conformational preferences of polyQ might be of particular relevance to its aggregation propensities which are known to be modulated by its flanking sequences (see below).

Evidence for a toxic monomer conformation of polyQ : The toxic monomer hypothesis suggests that polyQ expansion is linked to a toxic structural transition in the monomeric state (Fig 1-3). This hypothesis originated from observations of polyQ-specific monoclonal antibodies binding longer-polyQ repeats better than shorter repeats which was ascribed to the presence of a specific structural conformation at higher repeat lengths. Subsequent studies showed that such stronger binding of mAbs to longer polyQ repeats can be explained based on a "linear-lattice" mode of binding (92), at least for some of these antibodies. Thus, longer polyQ repeats present more binding epitopes and hence are bound to a greater extent by mAbs such as MW1. However, recent studies with the 3B5H10 antibody suggest that this antibody does bind a specific conformation in longer polyQ repeat constructs of htt exon-1 in a non "linear-lattice" binding mode. Thus, SAXS based studies of the 3B5H10-htt exon-1 complex indicate that the polyQ epitope is an anti-parallel β-hairpin structure (96). A greater propensity for an average β rich structure at higher polyQ repeat lengths has also been reported based on CD (91, 97) , FRET (98) and SAXS (96) studies of different polyQ repeat peptides. The ability of 3B5H10 antibody to bind a β strand rich monomeric conformer of polyQ coupled with the finding that 3B5H10 is a better predictor of neurodegeneration, based on correlative studies looking at neuronal lifetimes, has been used to support the argument that polyQ expansion is associated with the population of a toxic conformer in the monomeric state. Other studies in support of this argument include greater toxicity observed in the case of artificial htt exon-1 constructs engineered to form β hairpin structures (99) and also

enhanced toxicity observed upon microinjection of a β sheet conformer of an expanded polyQ construct into cultured cells (97).

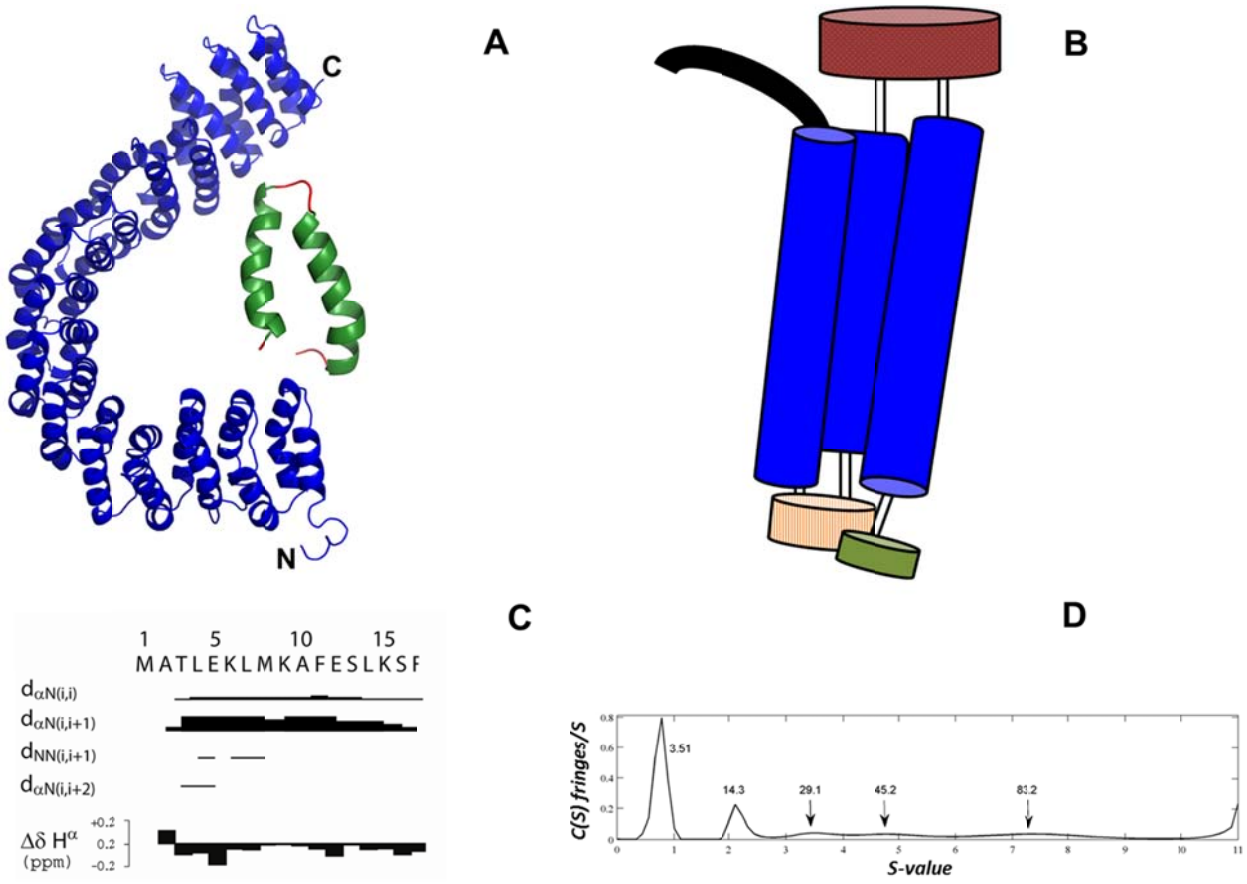

Figure 1-2: Solution structure of huntingtin and its fragments. (A) Structure of 15 tandem-repeats in the PR65/A subunit of protein phosphatase 2A (84). PDB ID: 1B3U. (inset) A single anti-parallel HEAT repeat. (B) Proposed model (85) of 3-D structure of htt mediated by interactions between HEAT clusters (blue cylinders). The N-terminal sequence including the polyQ tract is shown as a curved (black). Also, shown are domains adjacent to HEAT clusters (elongated cylinders) (C) NOEs from proton-NMR analysis of htt^{NT} shows the lack of any stable secondary structure. (D) AUC analysis indicates the presence of tetramers, octamers and higher-order species in equilibrium (100).

While the presence of a specific conformer at higher polyQ repeat lengths is possible, one must consider the caveats with the existing evidence for this hypothesis. It is likely that the putative β-strand conformation at higher polyQ repeat lengths is populated only in the presence of antibody. Such "conformational enrichment" has been reported in other systems (101) and is particularly relevant to disordered proteins that are known to have a propensity to fold when bound to a more structured partner (102). Of course the presence of a β-rich conformer at higher polyQ repeat lengths has also been observed as the average conformation (96) in the largely disordered monomeric ensemble (92) in the absence of the antibody. However, one would anticipate that given the higher propensity of longer polyQ repeats to aggregate, such a shift towards a β rich conformer might be explained, in part at least, by enhanced aggregation tendencies (103). In fact, the presence of small oligomeric species in some of these studies cannot entirely be discounted (96, 99). In any case, direct evidence linking a specific polyQ conformation to pathological events is needed to unequivocally demonstrate a toxic role for such species.

1.4.2.2 Polyproline stretch.

Unlike with other constituents of the htt N-terminal sequence, most experimental (96) and computational studies seem to concur that the polyPro sequence in htt adopts a PPII-helical conformation in solution. Functionally, this may stem from the importance of this structural motif to recognition by SH3 domains (77) though it might also be responsible for the inhibitory effect of the polyPro sequence on the aggregation of polyQ (91).

1.4.2.3 Solution structure of htt^{NT}.

In the past few years, considerable attention has been given to determining the solution structure of the first seventeen residues in htt in part because of the crucial role that these residues play in determining htt's aggregation, localization and interactions with other partners, in the cell. As mentioned above, the htt^{NT} segment is characterized by a mix of hydrophobic and hydrophilic residues prompting the hypothesis that this sequence adopts an α-helical conformation in solution. Earlier, circular dichroism studies of this sequence had identified substantial helical propensities displaying up to 50%-60% helical character (31). Supporting this finding, several computational simulations have also confirmed the helical propensities of this sequence (95, 104). On the other hand, higher resolution solution NMR studies did not find any stable elements of α-helix in the htt^{NT} sequence which was observed to exist as a random coil in solution though there were hints of transient helix conformation in some residues (31). One way to rationalize these seemingly disparate findings is that htt^{NT} exists as a random coil, transiently sampling helical states, which are stabilized under certain conditions like inter-molecular interactions or upon binding partners. Not surprisingly therefore, algorithms based on primary sequence analysis have identified htt^{NT} to belong to the larger group of MoRFs (molecular recognition features) which are typically compact coils in solution lacking any stable secondary structure but often adopt a α-helical conformation upon binding their interacting partners (31). Experimental support for this hypothesis comes from the X-ray diffraction studies by Kim *et al* which (80) showed that htt^{NT} adopts a helical conformation under crystallization conditions and also from the concentration dependence of helicity in the htt^{NT} sequence as assessed by circular dichroism (100). Overall, these findings are consistent with the idea that htt^{NT} though disordered at lower concentrations does have substantive helical propensities which are stabilized at high

concentrations. This "disorder to order" transition is particularly relevant to the aggregation of htt, as discussed below.

Tetrameric assemblies of htt in solution. A discussion of the solution structure of a protein has to also account for any evidence of quaternary structure. Recent studies have found evidence for the ability for htt^{NT} to exist in equilibrium between monomeric, tetrameric and higher order oligomeric forms (100). Some cellular studies with green-fluorescence protein tagged htt exon-1 have also observed the existence of oligomeric species in the pentameric to nonameric range (105). While the formation of a tetramer/multimer (100) might be an early step in the aggregation pathway of htt (discussed below), it is also likely that htt (or its fragments) can exist in solution in a tetrameric state. At the very least, the formation of such multimeric species circumvents the energetic penalties associated with the exposure of hydrophobic residues to the solvent as would be expected for a disordered sequence. A closer examination of the association states of htt in solution could yield some interesting insights into the structural facets of HD pathology and will be a major area of focus in the field in the future.

1.5 AGGREGATION OF HTT FRAGMENTS.

1.5.1 Aggregation of htt fragments: Role in HD.

Initially proposed as a mechanism to explain the neurodegeneration observed in HD (106), the case for a role of protein misfolding and/or aggregation in HD pathology was strengthened by the observation of neuronal intra-nuclear inclusions (NIIs) of htt fragments in tg HD mice (106) and subsequently in post-mortem HD brains (2). The polyQ dependence of NII

accumulation (107), the observation of these inclusions in specific regions of the brain that are affected in HD (2) and the appearance of NIIs just prior to observation of HD symptoms point to an intricate link between htt aggregation and disease pathology (106).

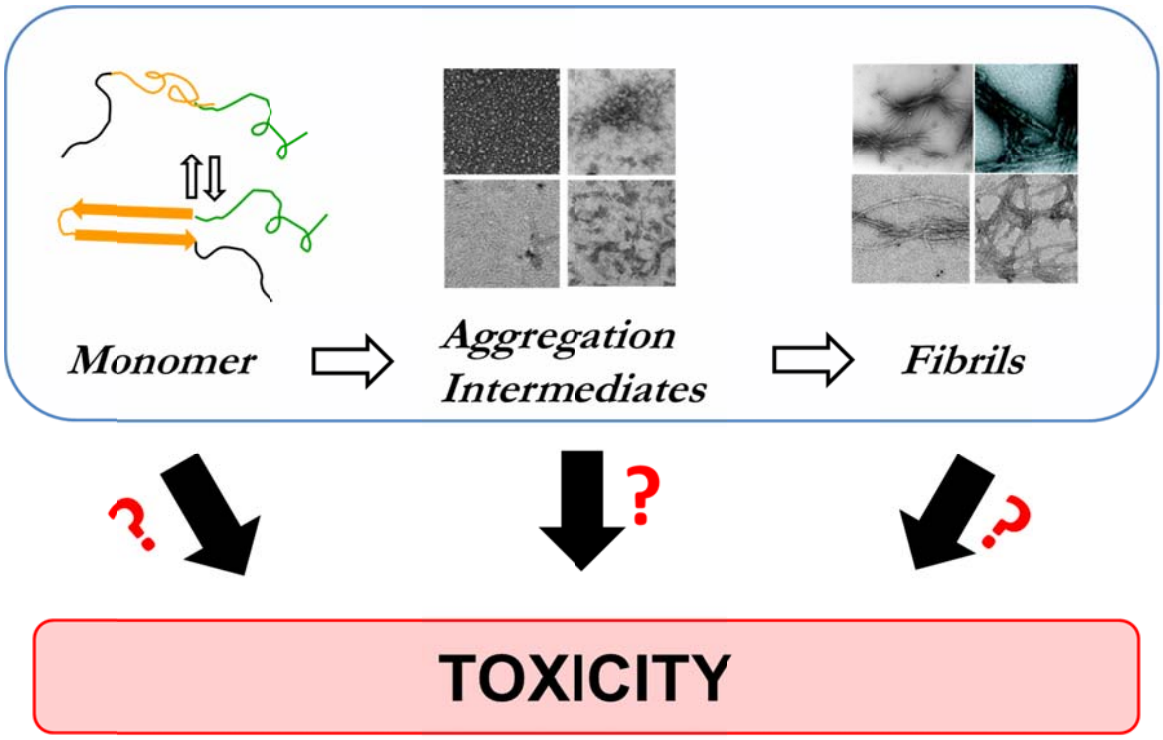

Figure 1-3: Link between aggregation and toxicity. Shown are the different stages of aggregation pathway . There is significant discussion and difference of opinion in the literature about the role in toxicity, and in some cases, the existence in the cell, of these various states. The polyQ in the monomeric species is essentially disordered but there are suggestions in the literature for either α-helix rich (97)or β-sheet-rich (96) monomers at higher polyQ repeat lengths that have been linked to toxicity (99, 108). Aggregation intermediates shown here oligomers and protofibrils (109) which could also be linked to toxicity (110, 111). Finally, the end-point of aggregation shown as fibrillar structures (112) (113) (109) with a putative role in mediating cellular toxicity (114, 115).

Toxicity of aggregates: While there has been substantial work devoted towards understanding the link between aggregation and toxicity, a complete picture still remains elusive. Several

studies have delineated a toxic role for final aggregates. For instance, the formation of inclusion bodies in cells expressing htt was observed to correlate with cell death (114, 116). Similarly, the specific delivery of aggregates into the nucleus was observed to promote cell-death (115). Consistent with such a toxic role for aggregates in cellular models of HD, are observations of correlations between aggregate formation and appearance of HD phenotypes in a tg mouse model. On the other hand, there is also some evidence for a neuroprotective role for aggregates. For instance, studies with tg mice expressing a mutant htt N –terminal fragment that formed inclusions but did not give rise to any HD like phenotype argue against a toxic role of inclusions (117). Similarly, it has also been postulated that aggregates can play a neuroprotective role by simulating the autophagic clearance of mutant htt (118). As an additional level of complexity, there is a growing body of evidence that suggests that aggregation intermediates (like monomers (99, 108) or oligomers (111, 119)) and perhaps even a misfolded monomer (96) might be toxic to cells (Fig 1-3). In fact, as the subsequent sections will indicate, the aggregation of htt fragments exhibits substantial diversity in terms of aggregation intermediates, aggregation pathways and response to PTMs and other cellular conditions. This diversity might explain the seemingly paradoxical viewpoints on the role of htt aggregation in HD pathology. Nevertheless, while the finer details of the relationship between htt aggregation and HD pathology get worked out, it has now become clear that a study of htt misfolding and aggregation is crucial to our understanding of the disease.

1.5.2 Aggregation mechanisms *in vitro*.

1.5.2.1 Aggregation of polyQ sequences.

Since the polyQ stretch in htt is directly linked to the occurrence of HD, most studies have focused on examining the aggregation properties of simple polyQ peptides. The study of aggregation of the simple polyQ repeats also assumes particular significance in the light of the finding that under certain conditions polyQ containing htt fragments can aggregate via a pathway that is entirely driven by their polyQ segments (120). Most studies of polyQ aggregation typically incorporate a few residues (like lysines) adjacent to the polyQ stretch to overcome the insolubility inherent to polyQ sequences (89, 121). Using synthetic peptides of the form $K_2Q_nK_2$, the lab had earlier shown that aggregation of polyQ peptides *in vitro* is directly correlated to the polyQ length. The aggregation of these peptides proceeds through a random-coil to beta-sheet transition during aggregation, ending up in beta-sheet rich amyloid fibrils (122).

Most aggregating systems are associated with a nucleation step, the rate-limiting step in the aggregation pathway that is concurrent with the formation of the nucleus, an unstable, experimentally inaccessible species on the aggregation pathway. The presence of such a nucleation phase in the aggregation pathway can be discerned by studying the dependence of aggregation rates on the concentration of the protein/peptide. A study of the concentration dependence of initial aggregation rates of $K_2Q_nK_2$ peptides identified a nucleated growth mechanism underlying aggregation of these peptides (122). However, there exist subtleties in the nucleation step in the aggregation of polyQ peptides of different lengths. Thus, while $K_2Q_{18}K_2$ and $K_2Q_{23}K_2$ peptides aggregate through the formation of a tetrameric nucleus, $K_2Q_{24}K_2$ and $K_2Q_{25}K_2$ peptides aggregate through a dimeric nucleus whereas $K_2Q_{26}K_2$ (and peptides with higher polyQ repeat lengths) aggregate via a monomeric nucleus (121). This relationship

between polyQ repeat length and nucleation mechanisms might portend some crucial insights into the underlying structural aspects of polyQ aggregates.

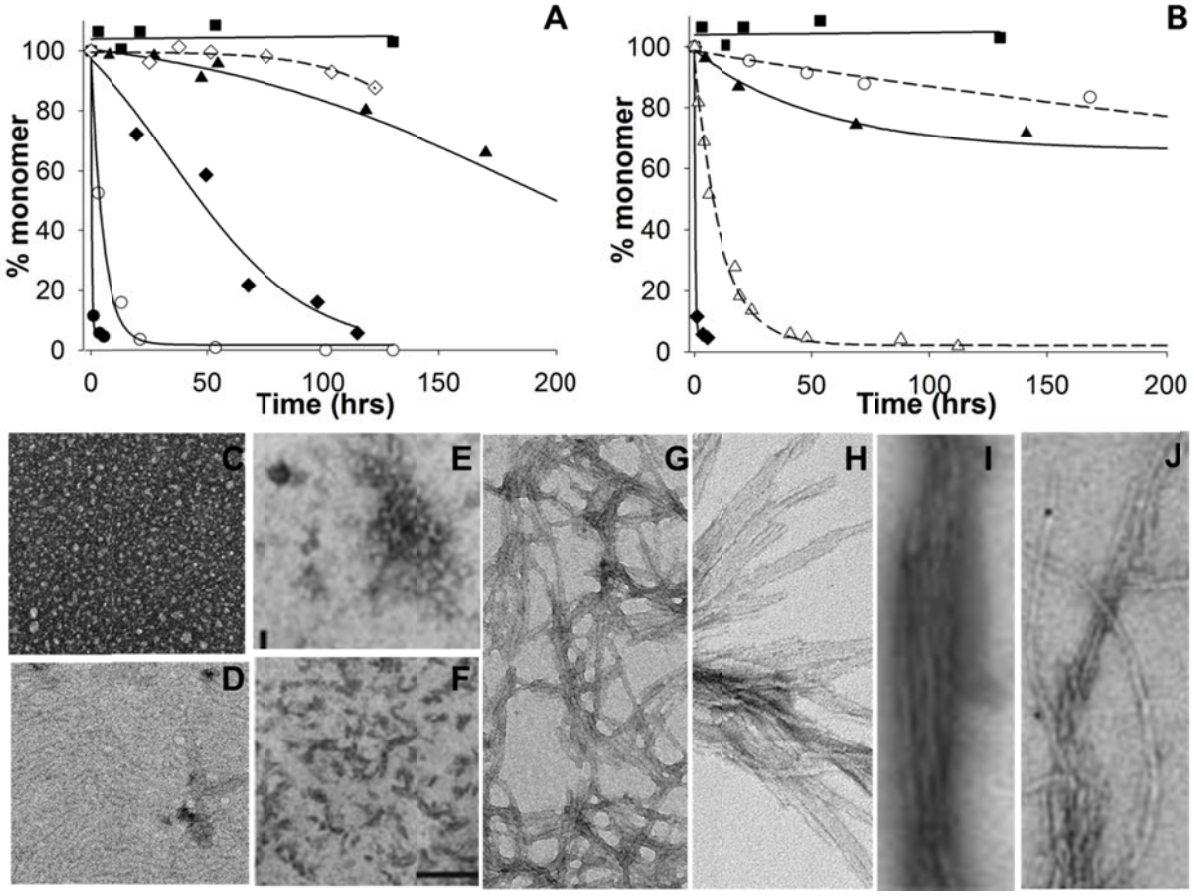

Figure 1-4: Aggregation of htt constructs. (A) Aggregation of equivalent concentrations (~5μM) of htt^{NT} (■), $htt^{NT}Q_{35}K_2$ (●), $htt^{NT}Q_{36}P_{10}K_2$ (○) and $K_2Q_{35}K_2$ peptides (◊). Also shown are the aggregation profiles of higher concentrations (~25μM) of $K_2Q_{35}K_2$ (♦) and $K_2Q_{35}P_{10}K_2$ (▲). (B) polyQ dependence of the aggregation of polyQ containing htt fragments. Aggregation of ~5μM htt^{NT} (■),$htt^{NT}Q_{10}K_2$ (○), $htt^{NT}Q_{15}K_2$ (▲), $htt^{NT}Q_{25}K_2$ (Δ) and $htt^{NT}Q_{35}K_2$ (♦). Adapted from (31). EM morphologies of different aggregates formed *in vitro*. Early oligomers (C), protofibrils (D) , end-stage aggregates of polyQ containing htt fragments (G) and final aggregates of simple a MF-$Q_{37}P_{10}K_2$ peptide (H). Also shown are morphologies of aggregates isolated from brains of tg HD mice showing oligomeric (E), protofibrillar (F) and fibrillar (I-J) species.

The nucleus, by definition, is highly unstable and hence inaccessible to most experimental studies. It has been suggested, that the nucleus in polyQ aggregation is a transiently populated β-sheet structure (122). At smaller polyQ repeat lengths, multiple molecules are required to form a stable nucleus, hence the formation of tetrameric and dimeric nuclei. As the polyQ repeat length increases, the monomers can themselves form stable beta-rich structures (Fig 1-5.B, g). Such a scheme is supported by studies that incorporate $_{D}$-Pro-Gly sequence within a polyQ context, to favor the formation of β-hairpins, which showed that such peptides aggregate faster than a peptide of identical polyQ repeat length without the $_{D}$-Pro-Gly interruption (123, 124). These studies also add weight to the hypothesis that anti-parallel beta structures might be crucially tied to the aggregation of polyQ repeat peptides (refer discussion below).

Another characteristic feature of nucleation driven aggregation is that the rate of aggregation can be substantially accelerated by the addition of pre-formed aggregates as seeds, a characteristic that is also true of polyQ peptides. This property has been exploited in a biotin tagged polyQ recruitment assay that allows for quantification of seeding capacities of aggregates and provides crucial thermodynamics of polyQ aggregation (122). Thus, while the $\Delta G_{nucl.}$ is -12kcal/mol for a $K_2Q_{47}K_2$ peptide (122), for an equivalent concentration of $K_2Q_{23}K_2$ peptide this values is ~ -24kcal/mol (121). Two points becomes evident from such an analysis. First, an expansion of polyQ makes nucleation of aggregation comparatively more favorable. Second, the ΔG_{nucl} (especially for higher polyQ repeats which aggregate via a monomeric nucleus, a process that can be compared to an unfavorable folding event) is substantially higher than those of typical ΔG_{fold} of proteins (-5 to -15 kcal/mol) (125) highlighting the ephemeralness of nucleation.

Overall, the aggregation of polyQ peptides can be described by a nucleated-polymerization model (Fig 1-5.B). In the monomeric state, polyQ sequences exist in collapsed, random-coil conformations (89). The nucleus, thought to be a β-rich structure that can either be monomeric or multimeric depending on the polyQ repeat length (121), is in equilibrium with the monomer. The nucleus can also indulge in elongation steps presumably by monomer addition, consolidating amyloid-like features in stable assemblies. The elongation step has been described by invoking a "dock and lock" mechanism whereby an incoming monomer, latches onto the growing face of the fibril and re-arranges on the surface presenting a new growing end to subsequent monomer additions.

Alternate mechanisms of polyQ aggregation: The nucleated growth pathway described above lacks any soluble, non β-sheet rich intermediates (oligomers). However, based on results from simulations of polyQ aggregation that suggest the formation of dimeric species (94) and amorphous aggregates (126) and based on the observation of oligomeric assemblies of polyQ peptides under certain conditions (127), it has been proposed that aggregation of these peptides proceeds through nucleation within such oligomeric species. The conversion of these oligomers into aggregates has however not been demonstrated, neither experimentally nor computationally, due to the rarity and transience of such an event. It is quite likely that these differences viz. oligomeric species between different studies stems from the differences in sample preparation and handling especially in the light of the fact that polyQ peptides are known to form oligomers under certain conditions (128). The importance of growth conditions in the aggregation of polyQ peptides is also driven home by the observation that aggregates of polyQ grown at -20^{o}C display altered morphologies and seeding properties than those grown at 37 ^{o}C (129, 130). Temperature

effects on polyglutamine aggregate structure and toxicity have also been observed in other studies (131). It is likely that similar to other aggregating systems, polyQ peptides too display polymorphisms in aggregate structure/property depending on growth conditions (132). In addition to growth conditions, sequence contexts can also affect the aggregation mechanisms and aggregate properties of polyQ rich peptides. Thus, a $K_2Q_{30}K_2$ peptide with histidine insertions (mimicking sequences encoded by the SCA1 gene (133)) aggregates through the formation of oligomers at acidic pH (134). Oligomeric intermediates have also been reported in the aggregation of polyQ containing htt fragments (see below). Overall, these results underscore the complexities of polyglutamine aggregation. Of course, it is possible that inside the cell aggregation of polyQ sequences proceeds through either (or even both) of these mechanisms.

1.5.2.2 Flanking sequences modulate aggregation of htt fragments.

Sequences flanking the polyQ stretch in htt have been shown to play a crucial role in modulating aggregation of polyQ sequences. Initial studies investigating the effects of flanking sequences on polyQ aggregation focused on the role of the proline rich C terminal sequence of htt exon-1. Addition of a proline sequence to $K_2Q_nK_2$ peptides was also observed to impair the kinetics of (Fig 1-3.A), and destabilize the thermodynamics of, aggregation though it did not change the aggregation mechanism (89). Studies with yeast models of HD showed that the polyproline stretch in htt exon-1 abrogates polyQ expansion induced toxicity in addition to altering aggregate morphologies (32). From a structural stand-point, this "auto-inhibitory" effect of polyproline has been explained based on its ability to induce PPII helical conformations in glutamines adjacent to it thereby interfering with the tendency of these sequences to form β-sheet rich structures (91).

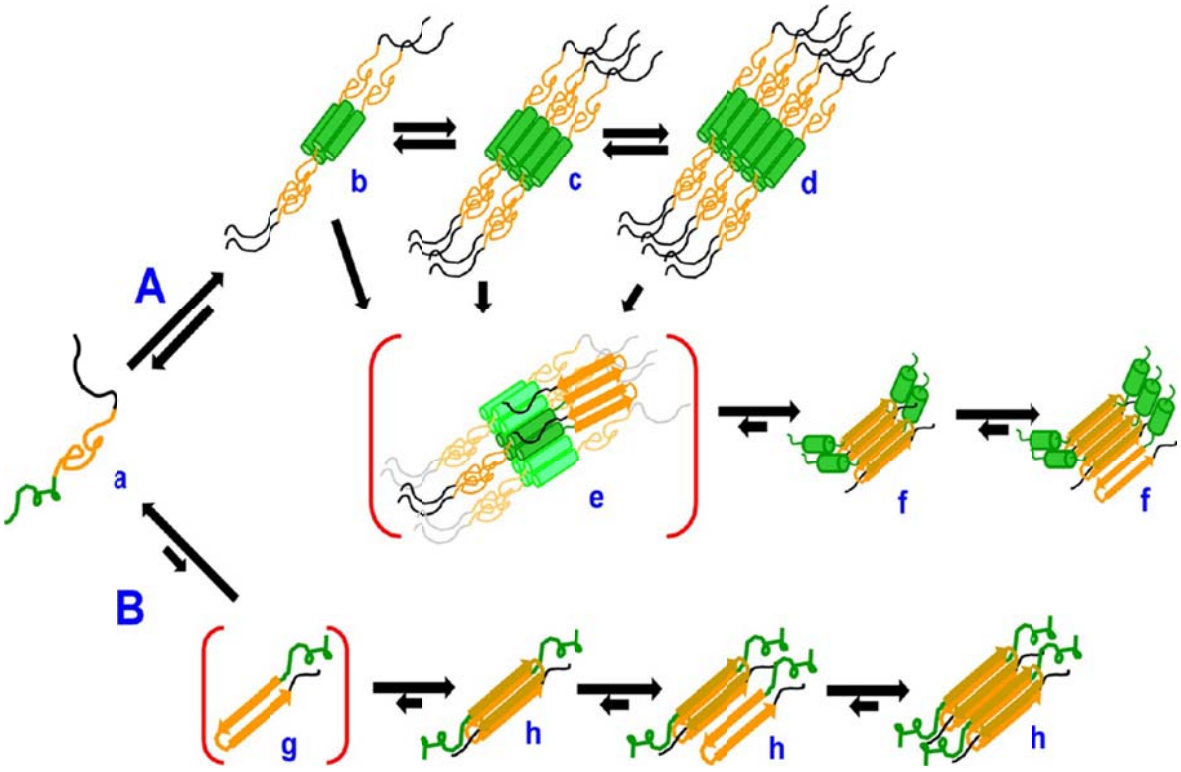

Figure 1-5: Putative aggregation mechanisms of polyQ containing htt fragments. (A) htt^{NT} (green) mediated aggregation pathway. Monomers of polyQ containing htt fragments (a) are in equilibrium with tetramers (b), octamers (c) and do-decamers (d). The htt^{NT} sequence is believed to adopt a helical conformation within these oligomeric species (green cylinders). Each of these oligomers has some probability to be the site of stochastic nucleation (e) of amyloid-like structure within polyQ (orange). Post-nucleation elongation (f) of amyloid structure can proceed, presumably via monomer addition to form amyloid-fibril like final aggregates (11). Oligomers that do not nucleate might act as reservoirs of monomer which fuel elongation. Also shown in black are the C-terminal polyProline sequences that are believed to be extruded from the amyloid core and exposed. (B) polyQ (black) driven aggregation pathway. Monomeric htt fragments are disordered (a). Under certain conditions (viz. in the presence of inhibitors or when htt^{NT} is cleaved) aggregation is driven by the polyQ stretch. The rate-limiting step is the nucleation of amyloid structure in polyQ (g) which might require the participation of 1,2 or 4 monomers depending on polyQ repeat length (121). Nuclei, thus formed, can elongate via monomer addition to form mature fibril structures (h). Elongation proceeds through a "dock and lock "mechanism by which incoming monomer first latches onto the growing face of the fibril and then undergoes conformational-rearrangement to present a new growth face (4). Adapted from (120)

Contrary to the inhibitory effect of the flanking proline residues, the addition of the seventeen residue N-terminal sequence, htt^{NT}, produced a dramatic acceleratory effect on aggregation of htt fragments (31, 76). Studies with peptides resembling htt exon-1fragments (polyQ containing htt fragments) showed that the htt^{NT} sequence accelerates aggregation (Fig 1-4.A), apparent in the dramatic differences in the initial phases of aggregation. Thus, while polyQ peptides display strong concentration dependence in their initial aggregation rates, these htt fragments have much shallower concentration dependence (31). At the mechanistic level, this difference in initial aggregation is manifested through the rapid formation of oligomers (Fig 1-4.C) which are believed to serve two crucial roles in the aggregation pathway: *a.* by concentrating polyQ segments locally, these oligomers can act as nucleating centers for the stochastic re-arrangement of polyQ chains into nascent amyloid-like structures and *b.* Oligomers that do not go through stochastic nucleation can act as monomer reservoirs, dissociating to monomers which can participate in elongation. The htt^{NT} sequence by itself is sufficient to form oligomers either under high concentrations (135) or after long incubations (136). These oligomers are predominantly helical in nature and seem to be formed through the ability of htt^{NT} to associate into tetramers, octamers and dodecamers in the native state (100). The hydrophobic residues have been hypothesized to play a crucial role in oligomerization (31, 76) while the polyQ stretch does not seem to be involved in the oligomer structure and remains accessible to binding by the polyQ specific MW1 antibody (31). Stochastic nucleation within these oligomers is believed to drive aggregate formation, presumably through monomer addition, forming fibril like structures (Fig 1-3.G) that display features characteristic of amyloid including ThT binding, seeding competence and β-sheet rich FTIR spectra (31) though they are morphologically

different from the final aggregates formed by simple polyQ peptides (Fig 1-3. H). This htt^{NT} mediated aggregation of polyQ containing htt fragments is also crucially linked to the glutamine repeat length with longer repeat lengths associated with faster aggregation kinetics (Fig 1-4.B). While, it has been suggested that polyQ expansion can alter monomeric conformations of polyQ containing htt fragments (31, 100), it is also quite likely that increasing the polyQ repeat length affects other stages of pathway including oligomerization, nucleation and/or elongation. While the point can be made that such peptide models do not accurately reflect the aggregation properties of htt exon-1, the lab has found that mechanistic features in play in the aggregation of such polyQ containing htt fragments are also largely conserved in the aggregation of chemically synthesized htt exon-1 (Sahoo *et al*, manuscript in preparation).

The aggregation enhancing role of htt^{NT} both in vitro and in vivo (28, 76, 137) has also been observed in several independent studies though different aggregation mechanisms to explain this acceleratory role have been posited. Thus, based on the ability of the htt^{NT} sequence to interact with the polyQ stretch, it has been suggested that the sequence promotes an amyloidogenic conformation within the polyQ stretch that can grow into amyloid aggregates (76). The ability of the htt^{NT} sequence to accelerate the aggregation of a Q51 fragment in trans was cited in support of such a model (76) though similar experiments in other systems do not yield similar results (138). It has also been suggested, based on some experimental (139) and computational (140) results, that oligomers of polyQ containing htt fragments are held together primarily by polyQ interactions though the results of other computational studies (95) suggest that initial aggregation (in as much as dimerization can be used as an indicator of aggregation) of polyQ containing htt fragments is mediated by htt^{NT}.

Cellular implications of aggregation: In the light of the crucial role that htt^{NT} plays in the aggregation of polyQ containing htt fragments, it can be reasoned that cellular conditions that selectively target this sequence can affect aggregation as well. One such trigger can be post-translational modifications within the htt^{NT} sequence (Fig 1-1). Thus, mutation of the two Ser residues at positions 13 and 16 within htt^{NT} to Asp to mimic phosphorylation completely abrogated aggregation and neurodegeneration in a tg mice. *In vitro* studies of a htt^{NT} $Q_{37}P_{10}K_2$ peptide with an identical mutation showed that this mutation serves to impair aggregation kinetics and alter final aggregate morphology (16). In another case, phosphorylation of the lone threonine residue in htt^{NT} was observed to alter aggregation of htt exon-1 *in vivo* and reduce lethality in a drosophila model of HD (17).

While, the aggregation of polyQ containing htt fragments is substantially different from that of polyQ-only sequences, recent evidence suggests that polyQ containing htt fragments can also aggregate through the nucleation growth pathway that is observed with simple polyQ sequences (Fig 1-4.B). However, this pathway is strongly disfavored kinetically and has thus far been observed only when the oligomer-driven pathway is blocked (for example with inhibitors, see below). It is possible that a similar situation exists inside the cell with htt exon-1 fragments retaining the ability to form different aggregates under different cellular conditions. For instance, there have been examples of osmolytes changing the final aggregation products of htt exon-1 (141). In fact, the presence of multiple pathways of htt fragments that can be activated selectively under different conditions (or triggers) might underlie the observation that different polyQ aggregates with different toxicities (131).

1.5.3 Structural features of aggregates.

Aggregates formed by both polyQ peptides and polyQ containing htt fragments display the characteristic β-sheet signature typified by amyloid fibrils in CD, FTIR, X-ray and ssNMR studies (31, 136, 142). One of the earliest structural models for aggregates proposed a β-helical structure for polyQ sequences (143). While, there is some support for such models, both experimental (144) and computational (126, 145-147), the current view seems to slant towards a more conventional, slab-like (142, 148) β-structure in aggregates. While, there have been some reports of a parallel orientation of β-sheets in polyQ aggregates (149, 150), the consensus view seems to favor an anti-parallel conformation. Early evidence for an anti-parallel β-sheet conformation adopted by polyQ sequences in final aggregates came from studies with synthetic polyQ constructs rationally designed to stabilize anti-parallel conformation. Thus, synthetic polyQ peptides with ^{D}Pro-Gly interruptions (that favor β-turn but destabilize extended strands) were observed to aggregate with similar kinetics and form morphologically similar aggregates as equivalent polyQ peptides without interruptions (123). Subsequently, the case for an anti-parallel arrangement of β-strands in polyQ aggregates was strengthened by the results from high-resolution structural techniques. Both ssNMR (151) and X-ray fiber diffraction studies of final aggregates formed by synthetic polyQ peptides indicate an anti-parallel β-sheet aggregate structure (142, 148).

The propensity of polyQ sequences to adopt anti-parallel β-sheet conformations in aggregates of simple polyQ peptides is also maintained in aggregates of polyQ containing htt fragments. Thus, ssNMR analysis of final aggregates of polyQ containing htt fragments indicated that the polyQ core in both “simple” polyQ peptides and in polyQ containing htt fragments are spectroscopically identical, most probably in an anti-parallel β-sheet conformation. Interestingly,

polyQ sequences in aggregates of both simple polyQ peptides (151) and polyQ containing htt-fragments (136) indicate that glutamine residues are present in two conformations, the structural basis of which is not entirely understood. Surprisingly, the major portion of the htt^{NT} segment is present in an α-helical conformation even in the final aggregates highlighting the strong preference of this sequence to adopt helical conformations. The transition from the β-sheet conformation adopted by polyQ to the α-helical conformation occurs towards the C-terminal end of the htt^{NT} sequence with both S16 and F17 adopting β-sheet conformations in the final fibrils. The proline residues adopt a PPII helical conformation in the aggregates (96) and are probably not involved in the aggregate core (31).

Given their potential role in HD pathology (see below), it becomes all the more important to gain structural insights into the organization of aggregation intermediates of polyQ containing htt fragments. While the transience of these species makes their study challenging, the use of htt peptides with shorter polyQ repeats has allowed us to glean some structural insights. Thus, htt^{NT} when incubated at high concentrations forms oligomers that display predominantly α-helical spectra (Fig 1-6.A).

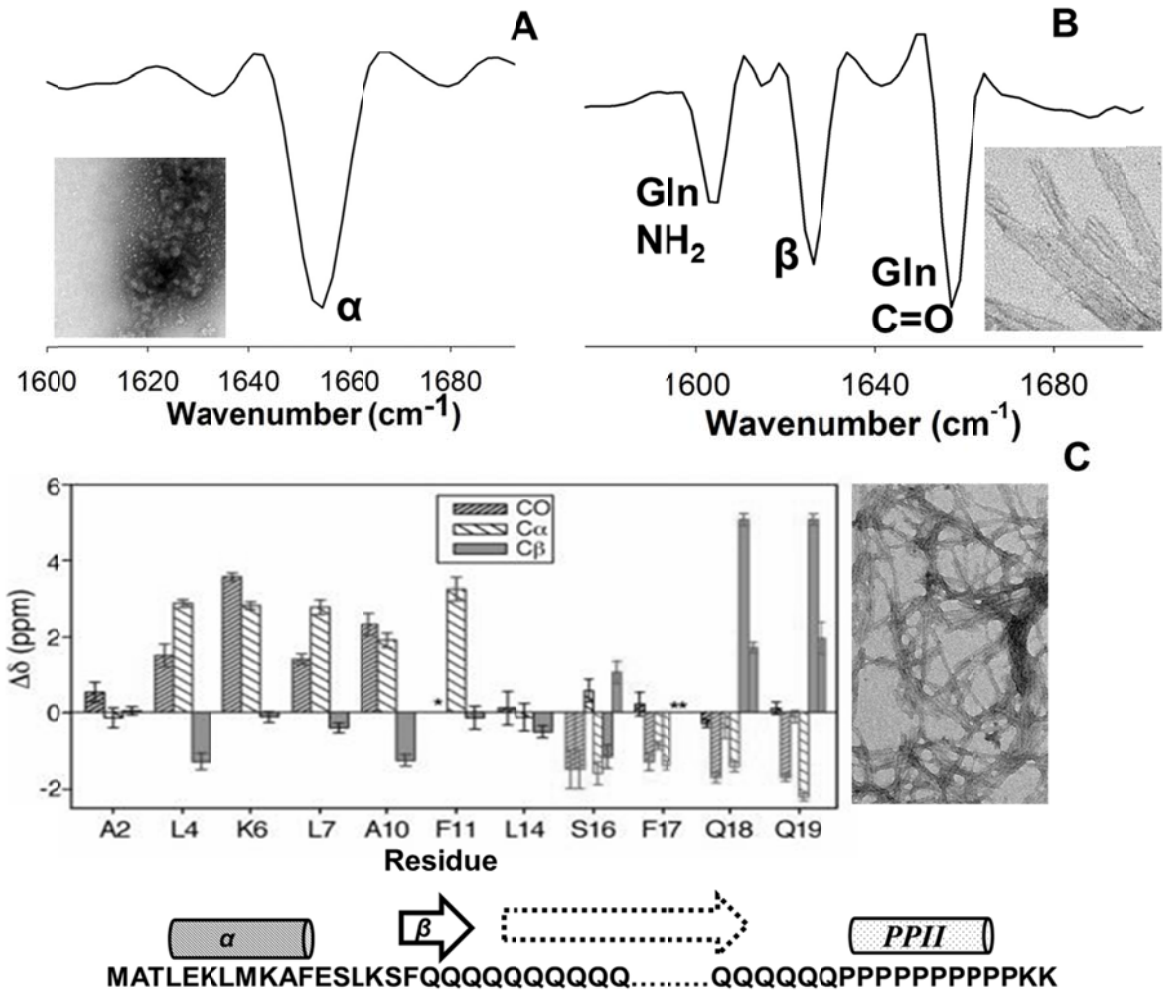

Figure 1-6: Structural features of aggregates. (A) FTIR spectra of oligomers (inset) formed by htt^{NT} indicates a predominantly helical conformation. (B) FTIR spectra of final aggregates (inset) formed by the fibrils of $K_2Q_nK_2$ fibrils indicates a strong β-sheet structure (~1626 cm^{-1})with ordered Gln side chains (~1650cm-1). (C) ssNMR studies of final fibrils formed by polyQ containing htt fragments indicate that residues Leu 4-Phe 11 retain α-helical secondary structure, Ser 16, Phe 17 and glutamine residues are in predominantly β-sheet conformation and the proline residues in predominantly PPII conformation(schematic). Adapted from (136).

Similarly, FTIR studies with aggregates of $htt^{NT}Q_8K_2$ isolated at different times showed a transition from α-helical to β-sheet structures consistent with the role of these intermediates as sites for nucleation of amyloid structure (100).

1.5.4 Inhibitors of aggregation.

In the light of the potentially toxic role that htt aggregation plays in HD pathology, considerable efforts have been directed towards the identification of aggregation inhibitors that might ameliorate disease phenotype. In addition to their potential significance as therapeutics, aggregation inhibitors are also useful reagents that can considerably add to our understanding of htt aggregation and its role in HD pathology. Based on their chemical structures, inhibitors of htt aggregation can be grouped into two classes: small molecule inhibitors and peptide/protein based inhibitors.

1.5.4.1 Small-molecule inhibitors of aggregation.

A wide range of small-molecule inhibitors with diverse chemical structures have thus far been identified as inhibitors of htt aggregation. Using an automated filter-trap assay to quantify aggregates, Heiser *et al* identified benzothioazoles as polyglutamine aggregation inhibitors reducing the amount of SDS insoluble (fibrillar) aggregates with IC_{50} values in the micromolar range. Some of these molecules were also identified to be potent inhibitors of aggregation *in vivo* through a cell-based assay (152) as well as reduce aggregate burden in tg HD mice (153) . A similar approach also led to the discovery of the polyphenol (-)-epigallocatechin-3-gallate also known as EGCG as an inhibitor of htt aggregation both *in vitro* and *in vivo (154)*. Inhibition by EGCG has been suggested to be mediated through an active redirection of htt aggregation via the formation of off-pathway aggregates (oligomers). In addition to filter-trap based analysis of aggregates, fluorescence techniques have also been used in identifying other small molecule inhibitors of htt aggregation *in vivo* (155-157) though the exact mechanism of action of such molecules remains unknown. Interestingly, some compounds that are effective in inhibiting htt

aggregation *in vivo* are not as effective in inhibiting the aggregation of simple polyQ sequences suggesting the existence of divergent aggregation mechanisms though it is also likely that these differences might arise out of different cellular fates of these constructs (like binding for instance, Table 1-1) (157). Further studies aimed at delineating the exact mechanism(s) of aggregation inhibition are indispensable to our goal to gain a clearer picture of htt aggregation and its role in HD pathology.

1.5.4.2 Peptide/protein based inhibitors of aggregation.

In contrast to small-molecule inhibitors, the bases of inhibition of which are obscure in most cases, a large number of peptide/protein based inhibitors of htt exon-1 aggregation have been identified whose inhibitory actions can be explained from a structural/mechanistic standpoint. The target binding site of these peptide/protein inhibitors span the entire sequence of htt exon-1 but can broadly be grouped into the three sequence domains described above i.e the htt^{NT} sequence, the polyQ stretch and the C-terminal polyPro region.

Inhibitors targeting polyQ sequence: Using a phage-display strategy, Nagai *et al* identified a tryptophan-rich peptide, QBP1, as an inhibitor of polyQ aggregation both *in vitro* (158) as well as *in vivo* (159, 160). Subsequent, structure-function studies (161) and sequence optimization studies (162) showed the importance of the tryptophan core in these peptides that contribute to the stability of the binding of these peptides (K_d ~5μM) in addition to stereospecificity of these interactions (161). Even though the QBP1 peptide itself lacks any stable secondary structure (161) the mechanism of inhibition is believed to be based on its ability to bind a β-sheet rich monomer populated at high polyQ repeat lengths (Fig 1-7.A) (97). The elongation step in polyQ aggregation is characterized by two successive events, binding of the incoming monomer to the

fibril/nuclei (dock) and subsequent re-arrangement of this monomer to present a new growth surface for the next round of elongation (lock). Exploiting the destabilizing effect of proline residues on β-sheet structures, a class of inhibitors have been designed that though capable of binding the growth face of a fibril (i.e docking) are incapable of the conformational rearrangement required to elongate the bound fibril (i.e incapable of locking) because of the strategic positioning of proline residues in the middle of the β-strand at the new growth face. Such hybrid polyQ-polyPro inhibitors reversibly inhibit polyQ aggregation (IC_{50} ~1μM) both *in vitro* and *in vivo* (163).

The presence of side-chains with H-bonding potential has often been cited to explain the high aggregation propensities of polyQ peptides (164). Thus, it is to be expected that impairing the ability of the side-chains to participate in hydrogen bonds can substantially impair aggregation of polyQ sequences. Using peptides that have alternately N-methylated glutamine side-chains, Lanning *et al* were able to demonstrate substantial reduction of *in vitro* aggregation of polyQ rich constructs presumably by interfering with the nucleation/elongation mechanism (165).

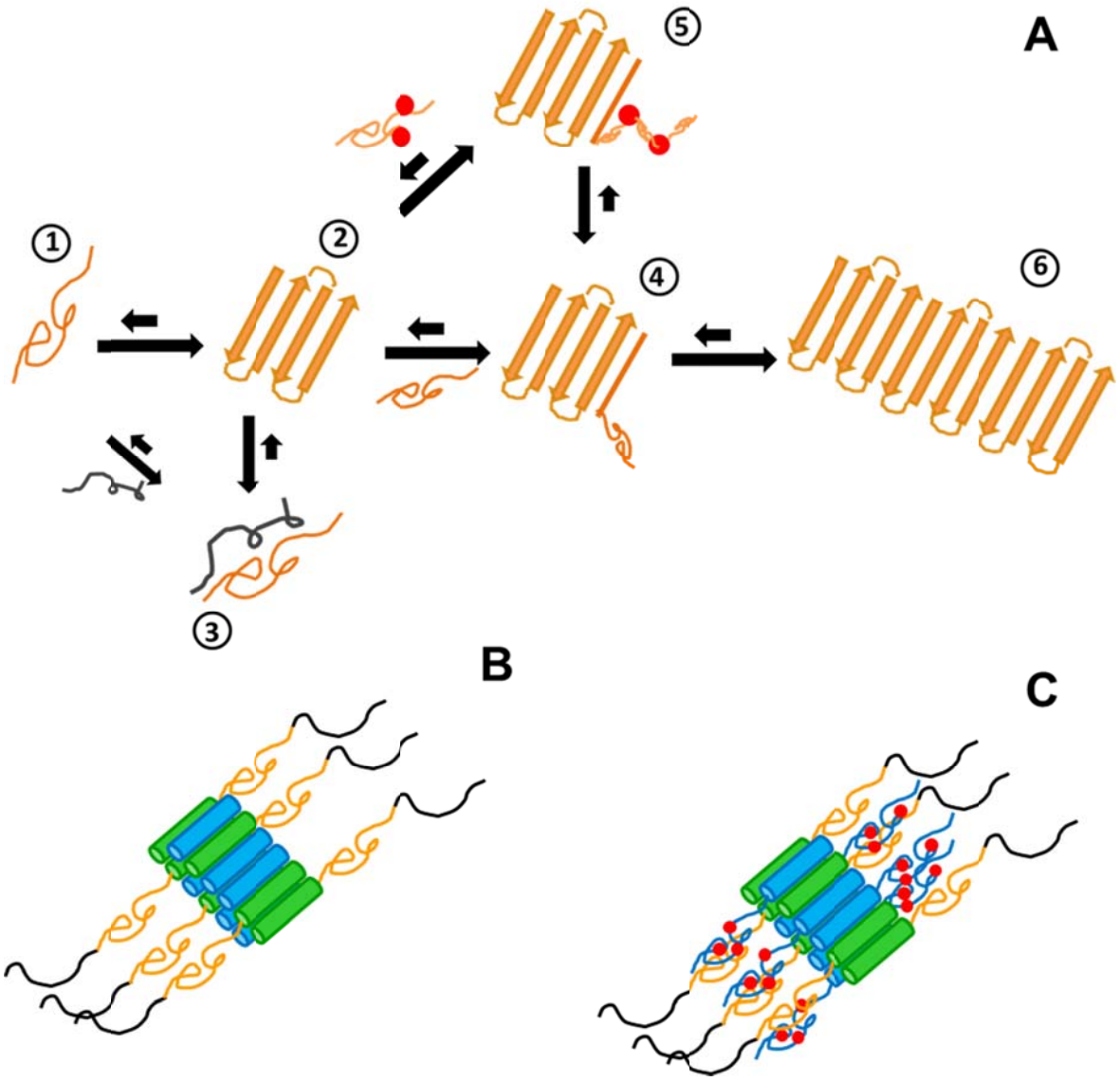

Figure 1-7: Mechanisms of protein/peptide based inhibition. (A) Peptide based inhibitors of simple polyQ aggregation can either act by binding the monomer (3) (like QBP1) or by reversibly inhibiting the elongation stage of aggregation (4) because of an ability to present a growth face (red dots, 5) such as observed in the case of the PGQ_9P^ninhibitors that have the β-sheet destabilizing proline residues or in the case of peptides with N-methylated Gln side chains. (B) Putative inhibition complex between htt^{NT} (blue) and polyQ containing htt fragments (htt^{NT} shown as green and polyQ as orange). (C) Proposed inhibition complex of $htt^{NT}PGQ9P^{1,2,3}K_2$ (blue with red circles indicating proline residues) and polyQ containing htt fragments.

Inhibitors targeting htt^{NT} *mediated aggregation.* As was described above, htt^{NT} is crucial to the aggregation of polyQ containing htt fragments. Thus, peptide/proteins that can bind and hence sequester the htt^{NT} sequence might be expected to inhibit htt^{NT} mediated aggregation. A direct significance of such sequestration based inhibition might be the ability of cellular chaperones to impair aggregation or redirect aggregation pathway by binding this sequence as has been reported in the case of the Hsp chaperone system (139). In fact, the htt^{NT} sequence has been shown to be the primary binding site of the chaperonin TRic to htt exon-1 (76). As an extension of this notion, the single domain V_L(12.3) intrabody, that reduces *in vivo* htt aggregation and rescues neuronal toxicity (166), was shown to bind a helical conformation of the htt^{NT} .

The primary role of the htt^{NT} sequence in the aggregation of polyQ containing htt fragments is to mediate the formation of oligomers that can act as centers for stochastic nucleation of amyloid structure within polyQ fragments. Expectedly therefore, a class of peptide inhibitors have been identified that can inhibit aggregation of polyQ containing htt fragments based on their ability to form co-oligomers. Thus, the addition of htt^{NT} (and variants) *in trans*, inhibits aggregation of polyQ containing htt fragments presumably based on its propensity to form amphipathic helices within mixed oligomers (Fig 1-7.B) of the substrate and inhibitor (138). However, these inhibitors only delay, instead of abrogating, nucleation by reducing the local concentration of polyQ segments which probably explains the incomplete nature of such inhibition. On the other hand, a hybrid inhibitor that contains both the htt^{NT} and the polyQ-elongation inhibitory sequence ($PGQ_9P^{1,2,3}$) completely blocks nucleation within these oligomers (Fig 1-7.C) (138).

Intrabodies targeting polyPro sequences. The polyproline tract has been demonstrated be crucial for both protein binding (Table 1-1) and for destabilizing aggregate formation both *in vitro* (89) and *in vivo* (32). Intrabodies targeting either the polyPro sequence or the proline-rich sequence in the C terminal region of htt exon-1 have been observed to have anti-aggregation and anti-toxicity roles *in vivo* which are believed to be mediated by an increased turnover of the soluble form of htt exon-1 (167). Such antibody mediated preferential turnover of mutant htt exon-1 over the wild-type presents yet another potential avenue of therapeutic intervention in HD.

1.5.4.3 Aggregation of htt *in vivo*.

High resolution electron micrographs of tissues from brains of post-mortem HD patients and tg HD mice often resemble fibril-like structures that are reported in the aggregation of htt fragments *in vitro* (2, 168). A more recent study that uses an amphipathic polymeric ligand to identify and isolate aggregates from the brains of HD mice has also been able to capture aggregation intermediates in addition to final fibrils which resemble oligomeric and protofibrillar species observed *in vitro* in the aggregation of htt fragments (Fig 1-4 E,F). In addition, to morphological similarities with fibrils grown *in vitro*, htt aggregates grown *in vivo* also display additional amyloid-like characteristics including Congo-red birefringence (169) and the ability to bind polyQ-biotin in a recruitment stain that is based on an amyloid-specific elongation mechanism (170). Overall, these results suggest that aggregates of htt *in vivo* do end up in fibril-like structures, possibly through intermediates similar to those observed *in vitro*.

In addition to such morphological assessments of aggregates, a major focus of recent studies has also been to look at the mechanisms and intermediates of aggregation *in vivo*. Using fluorescence and size-fractionation based techniques, a large number of studies have identified the presence of oligomeric species in cells ranging in sizes from 5-15 monomers (111, 171, 172)

to ~80 monomers (110). Interestingly, hetero-oligomers of wt and mutant htt exon-1 have been observed *in vivo* (171) consistent with *in vitro* studies that posit such hetero-oligomerization based on interactions within htt^{NT} (138). In addition to oligomeric species, larger inclusion bodies have also been the focus of several biophysical studies (110) (172). Such large inclusions, rich in β-sheet aggregates (106), are believed to form after a nucleation event (172). As more studies are conducted to look into htt aggregation *in vivo*, one hopes that we will be able to clarify the finer structural aspects of these and other aggregate species and their role in mediating HD pathology.

1.6 CONCLUSIONS.

The polyQ stretch in htt is the primary locus of HD pathology. However, despite their relatively monotonous appearance, polyQ sequences display considerable diversity in both their solution and aggregation properties. While, the results from a variety of experimental and computational techniques have considerably improved our understanding of the solution properties of polyQ peptides, it is increasingly becoming clear that the aggregation of these seemingly monotonous sequences is not as simple as previously thought. In addition to the repeat length expansion effects, polyQ aggregation is also intricately tied to a horde of other factors not the least of which is the chemical environment surrounding these sequences. Thus, the existence of divergent views of aggregation mechanisms of these sequences probably stems from the polymorphisms inherent in polyQ aggregation. It also raises the possibility of the existence of a multitude of aggregation mechanisms *in vivo* modulated perhaps by cellular localization and the presence of binding partners. The development of new reagents and techniques that can

distinguish between such subtle differences in aggregation will thus have to be a major focus of research in the field.

PolyQ expansion is the shared molecular trigger in at least nine neurodegenerative diseases and yet there exist substantial differences in the pathologies and manifestations of these diseases. It is now becoming clear that these differences can be explained, at least in part, based on the differences in sequence contexts. A major milestone in HD research over the past decade has been the identification of the crucial role that sequences flanking the polyQ stretch in huntingtin play in modulating its aggregation and associated toxicity. In addition to directly modulating aggregation, these flanking sequences are also sites of crucial interactions, interactions that span a wide-range of cellular processes and functions. Thus, while aggregation can lead to a potentially toxic "gain-of-function", it could also precipitate HD pathology through the loss of an essential function. It is quite likely that cellular fate of htt is ultimately decided by the winner of this tug-of-war between aggregation and normal cellular function.

The use of peptide and protein models has been indispensable to our understanding of the biophysical and structural drivers of htt aggregation. However, it is possible, and especially so in the light of the observed polymorphisms in aggregation, that that the aggregation of htt in the cell is more complicated than that observed *in vitro*. While, our ability to study aggregation of htt *in vivo* has thus far been impaired by experimental constraints, the discovery of new reagents that can distinguish between aggregates and the application of techniques/strategies such as *in vivo* FRET, split-GFP fluorescence and AUC of cellular constituents present the possibility of gleaning some crucial insights into *in vivo* aggregation of htt and its eventual role in HD pathology.

2.0 INTRODUCTION (II): PRELIMINARY STUDIES

2.1 BACKGROUND.

The purpose of this chapter is to review some of the preliminary results that have aided the development of the hypotheses that the subsequent chapters aim to address. The work presented here includes some of my own results along with results that have stemmed from collaborations with other members of the lab (and work of other interns that I have supervised and directed).

2.2 INTRODUCTION.

Protein misfolding and aggregation has been hypothesized to play a crucial role in mediating the pathology of HD. While it is still unclear whether the relationship of protein aggregation to HD pathology is one of causality, consequence, or both, the importance of a detailed study of htt aggregation (and its driving forces) to our understanding of HD cannot be understated. The crux of this thesis has thus been to identify the biophysical driving forces and glean mechanistic insights into the aggregation of htt fragments.

Htt exon-1 is the smallest fragment of htt that has been reported to be capable of inducing HD pathology (173, 174). However, the size of this fragment and its propensity to aggregate make the study of its aggregation particularly challenging. Our method of circumventing these challenges is based on the use of chemically synthesized peptide mimetics of htt exon-1 (referred to as polyQ containing htt fragments). These peptides differ from the htt exon-1 in that they contain a short polyPro instead of the entire sequence C-terminal to the polyQ segment in htt exon-1. This approach can be rationalized on multiple grounds:

a. We have thus far not seen any qualitative differences between the aggregation of polyQ containing htt fragments and the htt exon-, either chemically synthesized (B.Sahoo *et al*, unpublished) or biosynthetic (112, 113)

b. The size of the htt "toxic fragment" is not clearly known. While the sufficiency of htt exon-1 for eliciting a HD phenotype is known, theoretically it is possible that shorter fragments can elicit a similar response as well.

c. Unlike other methods of working with htt exon-1, the use of chemically synthesized fragments (when used in conjunction with the dis-aggregation protocol, Chapter 2) has the advantage of removing any pre-formed (seed) aggregates that might complicate analysis of aggregation.

While the lab has in the past focused, and continues to focus, on examining the aggregation of simple polyQ peptides, the work presented in this thesis is almost entirely concerned with investigating the aggregation of polyQ containing htt fragments. At the outset of this work, this lab (along with others) had just identified a "pro-aggregation" role of the htt^{NT} sequence. The next few sections delineate some of the preliminary work that has contributed to

the overall understanding of the aggregation of polyQ containing htt fragments and that forms the basis to the work presented in subsequent chapters.

2.3 RESULTS.

2.3.1 Aggregation of polyQ containing htt fragments.

While the polyQ stretch is directly linked to HD pathology, this stretch is also flanked by other sequences that might have an effect on its aggregation. Earlier, the lab had showed that the polyproline stretch C-terminal to the htt sequence acts an "auto-inhibitor" of aggregation though it does not alter the aggregation mechanism. On the other hand, studies from the lab had found that the addition of the htt^{NT} sequence to polyQ (or polyQ-Pro) peptides dramatically accelerates the rates of aggregation (31).

Thus, the aggregation of a $htt^{NT}Q_{37}P_{10}K_2$ peptide (Fig 2-1.A, ●) is substantially faster than an equivalent concentration of the MF-$Q_{37}P_{10}K_2$ (Fig 2-1.A, ○) (120). In addition to altering aggregation kinetics, addition of htt^{NT} also alters the properties of final aggregates which are morphologically different from those of polyQ peptides (Fig 2-2 G vs. B) (31). More importantly, we have seen evidence for the formation of oligomeric species during aggregation (Fig 2-2. C, D) (31), something that is not observed in the aggregation of simple polyQ peptides under similar conditions (121). Finally, the aggregation rates of these polyQ containing htt fragments, in spite of the strong htt^{NT} effect, are also directly modulated by the length of the corresponding polyQ stretch (Fig 2-1.A), consistent with the reported effects of polyQ expansion on aggregation propensities in simple polyQ peptides (88).

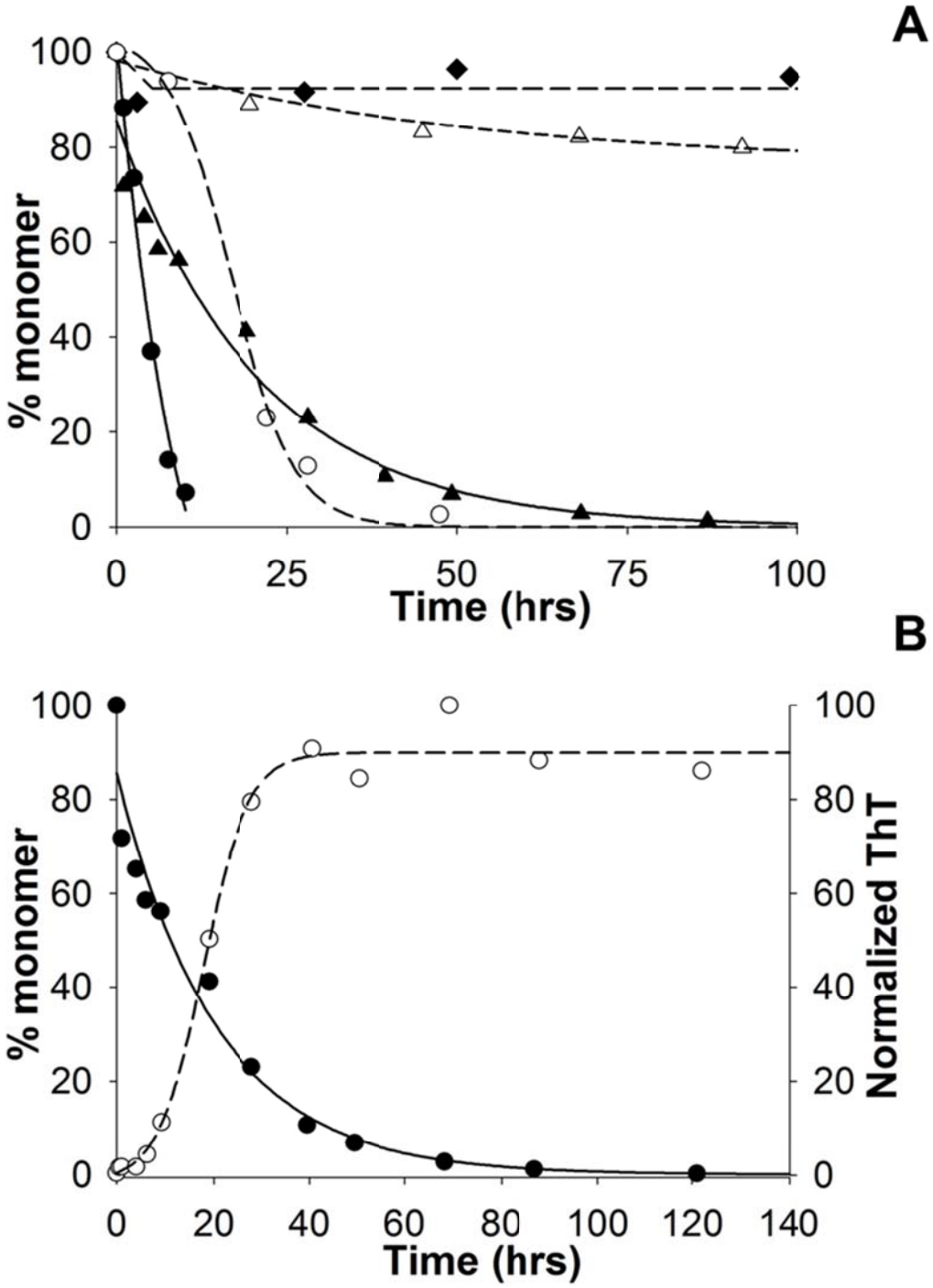

Figure 2-1: Aggregation of different polyQ containing htt fragments. (A) Sedimentation assay based analysis of aggregation of $htt^{NT}Q_{37}P_{10}K_2$ (●), $htt^{NT}Q_3$ (♦), $htt^{NT}Q_8K_2$ (Δ), $ht^{tNT}Q_{30}P_6$ (▲) and MF-$Q_{37}P_{10}K_2$ (○). (B) Detailed analysis of $htt^{NT}Q_{30}P_6K_2$ by sedimentation assay (●) and ThT binding (○). [Data from B.S and R.M]

Thioflavin T binding is a feature common to almost all amyloids, believed to be associated with the unique features of the β-sheet architecture of amyloid fibrils. Consistent with the morphological assessments by electron microscopy, aggregates of polyQ containing htt fragments were found to bind ThT. Interestingly, the initial drop in monomer concentration observed in the aggregation of polyQ containing htt fragments through the sedimentation assay is not reflected in the ThT binding of these nascent species (Fig 2-1.B) suggesting that these initial oligomers (Fig 2-2.C) lack any β-sheet structure.

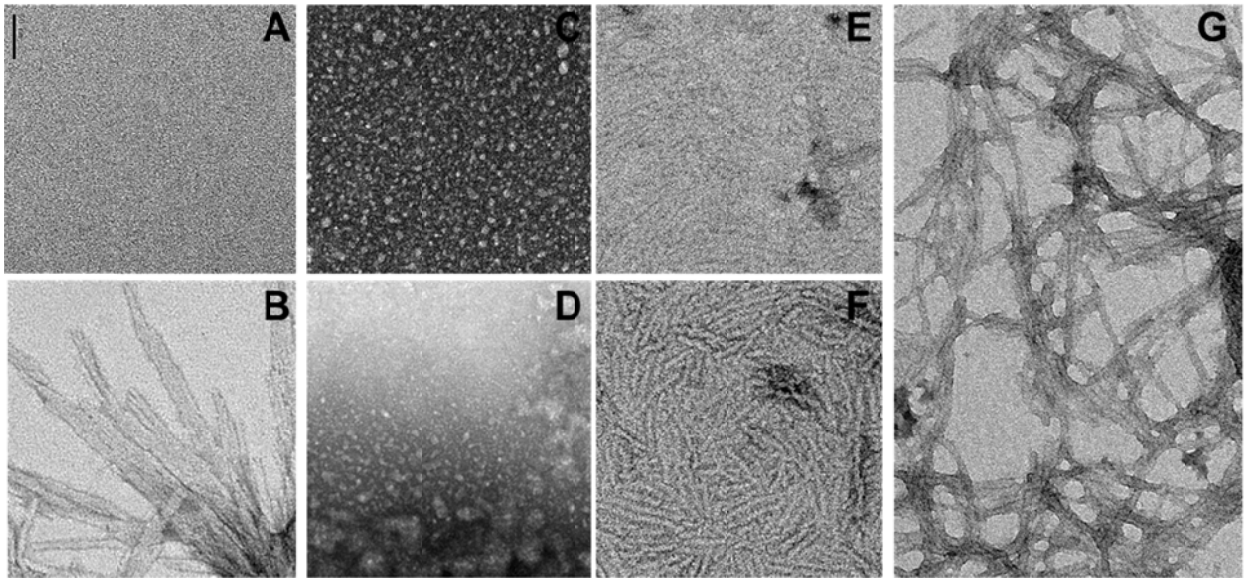

Figure 2-2: Morphologies of aggregates formed by polyQ containing htt fragments. Early aggregates isolated from a $htt^{NT}Q_{30}P_6K_2$ peptide (C) resemble oligomers formed by htt^{NT}-Q_3 peptide at high concentrations (D). Intermediate aggregates from $htt^{NT}Q_{30}P_6K_2$ (E) and $htt^{NT}Q_{37}P_{10}K_2$ (F) resemble small-protofibrillar species which eventually grow into mature amyloid-like fibrils (G). Also shown for comparison is an Empty grid (A) and final aggregates of MF-Q_{37} $P_{10}K_2$ (B). [Data from A.K.T, M.J and R.M]

A particularly characteristic feature of the aggregation of polyQ peptides is the presence of an initial lag-phase preceding aggregation. Furthermore, the length of this lag-phase depends

on the bulk concentration of the peptide. This dependence of aggregation rates on concentration can be quantified by calculating the slope of a plot of log (initial concentration) vs. log (initial aggregation rates) (Chapter 3). In the case of polyQ peptides, this slope is ~3 (Fig 2-3.A ○) consistent with the nucleated-growth aggregation mechanism of these peptides (122). On the other hand, a similar analysis of the concentration dependence of initial aggregation kinetics of polyQ containing htt fragments gave a slope of 1.2 (Fig 2-3.A ●, ▲) suggesting that the initial aggregation of these peptides is independent of concentration (31). This lack of concentration dependence of initial aggregation in the case of polyQ containing htt fragments is consistent with the rapid formation of oligomers observed in these peptides (31).

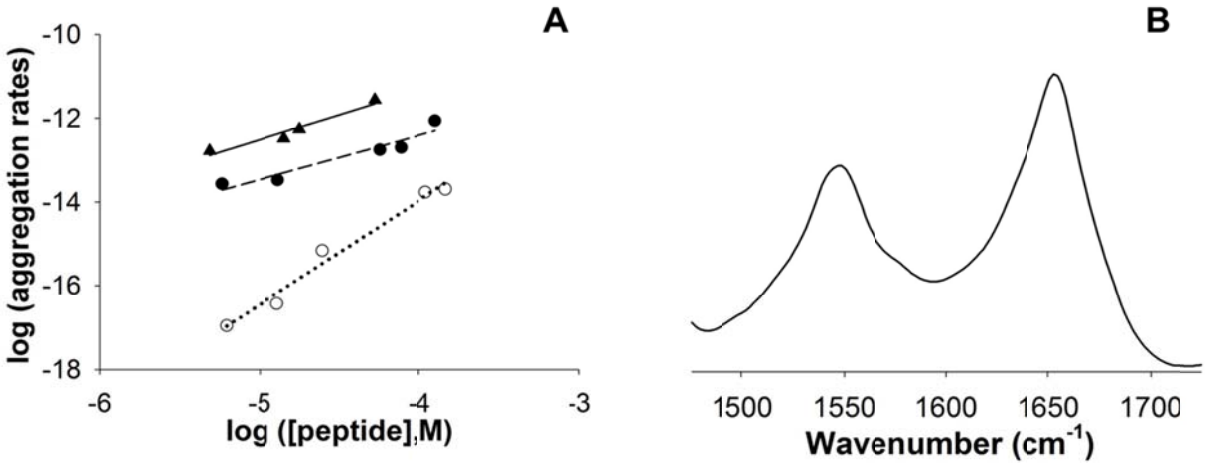

Figure 2-3: Role of htt^{NT} in initial aggregation. (A) polyQ containing htt fragments have a shallow concentration dependence of initial aggregation rates as shown for the htt$^{NT}Q_{30}P_6K_2$ (▲)and htt$^{NT}Q_{37}P_{10}K_2$ (●) peptides in comparison to the MF-$Q_{37}P_{10}K_2$ (○). (B) Oligomers formed by htt$^{NT}Q_3$ have a helical FTIR spectrum with an Amide I band at 1650cm^{-1} corresponding to α-helix. First reported in (31) and (136)

2.3.2 htt^{NT} drives oligomerization.

One of the major features of the aggregation mechanism of polyQ containing htt fragments that distinguishes it from that of simple polyQ peptides is the presence of oligomeric species "on-pathway". These oligomeric species are not only sites of stochastic nucleation of amyloid structure within the polyQ segment but are also believed to act as reservoirs of monomers that can fuel fibril elongation (100, 175). Earlier, a role for htt^{NT} in mediating oligomerization of polyQ containing htt fragments had been hypothesized based on the ability of this sequence to form oligomers with a characteristic helical FTIR spectrum (Fig 2-3.B).

Subsequently, we applied CD spectroscopy to study the thermodynamics of htt^{NT} mediated oligomerization. Thus, at low concentrations htt^{NT} displays a typical random-coil spectrum (Fig 2-4.A, —) consistent with previous proton NMR analysis (31).

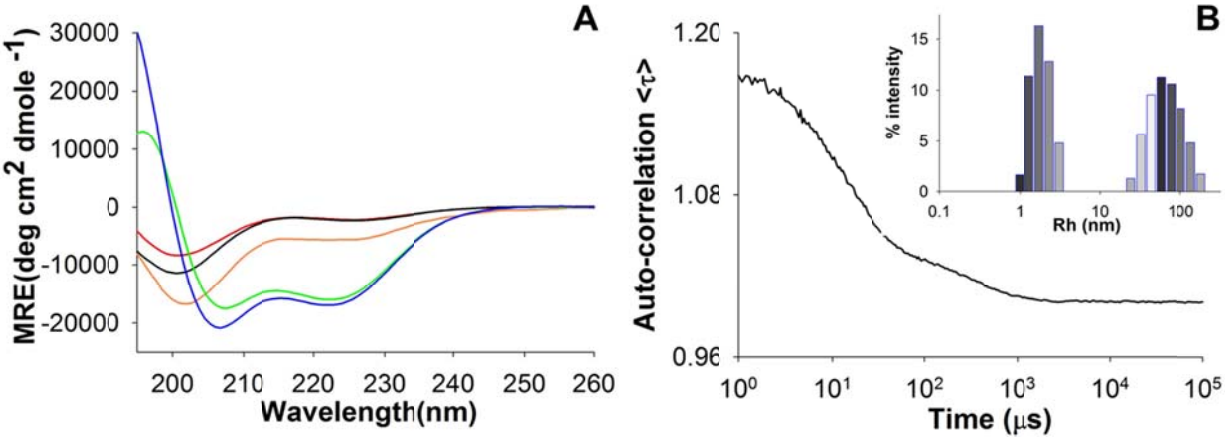

Figure 2-4: Concentration dependence of htt^{NT} oligomerization. (A) CD spectra of htt^{NT}Q peptide at different concentrations 1.3mM (—), 0.67mM(—), 0.3mM (—), .15mM (—) and 0.1mM (—) after dilution from a 0.7mM sample. (B) Dynamic light scattering experiments of 1.3mM sample (spun at 14,000 rpm for 2mins) indicates presence of at least two species with mean hydrodynamic radii of 2nm and 60nm respectively.

In contrast, at higher concentrations, the CD spectrum changes to a predominantly α-helical one (Fig 2-4.A,—) (100). This transition from a random-coil to α-helical spectrum is most likely due to a reversible association event since dilution of a high concentration sample, with a predominantly helical spectrum, (Fig 2-4,—) reverts the CD spectrum back to one that is predominantly random-coil (Fig 2-4,—). Furthermore, the DLS signatures and the morphologies of species populated at high concentrations are consistent with oligomers (Fig 2-4.B and 2-2. D). An analysis of the concentration dependence of helicity indicates that the mid-point of transition between random-coil to α-helix occurs at ~430μM (Chapter 5). Overall, these results are consistent with results from the analytical ultracentrifugation studies that indicate that monomeric htt^{NT} is in equilibrium with tetramers, octamers and higher-order oligomeric species (Fig 1-2.D) (100). The characterization of the biophysical driving forces of htt^{NT} mediated oligomerization form a crucial aspect of the work presented here (Chapters 5,6 and 7).

In addition to employing these low-resolution structural techniques to the study of htt^{NT} tetramers and other higher-order oligomers, we also tried characterizing these species by NMR spectroscopy. Unfortunately however, we did not observe any major difference in the 1-D NMR spectra of $htt^{NT}Q$ at high concentration and a similar htt^{NT} peptide at a lower concentration though the $htt^{NT}Q$ peptide did display substantial signal broadening consistent with the presence of oligomeric species at high concentrations (Fig 2-2.D and Fig 2-4.B). The only differences we observed were a shift in the methyl positions (from ~0.85ppm to ~0.71ppm) and a shift in the backbone amide HN peak of Leu4 (from 8.47ppm to 8.52ppm). The line broadening and the resonance shift exhibited by the spectrum of $htt^{NT}Q$ is probably indicative of exchange between monomer and oligomers.

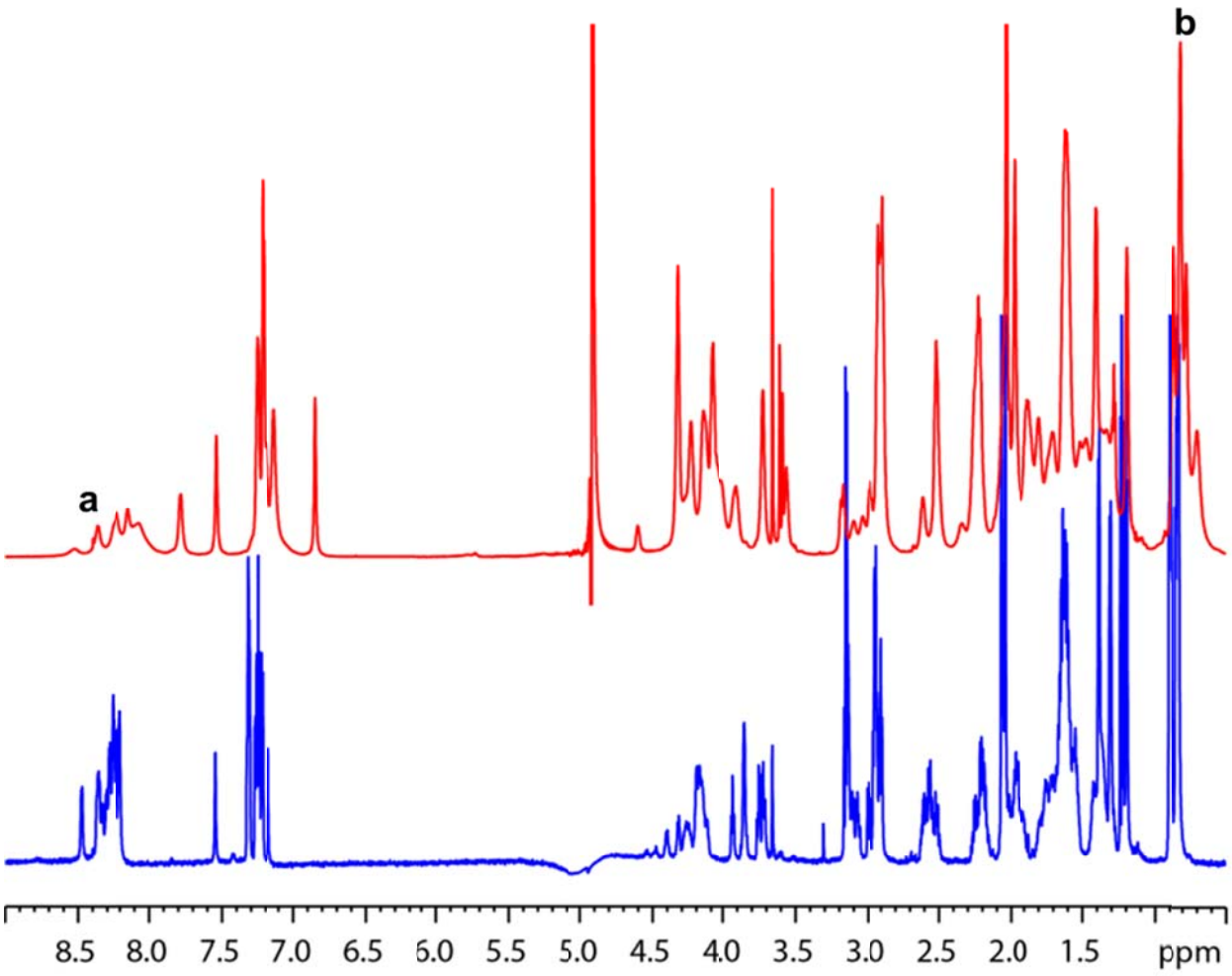

Figure 2-5: 1-D NMR spectra of htt^{NT}Q peptide at high concentration (1.35mM, —) and low concentration (—). Also marked are the methyl shifts (b) and the amide of Leu 4 (a). [Unpublished data of A.K.T, I.B and R.M]

2.3.3 Inhibition of aggregation of polyQ containing htt fragments.

Earlier work by A.K.T in the lab had identified a role for htt^{NT} in inhibiting the aggregation of polyQ containing htt fragments (176). Such htt^{NT} mediated inhibition is dose-dependent with optimal inhibition at an inhibitor: substrate ratio of 1:1 or greater (Fig 2-6.A).

There is also an initial drop in the htt^{NT} concentration during inhibition, suggesting that the inhibition by htt^{NT} is a consequence of interactions between htt^{NT} and substrate polyQ containing htt fragment (176)

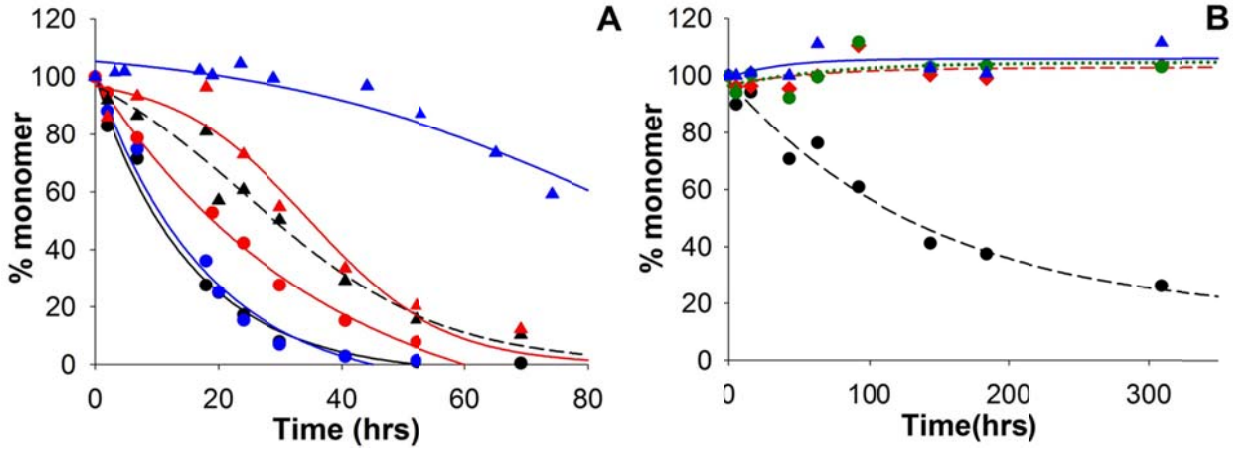

Figure 2-6: Inhibition of aggregation of polyQ containing htt fragment' by htt^{NT} and variants (I). Shown is the time-course of aggregation of the $htt^{NT}Q_{30}P_6K_2$ peptide by itself (●), or in the presence of different ratios of htt^{NT} to substrate- 0.05 (●), 0.2(●), 0.4 (▲), 0.9 (▲) and 1.6 (▲). (B) Aggregation of $htt^{NT}Q_{30}P_{10}K_2$ by itself (●) or in the presence of htt^{NT} (▲), D-htt^{NT} (♦) or RI-htt^{NT} (●). [Data from T.F, E.L, B.R and R.M]

We (R.M and E.L) thus set out to investigate the structural/mechanistic basis of htt^{NT} mediated inhibition of polyQ containing htt fragments. E.L started by assessing the abilities of variants of the htt^{NT} with altered stereo-specific properties. Thus, two peptides were designed, one with all residues in htt^{NT} in an all-D form (D-htt^{NT}) and the other a "retro-inverso" version which is basically the D-htt^{NT} peptide with sequence reversed (RI-htt^{NT}). Surprisingly, E.L found that both the D-htt^{NT} and RI-htt^{NT} peptides can inhibit the aggregation of the control $htt^{NT}Q_{30}P_{10}K_2$ peptide as effectively as the htt^{NT} peptide (Fig 2-6.B).

Name	*Sequence*	*Alpha Helical Content*[a]
$NT^{17}Q$	MATLEKLMKAFESLKSFQ	4.31
$NT^{17}Q$ #1	TMMKFQLLKSAEEKLFAS	0.69
$NT^{17}Q$ #2	MLSLKESAKMFFATKELQ	0.47
$NT^{17}Q$ #3	KQFTLEMAFLSKALSEMK	1.70
$NT^{17}Q$ #4	KLAFMLKQAELSSEKTFM	0.57
$NT^{17}Q$ #5	FAKFASEKKLESMTLMLQ	0.55
$NT^{17}Q$ #6	MLTFAEFKSMELKSQLAK	1.10
$NT^{17}Q$ #7	ASMFEAQLSKEKKMFTLL	1.58
$NT^{17}Q$ #8	ELLAKSEQAKSMLFTFMK	0.58
$NT^{17}Q$ #9	TKFSSFALLAQKEMLKME	1.29
$NT^{17}Q$ #10	ETLKMSMFLEAQFKKSAL	1.30
$NT^{17}Q$ #11	ASSQKKMKEMLAFFTLEL	2.84
$NT^{17}Q$ #12	MFSKMAKSLFLLAEKTQE	1.07
$NT^{17}Q$ #13	KLELKAASQMEFSFTMKL	0.39
$NT^{17}Q$ #14	KELKQELFFKASATLMMS	0.71
$NT^{17}Q$ #15	SAFMEKMLLLEKQFKAST	15.10

Table 2-1: Scrambled htt^{NT} sequences. Shown are the 15 scrambled sequences that were assessed for their abilities to inhibit aggregation of a $htt^{NT}Q_{30}P_6K_2$ peptide. Also shown are the theoretical helical propensities of these sequences. ***a.*** Helical contents were calculated using AGADIR program.

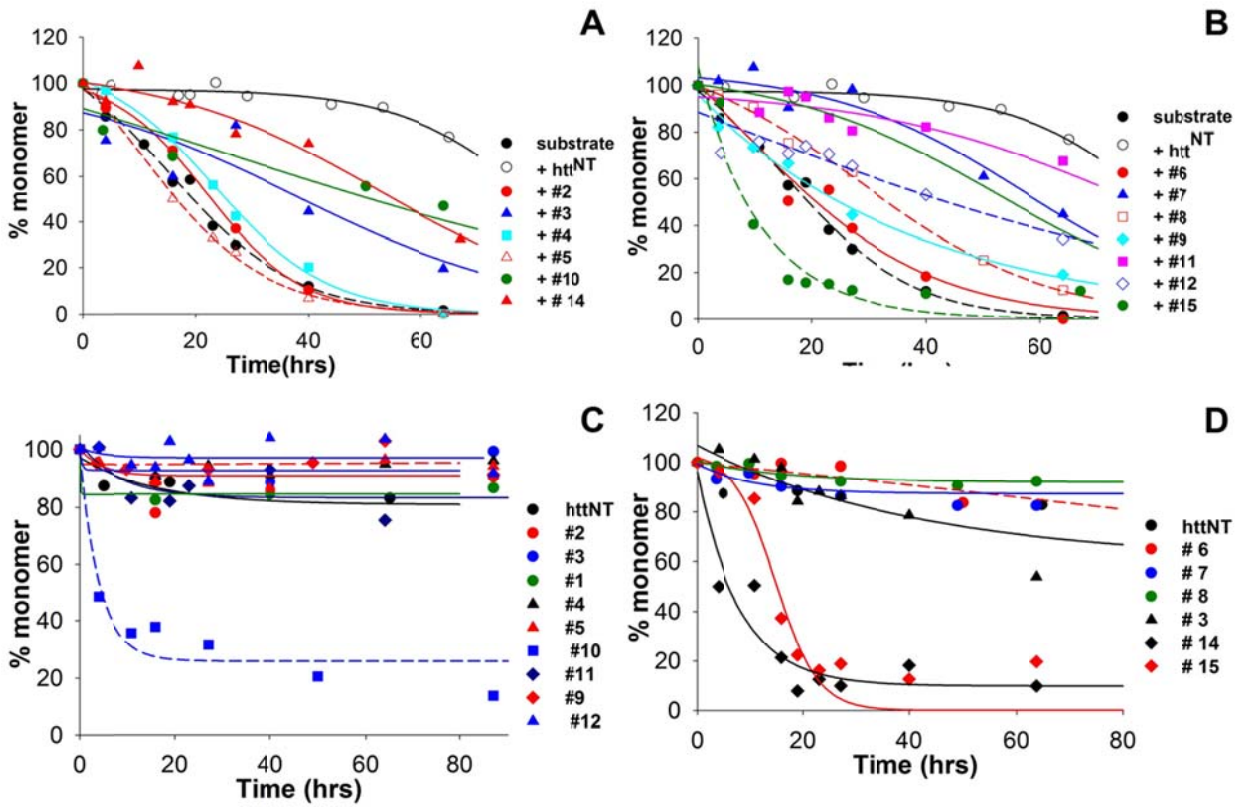

Figure 2-7: Inhibition of aggregation of polyQ containing htt fragment' by htt^{NT} and variants (II). (A-B) Aggregation of htt$^{NT}Q_{30}P_6K_2$ peptide by itself or in the presence of different scrambled htt^{NT} versions. (C-D) Aggregation of different scrambled htt^{NT} peptides by themselves.

One way to rationalize these results obtained from the D-htt^{NT} and the RI-htt^{NT} peptides is that htt^{NT} mediated inhibition lacks any specific structural specificity and might depend on the average properties of the sequence such as hydrophobicity or net-charge. In order to test this hypothesis, we decided to look at the inhibitory activities of 15 different scrambled versions of htt^{NT} (Table 2-1). Overall, we observed a wide-range of inhibitory activities ranging from no inhibition to inhibition as effective as the WT htt^{NT} sequence suggesting that htt^{NT} mediated inhibition is sequence-specific (Fig 2-7. A,B). Also, some of these scrambled peptides aggregated by themselves at low concentrations (Fig 2-7.C, D) adding yet another parameter (in

addition to inhibitory potential) to the classification of these scrambled sequences (Chapter 4). Overall, the results from these studies with scrambled variants of htt^{NT} indicate that average sequence properties (e.g. hydrophobicity/net-charge which remain unchanged in these peptides) cannot explain htt^{NT} mediated inhibition of polyQ containing htt fragments. One hypothesis that can explain the results of our studies, with scrambled inhibitors and from the D-htt^{NT} and RI-htt^{NT} inhibitors, is that inhibition proceeds through the formation of oligomers containing helical htt^{NT} segments that interact through an optimal arrangement of hydrophobic and/or charged residues. The rationale for this hypothesis stems from the ability of htt^{NT} (as well as D-htt^{NT} and RI-htt^{NT}) peptides to form helical oligomers (176).

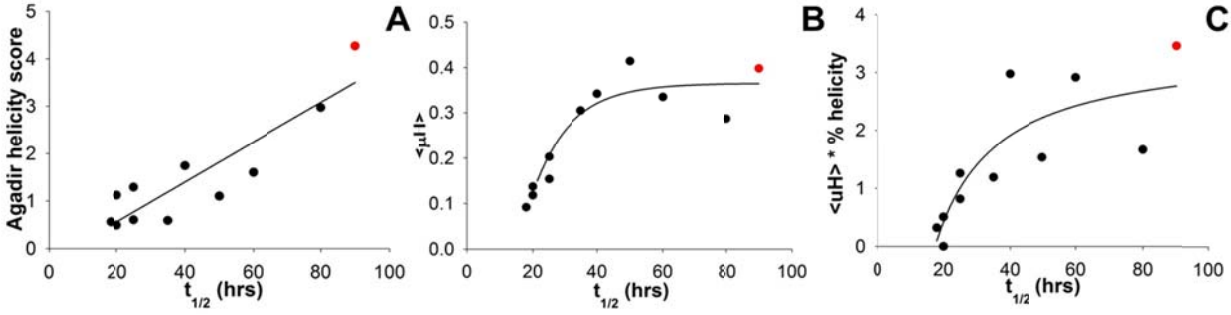

Figure 2-8: Role of amphipathic helix formation in htt^{NT} mediated inhibition. (A) Theoretical helical propensities of ten chosen scrambled sequences plotted against corresponding $t_{1/2}$ of inhibition shows a strong correlation (R^2= 0.8). (B) Hydrophobic moments of scrambled sequences plotted against $t_{1/2}$ (R^2= 0.9). (C) Normalized hydrophobic moments of scrambled sequences plotted against $t_{1/2}$ of inhibition (R^2=0.7). htt^{NT} is shown in red in all plots.

In order to test this hypothesis, we started by calculating the theoretical helical propensities of the ten scrambled peptides which did not aggregate at low concentrations to investigate any correlation between inhibitory activity ($t_{1/2}$ of aggregation in presence of inhibitor) and theoretical helical propensity (Fig 2-8.A). The presence of a strong correlation

(R^2=0.8) between these two parameters implicates a potential role of helicity in htt^{NT} mediated inhibition.

The adoption of an α-helical conformation by htt^{NT} also confers a certain degree of amphipathicity that stems from an optimal arrangement of polar and non-polar residues. Theoretically, this amphipathicity can be computed for a helical sequence by computing its hydrophobic moment (<μH>) (177, 178). Interestingly, a plot of <μH> versus the $t_{1/2}$ of inhibition (Fig 2-8.B) gave a robust correlation of (R^2=0.9) though this correlation drops to a R^2 of 0.7 upon normalizing the <μH> values by the actual helical propensities of these peptides, calculated by CD spectroscopy (Fig 2-8.C). It is possible that this drop in correlation is because of the experimental uncertainties in predicting helical propensities of disordered peptides and/or because of the inaccuracy of helical propensities in the monomeric ensemble in predicting inhibitory potential. Also worth noting is that in all these analyses, the htt^{NT} consistently ranks as the most potent sequence both in terms of amphipathic helix potential as well as inhibitory activity (Fig 2-8,●).

Overall, these results in conjunction with our prior results from D-htt^{NT} and the RI-htt^{NT}, the propensity of the htt^{NT} sequences to interact *in trans* through helical interactions (80) and the structural details of htt^{NT} oligomers (Fig 2-3) (100) suggest that amphipathic helicity within htt^{NT} is crucial to inhibition. Since both aggregation and inhibition are hypothesized to proceed through the formation of oligomers held together by interactions within htt^{NT}, it can be argued that the formation of amphipathic helicity is crucial to the aggregation of polyQ containing htt fragments, a hypothesis that is addressed in greater detail in Chapters 4 and 5.

2.4 THESIS FOCUS.

These preliminary results along with other studies from our lab and those of others have added considerably to our overall understanding of the aggregation pathway of polyQ containing htt fragments, especially the role that htt^{NT} plays in orchestrating different stages of this pathway. However, several aspects of htt^{NT}'s role in mediating the aggregation of polyQ containing htt fragments still remain unascertained. Over the next few chapters, we present our efforts in addressing some of these questions:

a. Role of helicity within htt^{NT} in polyQ containing htt fragment aggregation.

htt^{NT}'s propensity to adopt a helical conformation has received substantial attention in the field. While this sequence is essentially disordered (with some hints of helical structure) in the monomeric state (31, 100), there is a definite role for helicity within oligomers and the final fibrils (100, 136). Our studies assessing the inhibitory potential of htt^{NT} variants identified a role for amphipathic helicity in inhibition. Since both inhibition and aggregation proceed through oligomers that are mediated by htt^{NT} interactions, we hypothesize that amphipathic helicity in htt^{NT} is also crucial for the aggregation of polyQ containing htt fragments. We test this idea in greater detail by using scrambled versions of htt^{NT} in polyQ containing htt fragments (Chapter 4) and also rationally designed mutations within htt^{NT} (Chapter 5).

b. Effect of polyQ expansion on htt^{NT} mediated oligomerization of polyQ containing htt fragments:

PolyQ expansion is the fundamental molecular trigger of HD pathology. Thus, assessing the effect of polyQ expansion on the aggregation of polyQ containing htt fragments is crucial to

our understanding of the role that protein aggregation plays in HD. Within this context, it is interesting to explore the inter-dependence (if any) between polyQ expansion and the role of htt^{NT} in mediating aggregation. There have been some suggestions about the role of the polyQ sequence in modulating the conformation of htt^{NT} in the monomeric ensemble (31) and/or accelerating the subsequent oligomerization stage of the aggregation pathway. We explore these hypotheses in further detail in Chapter 7 by looking at the effect of polyQ expansion on the monomeric conformational ensemble as well as the energetics of oligomerization of polyQ containing htt fragments.

c. Implications of cellular PTMs on htt^{NT} mediated aggregation of polyQ containing htt fragments.

In addition to its role in driving the aggregation of polyQ containing htt fragments, the htt^{NT} sequence has also been implicated in several cellular processes. It is also the site of several post-translational modifications (PTMs) that modulate its biological activity. While PTMs have traditionally been examined based on their effects on cellular processes, we hypothesize that PTMs can affect the htt^{NT} mediated aggregation of polyQ containing htt fragments by altering the biophysical properties of the htt^{NT} sequence. Thus, we assessed the effects of most of the reported PTM's (17) of htt^{NT} on the aggregation of poly containing htt fragments (Chapter 5). Also, one of these mutations, the phosphorylation of the two serine residues was studied in great detail in terms of its effects on different stages of aggregation in the light of the crucial role it plays in HD pathology (16) (Chapter 6).

d. Structural insights into putative htt^{NT} tetramer.

htt^{NT} mediated oligomerization proceeds through the formation of a tetrameric state. Given the crucial role of this putative tetramer to aggregation, we have used our experimental data (Chapter 5) to guide modeling efforts based on protein-protein docking to obtain a putative structure of the htt^{NT} tetramer.

3.0 EXPERIMENTAL METHODS

3.1 PREPARATION OF MATERIAL.

3.1.1 Peptide Synthesis and Purification.

All of the peptides used in these studies were synthesized chemically by solid-phase synthesis and obtained in crude form. In most cases, the peptides were obtained from the Keck Biotechnology Center (http://medicine.yale.edu/keck/ssps/index.aspx) in synthesis scales of 25-100μM. In certain cases (sequences smaller than 20 residues in length), the peptides were obtained from Genscript Inc or from Sigma-Aldrich (PEPscreen). All crude peptides were stored at -80°C for future purification.

Crude peptides were purified using a reverse phase Agilent Zorbax C3 column as follows. Crude peptides were dissolved in 100% formic acid (Sigma) for ~2-3 minutes. Prior to injection into the reverse phase column the formic acid was diluted to ~20%. Peptides were purified in a Biorad Biologic Dual Flow system. The buffer systems used were water (Fisher Scientific, HPLC grade) + 0.05% TFA (Sigma) i.e solvent A and acetonitrile (Fisher Scientific, HPLC grade) + 0.05% TFA (Sigma) i.e solvent B. Each purification run was typically preceded by a couple of "blank runs" where 20% formic acid was injected, in order to ensure that there was no residual peptide bound to the column. During the purification run, the solvents were run

at a flow rate of 4ml/min with a gradient system that was specific to the peptide type. Fractions were collected using a Biorad fraction collector with a collection volume between 0.5-0.8 ml. Based on the absorbance signals at 218nm, fractions corresponding to the major peak were identified and their masses determined by mass spectrometry (see below). Pure fractions (including fractions with 1-2 glutamine deletions) were then pooled, lyophilized overnight and stored at either -20°C or -80°C for future use.

3.1.2 Disaggregation protocol.

In order to ensure that the study of aggregation properties was not compromised by the presence of pre-formed aggregates, each peptide was subjected to a disaggregation protocol to ensure that the starting material for experimental studies is monomeric. This protocol consisted of dissolving pure lyophilized peptide in a 1:1 mixture of TFA and HFIP at a peptide concentration of ~100µg/ml in glass scintillation vials for a period of 12-15 hours (overnight). At the end of this period, the solution was distributed across other glass vials (~ 5-10% of volume of vials) and the solvents were evaporated under a stream of nitrogen with the help of a commercially available manifold (Organomation N-EVAP evaporator, Fisher Scientific) leaving behind a peptide film on the walls of the vials. This film is then dissolved in acidic (pH 3) water (0.01% TFA) and centrifuged at 100,000 rpm (416640 x g) in an ultracentrifuge (Optima TLX, Beckman) for 2-3 hours. Subsequently, 60% of the supernatant is removed and used as stock solution for use in experiments.

In certain experiments with htt^{NT} and its mutants (for concentration dependence CD studies), in order to recover more peptide, a variant of the above protocol was used. Instead of dissolving in TFA/HFIP overnight, the lyophilized peptides were directly dissolved in water +

0.01% TFA (pH 3) and then centrifuged at 100,000 rpm for 2-3 hours (as above). No major changes in the CD spectra were observed with this variation of the protocol.

3.1.3 Determination of peptide concentrations.

The determination of peptide concentrations were done by measuring the peak area on a RP-HPLC system. Any particular sample was first injected into the Agilent C8 column using the in-built auto-sampler. Elution was monitored by following the absorbance signals through the A_{215nm} detector channel and area under the curve calculated using in-built analysis tools for any particular peptide. A standard slope was then used for each peptide to determine the amount of peptide injected and by extension, the concentration of peptide. Since different peptides can have different extinction coefficients at 215nm, the slope for each peptide was determined separately. This was done by first calculating the extinction coefficient for each peptide using the method of Kuipers and Gruppen. The calculated slope was then used to determine the concentrations of 4-5 calibrating samples using an absorbance spectrophotometer. Aliquots of these calibrated samples were also simultaneously injected into the RP-HPLC to determine the slope (peak area vs amount of peptide injected).

3.1.4 Isolation and quantification of aggregates.

Certain experiments require the use of isolated aggregates. In such cases, aggregates were isolated by centrifugation at 14,000 rpm (20,817 x g) for 45 mins in eppendorf tubes. The supernatant was then separated and the pellet washed with appropriate buffer and centrifuged under similar conditions to remove any residual monomer. This step was repeated 1-2 times. The

pellet from the last wash was then re-dissolved in an appropriate buffer. In order to determine the concentrations of the aggregates used, an aliquot was taken and re-dissolved in formic acid (typically ~90% formic acid), incubated for 1-2 hours and then injected into RP-HPLC for concentration determination. In addition, in certain cases the concentrations of the aggregates were calculated by subtracting the monomer left at any point in the aggregation reaction from the starting concentration

3.1.5 Mass spectrometric determination of peptide masses.

An Agilent electrospray 1100 mass spectrometer was used to determine the masses of the peptides. Any particular sample was first run through the Agilent C8 reverse phase column. The masses were determined by using the in-built analysis module.

3.2 EXPERIMENTAL ANALYSIS OF AGGREGATION.

3.2.1 Sedimentation assay.

The sedimentation assay was the primary method used to assess the aggregation propensities of the peptides studied in this work. The method comprised of taking aliquots from an ongoing reaction at any particular time and centrifuging it at 14,000 rpm on a bench top centrifuge (Eppendorf) for 45 minutes and then carefully isolating 50-60% of the supernatant. The concentration of peptide in the supernatant is then determined by injection into the RP-HPLC (as described above).

3.2.2 ThioflavinT binding.

A characteristic feature of amyloid aggregates is their ability to bind ThioflavinT, a dye, which universally binds amyloid structures, binding that is poorly understood structurally. Yet, this ability can be utilized to follow amyloid formation and in conjunction with the sedimentation assay provide additional information on the aggregation properties. For example, the detection of aggregates through the sedimentation assay which at the same time do not bind ThoiflavinT can point to the presence of oligomers.

To quantify Thioflavin T binding, an aliquot (260ul) of an ongoing reaction was taken at any particular time, mixed with an excess of ThioflavinT (12ul of 2.5mM stock) and the fluorescence measured using a Jobin Spectrofluorimeter. The instrumental parameters are as follows (λexc = 445 nm; excitation slit width = 2nm ; λ_{emm} = 489nm ; slit width = 2nm).

The ThioflavinT binding can be quantified were compared in two –different ways. In one method, the ThioflavinT binding per ug was determined for different kinds of aggregates in order to compare different aggregate. In the second method, the ThioflavinT binding can be converted to a "% aggregation" time-course, by equating a final ThioflavinT signal to equivalent % aggregation value based on the sedimentation assay and then re-calibrating early time ThioflavinT binding signals as % aggregation values.

3.2.3 Nucleation kinetics.

The concentration dependence of early phase of aggregation has historically been used in the lab as a probe to distinguish between the nucleated growth and oligomer-mediated aggregation mechanisms. In this study, such analysis was employed to ascertain the effect of mutations

within the htt^{NT} sequence on the aggregation mechanism of htt NTF peptides. The analysis hinges on two aspects of aggregation: (a) the linear dependence of aggregation on t^2 (time in secs squared) which gives the "nucleation rates" and (b) the concentration dependence of the nucleation rates calculated.

As described in detail elsewhere, the integrated equation describing the earlier phases of aggregation kinetics is given by:

$$\Delta = {}^{1}/_{2} JJ^{*}C^{*}t^{2}$$

where Δ is the concentration of monomers that have gone into polymers,J is the elongation rate of polymers, J* is the elongation rate of the nucleus, C* the concentration of the nucleus and t is the time.

Making the substitutions $J=k_{+}C$, $J^{*}= k_{+}{}^{*}C^{*}$, $C^{*}= K_{n*}C^{n*}$, where k_{+} is the forward elongation rate constant of the monomers, c is the bulk concentration of monomers, $k_{+}{}^{*}$ is the elongation rate constant of the nucleus , C^{*} is the concentration of the nucleus, n* is the number of monomers per nucleus, and K_{n*} is the equilibrium constant of the monomer-nucleus equilibrium, the equation above reduces to

$$\Delta = \frac{1}{2} k_{+}{}^{2} K_{n*}\, c^{(n*+2)} t^{2}$$

Thus a plot of Δ vs t^2 gives a slope

$$Slope = {}^{1}/_{2}\; k_{+}{}^{2}\, \mathrm{K}_{n*}\, c^{(n*+2)}$$

for any particular starting concentration of monomers under the assumption that the elongation rate of the aggregates (k_{+}) and the nucleus (k_{+}*) are identical. Since $C_{sol} = Co - \Delta$ where C_{sol} is the concentration of soluble monomer and C_o is the starting concentration, it follows that a plot of Csol vs t^2 gives the same slope as above.

Also,

$$\log(slope) = (n^* + 2)\log c + \log(\frac{1}{2} {k_+}^2 K_{n*})$$

it follows that a plot of log (slope) vs log c yields a slope that allows the determination of the number of monomers in the nucleus, n*. This values of n^* thus calculated allows for the comparison of the mechanism underlying the early stages of aggregation across different peptides or aggregation conditions.

Thus, aggregation reactions of different peptides were monitored by the sedimentation assay as described and the drop in concentration monitored over time. The concentration vs t^2 from the initial part of reaction (20%-35%) was then fit to the equation above to get the slope. The logarithms of the slope thus calculated at different starting concentrations of aggregation were then plotted against the logarithm of the corresponding starting concentration to get the slope and thus the value of n*.

3.2.4 Circular dichroism Spectroscopy.

Comparison of monomers: Circular dichroism spectroscopy was used to determine the secondary structure of different peptides used in this study. Freshly disaggregated peptides (above) were typically made in 10mM Tris buffer (pH 7.4). Far-UV CD spectra were recorded using a Jasco J-810 spectropolarimeter. Spectra were collected in either a 0.1mm (high concentrations) or 1mm cuvette with a resolution of either 0.5nm or 1nm using at a spectral rate of 100nm min^{-1}. Spectra were collected and averaged over four scans and corrected for the appropriate buffer. In certain cases, further secondary structure de-convolution was performed using the CONTIN program in

the CDPro analysis package (http://lamar.colostate.edu/~sreeram/CDPro) using the SP37 basis set (ibasis 5).

Monitoring aggregate formation: Aggregate formation was monitored by making freshly disaggregated samples in 10mM PBS (pH 7.4) and collecting the spectra at 37°C at defined intervals. Spectra were collected at 1 nm resolution at a rate of 100nm min^{-1} and corrected for the buffer. Secondary structure de-convolution was performed as described above.

3.2.5 Dynamic Light Scattering.

All dynamic light scattering measurements (DLS) were done using the DynaPro plate reader (Wyatt technology) equipped with a temperature control. The DLS was typically used to follow the time-course of aggregation to detect any concomitant oligomer formation. All samples were thus filtered with a 20nm syringe filter at the start of the reaction. Then at specific time-intervals, a given aliquot of the reaction (~75µl) was transferred into a fresh well of a 384-well microplate and the scattering data was recorded. Typically, the measurements were performed at 37°C with an acquisition time of 5secs/scan. In each of the experiments, the most representative of all collected scans were selected.

3.2.6 FTIR spectroscopy.

FTIR of the aggregates (or aggregation intermediates) were performed at a concentration of ~10mg ml^{-1}. Thus, for shorter polyglutamine repeat length peptides that do not aggregate appreciably, the starting concentration was typically in the 1.5mM-2mM range so that enough

aggregate could be isolated at the end of the reaction. Aggregates were isolated by centrifugation at 20817 x g , washed twice with PBS to remove any residual TFA and then re-dissolved in 4µl PBS to get a highly concentrated sludge. Spectra were acquired by then placing this sludge between two polished CaF_2 windows on an ABB Bomem FTIR instrument by using the in-built data acquisition module, BioCell (BioTools, Inc.). The data was acquired by averaging over 400 scans, at a scan rate of 4 cm^{-1}, at room temperature. The data was also corrected for residual buffer absorption.

3.2.7 Tryptophan fluorescence of aggregates.

In order to get some structural insights into the conformation of the htt^{NT} sequence, some of the eptides were synthesized with a F17W mutation. As shown earlier, this mutation does not appreciably alter the aggregation (neither kinetics nor the aggregation mechanism) of polyQ containing htt fragments (31) . Aggregates were isolated at different time intervals as described above and re-dissolved in PBS. Spectra were recorded in a quartz cuvette by exciting the sample at 280nm and monitoring the fluorescence between 290nm and 550nm on a FluoroLog spectrofluorometer (Horiba). The wavelength corresponding to the maximal intensity was then recorded ($\lambda_{max}{}^{Fluor}$).

3.2.8 FRET studies of peptide conformations.

In this study, we used ratiometric FRET to determine the distance between the donor and acceptor fluorophores as a proxy for peptide conformations. The donor –acceptor pair used in the study was tryptophan (incorporated as a F17W mutation) and EDANS.

All fluorescent measurements are performed with a Fluorolog from Horiba Scientific. FRET efficiencies are calculated based on a ratio-metric approach on the basis of measured donor (I_D) and acceptor (I_A) fluorescence intensities from the protein tagged with a pair of FRET fluorophores. In the traditional method of FRET efficiency measurement, one requires the fluorescence of the donor molecule in the presence and absence of the acceptor as well as an accurate determination of concentration.

However, in ratiometric FRET method, one only requires the fluorescence of the donor and acceptor from the same sample(s). The major advantage of this method is the eliminate of error due to the measurement of concentration. Additionally, by calculating the quantum yields of the donor and acceptor in the protein context, this method allows one to distinguish between two possible contributions to measured fluorescence and hence calculated FRET distances: *a.* the actual distance, and *b.* the quantum yields of the fluorophores and how they may be affected by local structure within the protein. This is particularly relevant in the context of polyQ containing htt fragments where we have observed changes in the quantum yields a tryptophan at a particular position in htt^{NT} depending on other sequence changes (B. Sahoo and R. Wetzel, unpublished). In fact, in the ratiometric FRET method, it is required that one knows the quantum yields of the fluorophores within the molecular context in which they are placed for the measurement (see below).

The ratiometric FRET method has been used previously in many applications where the traditional method may not be feasible. The FRET efficiency is given by

$$E_{FRET} = \frac{I_A}{I_A + \gamma I_D}$$

where I_A and I_D are the intensities at the fluorescence-maximum of acceptor and donor respectively.

Where γ is a correction factor that depends on the quantum yields (Φ) of the FRET pair and their detection efficiencies (η).

$$\gamma = \frac{\eta_A \phi_A}{\eta_D \phi_D}$$

Since we use the same spectrofluorometer to measure the fluorescence of both donor and acceptor, we assume the detection efficiency is same for both donor and acceptor. So the above equation can be modified to

$$\gamma = \frac{\phi_A}{\phi_D}$$

We determine the quantum yields of both the donor and acceptor using the comparative method described elsewhere (reference). The quantum yield of an unknown fluorophore is given by

$$\phi = \phi_R \left(\frac{m}{m_R}\right)\left(\frac{n^2}{n_R^2}\right)$$

Where *m* is the slope of the line determined from the plot of the absorbance against the integrated fluorescence intensities, *R* is the reference fluorophore with known quantum yield, and *n* is the refractive index of the solvents. Since the samples are made in same buffer as of the reference, the refractive indices are same for both. So Equation 3 reduces to

$$\phi = \phi_R \left(\frac{m}{m_R}\right)$$

We have used tryptophan and EDANS as the FRET pair for all our studies. We first determined the quantum yields of tryptophan in the $htt^{NT}Q_{37}P_{10}K_2$(F17W) and $htt^{NT}Q_{37}P_{10}K_2$(F17W, S13D,S16D) as described in Equation 3a above and using free tryptophan as the standard. There was no substantial difference in the quantum yields of the Trp residues in these two peptides. Similarly, the quantum yields of EDANS was calculated for the $htt^{NT}Q_{37}P_{10}K_2$(F17W) peptide using free EDANS as the standard. The quantum yields of both

free tryptophan and free EDANS have been determined elsewhere. Since the quantum yield of EDANS does not change with the protein context in htt peptides (B.Sahoo and R.W, unpublished), we used the quantum yield of the EDANS calculated for the $htt^{NT}Q_{37}P_{10}K_2$(F17W) peptide for the calculations with the S13D/S16D mutant. The quantum-yields thus computed were then used to calculate the correction factor (Eq 2a) which were almost identical for both the $htt^{NT}Q_{37}P_{10}K_2$(F17W) and $htt^{NT}Q_{37}P_{10}K_2$(F17W/ S13D/S16D) peptides (4.54 and 4.39 respectively).

In order to compute E_{FRET}, monomers of the $htt^{NT}Q^{37}P_{10}K_2$(¥/F17W) and $htt^{NT}Q_{37}P_{10}K_2$(¥/F17W/S13D/S16D) peptides were prepared using the disaggregation procedure described in phosphate buffered saline solution at concentrations of ~ 30μM. Emission spectra were collected between 290nm-750nm after excitation of sample at 280nm with excitation and emission slit-widths of 1nm and 5nm respectively. The intensities of the donor and acceptor at the respective maxima were then plugged into Eq 1 to compute E_{FRET}. The E_{FRET} values were then used to compute the donor-acceptor distance by using the equation

$$E_{FRET} = \frac{1}{1 + (\frac{r}{Ro})^6}$$

where Ro is the Forster's radius of the EDANS –Trp pair ($22A^0$).

3.2.9 Aggregate morphologies by electron microscopy.

Aggregate morphologies at different stages of aggregation were studied by transmission electron microscopy. 5µl of an on-going reaction of any particular peptide of interest was taken at defined time-intervals and transferred onto a freshly glow-charged carbon-coated grid, adsorbed for 3-4 minutes, washed twice with 5µl of deionized water by blotting after which 2µl of 1% (w/v) uranyl acetate was added. In order for optimal staining, the uranyl acetate was removed by blotting within 2-3 secs and the grid was washed with deionized water again. The grids thus prepared were either imaged immediately or were stored for visualization later. Grids were imaged on a a Tecnai T12 microscope (FEI) operating at 120kV and a magnification of 30,000. The microscope was equipped with an Ultrascan 1000 CCD camera (Gatan) with a post-column magnification of 1.4X.

3.2.10 Trypsin sensitivity of aggregates.

The htt^{NT} sequence has three trypsin cleavage sites at K6, K9 and K15. Thus the susceptibility of different aggregation intermediates (or mutants) to cleavage by trypsin can offer some insights into the conformation (and in certain cases dynamics) of the htt^{NT} domain in such conditions. For trypsin analysis, aggregates at defined time-intervals were isolated and quantified as described above. These aggregates were then incubated overnight at a ~25:1 ratio of peptide: trypsin (TRSEQZ, Worthington Biochem) in 50mM Tris pH 7.0 at 37°C. The pellet fraction was then isolated by centrifugation, washed with 1X Tris, dissolved in formic acid and then run on an Agilent 1100 LC-MS system. The A_{215nm} signal was integrated for the cleaved and uncleaved peaks and the fractional cleavage was obtained by normalizing the area of the cleaved peak to the

total area. The masses of the cleaved fragments were noted and the cut-sites were determined by using the Protein Prospector tool online (http://prospector.ucsf.edu/prospector/mshome.htm).

3.2.11 Accessibility of polyQ epitope to MW1 antibody.

Antibody binding is usually used qualitatively for the detection of presence. However, within caveats, accessibility of epitopes to antibody can yield conformational information (albeit qualitative) about aggregates. In this study, the accessibility of the polyQ segment to the MW1 antibody in the context of different mutations and/or aggregation states was probed.

Aggregates were isolated at defined time-intervals and quantified as above. A specific amount of aggregate (typically between 1µg – 3µg) was transferred onto a nitro-cellulose membrane with the help of the Bio-Dot apparatus (Biorad. Inc.). The blot was then blocked with TBST (10mM Tris-HCl, 0.1%v/v Tween-20, 150mM NaCl, 0.05% azide) containing 2.5% bovine serum albumin (Sigma) for 4-5 hours, washed with TBST thrice and transferred to a solution containing 30nM of the MW1 antibody dissolved in TBST and incubated at room – temperature (with gentle shaking) overnight. Subsequently, the membrane was washed with TBST 4-5 times before being incubated with a 1:5000 dilution of a peroxidase conjugate of an anti-mouse IgG (Sigma, A4416), made in TBS, for 2-3 hours. At the end of this incubation, the blot was washed 4-5 times with TBS and visualized using an enhanced chemiluminescence solution (Thermo Scientific SuperSignal West Pico Chemiluminescent Substrate). For qualitative comparisons, every time, the polyQ accessibility of a matched concentration of the corresponding monomeric peptide was also analyzed.

3.2.12 Determination of critical concentrations.

The critical concentration (C_r) of aggregate formation is an indicator of aggregate stability. An aggregation reaction of the peptide of interest was monitored until there was no change in the concentration of monomer. This monomer concentration at the end of the forward aggregation reaction was measured to obtain the critical concentration. In some cases, we also looked at the reversibility of aggregate formation by taking an aliquot of the aggregation reaction at a later time (when the monomer concentration is at equilibrium) and diluting into 1X PBS (0.05% azide) such that the total peptide concentration was well-above the C_r (as measured from the forward reaction). This was then incubated at 37°C and the monomer concentration monitored by sedimentation assay as described above until equilibrium. The final C_r for any particular peptide was determined by taking the average of the values obtained from the forward and reverse reactions.

3.2.13 DEER experiments.

All DEER experiments were performed on a Bruker EleXsys CW/FT X-band ESR spectrometer using the Bruker MD5 resonator. Temperatures were maintained using an Oxford ITC 503 temperature controller and CF935 dynamic continuous flow cryostat. Liquid helium was used to maintain temperatures at 40 K. The samples were flash frozen by plunging the capillaries into liquid nitrogen cooled propane.

The experiments were performed using an observer $\pi/2$ and π pulse of 16 and 32 ns respectively, and a pumping pulse of 12 ns. The pump pulse was located at the maximum of the

nitroxide spectrum with the observer pulse applied at a frequency ~70 MHz higher. The pump pulse began 40 ns before the echo so the zero time could accurately be determined.

The experimental data was analyzed using DeerAnalysis2009 in which the background (intermolecular signal) was subtracted by fitting to a 3D-homogeneous background model. The background subtracted data was then fit using a single Gaussian distribution.

3.3 DATA ANALYSIS.

3.3.1 Curve Fitting.

All curve fitting was done by using the fitting functions provided by the Sigma Plot 10.0 software. The choice of the fitting equation was determined based on an understanding of aggregation phenomenon as described below.

All aggregation kinetics of single-peptide systems (i.e aggregation reactions where only one peptide was present) were fit with a standard three-exponential decay equation given by :

$$y = yo + a * e^{-bx}$$

$$where\ x = time\ in\ hours\ ; y = \%\ monomer\ data$$

In the case of inhibition of polyQ containing htt fragments by htt^{NT} or related analogs, the aggregation profiles of the substrate was described by a sigmoidal three-parameter equation

$$f = \frac{a}{1 + e^{\frac{-(x-xo)}{b}}}$$

The choice of the sigmoidal function was dictated by our understanding of htt^{NT} inhibition of polyQ containing htt fragment aggregation which proceeds through a lag-phase as

described elsewhere in this thesis. The aggregation of the inhibitor was typically described by an exponential decay function as described above. Similarly, inhibition by the elongation inhibitor was modeled using the exponential decay function.

3.3.2 FTIR deconvolution.

FTIR spectra were collected as described above. The second-derivative of the spectra were then obtained by using the inbuilt PROTA software and the minima used to determine the spectral components. In certain cases, the relative preponderances of different secondary structural elements were determined by using the PeakFit program.

3.4 COMPUTATIONAL METHODS.

3.4.1 Peptide modeling.

The initial structures for molecular dynamics simulations and/or molecular docking where modeled using the Sybyl7.3 program. In the case of molecular dynamics simulations, the starting sequence was modeled as a random coil (unless otherwise mentioned).

3.4.2 Theoretical structural calculations on peptides.

Helical propensities of peptides were determined by using the AGADIR (http://agadir.crg.es/agadir.jsp) software that estimates helical propensities based on helix-coil transition theory (179-181). Calculations were performed at pH 7.4, 298K and 0.1M ionic strength. Hydrophobic moments (182) of different scrambled sequences in Chapter 2 were determined using the HeliQuest online server (http://heliquest.ipmc.cnrs.fr/) with a window-size of 18.

3.4.3 Molecular Dynamics Simulation.

All MD simulations were performed using the GROMACS software package. Starting conformations were either modeled using the Sybyl7.3 package or from existing crystal structures. Simulations were done using the GROMOS 96 force field with the SPC water model to mimic solvent. Excess charges were balanced using counter-ions. Post-solvation, the protein was energy minimized using the steepest descent algorithm with parameters as described below. The energy-minimized structure was then restrained and equilibrated in water for 50ps before setting up the simulation run was setup subsequently for a defined time length. The details of these runs are described below. Analysis of the trajectories was performed by using the in-built functions in GROMACS. Secondary structure evolution over time was done using the DSSP executable and the inbuilt do_dssp function. A detailed tutorial of the simulation setup and parameters can be accessed at http://www-personal.umich.edu/~amadi/fwspidr_tutor.pdf.

3.4.4 Modeling tetramer structure.

The workflow adopted in the modeling of tetramer structure is shown in Figure 3-1. Briefly, the starting helical conformation of htt^{NT} was obtained from a previously reported crystal structure (80). This was then supplied to the online ClusPro server (http://nrc.bu.edu/cluster/cluspro_v1.cgi) (183, 184) to generate tetramer models. Briefly, chain A (residues 371-387) of the pdb structure (3IO4.pdb) were supplied to the online ClusPro server following which tetrameric models were generated by using the default parameters (DOT, distance cut-offs of 5A$^{\circ}$). The DOT rigid body docking algorithm produces 20,000 conformations which is then reduced to 2000 based on electrostatic and desolvation energies (1500 structures with stable electrostatics and 500 with stable desolvation). These 2000 structures are then clustered using the ClusPro algorithm that groups neighbors below the selected clustering radius into clusters that are ranked based on the size of such neighbors. Each cluster center (the conformation with the maximum number of neighbors) is then CHARMM (185) minimized. A detailed description of the procedure is described elsewhere (186). Of the ten (default number of clusters) tetrameric models, we did an initial screen that comprised of calculating the side-chain solvent accessibilities by using the WHATIF webserver (http://swift.cmbi.ru.nl/servers/html/index.html) (187) to identify structures where the major hydrophobic residues were buried. Single-point alanine mutations (in addition to the K6, 9,15R) were then modeled across each of the four chains in these structures using the Sybyl software (ver 7.3) and the side-chains were locally minimized. The energy of the complex was then calculated by using the FastContact Server (http://structure.pitt.edu/servers/fastcontact/) (188) by summing the contributions of the desolvation and electrostatic components of the associations between Chains B,C and Chains A,D of the tetramer.

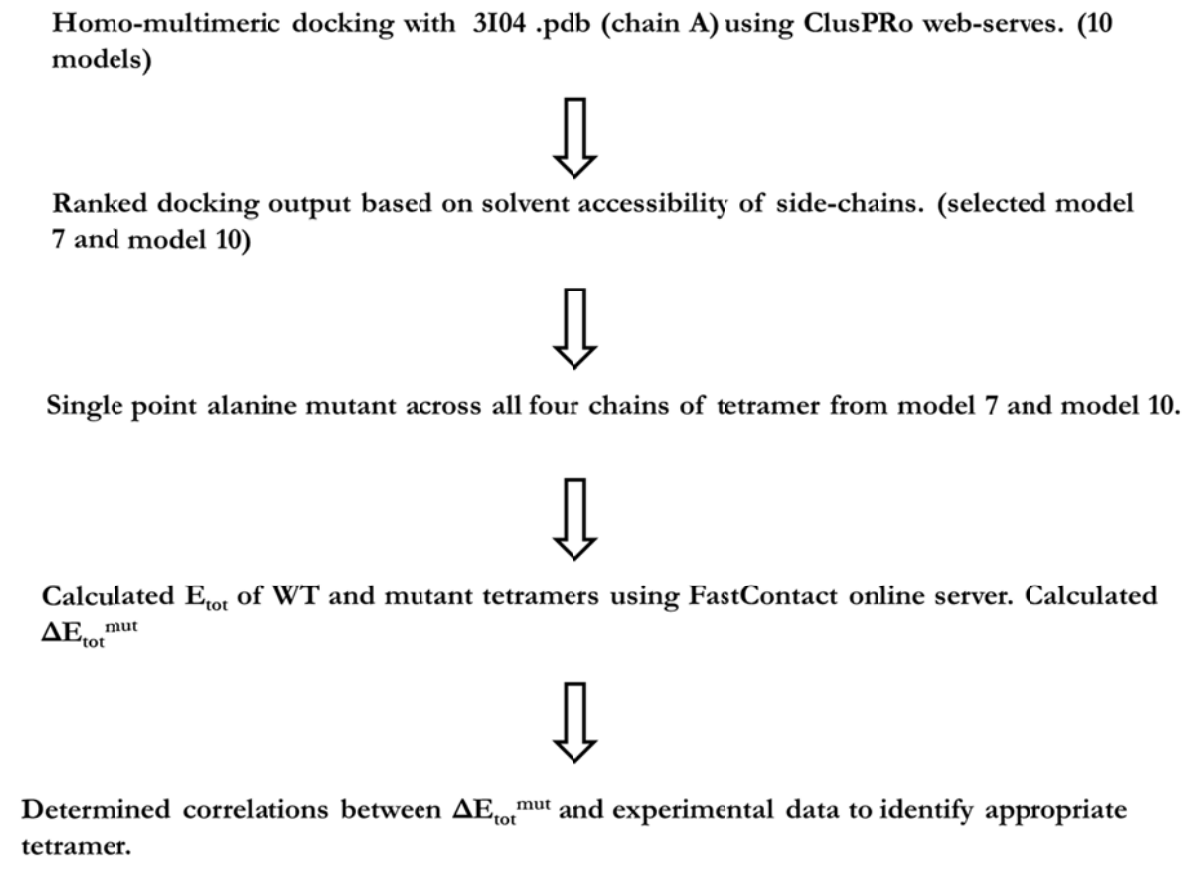

Figure 3-1: Workflow for htt^{NT} tetramer modeling.

4.0 IMPORTANCE OF AMPHIPATHIC HELICITY IN AGGREGATION OF POLYQ CONTAINING HTT FRAGMENTS (I): STUDIES WITH SCRAMBLED SEQUENCES

4.1 OVERVIEW.

Using different scrambled versions of the htt^{NT} sequence in polyQ containing htt fragments, we demonstrate that amphiphathic helix-formation underlies the htt^{NT} mediated aggregation of htt exon-1fragments. Our results suggest that amphipathic helix formation is necessary for initial oligomerization which mediates the observed rate acceleration in aggregation upon adding the htt^{NT} sequence to polyQ peptides. In addition, the htt^{NT} sequence seems to have a dual-role in polyQ containing htt fragment aggregation, acting on both the oligomerization and subsequent nucleation/elongation phases. Overall, these results add to the emerging picture about the role that htt^{NT} plays in the aggregation of polyQ containing htt fragments and lay the ground-work for a subsequent chapter that details the sequence-determinants of this role.

4.2 INTRODUCTION.

As has been described in previous chapters, the addition of the seventeen residue htt^{NT} sequence to polyQ peptides dramatically alters the mechanism of aggregation, primarily through the formation of oligomeric species that act as sites for stochastic nucleation of amyloid structure in the polyQ segment (31, 100). The htt^{NT} sequence that lies at the core of this altered aggregation mechanism is characterized by a mix of hydrophobic and hydrophilic residues and has been suggested to have substantial helical propensity (29, 31, 104).

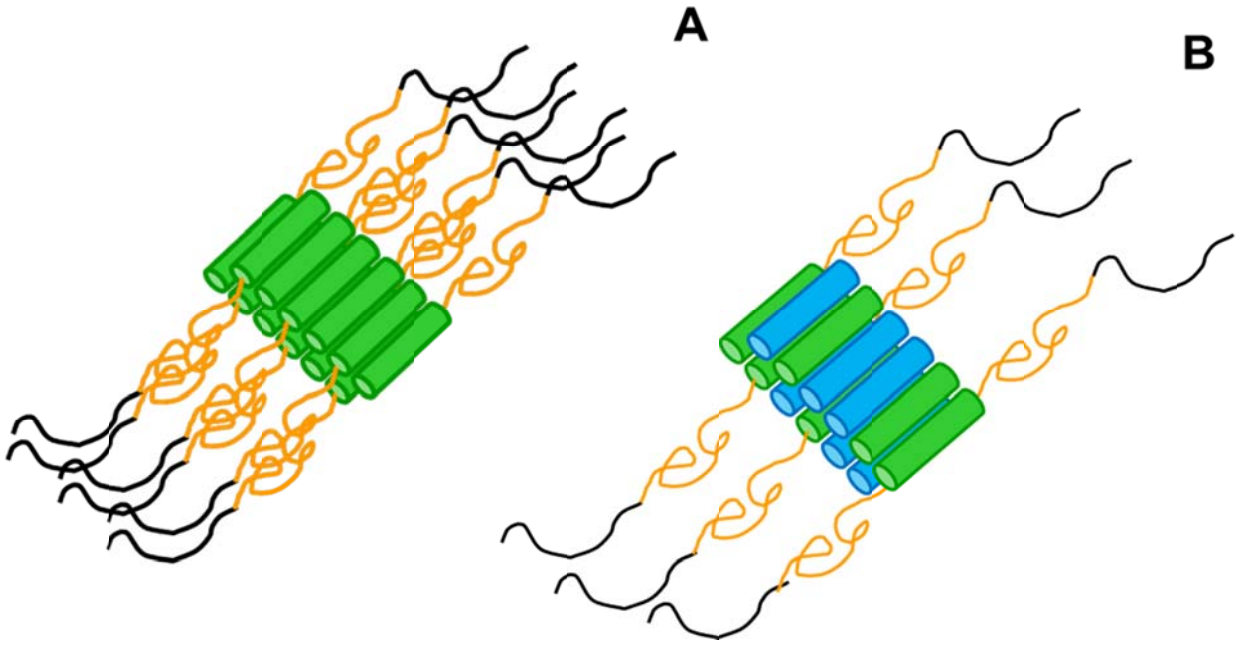

Figure 4-1: Mechanism of htt^{NT} inhibition. htt^{NT} sequence in polyQ cotnaining htt fragments (green) mediates the formation of oligomers (A). This ability to mediate oligomerization is also believed to lie at the core of htt^{NT} inhibition of aggregation of polyQ containing htt fragments presumably through the formation of mixed oligomers (B) mediated by the htt^{NT} sequences in the inhibitor (blue) and the substrate (green). The inhibition is believed to be incomplete since oligomers that have a lesser number of the inhibitor molecules can proceed through stochastic nucleation steps of the pathway.

Thus, within oligomers and final fibrils of polyQ containing htt fragments, the htt^{NT} sequence adopts a helical conformation (135, 136) though the sequence is essentially disordered within the monomer. The exact role that this putative helicity plays in the aggregation of htt fragments (and on which stage of aggregation) remains to be ascertained. Earlier, we had showed that the inhibition of polyQ containing htt fragment aggregation by htt^{NT} (and sequence variants thereof) seems linked to their ability to form amphipathic helices (Chapter 3). Thus, scrambled versions of htt^{NT} that have a high tendency to form amphipathic helices (based on their hydrophobic moments, $<\mu H>$) act as good inhibitors, presumably by presenting a hydrophobic interaction surface in co-oligomers with the aggregating substrate. This could also explain the inhibitory activity of the all-D and the retro-inverso versions of htt^{NT} (Chapter 3). Since aggregation inhibition by htt^{NT} is believed to occur through the formation of co-oligomers that require an amphiphathic helical conformation within htt^{NT}, it can be hypothesized that the aggregation of polyQ containing htt fragments that occurs through htt^{NT} mediated oligomerization has similar requirements for amphipathic helicity within htt^{NT} (Fig 4-1).

In order to directly test the role of amphipathic helicity within htt^{NT} in the aggregation of polyQ containing htt fragments, we decided to replace the htt^{NT} sequence in $htt^{NT}Q_{30}P_6K_2$ peptides with three of the different scrambled versions of the htt^{NT} sequence ($shtt^{NT}$), described previously. The three scrambled sequences were so chosen as to factor in both their tendency to form amyloid (evinced by their propensity to aggregate at low concentrations) and their ability to inhibit, *in trans*, the aggregation of a control $htt^{NT}Q_{30}P_6K_2$ substrate (Chapter 3). Based on these parameters, we chose three sequences: ***i.*** a sequence that has low amyloid propensity and is an effective inhibitor, $shtt^{(Olig)+}$ ***ii***. a sequence that has low amyloid propensity but is not an effective inhibitor, $shtt^{(Olig)-}$ and ***iii.*** a sequence that has a high amyloid propensity though not an effective

inhibitor of $htt^{NT}Q_{30}P_6K_2$ aggregation, $shtt^{(Amyl)+}$ (Table 4-1). We then investigated in detail the aggregation properties of model $htt^{NT}Q_{30}P_6K_2$ analogs containing these three different scrambled sequences.

Peptide	***Sequence***	***$t_{1/2}$ (hrs)***	***<μH>***	***% helix (theoretical)***
$htt^{NT}Q$	MATLEKLMKAFESLKSFQ	90	0.398	4.27
$shtt^{(Olig)+}$	ASSQKKMKEMLAFFTLEL	80	0.287	2.97
$shtt^{(Olig)-}$	FAKFASEKKLESMTLMLQ	18	0.092	0.56
$shtt^{(Amyl)+}$	SAFMEKMLLLEKQFKAST	9	0.282	15.1

Table 4-1: Details of scrambled sequences. Shown are the control htt^{NT} sequence and its three scrambled variants chosen in this study along with other properties such as inhibitory activity ($t_{1/2,}$ hrs), hydrophobic moments (<μH>) and theoretical helical propensities of these peptides. The choice of nomenclature is dictated by the underlying rationale. Thus, the scrambled htt^{NT} sequence that is a good inhibitor is presumed to form co-oligomers with the substrate and hence is designated $shtt^{(Olig)+}$ while the peptide that does not inhibit cannot form such co-oligomers and is called $shtt^{(Olig)-}$. The peptide with a high tendency to form amyloid fibrils is termed $shtt^{(Amyl)+}$

Overall, the results of the studies described in this chapter indicate that the aggregation of polyQ containing htt fragments is driven primarily by the ability of the htt^{NT} sequence to adopt amphipathic helical conformations that are crucial for the initial oligomerization of htt fragments.

4.3 RESULTS.

4.3.1 Studies with shtt^{NT} peptides.

Earlier, we had reported some initial work on characterizing the structural properties of the three shtt^{NT} sequences chosen here (Chapter 3). We thus set out to add to our existing knowledge about the structural properties of these sequences in order to better rationalize the results of the studies with the shtt^{NT} $Q_{30}P_6K_2$ peptides described here. Specifically, we were interested in determining the propensity for helical oligomer formation by these peptides.

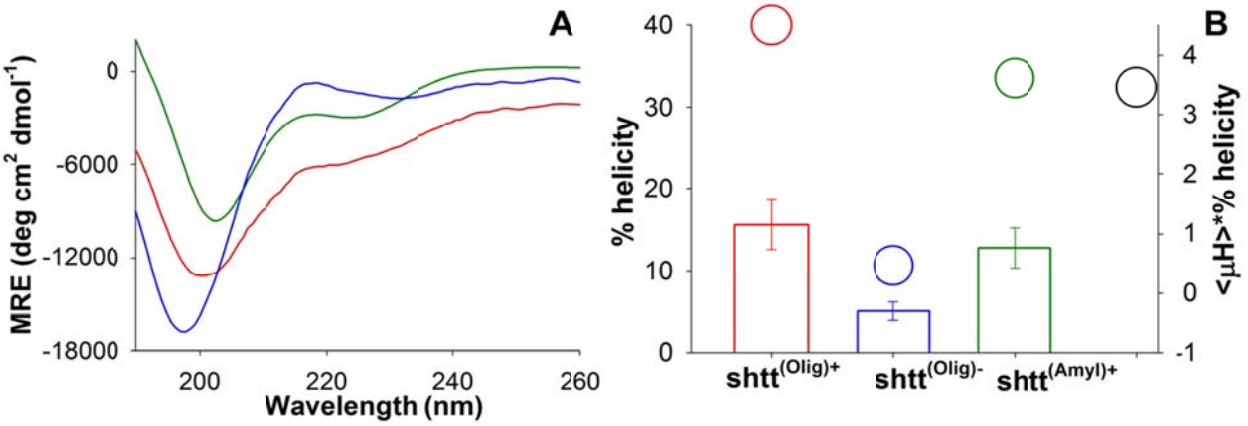

Figure 4-2: CD studies of monomeric shtt^{NT} peptides. (a) CD spectra of monomeric (averaged over multiple experiments) shtt^{NT} peptides: shtt$^{(Olig)+}$ (150μM, —), shtt$^{(Olig)-}$ (106μM, —), shtt$^{(Amyl)+}$ (160μM, —). (b) % helicity (vertical bar chart) of shtt^{NT} peptides determnined by deconvolution of CD spectra. Propensities for forming amphipathic helices (calculated as the product of <μH> and % helicity) are plotted as dots on the secondary (right) axis. Also, shown is the amphipahtic helical potential of the control htt^{NT}-Q sequence (black).

The CD spectrum of a htt^{NT} peptide displays a characteristic random-coil to α-helix transition at high concentrations (>~500μM), presumably through the formation of tetramers and

other higher-order oligomers (Chapter 2). We thus wanted to assess whether the three scrambled sequences display a similar propensity to form helical oligomers by investigating the concentration dependence of their CD spectra. Unfortunately however, all our efforts to prepare samples of these peptides at high concentrations were futile probably due to loss of material due to aggregation (see below). Nevertheless, an analysis of the CD spectrum and de-convolution of the individual contributions of different secondary structural sub-types to the spectrum confirms our previous results. Thus, of the three shtt^{NT} peptides, the shtt$^{(Olig)+}$ peptide displayed maximal helical propensity (~16%) while the shtt$^{(Olig)-}$ peptide had the least helical propensity (~5%). Interestingly, the shtt$^{(Amyl)+}$ sequence exhibited substantial helical propensity, almost matching that of the shtt$^{(Olig)+}$ peptide, consistent with the high helical propensity predicted for this sequence by secondary structure prediction algorithms (Table 4-1). It must be noted that though the relative helical propensities of the shtt$^{(Olig)+}$ and the shtt$^{(Olig)-}$ peptides found here are similar to the values determined before, the absolute numbers are slightly different. This difference most likely stems from the difference in sampling conditions (use of different cuvettes) and/or from the inaccuracy of de-convolution algorithms in predicting the relative percentages of different structures in disordered peptides. Overall, these results suggest that both the shtt$^{(Olig)+}$ and shtt$^{(Amyl)+}$ sequences have an amphipathic helical potential that matches that of the htt^{NT} sequence (Fig 4-2.B) in the monomeric state whereas the shtt$^{(Olig)+}$ has negligible amphipathic helical potential.

Our lab had previously demonstrated that htt^{NT} when incubated at high concentrations forms sedimentable oligomers which display a characteristic helical FTIR spectrum (136) (Fig 4-3.A). We thus wanted to investigate whether any of these scrambled peptides when incubated at high concentrations form similar helical oligomers. We were thus disappointed to find that at

high concentrations, all the three scrambled peptides aggregate to form β-sheet rich fibrillar structures (peaks at 1620 cm^{-1} and 1695 cm^{-1}) (Fig 4-3. B-D and E).

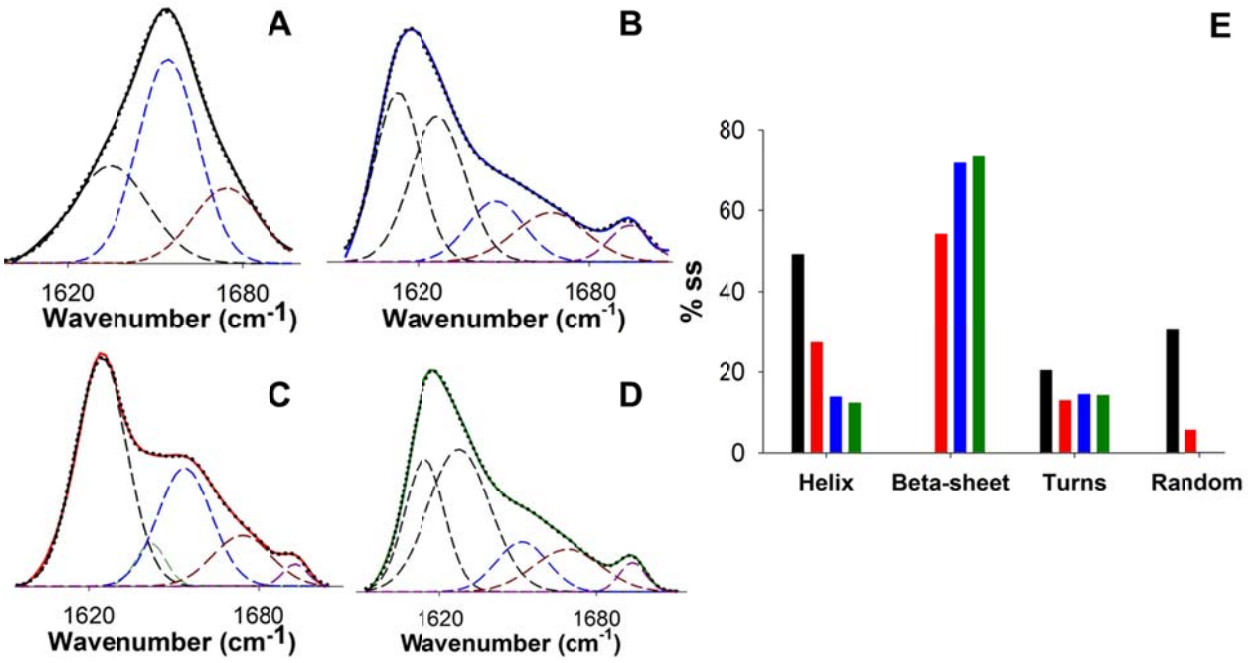

Figure 4-3: FTIR spectra of shtt^{NT} peptides. Aggregates isolated by centrifugation from WT (A, —), shtt$^{(Olig)+}$ (C, —), shtt$^{(Olig)-}$ (B, —) and shtt$^{(Amyl)+}$ (D, —) peptides incubated at high concentrations. All spectra were deconvoluted into contributions from individual structural subtypes (dashed lines). The theoretical fit (dotted line) was identical to the observed spectra in all cases (χ^2>0.999). Contributions from different structural sub-types are shown in E. The color scheme is same as detailed above. For deconvolution, we assigned peak at ~1650cm^{-1} to α-helix, peaks at 1620 cm^{-1} and 1690 cm^{-1} to β-sheet, 1635-1640cm^{-1} to random coil and 1665-1675 cm^{-1} to turns (189).

However, spectral deconvolution of the FTIR spectra to parse out contributions from individual structural elements throws up some interesting facts. Thus, the shtt$^{(Olig)+}$ peptide displays a pronounced helical component in the FTIR spectrum of aggregates formed at high concentrations (Fig 4-3.B, ~28%) while similar analysis on the shtt$^{(Olig)-}$ and shtt$^{(Amyl)+}$ peptides

displays substantially lower helicity values (~12%-13%). In comparison, the $htt^{NT}Q_3$ peptide forms helical oligomers that by the same deconvolution analysis are 50% helical. Of course, based on these data it is not possible to ascertain whether these different structural subtypes originate from a structurally homogeneous or heterogeneous mix of aggregates. Nevertheless, these data do suggest that amongst the three scrambled peptides, the $shtt^{(Olig)+}$ sequence has the maximal tendency to adopt helical conformations, an observation consistent with the CD results and its inhibitory effect on aggregation of polyQ containing htt fragments.

4.3.2 Studies with $shtt^{NT}Q_{30}P_6K_2$ peptides.

Each of the three scrambled sequences chosen in this study has different biophysical properties viz. amphipathic helix forming propensity, inhibitory activity and tendency to aggregate (Table 1). We were thus interested in examining how the addition of these scrambled htt^{NT} variants to a $Q_{30}P_6K_2$ peptide affects aggregation so as to better understand the role of the htt^{NT} sequence in mediating aggregation of polyQ containing htt fragments.

4.3.2.1 Structural characterization of the monomeric ensemble of $shtt^{NT}Q_{30}P_6K_2$.

One of the hypotheses to explain the enhanced aggregation of longer htt fragments invokes the presence of a toxic monomeric conformation (96, 131) at longer polyQ lengths. While in our system we have thus far not discovered any evidence of such a toxic monomeric conformation with polyQ containing htt fragments, it is theoretically possible that the addition of $shtt^{NT}$ sequences might preferentially stabilize any particular conformation within the monomer. We thus set out to look at the CD spectrum of the monomeric ensemble of the $shtt^{NT}Q_{30}P_6K_2$

peptides looking for any differences in secondary structure profiles as compared to the WT htt$^{NT}Q_{30}P_6K_2$ peptide which is essentially disordered with some hints of helical structure under similar conditions (Fig 4-4. —).

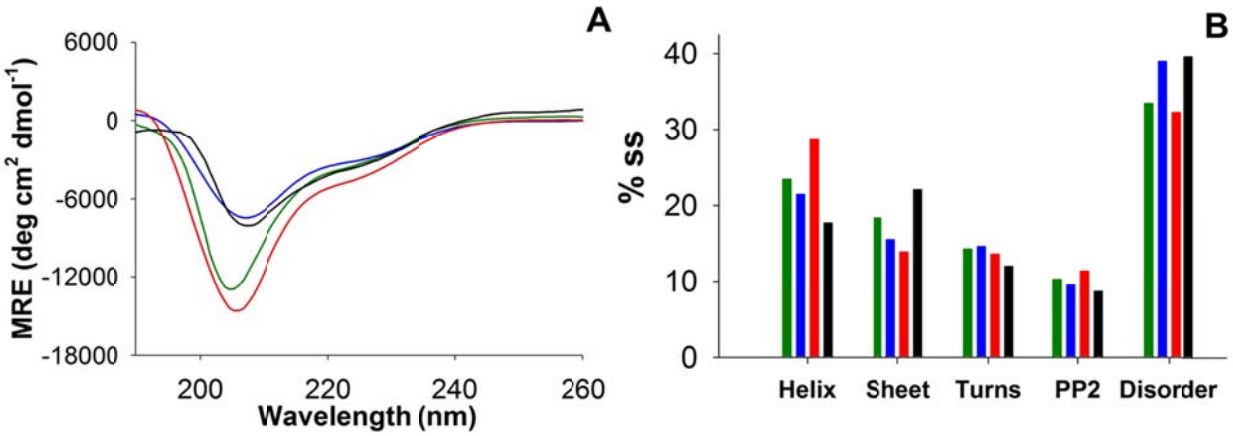

Figure 4-4: CD studies of monomeric shtt$^{NT}Q_{30}P_6K_2$. (A) Representative CD spectra of monomeric htt$^{NT}Q_{30}P_6K_2$ (22µM, —), shtt$^{(Olig)+}Q_{30}P_6K_2$ (78µM, —), shtt$^{(Olig)-}Q_{30}P_6K_2$ (34µM, —), shtt$^{(Amyl)+}Q_{30}P_6K_2$ (60µM, —). (B) Secondary structure deconvolution (vertical bar chart) of shtt$^{NT}Q_{30}P_6K_2$ peptides determined by deconvolution of CD spectra. Color scheme is same as in (A).

Overall, we did not observe any substantial differences in the secondary structural properties of the shtt$^{NT}Q_{30}P_6K_2$ peptides with all of them exhibiting predominantly random-coil spectra with varying hints of helical propensities (Fig 4-4.B).

4.3.2.2 Aggregation properties of shtt$^{NT}Q_{30}P_6K_2$.

Next, we progressed to examining the aggregation kinetics of these peptides. As shown in Fig 4-5, of the three scrambled peptides, the shtt $^{(Olig)+}Q_{30}P_6K_2$ peptide (●) aggregates the fastest ($t_{1/2}$ = 49hrs) though its aggregation is still substantially slower compared to the control htt$^{NT}Q_{30}P_6K_2$ peptide ($t_{1/2}$ = 15hrs,●). On the other hand, both the shtt $^{(Olig)-}Q_{30}P_6K_2$ (▲, $t_{1/2}$ = 93hrs) and shtt $^{(Amyl)+}Q_{30}P_6K_2$ peptides (♦, $t_{1/2}$ = 102hrs) aggregated substantially slower than both

the WT and the shtt$^{(Olig)+}$$Q_{30}P_6K_2$ peptides though not as slow as an equivalent concentration of the $K_2Q_{30}P_6K_2$ peptide (○). More interestingly however, the aggregation of these two peptides proceeded through an initial lag-phase characterized by a constant monomer concentration, similar to that observed in the case of $K_2Q_{30}P_6K_2$ (Δ) peptide.

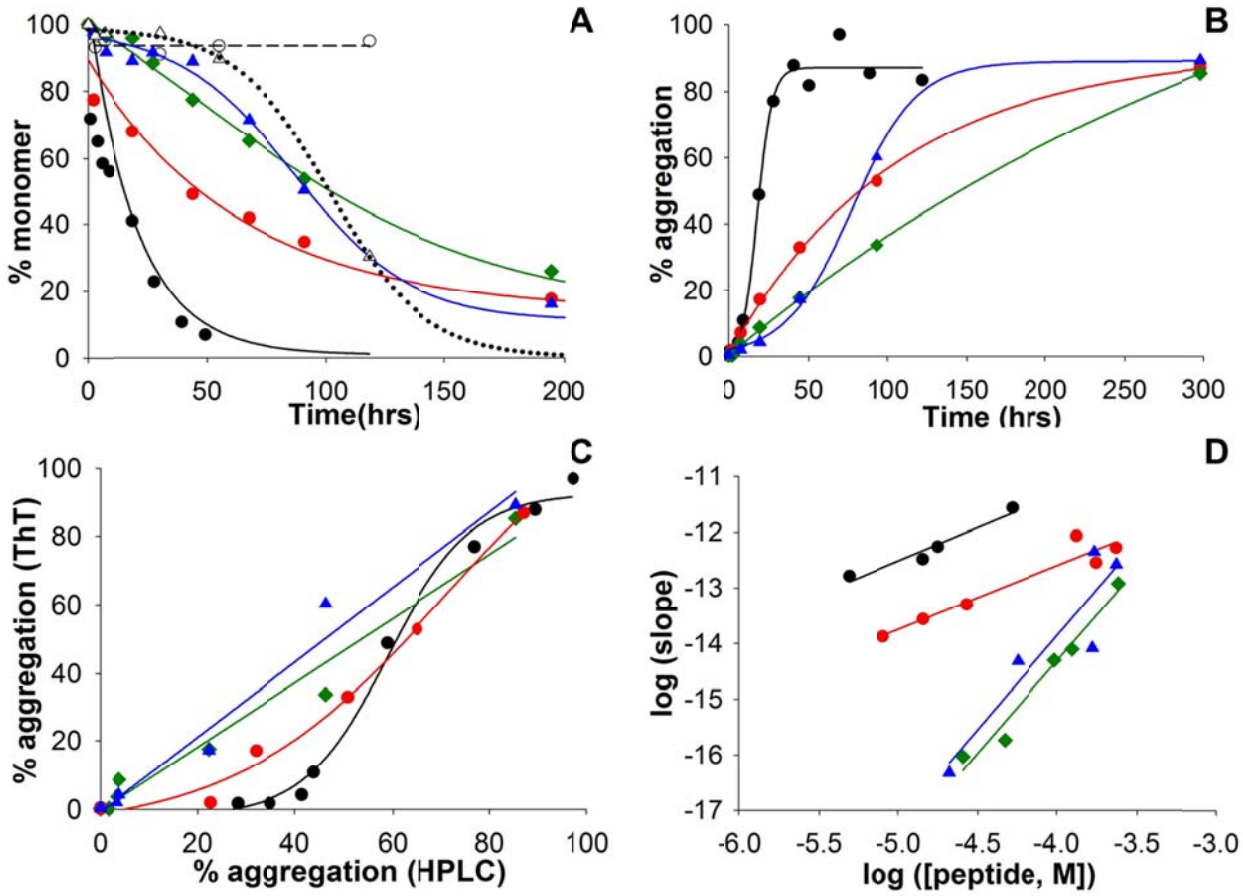

Figure 4-5: Aggregation of shttNT$Q_{30}P_6K_2$ peptides. Aggregate sedimentation (A) and ThT binding (B) were followed over time for htt^{NT}$Q_{30}P_6K_2$ (68μM ,●) shtt$^{(Olig)+}$$Q_{30}P_6K_2$ (51μM, ●), shtt$^{(Olig)-}$$Q_{30}P_6K_2$ (48μM, ▲), shtt$^{(Amyl)+}$$Q_{30}P_6K_2$ (46μM, ♦), $K_2Q_{30}P_6K_2$ (64 μM,○ and 195 μM, Δ). (C) Plot of % aggregation(s) determined by HPLC and ThT for htt^{NT}$Q_{30}P_6K_2$ (●) shtt$^{(Olig)+}$$Q_{30}P_6K_2$ (●), shtt$^{(Olig)-}$$Q_{30}P_6K_2$ (▲), shtt$^{(Amyl)+}$$Q_{30}P_6K_2$ (♦), (D) Concentration dependencies of initial aggregation rates determined by sedimentation assay of htt^{NT}$Q_{30}P_6K_2$ (●, slope =1.2, R^2=0.95) shtt$^{(Olig)+}$$Q_{30}P_6K_2$ (●, slope =1.15, R^2=0.93), shtt$^{(Olig)-}$$Q_{30}P_6K_2$ (▲, slope=3.4, R^2=0.85) and shtt$^{(Amyl)+}$$Q_{30}P_6K_2$ (♦, slope =3.3, R^2=0.97).

These differences in the aggregation properties of the scrambled peptides become all the more apparent in an analysis of the early-phase of aggregation. Thus, while the shtt$^{(Amyl)+}$$Q_{30}P_6K_2$ and shtt$^{(Olig)-}$$Q_{30}P_6K_2$ peptide hardly aggregate within the first 20hrs, both the WT and the shtt$^{(Olig)+}$$Q_{30}P_6K_2$ peptides display a sharp drop in monomer concentrations within the first 5 hrs suggesting these two peptides might behave similarly during the early phases of aggregation.

A characteristic feature of all amyloid aggregates is their ability to bind the ThioflavinT (ThT) dye. Thus, monitoring ThT binding of aggregates during the course of aggregation can provide insights into the aggregation that can complement information obtained from sedimentation analysis. As shown in Fig 4-5.B, we did not observe any substantial differences in the ThT binding of aggregates formed by the shtt^{NT}$Q_{30}P_6K_2$ peptides suggesting that the relative rates of formation of β-rich fibrillar aggregate, the binding target of ThT (190), are similar across the three scrambled peptides though substantially slower than that of the WT htt^{NT}$Q_{30}P_6K_2$ peptide. However, an analysis of the initial aggregation, as observed by ThT binding, does throw up some differences. Thus, a plot of % aggregation calculated from sedimentation assay vs that calculated from ThT binding shows that in the initial phase, the ThT based value lags behind the one calculated through the sedimentation assay for the WT (●) and the shtt$^{(Olig)+}$$Q_{30}P_6K_2$ (●) peptides but not for the shtt$^{(Olig)-}$$Q_{30}P_6K_2$ (▲) and shtt$^{(Amyl)+}$$Q_{30}P_6K_2$ (♦). In the case of the htt^{NT}$Q_{30}P_6K_2$ peptide, this property is believed to originate from the formation of non β-sheet oligomeric structures during the early-phases of aggregation which do not bind ThT (31). It is possible that a similar mechanism is in play in the case of the shtt $^{(Olig)+}$$Q_{30}P_6K_2$ peptide as well.

Overall, these results suggest that both the WT and the shtt$^{(Olig)+}$$Q_{30}P_6K_2$ peptides aggregate similarly, at least during the early phases of aggregation while the shtt$^{(Olig)-}$$Q_{30}P_6K_2$ and the shtt$^{(Amyl)+}$$Q_{30}P_6K_2$ peptides aggregate similar (mechanistically) to a $K_2Q_{30}P_6K_2$ peptide.

However, the formation of β-rich aggregates occurs at almost similar rates across all three shtt$^{NT}Q_{30}P_6K_2$ peptides.

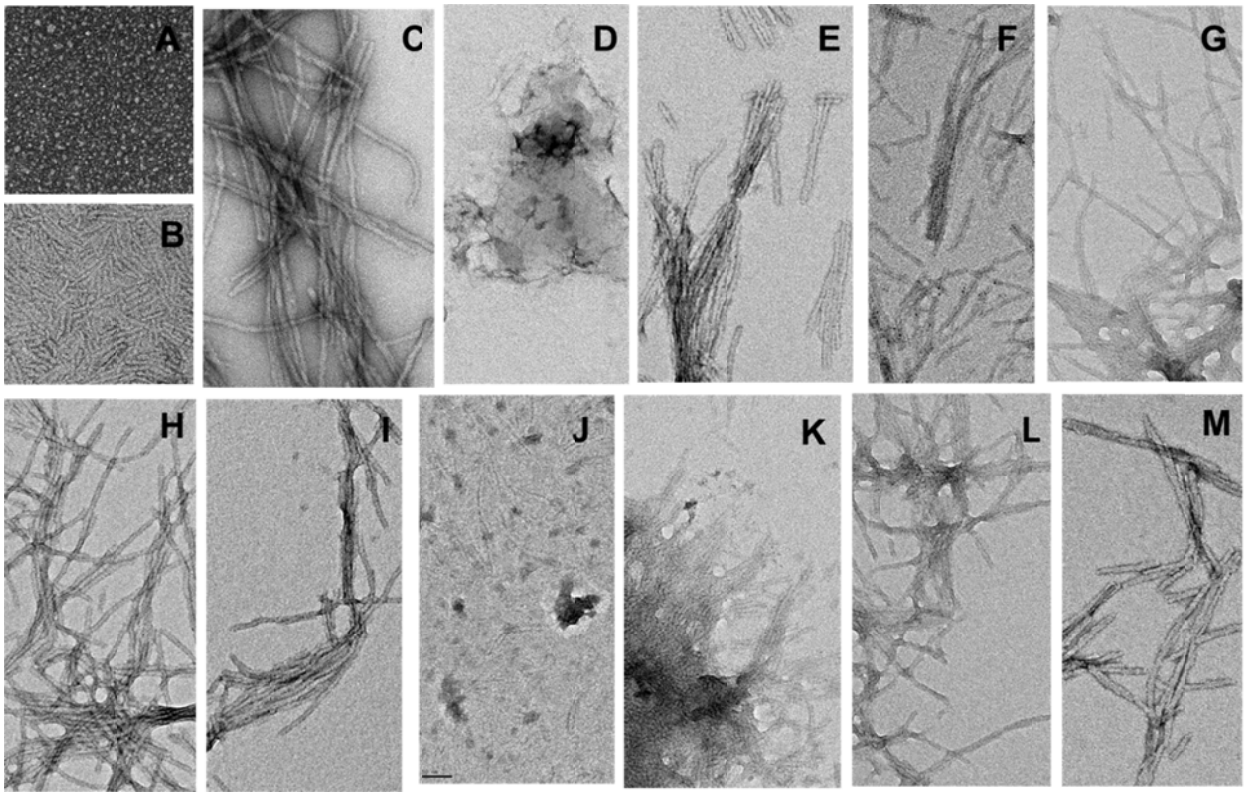

Figure 4-6: Morphologies of shtt$^{NT}Q_{30}P_6K_2$ aggregates. Aggregates of htt$^{NT}Q_{30}P_6K_2$ (isolated after ~5-10% ,A or 25% ,B and final, C (31); shtt$^{(Amyl)+}Q_{30}P_6K_2$ (isolated either after 25% aggregation, D or at completion, E-F), shtt$^{(Olig)-}Q_{30}P_6K_2$ (isolated after 10% , G or at completion H-I) and of shtt$^{(Olig)+}Q_{30}P_6K_2$ (isolated after 25% aggregation (J), 50% aggregation (K) and at completion L-M).

We also looked at the morphologies of the aggregates formed by the shtt$^{NT}Q_{30}P_6K_2$ peptides. The morphologies of the final aggregates isolated from both the shtt $^{(Olig)+}Q_{30}P_6K_2$ (Fig 4-6.L-M) and shtt$^{(Olig)-}Q_{30}P_6K_2$ (Fig 4-6.H-I) peptides resembled fibrillar structures that are typically observed in the aggregates of polyQ containing htt fragments (Fig 4-6.C). On the other hand, the final aggregates formed by the shtt$^{(Amyl)+}Q_{30}P_6K_2$ peptide (Fig 4-6.E-F) seemed slightly different morphologically, especially in their staining properties. Next, we looked at the

morphologies of the aggregates isolated at intermediate stages of aggregation. Thus, the shtt$^{(Olig)+}$$Q_{30}P_6K_2$ peptide aggregates through the formation of oligomers (Fig 4-6.J) and proto-fibrillar intermediates (Fig 4-6.K). On the other hand, the earliest aggregates of the shtt$^{(Olig)-}$$Q_{30}P_6K_2$ peptide resembled fibrillar (Fig 4-6.G) structures morphologically. The early aggregates of the shtt$^{(Amyl)+}$$Q_{30}P_6K_2$ peptide were a mix of amorphous aggregates (Fig 6A) and dark-staining protofibrillar intermediates (Fig 4-6.B). While it is tempting to speculate about aggregation mechanisms based on morphologies, especially in the context of shtt$^{(Olig)+}$$Q_{30}P_6K_2$ and shtt$^{(Olig)-}$$Q_{30}P_6K_2$ peptides, doing so can be misleading since aggregates with similar morphologies have been shown to have completely different properties (120).

4.3.2.3 Concentration dependence of initial aggregation rates of shtt^{NT}$Q_{30}P_6K_2$.

As was described in Chapter 1, one of the fundamental differences in the aggregation of polyQ peptides and that of polyQ containing htt fragments lies in the difference in the concentration dependence of the initial rates of aggregation, originating from differences in aggregation mechanisms. Since our analysis of the aggregation kinetics (Fig 4-5. A,B) uncovered differences in the early phases of aggregation between shtt$^{(Olig)+}$$Q_{30}P_6K_2$ and the other two scrambled peptides, we decided to explore whether such differences were also apparent in the concentration dependence of the initial aggregation rates of these peptides. Thus, a log-log plot (Fig 4-5.D) of the starting concentrations vs initial aggregation rates for the shtt$^{(Olig)+}$$Q_{30}P_6K_2$ (●) peptide gave a slope of 1.15 almost identical to the slope of 1.2 reported earlier (31) for the control htt^{NT}$Q_{30}P_6K_2$ peptides (●). On the other hand, both the shtt$^{(Olig)-}$$Q_{30}P_6K_2$ (▲) and the shtt$^{(Amyl)+}$$Q_{30}P_6K_2$ (♦) peptides gave almost identical slopes of ~3 similar to that observed in the case of simple polyQ peptides (122). Overall, these results are consistent with our results from the study of the aggregation kinetics of these peptides in suggesting that during the early phases

of aggregation, the shtt$^{(Olig)+}Q_{30}P_6K_2$ peptide aggregates similar to polyQ containing htt fragments, while the shtt$^{(Olig)-}Q_{30}P_6K_2$ and shtt$^{(Amyl)+}Q_{30}P_6K_2$ peptides aggregate similar to simple polyQ peptides.

4.3.2.4 Characterization of the early aggregation phase of shtt$^{NT}Q_{30}P_6K_2$.

The difference in the concentration dependence of the initial rates of aggregation between polyQ peptides and polyQ containing htt fragments is believed to be indicative of the different aggregation mechanisms of these peptides. Thus, polyQ containing htt fragments that show a shallow concentration dependence of initial aggregation rates aggregate through oligomeric intermediates. In contrast, simple polyQ peptides that display strong concentration dependence in their initial rates of aggregation do not form any oligomeric intermediates under similar conditions (121). We thus wanted to see whether the different concentration dependencies of the shtt$^{NT}Q_{30}P_6K_2$ peptides are also reflected in other indicators of aggregation mechanisms.

The DLS (dynamic light scattering) technique is particularly useful in identifying large scattering species that are populated during aggregation. Earlier, we had successfully used this technique in demonstrating that the early phases of aggregation of polyQ peptides lack any oligomeric species (121). Hence, we decided to apply this technique to the characterization of early aggregates formed by shtt$^{NT}Q_{30}P_6K_2$ peptides.

The aggregation of htt$^{NT}Q_{30}P_6K_2$ peptides was observed to proceed through the rapid formation of larger-scattering species (Fig 4-7.A) with the average size of these species increasing within an hour from 40Å to 300Å (Fig 4-7.C). Similarly, the early phases of shtt$^{(Olig)+}Q_{30}P_6K_2$ aggregation were also characterized by the rapid formation of large, highly scattering species (Fig 4-7.B) with progressively increasing sizes (Fig 4-7.D). It is worth pointing

out that within this timeframe (60-90mins), aggregates of both these peptides do not display any ThT binding (Fig 4-5.D) consistent with the non β-sheet nature of these aggregates.

In contrast, the initial phases of both the shtt$^{(Olig)-}Q_{30}P_6K_2$ and the shtt$^{(Amyl)+}Q_{30}P_6K_2$ do not exhibit formation of any large-scattering species (Fig 4-7.E and 4-7.F), behavior that is similar to what has been reported with simple polyQ peptides (121). Eventually, upon completion of ~35%-45% of aggregation, both shtt$^{(Olig)-}Q_{30}P_6K_2$ and the shtt$^{(Amyl)+}Q_{30}P_6K_2$ form larger scattering species with average radii of 100 Å -200Å respectively (Fig 4-7.G and 4-7.H). Based on the ThT binding of aggregates formed at an equivalent point in the aggregation reaction, it is likely that these scattering species (formed by shtt$^{(Olig)-}Q_{30}P_6K_2$ and the shtt$^{(Amyl)+}Q_{30}P_6K_2$) are nascent β-sheet rich fibrils.

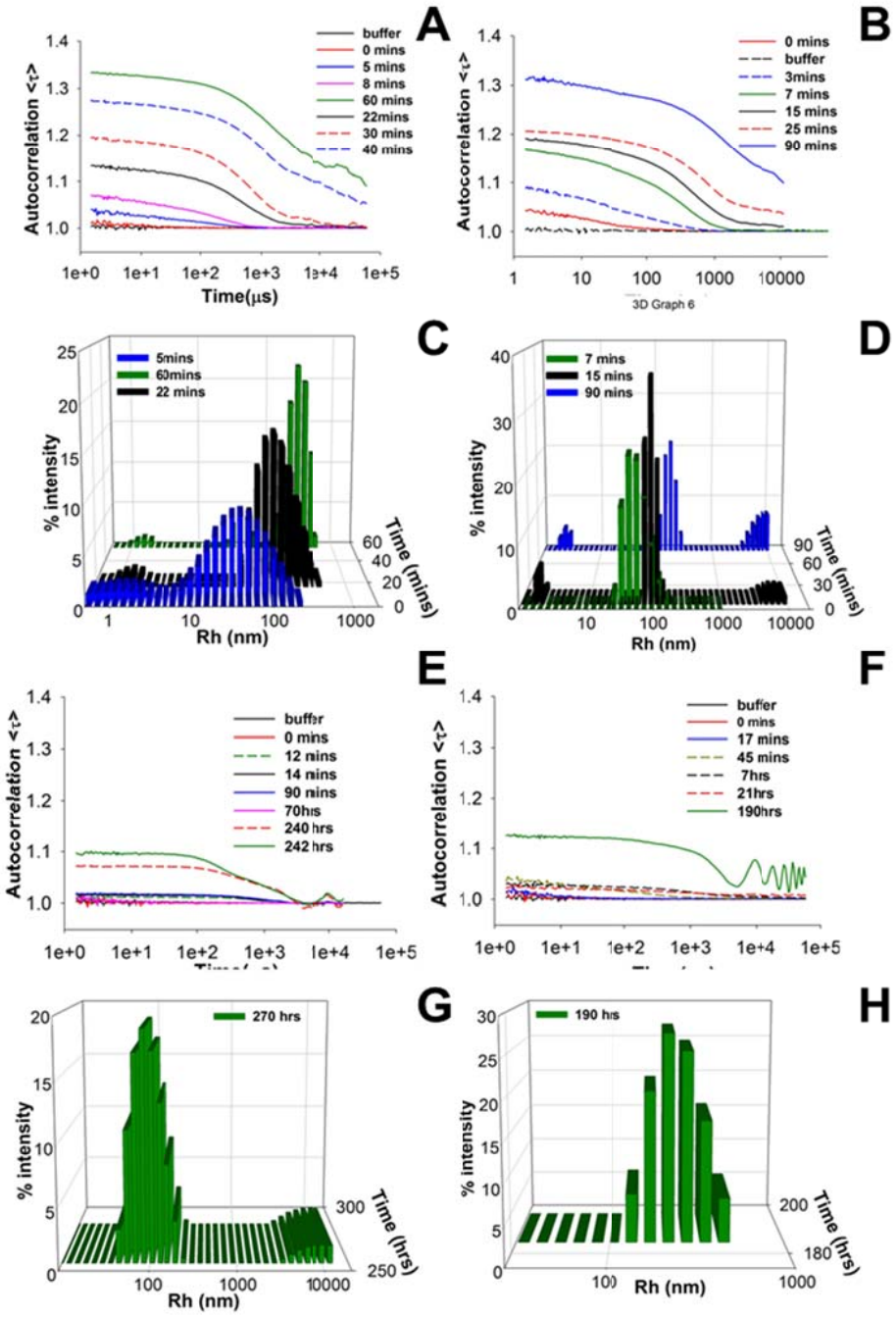

Figure 4-7: DLS experiments with shtt$^{NT}Q_{30}P_6K_2$ peptides. Aggregation of different scrambled peptides monitored by DLS. Shown are the temporal scattering profiles and hydrodynamic radii distributions of htt$^{NT}Q_{30}P_6K_2$ (A,C), shtt$^{(Olig)+}Q_{30}P_6K_2$ (B,D), shtt$^{(Olig)-}Q_{30}P_6K_2$ (E,G) and shtt$^{(Amyl)+}Q_{30}P_6K_2$ (F,H) peptides.

As an additional probe of amyloid nucleation mechanisms, we also assessed the ability of the htt^{NT} peptide to inhibit the aggregation of the $shtt^{NT}Q_{30}P_6K_2$. Earlier, we had shown that the addition of the htt^{NT} sequence (with or without a few glutamine residues) inhibits the aggregation of polyQ containing htt fragments based on their ability to form mixed oligomers (Fig 4-1.B). Thus, we reasoned that $shtt^{NT}Q_{30}P_6K_2$ peptides that can form oligomers should display inhibition by the htt^{NT} peptide.

As was reported earlier, adding the htt^{NT} peptide to $htt^{NT}Q_{30}P_6K_2$ peptide in a 1:1 ratio (or greater) substantially reduces the rate of aggregation, increasing the $t_{1/2}$ of aggregation by ~ten-fold (Fig 4-8.A,B, ○). Similarly, addition of htt^{NT} was also observed to inhibit the aggregation of $shtt^{(Olig)+}Q_{30}P_6K_2$ (Fig 4-8.A, ○) though the degree of inhibition was substantially lower than observed in the case of the WT $htt^{NT}Q_{30}P_6K_2$ (increasing $t_{1/2}$ by ~2.5 fold). More importantly, the aggregation of $shtt^{(Olig)+}Q_{30}P_6K_2$ peptide in the inhibition reaction proceeds through an initial lag-phase, similar to that observed with the WT $htt^{NT}Q_{30}P_6K_2$ peptide (○), consistent with the hypothesis that htt^{NT} reversibly inhibits homo-oligomerization of these peptides.

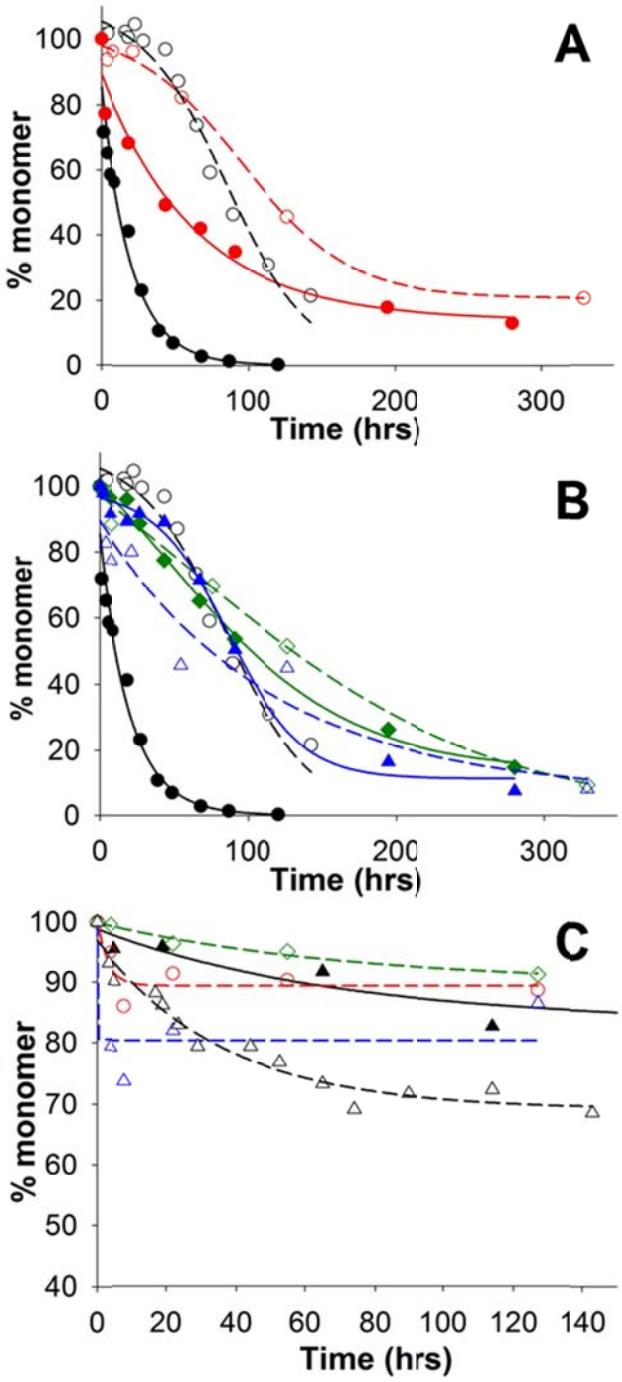

Figure 4-8: htt^{NT} mediated inhibition of aggregation. Inhibition by htt^{NT} (added 1.5 times in excess) of aggregation of 14μM $htt^{NT}Q_{30}P_6K_2$ (A,B, ○), 66μM $shtt^{(Olig)+}Q_{30}P_6K_2$ (A,○), 85μM $shtt^{(Olig)-}Q_{30}P_6K_2$ (B,Δ) and 75μM $shtt^{(Amyl)+}Q_{30}P_6K_2$ (B,◊) peptides. Also shown are the uninhibited controls for WT (●), $shtt^{(Olig)+}Q_{30}P_6K_2$ (●) , $shtt^{(Olig)-}Q_{30}P_6K_2$ (▲)and $shtt^{(Amyl)+}Q_{30}P_6K_2$ (♦). (C) Aggregation of htt^{NT} by itself (▲) or in the presence of $htt^{NT}Q_{30}P_6K_2$ (Δ), $shtt^{(Olig)+}Q_{30}P_6K_2$ (○), $shtt^{(Olig)-}Q_{30}P_6K_2$ (Δ) and $shtt^{(Amyl)+}Q_{30}P_6K_2$ (◊) peptides.

Consistent with htt^{NT}'s role in inhibition, we did observe a drop in the concentration of the htt^{NT} peptide in the mixed reaction with both the WT (Fig 4-8.C, Δ) and the $shtt^{(Olig)+}Q_{30}P_6K_2$ peptides (Fig 4-8.C, ○).

On the other hand, the addition of htt^{NT} did not have any effect on the aggregation of the $shtt^{(Amyl)+}Q_{30}P_6K_2$ peptide (Fig 4-8.B, ◊) which aggregates similar to the uninhibited control (Fig 4-8.B,♦). Expectedly, we did not see any difference between the aggregations of the htt^{NT} in this mixed reaction (Fig 4-8.C, ◊) or by itself (Fig 4-8.C, ▲), consistent with its inability to interact with the $shtt^{(Amyl)+}Q_{30}P_6K_2$. Interestingly the aggregation of the $shtt^{(Olig)-}Q_{30}P_6K_2$ peptide was slightly accelerated upon addition of the htt^{NT} peptide (Fig 4-8.B, Δ) in comparison with the uninhibited control (Fig 4-8.B,▲) especially during the early-phases of aggregation. The involvement of htt^{NT} in this rate acceleration of aggregation is also suggested by the drop in the htt^{NT} concentration in the mixed reaction (Fig 4-8.C,Δ).

Overall, both the DLS and inhibition studies demonstrate that the $shtt^{(Olig)+}Q_{30}P_6K_2$peptide aggregates via the formation of oligomers, similar to the WT $htt^{NT}Q_{30}P_6K_2$ peptide while the $shtt^{(Amyl)+}Q_{30}P_6K_2$ and $shtt^{(Olig)-}Q_{30}P_6K_2$ peptides like simple polyQ peptides, do not aggregate through the formation of oligomers.

4.3.2.5 Low-resolution structural characterization of $shtt^{NT}Q_{30}P_6K_2$ aggregates.

Next, we moved to structurally characterizing aggregates isolated at different times in the aggregation reactions of $shtt^{NT}Q_{30}P_6K_2$ peptides. First, we looked at the accessibilities of the polyQ segments, in isolated aggregates, to the polyQ specific monoclonal antibody MW1 (92). Earlier, we had demonstrated that the polyQ stretch in oligomers of the WT $htt^{NT}Q_{30}P_6K_2$ peptide is accessible to MW1 binding though this accessibility is lost in the final fibrils (31).

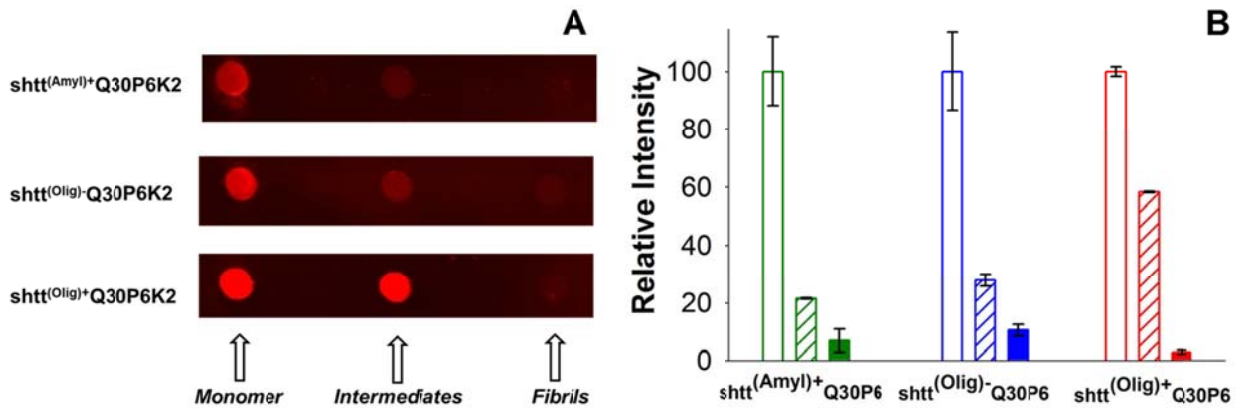

Figure 4-9: MW1 binding to shtt$^{NT}Q_{30}P_6K_2$ aggregates. (A) Accessibility of polyQ segments in aggregates of shtt$^{NT}Q_{30}P_6K_2$ isolated early (15%-18% completion) or at the end of the aggregation reaction, to the MW1 antibody. (B) Densitometric analysis (duplicates) of MW1 binding.

Similarly, the polyQ segment in early oligomers of the shtt$^{(Olig)+}Q_{30}P_6K_2$ peptide are substantially exposed (Fig 4-9.A), with almost 60% of the polyQ epitope available for MW1 binding (Fig 4-9.B). In contrast, the polyQ segments in the early aggregates isolated from both shtt$^{(Olig)-}Q_{30}P_6K_2$ and the shtt$^{(Amyl)+}Q_{30}P_6K_2$ (Fig 4-9.A) are substantially buried with the accessibility to MW1 of only ~20% -30% of that in the monomeric state (Fig 4-9.B). As expected, the polyQ segment in all the three shtt$^{NT}Q_{30}P_6K_2$ fibrils were buried, inaccessible to MW1 binding. (Fig 4-9.A and 4-9.B). Thus, these results suggest that while the early stages of shtt$^{(Olig)+}Q_{30}P_6K_2$ aggregation are driven by the shtt$^{(Olig)+}$sequence (similar to the htt^{NT} driven oligomerization of the WT peptides), those of the shtt$^{(Olig)-}Q_{30}P_6K_2$ and shtt$^{(Amyl)+}Q_{30}P_6K_2$ peptides are most likely driven by the polyQ segment.

4.4 DISCUSSION.

The htt^{NT} sequence is highly conserved across species (27) consistent with the crucial role that this sequence plays in a wide-range of cellular processes (28, 29). This sequence has also been shown to take the lead in mediating the aggregation of polyQ containing htt fragments (31, 76) through the formation of oligomeric species that accelerate nucleation of the polyQ segments. In this work, we have tried to understand in greater detail the role that the htt^{NT} sequence plays in the aggregation of polyQ containing htt fragments.

Our studies of the abilities of scrambled variants of the htt^{NT} sequence to inhibit aggregation of polyQ containing htt fragments, led us to hypothesize that the adoption of amphipathic helical structures by htt^{NT} is crucially linked to the initial oligomerization of these peptides. We further tested this hypothesis by replacing the htt^{NT} sequence within polyQ containing htt fragments by three of the scrambled variants studied in Chapter 2. These sequences were chosen based on their different properties (Table 4-1). Thus, while the $shtt^{(Olig)+}$ sequence inhibited the aggregation of $htt^{NT}Q_{30}P_6K_2$ peptides, the $shtt^{(Amyl)+}$ and $shtt^{(Olig)-}$ sequences did not. In addition, both the $shtt^{(Olig)+}$ and $shtt^{(Amyl)+}$ sequences display similar amphipathic helix forming propensities which are similar to that of the htt^{NT} sequence but substantially higher than that of the $shtt^{(Olig)-}$ sequence. Finally, the tendency to form amyloid structures at low concentrations acts as another differentiating feature between these sequences with only the $shtt^{(Amyl)+}$ sequence capable of aggregating into amyloid structures at low concentrations. These helical propensities are also reflected in the structures of the aggregates formed by these sequences at high concentrations (Fig 4-3.E) with aggregates of $shtt^{(Olig)+}$ sequence displaying maximal helical propensity of these three sequences. Thus, despite our inability to directly isolate helical oligomers, these results in conjunction with the inhibitory

activity of these peptides (Table 1) suggest that of the three peptides only shtt$^{(Olig)+}$ is capable of forming amphipathic helical oligomers.

Consistent with its amphipathic helical propensity, the shtt$^{(Olig)+}$ sequence within the context of a htt$^{NT}Q_{30}P_6K_2$ peptide was observed to aggregate the fastest amongst all the three shtt$^{NT}Q_{30}P_6K_2$ peptides (Fig 4-5.A), with its initial aggregation kinetics almost matching that of the WT htt$^{NT}Q_{30}P_6K_2$ peptide (Fig 4-5.C). This equivalence in initial aggregation of the WT htt$^{NT}Q_{30}P_6K_2$ and the shtt$^{(Olig)+}Q_{30}P_6K_2$ peptides are also reflected in the similarly shallow concentration dependencies of their initial aggregation rates (Fig 4-5.D). While it is theoretically possible that the pro-acceleratory role of the shtt$^{(Olig)+}$ sequence is mediated by a change in the monomeric conformation, CD measurements of the average structure argue against this (Fig 4-4.A,B). Rather, the effects of the shtt$^{(Olig)+}$ sequence on aggregation are almost entirely mediated during the oligomerization phase. Thus, both the WT htt$^{NT}Q_{30}P_6K_2$ and the shtt$^{(Olig)+}Q_{30}P_6K_2$ peptides aggregate via the rapid formation of oligomers (Fig 5I) that have typical DLS profiles (Fig 6A and Fig 6B) . This shared tendency to form oligomers also explains the inhibition of the htt$^{NT}Q_{30}P_6K_2$ and the shtt$^{(Olig)+}Q_{30}P_6K_2$ peptides by htt^{NT} (Fig 4-7.A), presumably through co-oligomerization of the substrate and inhibitor (Fig 4-7.C). Furthermore, the substantial exposure of the polyQ segment in these initial oligomers (Fig 4-9.A and 4-9.B) suggests that the shtt$^{(Olig)+}$ sequence, primarily mediates the formation of these oligomers.

The low propensity of the shtt$^{(Olig)-}$ sequence to form amphipathic helices (Fig 4-2.B) and its inability to inhibit the aggregation of htt$^{NT}Q_{30}P_6K_2$ (Table 4.1) make it an excellent negative control in testing the hypothesis that amphipathic helicity is crucial to aggregation of polyQ containing htt fragments. Overall, the shtt$^{(Olig)-}Q_{30}P_6K_2$ peptide behaved as expected, aggregating much slower than the htt$^{NT}Q_{30}P_6K_2$ peptide and displaying an initial lag-phase in its aggregation

that is similar to that observed in simple polyQ peptides (Fig 4-5.A). Also, the initial aggregation rates of this peptide were found to scale linearly with the peptide concentration, almost identical to the relationship observed in polyQ peptides. More importantly, we did not observe any indication of this peptide forming oligomeric structures during the initial phase of aggregation (Fig 4-6.E).

The propensity of the shtt$^{(Amyl)+}$ peptide to form amphipathic helices (Fig 4-2.B) coupled with its high tendency to aggregate and its inability to inhibit aggregation of polyQ containing htt fragments, made this sequence particularly interesting . Thus, it could be hypothesized that the addition of this sequence to a $Q_{30}P_6K_2$ peptide would drive aggregation through an oligomer driven mechanism similar to that observed in htt$^{NT}Q_{30}P_6K_2$ peptides, mediated by its amphipathic helical propensities. On the other hand, the high tendency of this peptide to aggregate into β-sheet rich fibrils could mean that population of amphipathic helical oligomers of shtt$^{(Amyl)+}Q_{30}P_6K_2$ is not favored. Our results indicate the latter to be the case. Thus, aggregation of the shtt$^{(Amyl)+}Q_{30}P_6K_2$ was observed to be substantially slower than htt$^{NT}Q_{30}P_6K_2$ proceeding through an initial lag-phase similar to the ones observed with the shtt$^{(Olig)-}Q_{30}P_6K_2$ and $K_2Q_{30}P_6K_2$ peptides. Furthermore, the concentration dependencies of initial aggregation and the lack of any oligomeric species during the lag-phases of aggregation are consistent with an aggregation mechanism that is similar to that of polyQ peptides. Even though these data demonstrate the lack of any oligomers mediated by amphipathic helical interactions, it is still possible that nucleation of amyloid formation involves elements of the shtt$^{(Amyl)+}$ sequence.

Overall, these results suggest that the major role of the htt^{NT} sequence lies in the mediation of oligomerization, driven by its propensity to adopt amphipathic helical conformations. This property of htt^{NT} also underlies the rapid initial aggregation that is observed

in polyQ containing htt fragments. However, is the mediation of amphipathic helical oligomers the only role of the htt^{NT} sequence? Our results with the scrambled htt^{NT} sequences seem to suggest otherwise. ssNMR studies of final fibrils showed that the C-terminal region of the htt^{NT} sequence (Ser16, Phe17) adopts the β-sheet conformation that characterize the polyQ segments (136) suggesting that at least part of the htt^{NT} sequence plays a role in nucleation/elongation stages of the aggregation pathway (Chapter 1). Our results with the shtt $^{(Olig)+}Q_{30}P_6K_2$ peptide provide some additional insights. Thus, this peptide is similar to the WT sequence in terms of its tendency to form amphipathic helices, its ability to aggregate via oligomeric intermediates and its concentration dependencies of its initial aggregation. Yet, the formation of β-sheet aggregates is substantially slower in the case of this sequence than the WT. Similarly, the shtt $^{(Olig)+}$ sequence is substantially more accessible to cleavage by trypsin (Fig A-6 and Table A-1) than the WT sequence (31). These results suggest that mimicking the amphipathic helical propensities of the htt^{NT} sequence is not sufficient to match the aggregation observed with polyQ containing htt fragments. Thus, it would appear possible that another (probably secondary) role of htt^{NT} lies in its ability to engage in β-sheet structures especially in the polyQ proximal region of this sequence. Of course, it must be stressed that this argument in its current form is mostly speculative and needs to be experimentally validated. For instance, differential stabilities of oligomers formed by the htt^{NT} sequence and the shtt $^{(Olig)+}$ sequence could explain the differences in kinetics of formation of β-sheet aggregates observed in these peptides.

In conclusion, our work with the scrambled htt^{NT} sequences ascribes a crucial role for amphipathic helicity within htt^{NT} in the oligomerization of polyQ containing htt fragments. In the subsequent chapter, we have adopted a mutational analysis approach to confirm and to determine the major residues within htt^{NT} that are crucial to this "pro-aggregation" role of htt^{NT}.

5.0 IMPORTANCE OF AMPHIPATHIC HELICITY IN AGGREGATION OF POLYQ CONTAINING HTT FRAGMENTS (II): A MUTATIONAL ANALYSIS.

5.1 OVERVIEW.

Using a combination of single point alanine mutations and other functionally important mutations, we show that amphipathic helix formation is the major driving force in the oligomerization of polyQ containing htt fragments, controlling the kinetics and thermodynamics of oligomer formation. This ampiphilicity driven oligomerization underlies the differences in the aggregation mechanism (concentration dependence) between polyQ containing htt fragments and polyQ-only (simple polyQ) sequences. Within this context we also assessed the effects of some of the reported post-translational modifications (PTMs) of htt^{NT} on aggregation. These results provide an additional dimension to the analysis of the role that PTMs play in HD pathology. Finally, we have used the mutational data described here in modeling *in silico* a putative structure of the htt^{NT} mediated tetramer that is populated during aggregation. We anticipate the structure provided here to be a useful tool in guiding future experiments and to be a starting point for pharmacophore screening studies to identify chemical targets that can block tetramer formation.

5.2 INTRODUCTION.

The addition of the htt^{NT} sequence to a polyQ (or a polyQ-polyPro) peptide was observed to ***a.*** accelerate the kinetics of aggregation and ***b.*** alter the aggregation mechanism from a nucleated-growth (with a monomeric nucleus) mechanism to one that is driven by stochastic nucleation within an oligomeric pool. Such htt^{NT} mediated oligomerization proceeds through the formation of tetrameric, octameric and dodecameric species in equilibrium with each other (100). While in the monomeric state the htt^{NT} sequence adopts a random-coil structure (31), within oligomers this sequence is almost entirely helical and a major portion of the htt^{NT} sequence remains helical (136) even in the final fibrils highlighting the preference of this sequence to adopt a helical conformation (Fig 5-1).

A number of experimental and computational studies have identified a crucial role for htt^{NT} helicity in mediating the aggregation of polyQ containing htt fragments (31, 76, 95, 100). However, the role of the different parts of the htt^{NT} sequence and the exact role of helicity (and by extension amphipathicity) in the different stages of polyQ containing htt fragment aggregation remains to be ascertained. This is crucial not only to our understanding of the aggregation pathway but might also hold potential for the discovery of active molecules that inhibit aggregation.

The htt^{NT} sequence is not only crucial to the aggregation of polyQ containing htt fragments but also has several crucial cellular roles. For instance, the htt^{NT} sequence has been implicated as the site of several post-translational modifications (PTMs) *in vivo* with crucial implications in HD pathology (16, 17, 37) . It can be reasoned that PTMs within htt^{NT} can also affect the aggregation of polyQ containing htt fragments as has been described for the phosphorylation of serines at positions 13 and 16 in htt^{NT} (Chapter 6). Given the potential

relevance of PTMs to HD pathology, a study of the effects of the PTMs on polyQ containing htt fragments' aggregation is crucial to our understanding of the cellular and pathological roles of such modifications.

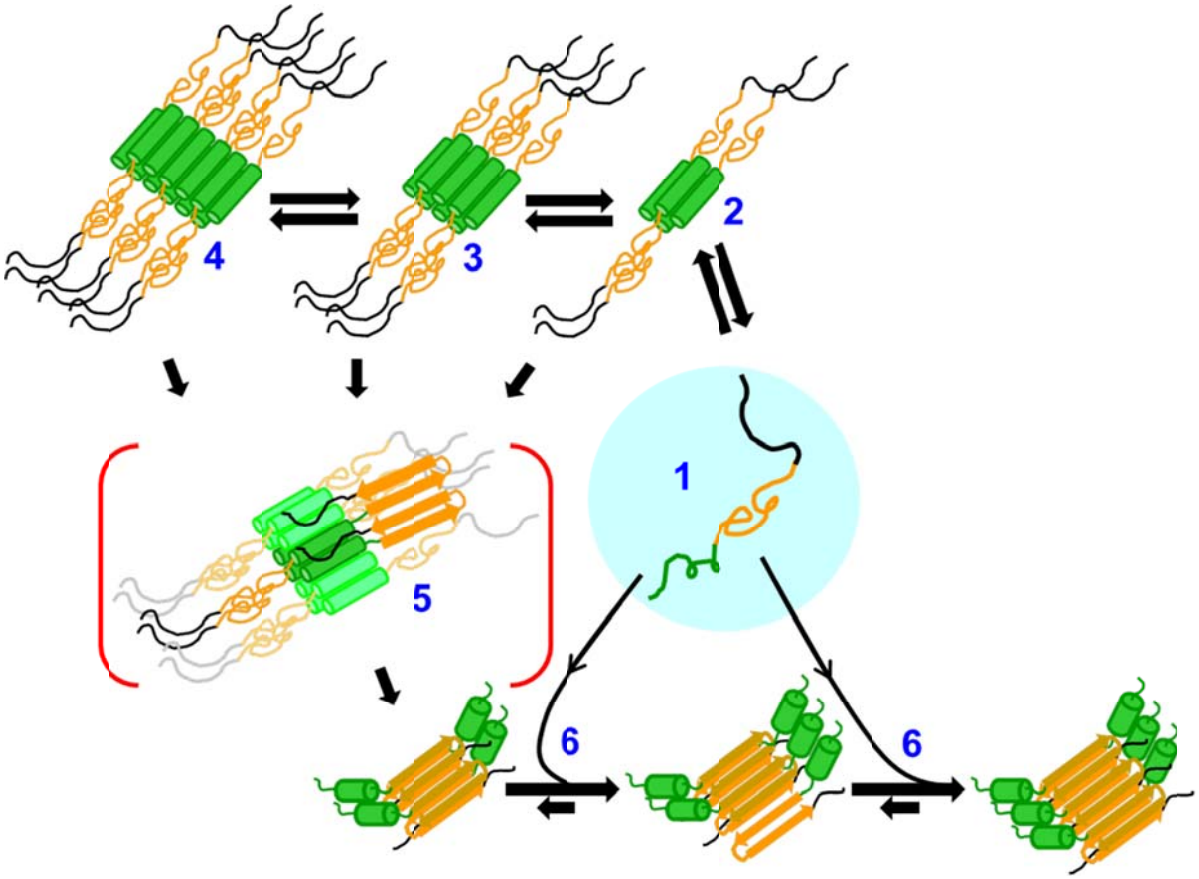

Figure 5-1: htt^{NT} mediated aggregation of polyQ containing htt fragments. PolyQ containing htt fragments lack any stable secondary structure in the monomeric state (1). Aggregation proceeds through the formation of tetrameric (2), octameric (3) ,do-decameric (4) and larger oligomeric species that are held together by a helical htt^{NT}. Each of these intermediates has some probability of nucleation (5), presumably dependent on the length of the adjoining polyQ segment. Post-nucleation aggregation proceeds through monomer addition (6) to form amyloid –like aggregates. Oligomers that do not undergo nucleation can dissociate to monomers to fuel elongation.

We have used a series of single point alanine and other functional mutations in assessing the importance of amphipathicity in the aggregation of polyQ containing htt fragments. Within this context, we have also determined the effects of some of the reported PTMs of htt^{NT} on aggregation kinetics and aggregate morphology. We have also used the data from our mutational analysis of polyQ containing htt fragments' oligomerization and aggregation in guiding *in silico* based modeling of the htt^{NT} mediated tetramer populated during aggregation and obtained a putative structure which could be a useful tool in future pharmacophore screening experiments.

5.3 RESULTS.

5.3.1 Effect of PTMs on aggregation.

In order to look at the effect of post-translational modifications on the aggregation of polyQ containing htt fragments, we used mutations that have been shown to chemically mimic a particular PTM. Thus, in order to mimic acetylation, we mutated lysines to glutamine while arginine mutations were used to mimic the modification –resistant state. Similarly, threonine was mutated to aspartate to mimic phosphorylation or alanine to mimic the alternate state. These studies were performed in the $htt^{NT}Q_{37}P_{10}K_2$ (F17W) background which exhibits aggregation properties similar to the huntingtin exon-1 (B.Sahoo *et al*, unpublished). The use of chemically synthesized peptides allows us to not only to study modification-mimicking mutations (similar to ones studied by cell biologists) but also look at the effect of the actual chemical modifications on aggregation properties.

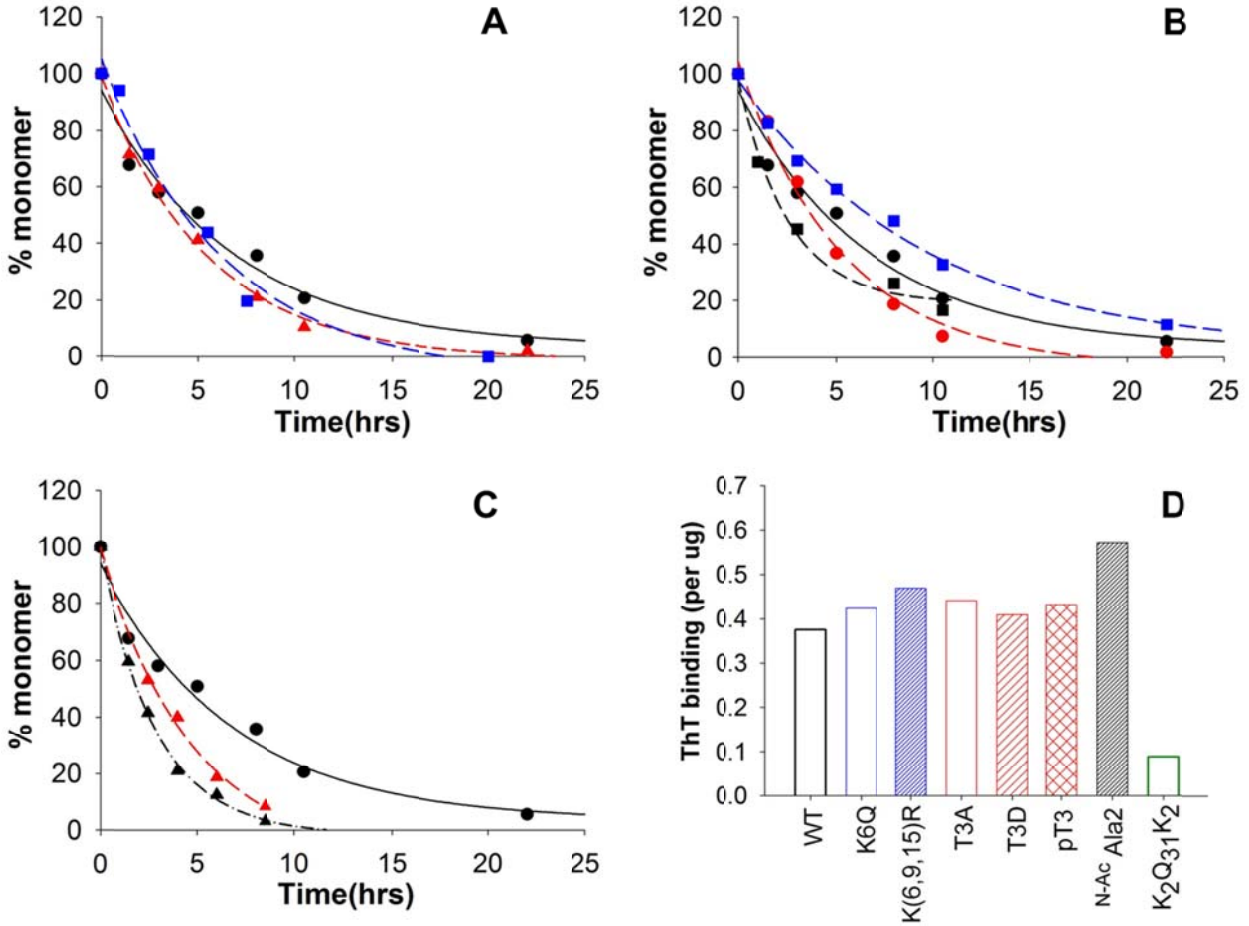

Figure 5-2: Effect of PTMs on aggregation. Effect of PTMs on the aggregation kinetics of $htt^{NT}Q_{37}P_{10}K_2$ (F17W) peptides at ~15uM. (A) Aggregation of WT (●), des-Met (■) and N-Ac Ala2 (▲). (B) Aggregation of WT (●), T3D (●), pT3 (■) and T3A (■). (C) Aggregation of WT (●), K (6, 9, 15) R (▲) and K6Q (▲). (D) Relative ThT binding per µg of aggregates of surveyed PTMs.

We started by looking at the effect of cleavage at Met1 after translation on aggregation. A peptide sequence lacking methionine at position 1 (des-Met peptide) (Fig 5-2.A, ■) was seen to aggregate within the same time-frame (and with almost identical kinetics) as the corresponding wild-type (wt) sequence (Fig 5-2.A, ●). Furthermore, the final aggregate morphologies, as observed by electron microscopy, of the des-Met (Fig 5-3.B) and the WT peptide (Fig 5-3A)

were almost identical, displaying a characteristic network of amyloid fibril structures that we observe in our htt exon-1 models. We also confirmed that the acetylation of the N-terminus of the newly generated peptide upon methionine cleavage does not affect the aggregation kinetics (Fig 5-2.A, ▲) nor the final aggregate morphologies of polyQ containing htt fragments by EM (Fig 5-3.C). As an additional probe of aggregate morphology we looked at the ability of the final aggregates of these peptides to bind ThT, a property that can distinguish the aggregates formed by polyQ containing htt fragments and simple polyQ sequences. The ThT binding ability of the N-Ac Ala2 peptide was slightly greater than that of the WT though the difference is not as pronounced as that between the WT $htt^{NT}Q_{37}P_{10}K_2$ peptide and a $K_2Q_{31}K_2$ peptide (Fig 5-2.D). Since there is not much difference in the aggregation behavior of the des-Met peptide and that of the WT, we chose to maintain Met 1 in all our subsequent studies of PTMs.

Phosphorylation of the two serine residues has been shown to alter the aggregation of polyQ containing htt fragments (16). We thus assessed whether phosphorylation of the lone threonine residue, Thr3, has any effects on the aggregation kinetics of a $htt^{NT}Q_{37}P_{10}K_2$ peptide. The T3D mutation had previously been shown to reduce lethality and neurodegeneration in a drosophila model of HD (17). We did not observe any significant difference in the aggregation kinetics of the phosphomimetic T3D (Fig 5-2.B, ●) nor a peptide with phosphothreonine (pT3) (Fig 5-2.B, ■) compared to the WT. Similarly, the final aggregates formed by these peptides were similar to the WT peptide in terms of their ThT binding ability (Fig 5-2.D) and EM morphologies (Fig 5-3). As an additional control, we also examined the aggregation behavior of the non-modifiable T3A mutation but found no significant difference in the aggregation kinetics (Fig 5-2, ■), aggregate morphologies (Fig 5-3) nor ThT binding (Fig 5-2.D). In contrast, mutating the serine residues at positions 13 and 16 to aspartate or phosphoserine not only impairs

aggregation kinetics but also alters aggregate morphologies (Fig 5-3.H-J, Chapter 6) suggesting that the location of these modifications within htt^{NT} segment can have different consequences possibly due to different effects on biophysical properties.

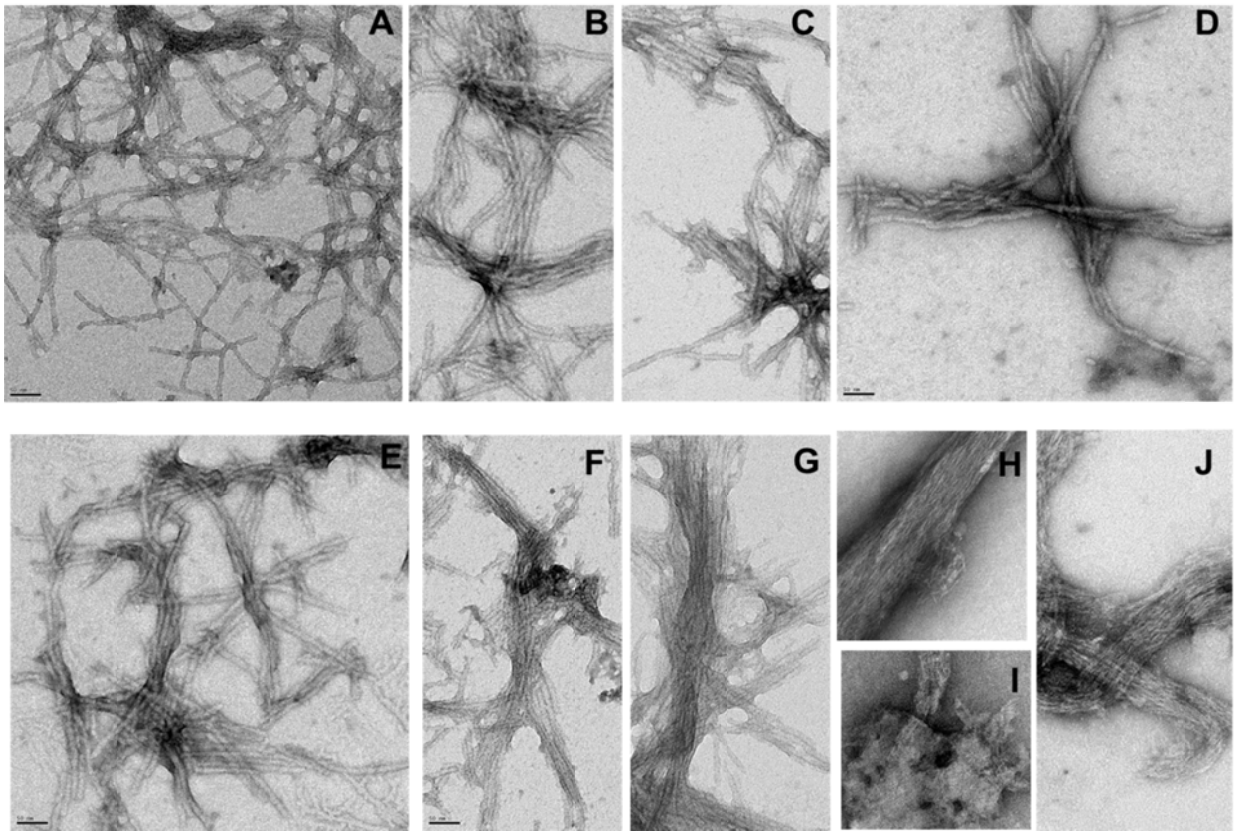

Figure 5-3: Effect of PTMs on aggregate morphologies. Final aggregate morphologies of different $htt^{NT}Q_{37}P_{10}K_2$ variants- WT (A), des-Met (B), N-Ac Ala2 (C), pT3 (D), T3D (E), K6Q (F), K (6, 9, 15) R (G), S13D/S16D (H-I) and S13p/S16p (J). All images were taken at the same magnification with the scale bar (i) representing 50nm.

Next we examined the effect of lysine acetylation on the aggregation of polyQ containing htt fragments. We started by looking at the effect of K6Q mutation (Fig 2c, ▲) which aggregated faster than the WT, consistent with the increase in hydrophobicity and loss of charge, forming aggregates that are similar to the WT in terms of their ThT binding and morphology. Next, we proceeded to investigate the effect of the K6, 9,15R mutation that mimics the modification

resistant states of lysine. Since lysine and arginine are both charged residues, we expected the aggregation kinetics of the K6, 9,15R mutation to be similar to that of the WT. We were thus surprised to observe that this mutation accelerated aggregation (Fig 5-2.C, ▲), as much as if not faster than, the K6Q mutation even though the final aggregate products are similar to the WT and K6Q peptides (Fig 5-3 and Fig 5-2.D) in morphology and ThT binding. Interestingly, a single point K-R mutation has also been observed to increase aggregation *in vivo* (156). Earlier, we had shown that mutations within htt^{NT} that alter hydrophobicity alter aggregation kinetics (31). However, the data discussed above suggest that in addition to changes in hydrophobicity, the position of these mutations within htt^{NT} also plays a role in aggregation. For instance, mutations that increase or decrease hydrophobicity of Thr3 do not seem to affect kinetics of aggregation by much whereas a single mutation at Lys6 that increases hydrophobicity slightly, increases aggregation substantially. One hypothesis for this sequence dependence of hydrophobicity is that mutations that affect aggregation do so by affecting amphipathicity (rather than net hydrophobicity) which is a property that is tied to htt^{NT}'s helical propensities. It is also possible that different parts of the helix might make different contributions to helical packing.

As described already in chapter 3, htt^{NT} displays a concentration dependent transition from a random coil conformation to an entirely helical conformation (presumably through the formation of tetramers and other species). Thus, mutations that change ampiphilicity should also change this concentration dependence of helicity within htt^{NT}, evinced by a change in the mid-point concentration of the random coil to helix transition in CD spectra. In order to test this hypothesis, we decided to look at the effect of the K6, 9,15R mutation on the concentration dependence of htt^{NT} helicity. Our choice of this mutation was dictated by its drastic effect on the aggregation kinetics and the overall conservative nature of this mutation. Consistent with the

observation of increased aggregation rates, the htt^{NT} (K6, 9, 15) R (—) mutation exhibited a characteristic helical conformation while an equivalent concentration of the WT htt^{NT} (—)sequence is mostly random-coil in nature (Fig 5-4.A). A detailed concentration dependence study indicated that the $C_{1/2}$ of the random coil to helix transition was 282μM for the K6, 9,15R mutation as compared to 430μM for the WT sequence (Fig 5-4.B).

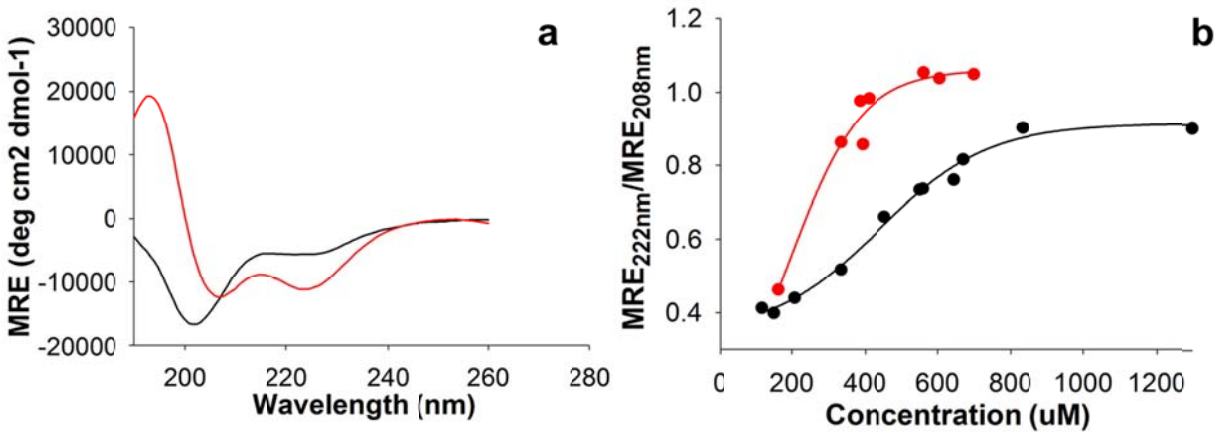

Figure 5-4: Effect of K (6, 9, 15)R on htt^{NT} oligomerization. (A) CD spectra of ~300μM of htt^{NT}Q (—) and htt^{NT} K(6, 9, 15)R (—). (B) Concentration dependence of CD spectra of htt^{NT}Q (●) and htt^{NT} K (6, 9, 15) R (●).

5.3.2 Alanine scan studies of polyQ containing htt fragments' aggregation.

5.3.2.1 Alanine scan studies of aggregation.

Our results with the post-translational modifications, especially the K6, 9,15R mutation highlight the role that ampiphilicity of the htt^{NT} sequence plays in the aggregation of polyQ containing htt fragments. In order to examine this in greater detail, we decided to conduct an alanine scan study of the htt^{NT} sequence. Thus, we mutated each of the fifteen non Ala residues

in htt^{NT} to alanine in the $htt^{NT}Q_{37}P_{10}K_2$ peptide background and assessed the effects of the mutations on aggregation kinetics and aggregate morphology.

The htt^{NT} sequence has three neutral, polar residues: the lone threonine residue at position 3 and the two serine residues at positions 13 and 16. Sedimentation analysis of aggregation indicates that the S16A (Fig 5-5.A, -○-) and the T3A (Fig 5-5.A, -■-) mutants aggregate similar to the WT (Fig 5-5.A, ●) sequence, aggregating to 50% within 4hrs and 3hrs respectively. On the other hand, the S13A mutant (Fig 5-5.A, -▲-) aggregates slightly faster than the WT sequence ($t_{1/2}$= 2.5hrs). An examination of the morphologies of the final aggregates formed by these mutants reveals the characteristic meshwork of fibril-like structures that characterize the WT sequence (Fig 5-3.A). Similarly, the ThT binding ability of the final aggregates of these mutants is similar to those of the WT (Fig 5-5.D).

Next we looked at the role of the charged residues (glutamate at positions 5 and 12 and lysines at positions 6, 9 and 15) in modulating polyQ containing htt fragment aggregation. We did not observe any major changes in the aggregation kinetics nor aggregate morphologies upon mutating glutamates at positions 5 (Fig 5-5.B, ● and Fig 5-6) and 12 (Fig 5-5.B, ○ and Fig 5-6) nor the lysines at position 9 (Fig 5-5.B, ▲ and Fig 5-6) or 15 (Fig 5-5.B, ■ and Fig 5-6). On the other hand, mutating the lysine at position 6 to alanine substantially enhances aggregation kinetics (Fig 5-5.B, ●), aggregating to 50% within 1.8 hrs though there is no visible change in the morphologies of the final aggregate products (Fig 5-6). The ThT binding abilities of the final aggregates of all mutations at charged residues were found to be more or less similar to those of the WT.

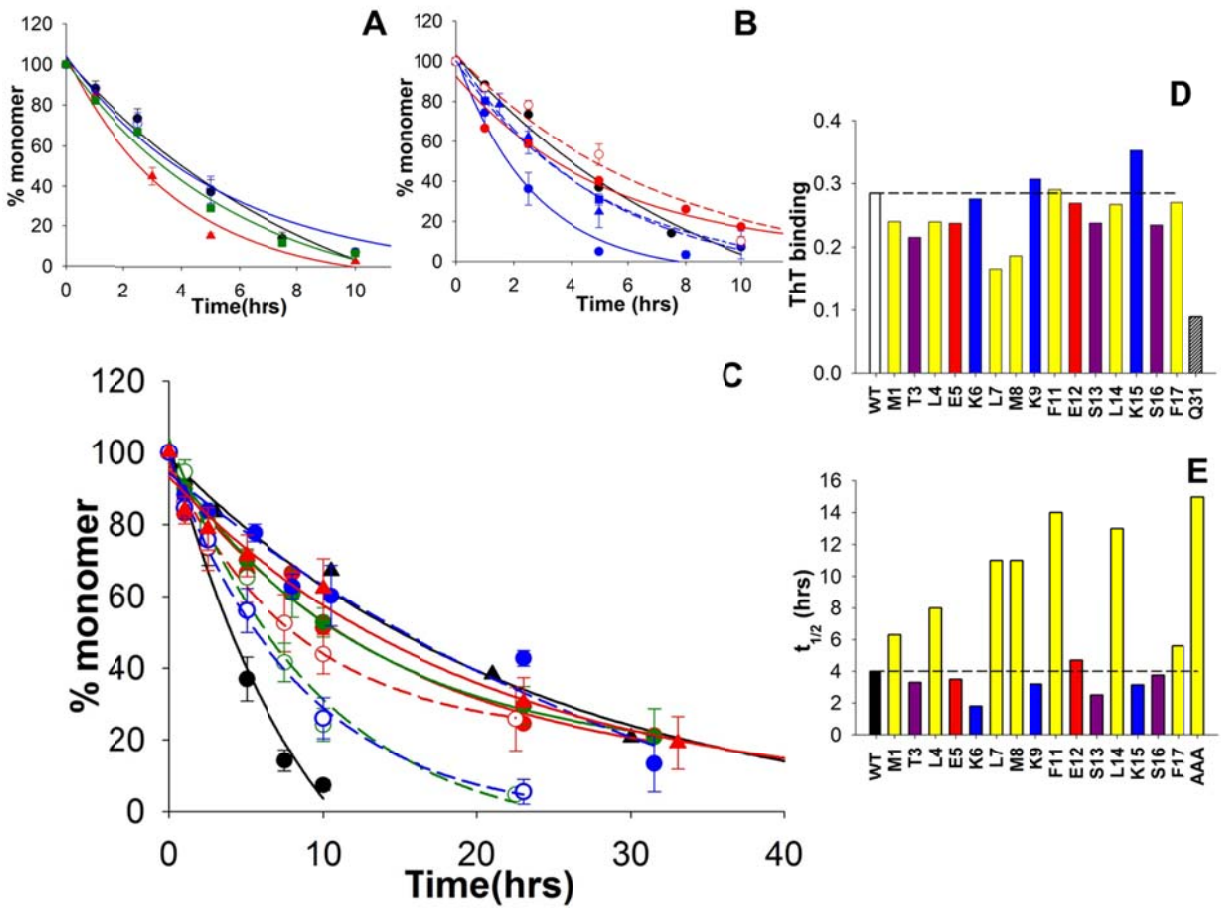

Figure 5-5: Effect of point alanine mutations within htt^{NT} on aggregation. Effect of alanine mutations on aggregation kinetics of ~ 20μM htt$^{NT}Q_{37}P_{10}K_2$ peptides. (A) Aggregation of WT (●), S13A (▲), S16A (○), T3A (■). (B) Aggregation of WT(●), K6A(●), K9A (▲), K15A (■), E5A (●) and E12A (○). (C) Aggregation of WT (●), M1A (○), L4A (○), L7A (●), M8A(●), F11A (●), L14A (▲), F17A (○) and M8A/F11A/F17A a.k.a AAA (▲) (D) Relative ThT binding abilities per μg of the final aggregates. (E) $t_{1/2}$ of aggregation of mutants.

The results mentioned here are contrary to those reported by Tam *et al* who had found that a E5A/K6A/K9A mutation reduces the aggregation yield of a GST-httQ51 variant by 50% (76). While the differences in results can be attributed to a difference in assays, or non-additive effects of using such multiple mutants, it is interesting to note that the initial aggregation kinetics

of this triple mutant are actually faster than the WT in their study which is consistent with the results presented here.

By far, the most dramatic effects on aggregation kinetics were observed upon mutating the hydrophobic residues into alanine which in each case reduced the kinetics of aggregate formation. In fact, a pattern can be identified in the effects of hydrophobic residues on aggregation. Thus, the inhibitory effect of mutating the hydrophobic residues to alanine increases gradually from M1A (Fig 5-5.C --○--) to L4A (Fig 5-5.C --○--) through L7A (Fig 5-5.C -●-) and M8A (Fig 5-5.C -●-) , before peaking at F11A (Fig 5-5.C -●-) and L14A (Fig 5-5.C -▲- and inset) and then dropping back to near WT level with the F17A mutation (Fig 5-5.C --○--). Interestingly, the aggregation kinetics of a triple alanine mutant M8A/F11A/F17A (Fig 5c, ▲, AAA in E) are almost identical to those of the F11A and L14A mutations and just marginally slower than the L7A, M8A mutants, suggesting that disruption of hydrophobic interactions at any of these positions is sufficient to reduce aggregation rates to similar extents.

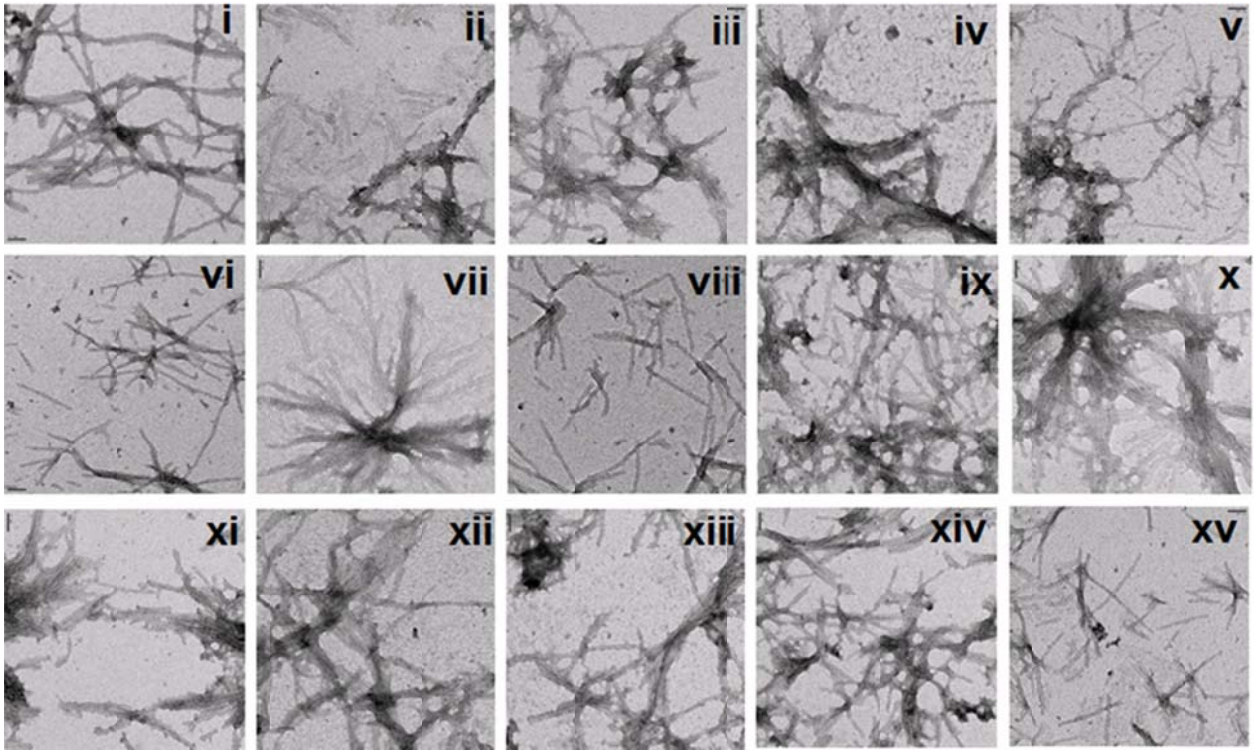

Figure 5-6: Morphologies of the final aggregates of htt$^{NT}Q_{37}P_{10}K_2$ peptides studied by EM. M1A (i), L4A (ii), E5A (iii), K6A (iv), L7A (v), M8A (vi), K9A (vii), F11A (viii), E12A (ix), S13A (x), L14A (xi),K15A (xii), S16A (xiii), F17A (xiv) and M8A/F11A/F17A (xv). All images were taken at the same magnification with the scale bar (i) representing 50nm.

These results suggest that residues between L4-L14 form the "helical core" within htt^{NT} and have the most pronounced effects on polyQ containing htt fragment aggregation. The ThT binding abilities of the final aggregates of these peptides were more or less similar to the WT though we did observe slightly lower ThT binding in the case of the L7A and M8A the significance of which (if any) is not entirely clear (Fig 5-5.D). We also looked at the final aggregate morphologies of these hydrophobic mutants and did not observe any drastic morphological differences compared to the WT (Fig 5-6).

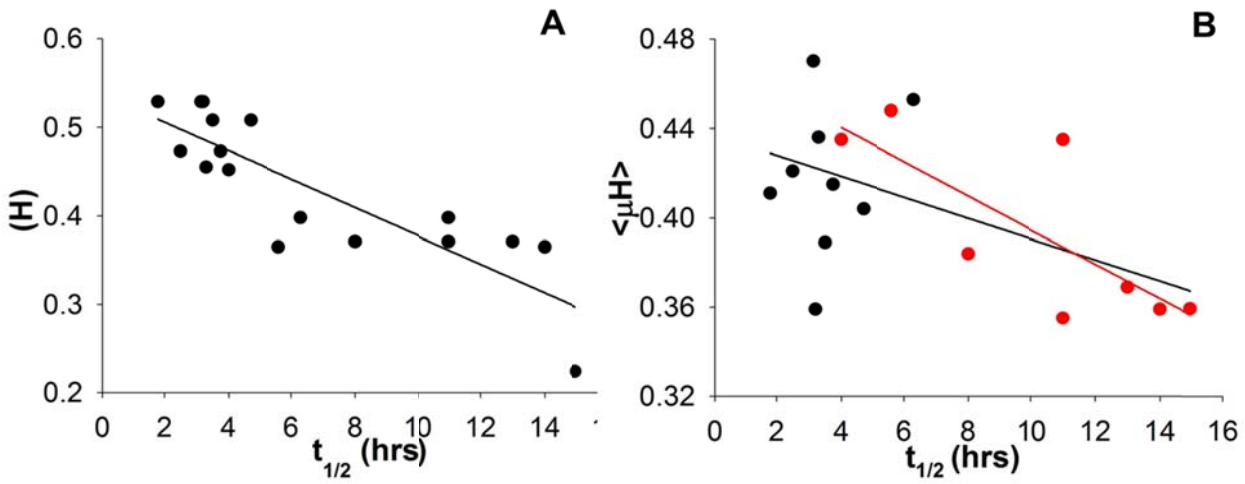

Figure 5-7: Contributions of hydrophobicity and ampiphilic helicity on polyQ containing htt fragment aggregation. (A) Plot of average hydrophobicity of the htt^{NT} sequence in different alanine mutants vs. t1/2 of aggregation of corresponding mutant in a $htt^{NT}Q_{37}P_{10}K_2$ peptide. (R^2 =0.72) (B) Plot of hydrophobic moment of the htt^{NT} sequence across all alanine mutants and the WT vs. $t_{1/2}$ of aggregation in the corresponding $htt^{NT}Q_{37}P_{10}K_2$ peptides (—, R^2=0.3). The hydrophobic mutations and the WT are shown in red. A separate fit of only hydrophobic residues and the WT (—) gave a correlation with a R^2 of 0.6.

Overall, the data above seems to suggest that hydrophobicity plays a crucial role in the htt^{NT} mediated aggregation of polyQ containing htt fragments. A plot of the $t_{1/2}$ of aggregation vs. the average hydrophobicity (H) of the htt^{NT} sequence in the corresponding mutants (Fig 5-7.A) gives a linear correlation with a R^2 of 0.73. However, a cursory examination of the data presented above also highlights the importance of sequence context especially in the case of the hydrophobic residues. Thus while M1A and F17A aggregate marginally slower than WT, such inhibitory effect is much more pronounced in the case of the M8A and F11A mutation. In order to explore these minutiae further, we decided to look at the changes in the ampiphilicity upon

making these mutations (based on a determination of the hydrophobic moments, <μH>). A plot of the <μH> vs $t_{1/2}$ of aggregation of all alanine mutants did not display any correlation (R^2 =0.3) (Fig 5-7.B, ▬) though a plot of the <μH> vs $t_{1/2}$ of aggregation of just the hydrophobic mutations gave a correlation (R^2=0.6) (Fig 5-7.B, ▬) that almost matches that between $t_{1/2}$ and net hydrophobicity. Based on the analysis described above and the results from the PTMs, a picture begins to emerge that suggests that amphipathicity (arising out of a helical htt^{NT} sequence) within htt^{NT} drives the aggregation of polyQ containing htt fragments with the hydrophobic residues as the major drivers. We thus decided to explore in details how amphipathicity might affect the different stages of the aggregation pathway shown in Figure 1.

5.3.2.2 Ampiphilicity in the monomeric ensemble.

It is possible that the effects of the alanine mutations described here on aggregation are exerted via a change in the monomer conformation. In order to test this, we first assessed the effect of some of these mutations on the monomeric conformational ensemble. Thus, after disaggregation, peptides were filtered through a 20nm syringe filter before CD sampling to ensure that the results of the analysis are not complicated by the presence of oligomeric species (Fig 5-8). Except for the K9A (- -) peptide which had slightly more helical character, all the peptides surveyed displayed typically random coil spectra with some hint of helical propensity as has been reported before. This point is also reinforced by looking at the ratios of mean residue ellipticities at 222nm and 208 nm (Fig 5-8, insets) which is often used to characterize helicity (for a helical peptide, this ratio is ~0.86 or greater). Even though we looked at only nine of the fifteen Ala mutants, the mutations studied here span the region from Leu4-Phe11 that was observed to be helical in ss NMR studies of final aggregates and that can be argued to constitute the "helical core" of the htt^{NT} sequence. In the monomeric state, polyQ containing htt fragments

are believed to sample helical conformations transiently (31). Thus, it is theoretically possible that loss of amphipathicity can affect the monomeric ensemble by making even such transient sampling events unfavorable. Nevertheless, the data here suggests that none of the mutations studied here change the average conformational properties of polyQ containing htt fragments in the monomeric state.

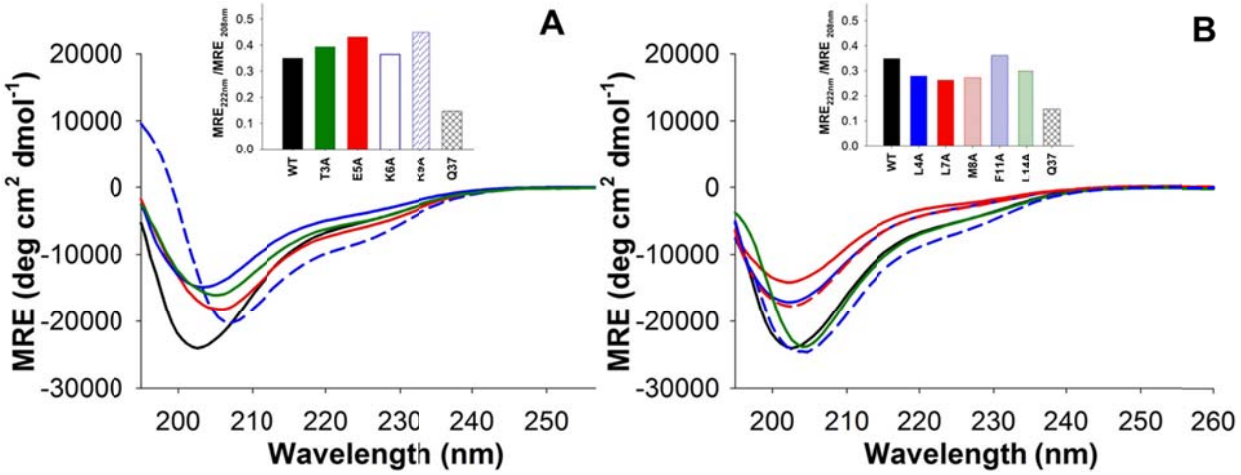

Figure 5-8: Effect of alanine mutants on monomeric conformation of htt^{NT}Q$_{37}$P$_{10}$K$_2$ peptides. (A) CD spectra of WT (—, 38μM), K6A (—, 45μM), K9A (- - -, 40μM), E5A (—, 22μM), T3A (—, 14μM). (B) CD spectra of WT (—, 38μM), L4A (—, 32μM), F11A (- - -, 28μM), L7A (—, 27μM), M8A (- - -, 32μM) and L14A (—, 40μM). (insets) Ratio of mean residue ellipticities at 222nm and 208nm for corresponding mutants including a Q$_{37}$P$_{10}$K$_2$ peptide for comparison.

5.3.2.3 Ampiphilicity drives htt^{NT} oligomerization.

Next, we examined whether the effects of these point Ala mutations can be explained on the basis of changes in the oligomerization stage of the aggregation pathway of polyQ containing htt fragments (Fig 5-1).

Since htt^{NT} can associate into α-helical oligomers (100, 136) but not β-sheet fibrils even after prolonged incubation at highest concentrations, this peptide context provides a nice way to

assess the effect of alanine mutants on the initial oligomer formation. As shown in Fig 5-9, at high concentrations (>~600μM), the htt^{NT} sequence displays a predominantly helical spectra (—). Thus, we first started by looking at the effect of the point alanine mutations on the helicity of htt^{NT} at high concentrations. We found that mutating the hydrophobic residues to alanine completely abrogated the formation of helical oligomers of htt^{NT} with these mutants exhibiting typical random coil spectra even at the highest concentrations studied with the exception of F17A which displays substantial helicity at concentrations higher than 1mM (Fig 5-10.C). These results are consistent with the notion that the hydrophobic residues form the interaction interface within the oligomers and hence mutating the hydrophobic residues destabilizes the association of htt^{NT} into helical assemblies.

All of the other mutations (Fig 5-9.A and 5-9.B) gave typically helical spectra under similar concentrations with the exception of the K9A mutation which yielded a seemingly helical spectrum with lower mean residue ellipticity values. It should be noted though that all our efforts to obtain higher concentrations of this mutant were futile because of considerable peptide loss in the preparatory centrifugation step, presumably as larger aggregates/oligomer.

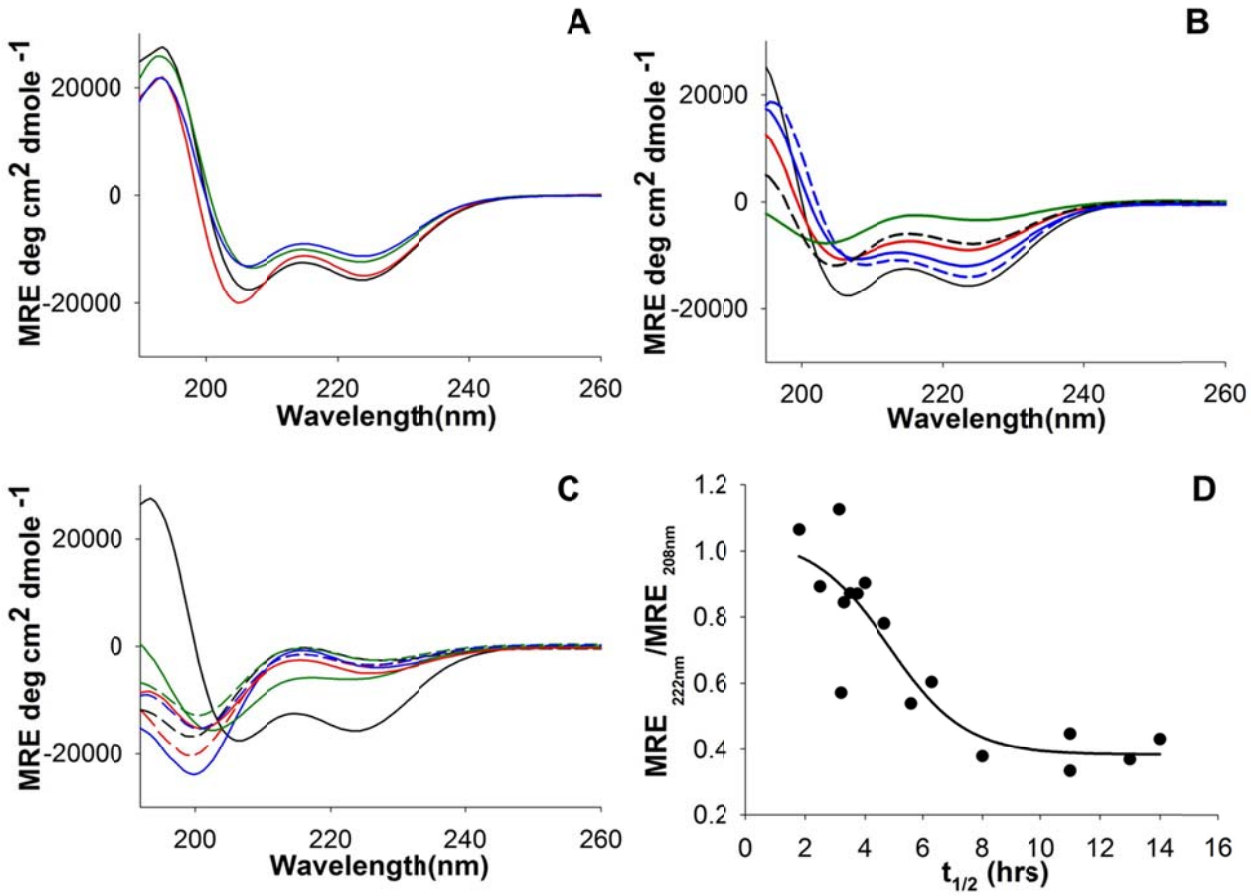

Figure 5-9: Role of amphipathicity in htt^{NT} oligomerization. CD spectra of ~ 1mM of different htt^{NT} peptides. (a) WT (—) , T3A (—), S13A (—), S16A (—). (b) WT (—), K6A(—), K9A(—), K15A (---), E5A (—) and E12A (---). (c) WT (—), M1A (—),L4A(—), L7A (---),M8A (---), L14A (---), F11A (---) and F17A (—). (d) A plot of ratio of mean residue ellipticities at 222nm and 208 nm of different alanine mutants vs. the $t_{1/2}$ of aggregation in corresponding htt$^{NT}Q_{37}P_{10}K_2$ peptides. (R^2= 0.8).

This also suggests that for this peptide, the lower MRE values might be due to scattering because of the presence of larger oligomeric species in the sample. A plot of the ratios of the mean residue ellipticities at 222nm and 208 nm (a proxy for helicity (191) of each alanine mutant vs the $t_{1/2}$ of aggregation of the same mutation in the htt$^{NT}Q_{37}P_{10}K_2$ background gave a strong correlation (R^2=0.8) when fit to a sigmoidal function (Fig 5-9.D). This correlation improves to a

robust $R^2$of 0.92 if the K9A mutation is not considered. Regardless of this nuance, the strong correlation suggests that the effects of alanine mutations on the aggregation of polyQ containing htt fragments are exerted primarily through htt^{NT} oligomerization.

In order to parse out subtle differences in the oligomerization ability of these different alanine mutants, we also decided to look at the concentration dependence of helicity of the alanine mutants (Appendix A, Fig A-3). To this end, we calculated the concentration ($C_{1/2}^{helix}$) at which the mid-point of the helical transition is reached for some of these mutations by plotting the ratio of molar ellipticities at 222nm and 208nm versus the concentration. The $C_{1/2}^{helix}$ provides us with some information regarding the comparative thermodynamics of oligomerization across these different mutations. As mentioned above, for the hydrophobic mutants even the highest concentrations gave characteristic random coil spectra and hence the $C_{1/2}^{helix}$ was assigned a value greater than the highest concentration studied. Amongst the other mutations, only the charged mutations K6A and E12A had any substantial effect on the helicity of htt^{NT}, with both of these mutations stabilizing helicity by reducing the $C_{1/2}^{helix}$. A plot of the $C_{1/2}^{helix}$ (Table 5-1) vs. the $t_{1/2}$ of aggregation gave a correlation of R^2=0.9 when fit to a sigmoidal function (Appendix A) similar to the results obtained in Fig 5-9.D

Peptide	**$C_{1/2}^{helix}$ [μM]**	***Peptide***	**$C_{1/2}^{helix}$ [μM]**
WT	432μM	K9A	n.d
M1A	>1012 μM	F11A	>1490 μM
T3A	460 μM	E12A	382 μM
L4A	>740 μM	S13A	614 μM
E5A	437 μM	L14A	1246 μM
K6A	330 μM	K15A	638 μM
L7A	>1105 μM	S16A	525 μM
M8A	>1015 μM	F17A	871 μM

Table 5-1: Mid-point concentrations of coil-helix transition of htt^{NT} mutants. Data used in the calculation of mid-points is shown in Appendix A.

In addition to CD studies of the effects of alanine mutations on htt^{NT} mediated oligomerization, we also looked at the effect of a couple of hydrophobic mutations, L4A and M8A, on the oligomerization kinetics and oligomer structure of htt^{NT}Q3 peptides (Appendix A, Fig A-1). Consistent with the results described above, mutating these hydrophobic residues to alanine was observed to disfavor oligomerization.

5.3.2.4 Role of amphipathic helicity in nucleation.

The results from our studies of alanine mutants in the htt^{NT} background showed that amphipathic helicity plays a crucial role in the initial htt^{NT} mediated oligomerization stage of the aggregation pathway. However even mutating the hydrophobic residues that completely destabilize helicity in a htt^{NT} background (L4A, M8A, F11A, L14A) does not abrogate aggregation in the $htt^{NT}Q_{37}P_{10}K_2$ background suggesting that either *a.* these mutations can still aggregate through the normal pathway (i.e through stochastic nucleation within oligomerization) albeit less efficiently or *b.* These peptides aggregate through a different pathway.

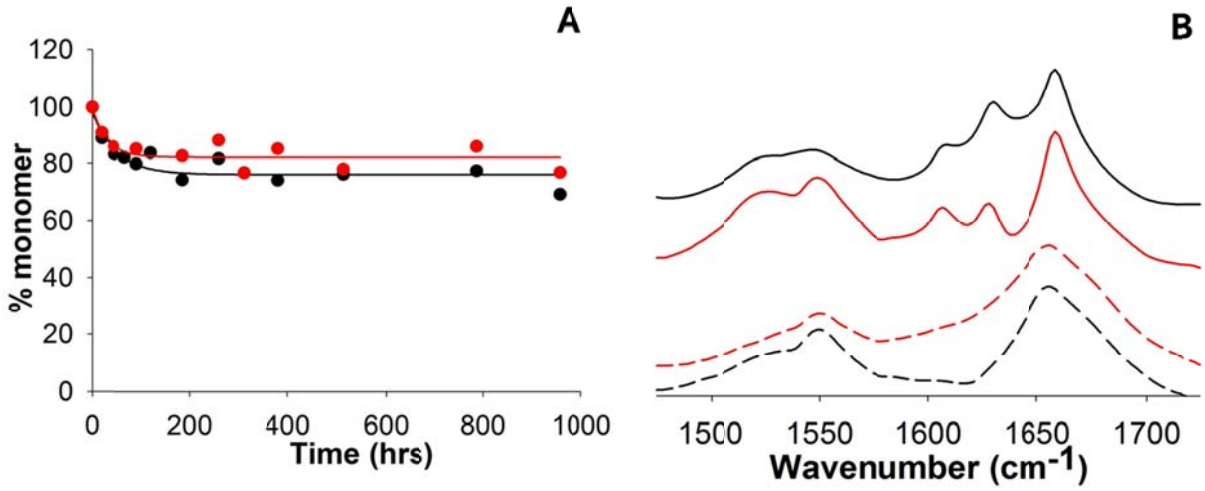

Figure 5-10:Nucleation/Elongation in $htt^{NT}Q_8K_2$ peptides. (A) Aggregation of WT (●) and M8A(●) mutants. (B) FTIR spectra of isolated aggregates. Early aggregates of WT (---) and M8A (---) and end-stage aggregation products of WT (—) and M8A (—).

Earlier we had shown that pelletable aggregates isolated from a htt^{NT}-Q_8K_2 peptide display a transition from helical oligomers (in the early stages) to β sheet aggregates with ordered Gln side chains (Fig 5-10) (100). We adapted the htt^{NT}-Q_8 K_2 system to assess whether the M8A mutation that abrogates helicity in a htt^{NT} sequence and impairs aggregation in a

$htt^{NT}Q_{37}P_{10}K_2$ sequence displays the same transition from helical oligomer to ordered β-sheet aggregates. The early aggregates of M8A are helical oligomers (Fig 5-10.B, --) that over time mature into β-sheet aggregates (Fig 5-10.B, —) with ordered Gln side chains. Furthermore, both the WT (Fig 5-10.A, ●) and the M8A (Fig 5-10.A, ●) peptides aggregate to almost the same extent suggesting that there is not much difference in the net efficiency of nucleation/elongation between these peptides. Thus, it seems unlikely that alanine mutants that impair oligomerization and by extension aggregation, aggregate via any alternate pathway. The observation that the M8A mutation is incapable of helical oligomer formation in a htt^{NT} background but can do so in a htt^{NT}-Q_8 K_2 peptide points to a potential effect of glutamines on the thermodynamics of htt^{NT} mediated oligomerization, a hypothesis that is tested in detail in Chapter 7.

5.3.2.5 Studies of the helix disrupting M8P mutation.

The M8P mutation has been shown to almost entirely abrogate helical propensities in a htt^{NT} sequence (29). Furthermore, the M8P mutation in a 1-171 htt fragment with 128 glutamines was observed to be substantially more toxic than the control despite the lack of large inclusions in the cells as were observed with the WT. Other studies have also found that the M8P mutation in cells expressing htt exon-1 to completely disrupt aggregation (156).We thus decided to utilize the M8P mutation in our studies of polyQ containing htt fragments' aggregation.

5.3.2.6 M8P mutation impairs formation of htt^{NT} oligomers.

We first looked at the effects of the M8P mutation on the ability of a htt^{NT}Q3 construct to form helical oligomers. Thus, while pelleted oligomers of WT htt^{NT}-Q_3 display a predominantly α-helical FTIR spectrum (Appendix A, Fig A-1, —), the M8P mutant grown under similar conditions formed oligomers (Fig A-1,- - -) that show a broad FTIR Amide I spectra with a

mean position of 1640cm-1 which is characteristic of random coil structures. While the broadness of the Amide I peak could indicate the presence of different structural subtypes within the oligomers, overall the data suggests that the M8P mutant, unlike the WT, does not form helical oligomers.

5.3.2.7 M8P mutation impairs aggregation.

Next, we examined the effect of the M8P mutation on the aggregation of a $htt^{NT}Q_{37}P_{10}K_2$ peptide (Fig 5-11). We observed the M8P mutant (●) to aggregate considerably slower than the WT peptide (●). The aggregation kinetics of the M8A mutation (○) in the same peptide background (Fig 5-5) is intermediate between that of the WT and the M8P mutation suggesting that a good portion of the inhibitory effects of the M8P mutation can be explained based on a general reduction in side-chain hydrophobicity. The rest of the rate differences between WT and M8P is most likely attributable to the loss of the backbone conformation. Even though the aggregation rate is impaired in the M8P mutation, it is still much faster than an equivalent concentration of a MF-$Q_{37}P_{10}K_2$ peptide (○) that lacks the majority of the htt^{NT} peptide suggesting that despite the loss of helicity (upon mutating the Met to Pro), the net hydrophobicity of the htt^{NT} segment still plays a role in polyQ containing htt fragment aggregation. Interestingly, the morphology of the final aggregates of the M8P mutation are typically shorter than mature fibrils (Fig 5-11.C-F), and look more like intermediate aggregates observed on the polyQ containing htt fragment aggregation pathway suggesting that the properties of these aggregates might be different than those of the WT. As a positive control, we also looked at the aggregation of a peptide with a proline residue inserted between the htt^{NT} and the $Q_{37}P_{10}K_2$ domains (referred to here as the Q0P mutant). The addition of this mutation does not affect aggregation as both the Q0P (●) and the WT (●) peptide have similar aggregation profiles. The final aggregates of the

Q0P mutant (Fig 5-11.G) resemble those of the WT (Fig 5-3.A), displaying the characteristic meshwork of long, and amyloid-like fibrils.

5.3.2.8 M8P alters initial aggregation rates.

As was described before, one of the major differences between the aggregation of simple polyQ (or polyQ-polyPro) sequences and that polyQ containing htt fragments lies in the concentration dependence of initial aggregation. One explanation for this difference could be that this difference is linked to the helicity in the htt^{NT} which is responsible for oligomerization. Thus, the M8P mutation which impairs helicity and oligomerization might be expected to exhibit a concentration dependence that is more in-line with that of simple polyQ peptide. We thus looked at the concentration dependence of the initial aggregation rates (refer experimental methods for a detailed analysis of the model) of the WT, Q0P and M8P mutants in the $htt^{NT}Q_{37}P_{10}K_2$ background (Fig 5-11.B). Both the WT (●) and the Q0P (●) display log-log slopes of ~1 as has been reported for polyQ containing htt fragments (31). On the other hand, the M8P mutant (●) gave a slope of 3.46 consistent with the concentration dependence of a $K_2Q_{37}P_{10}K_2$ peptide that has been reported to give a slope of 3 (122) and the $shtt^{(Amyl)+}Q_{30}P_6K_2$ peptide (Chapter 4) that has a slope of 3.3 (Fig 5-11.B, ♦). Thus, while the M8P mutation stimulates aggregation compared to the $MFQ_{37}P_{10}K_2$ peptide (Fig 5-11), this peptide nonetheless undergoes nucleation of aggregation by a mechanism that does not involve htt^{NT} mediated oligomerization similar to the $shtt^{(Amyl)+}Q_{30}P_6K_2$.

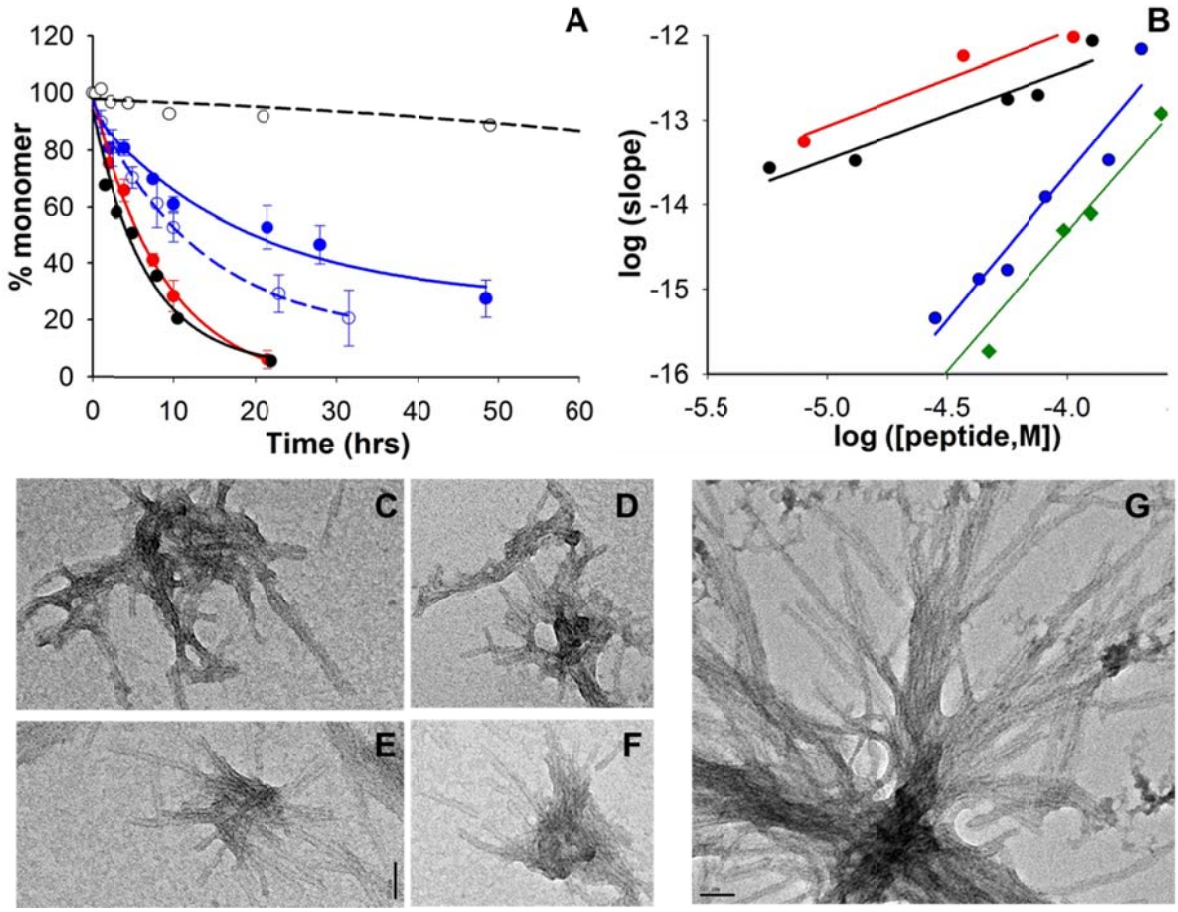

Figure 5-11: Effect of helix-breaking M8P mutation on htt^{NT}Q$_{37}$P$_{10}$K$_2$ aggregation. (A) Aggregation kinetics of WT (15µM, ●), Q0P (15µM, ●), M8P (12µM, ●), M8A (20µM, ○) and MF-Q$_{37}$P$_{10}$K$_2$ (10µM, ○) peptides. (B) Concentration dependence of early aggregation kinetics. WT (●, R2= 0.92, slope =1.1), M8P (● R^2=0.93, slope = 3.46) and Q0P (●, R^2=0.95, slope =1.11). Also shown for reference is the data for the shtt$^{(Amyl)+}$Q$_{30}$P$_6$K$_2$ peptide (♦). Morphologies of final aggregates of M8P (C-F) and Q0P (G) studied by EM.

5.3.2.9 M8P aggregates have altered properties.

Though the M8P mutation impairs oligomerization of htt^{NT}, it does not abrogate aggregation. EM studies of the M8P mutant showed that it forms shorter fibrillar intermediates

unlike the meshwork of amyloid fibrils observed in the WT and the Q0P constructs. We thus chose to investigate any differences in the aggregate properties of the M8P mutant from the WT.

We first looked at the accessibility of M8P aggregates to cleavage by trypsin. The htt^{NT} sequence has three trypsin cut-sites at K6, K9 and K15. Such trypsin accessibility experiments are useful tools, though of a lesser resolution, in elucidating structural features of aggregates (Fig 5-12.A). As has been reported before (31), the htt^{NT} sequence in the final aggregates of polyQ containing htt fragment peptides are resistant to proteolysis. Thus, a WT $htt^{NT}Q_{37}P_{10}K_2$ sequence gets cleaved by only about 10% (—). On the other hand, a M8P mutation in the same peptide background is cleaved to a much greater extent, ~31% under similar conditions (—). Analysis of the mass of the cleaved peptide indicates that the major scission event occurs at Lys 9 in the M8P mutant. These results are consistent with the helix-breaking property of the proline mutation at Met 8 which would be expected to increase the accessibility of the adjacent Lys 9 residue to trypsin.

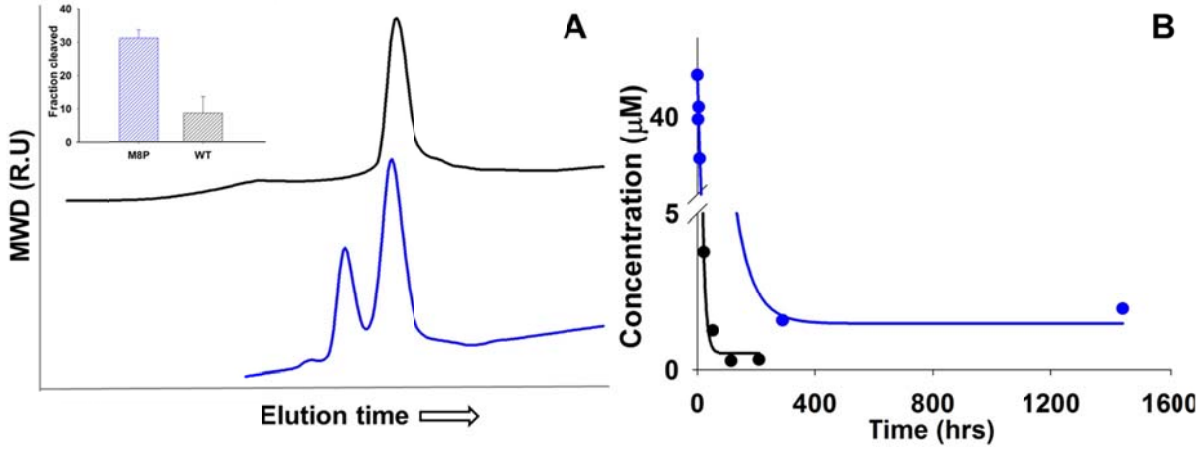

Figure 5-12: Effect of M8P mutation on aggregate properties. Characterization of aggregates of WT (—) and M8P (—). (A) Susceptibility of aggregates to trypsin. Shown is the LC-MS chromatogram of the cleaved aggregates with the fraction cleaved calculated and plotted (inset). (B) Forward aggregation reactions for critical concentration calculations.

The critical concentration of aggregation is another useful parameter to compare the relative stabilities of different aggregates. By definition, the critical concentration is the concentration of monomer in equilibrium with the aggregates towards the end of an aggregation reaction. In other words, the higher the critical concentration, the greater the instability of the aggregates. We thus measured the critical concentrations of aggregation for the WT and the M8P mutant (Fig 5-12.B).While the WT $htt^{NT}Q_{37}P_{10}K_2$ aggregates to a critical concentration of ~0.3-0.4μM (▬), the M8P mutation was observed to aggregate to ~1.5μM (▬). Based on the calculated critical concentration, the destabilization in the free energy of elongation upon mutation, $\Delta\Delta G_{M8P}^{elong}$ would be ~ 1 kcal/mol. It is worth mentioning that other mutations within htt^{NT} have been known to destabilize aggregation to a greater extent (Chapter 6).

5.3.3 Modeling a htt^{NT} tetramer structure

As was described earlier, the oligomerization of polyQ containing htt fragments proceeds through the formation of a tetrameric species held together by interactions within htt^{NT}. A structure of this tetrameric species would not only facilitate a better understanding of the disease but could also have drug-screening potential as a viable target. We thus decided to utilize the experimental data that we had obtained from the different mutations described in this chapter in conjunction with protein-protein docking to model the htt^{NT} tetrameric species. Our goal in this study was to obtain a preliminary structure that can form the basis to future experiments.

Chapter 3 describes the methodology that we adopted to determine a putative structure of the htt^{NT} tetramer. Briefly, the previously reported X-ray structure of a polyQ containing htt fragment was used to model the starting structure of the htt^{NT} monomer.

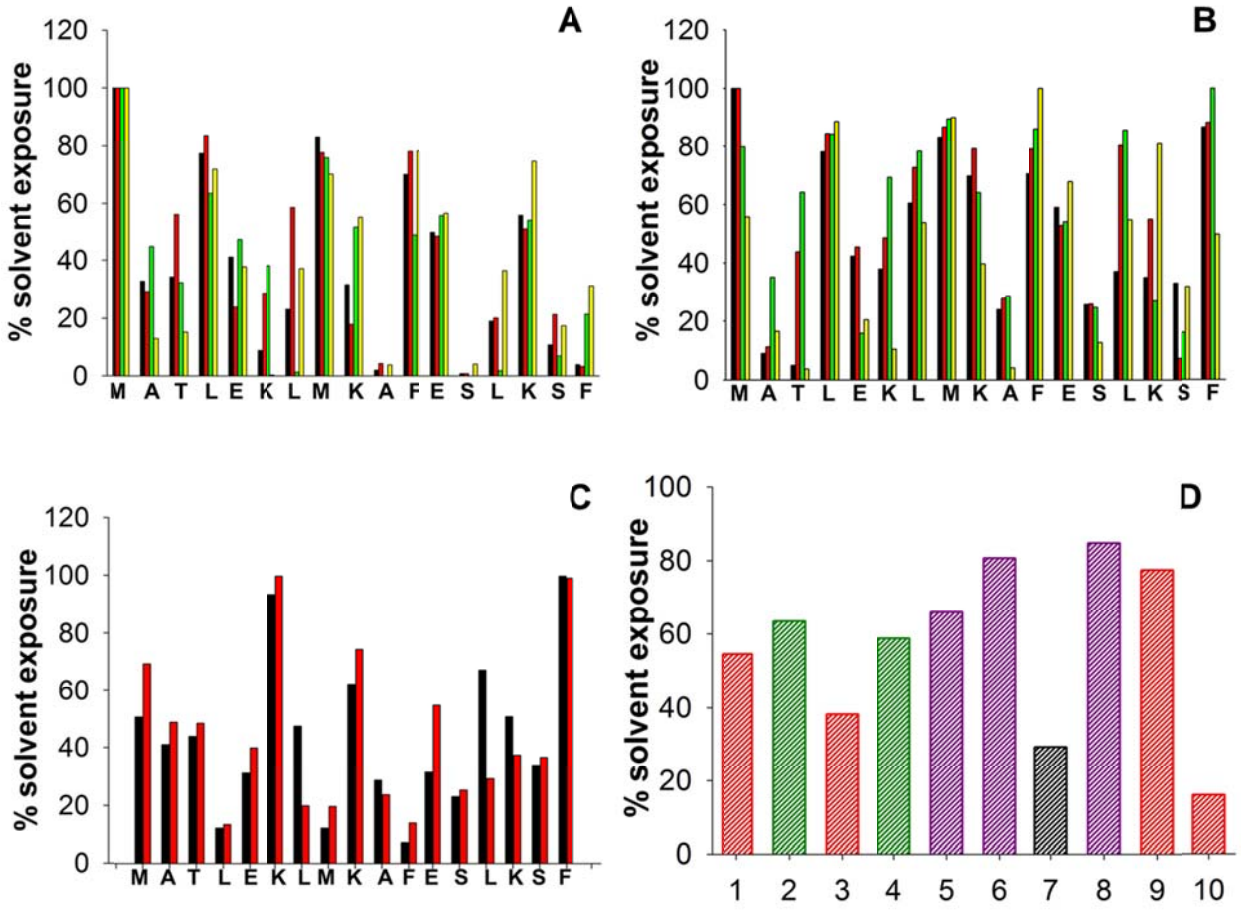

Figure 5-13: Side-chain solvent accessibilities of initial docked structures. (a) Solvent exposure of side-chains in model numbers: 1(—), 2(—), 3(—) and 4(—). (b) Solvent exposure of side-chains in model numbers: 5(—), 6(—), 8(—) and 9(—). (c) Solvent exposure of side-chains in model numbers: 7 (—) and 10 (—). Reported side-chain accessibilities for each position are averaged over all the four chains of the tetramer. (d) Average side-chain exposure of residues Leu4, Leu 7, Met 8, Phe 11 and Leu 14 which constitute the putative helical core in htt^{NT} plotted for all the ten models. Color scheme: Anti-parallel arrangements (red), parallel arrangements (black), other arrangements (purple) and irregular structures (green).

This was then submitted to ClusPro and 10 docking models were obtained. Next, we calculated the side-chain exposure of each residue in all models (Fig 5-13.A-C). Since the hydrophobic residues are known to be involved in the formation of the tetramer, the argument can be made that models that have the hydrophobic side-chains most buried are probably the best representations of the tetrameric structure.

Thus, we calculated the average side-chain accessibility of the hydrophobic residues in the "helical core" within htt^{NT} (Fig 5-13.D) across all the ten models to identify models 7 and 10 as the two best representations. The major difference between these two models is that while model 7 had the four helices arranged in a parallel fashion (Fig 5-14.B), model 10 had them in an anti-parallel configuration (Fig 5-14.A).

Next, we made *in silico* mutations at each position within htt^{NT} across all the four chains in the tetrameric structures obtained from model 7 and model 10. Each of these structures thus obtained were then minimized locally at the site of the mutation and the energy of the complex determined by summing the electrostatics and de-solvation energy components obtained from the FastContact analysis and this energy term was used to calculate the ΔE_{tot}^{mut} for each mutant. In addition to the point alanine mutants, we also repeated the above procedure for the K (6, 9, 15) R mutant. To test whether the tetramers from model 7/model 10 had any relevance to our experimental system, we computed a. the correlation between the ΔE_{tot}^{mut} and the $t_{1/2}$ of aggregation and b. the correlation between $\Delta E_{tot}^{mut}{}_{t}$ and the ratio of mean residue ellipticities at 222nm/208 nm (Fig 5-15).

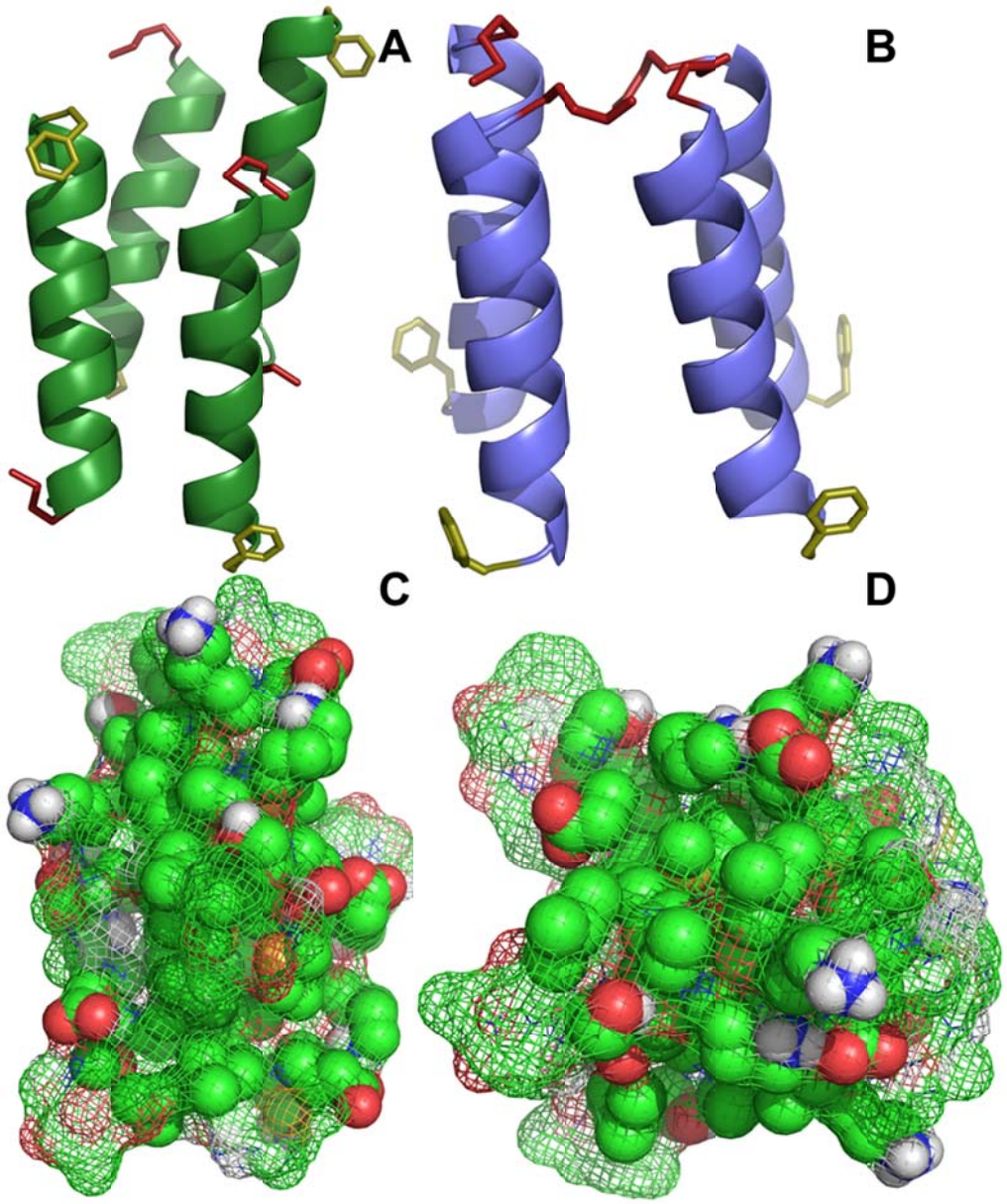

Figure 5-14: Structures of tetramers chosen for in silico mutagenesis. Backbone representations of model 10 (A) and model 7 (B). The side-chains of Met 1 and Phe 17 are shown in red and olive respectively. Both structures have a buried hydrophobic core. Shown is a mesh representation of the tetrameric structures with the side –chains of the helical core (residues Leu4-Leu 14) shown as spheres for model 10 (C) and model 7 (D).

We did not find any correlation between ΔE_{tot}^{mut} and $t_{1/2}$ of aggregation nor ΔE_{tot}^{mut} and ratio of molar ellipticities in the case of model 7 (Fig 5-15.A,B). On the other hand, with model 10 we saw a pretty strong correlation between ΔE_{tot}^{mut} and ratio of molar ellipticities (Fig 5-15.D, $R^2 = 0.7$) and a weak correlation between ΔE_{tot}^{mut} and $t_{1/2}$ of aggregation (Fig 5-15.C, $R^2 = 0.5$).

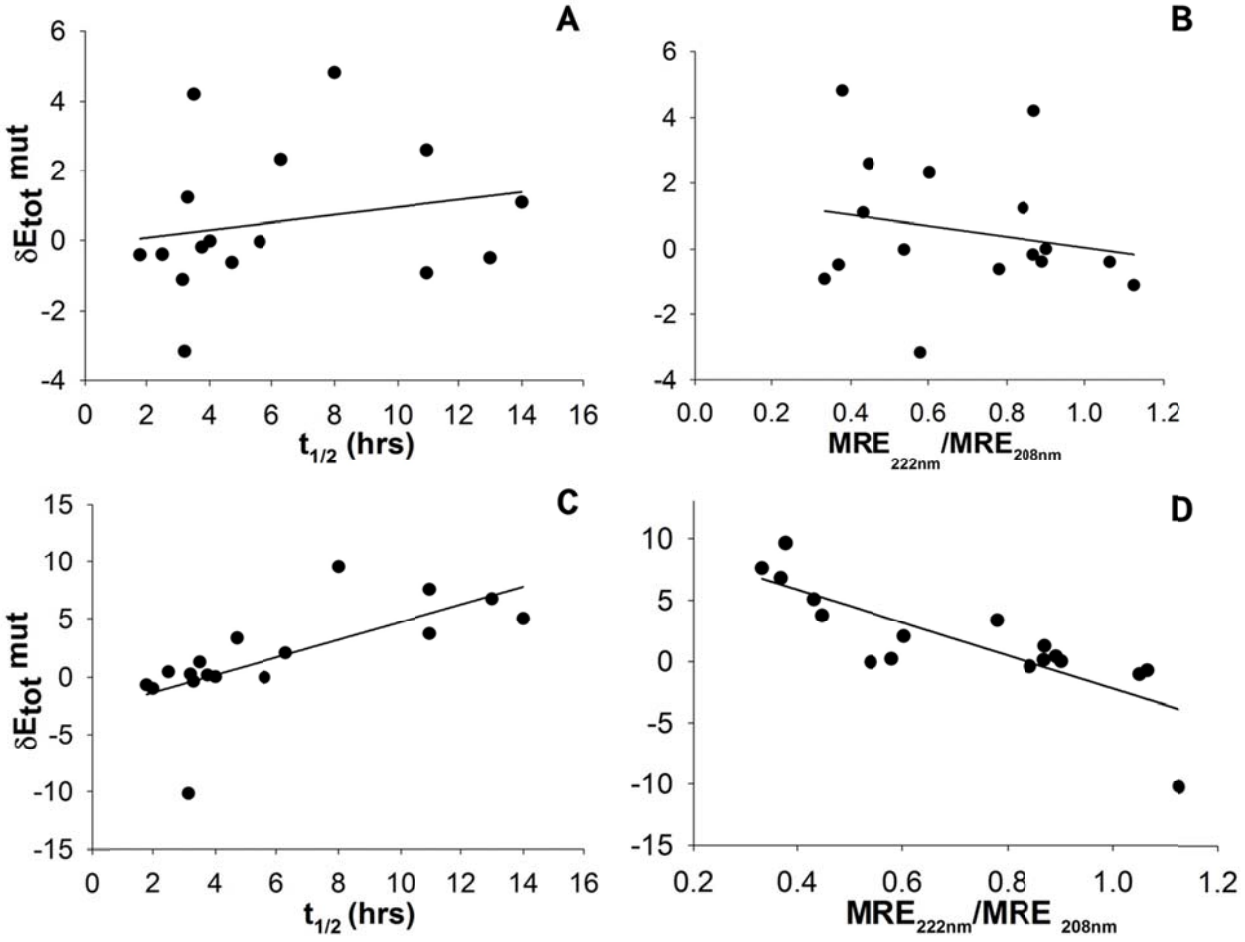

Figure 5-15: Validation of docking results. Computed ΔE_{tot}^{mut} were plotted against $t_{1/2}$ of aggregation (model 7: (A) R^2=0.04; model 10: (C) R^2=0.5) for corresponding $htt^{NT}Q_{37}P_{10}K_2$ peptides and against the ratio of molar ellipticities at 222nm and 208 nm (model 7 : (B) R^2=0.04; model 10: (D) R^2=0.7) for corresponding htt^{NT} peptide.

Since the $t_{1/2}$ of aggregation can also be influenced by other mechanistic features of polyQ containing htt fragments' aggregation, in addition to tetramer formation (viz. stochastic nucleation, fibril stabilities etc.), one can rationalize such a weak correlation. However, this analysis clearly suggests that model 10 is a more accurate representation of the tetramer structure than model 7. It is imperative to point out that the structures reported here are preliminary and will have to be refined for a more accurate model. The refinement strategy would include getting distance constraints and/or adding more mutations to the dataset. Notwithstanding these limitations of accuracy, the structure of the tetramer proposed here should still be useful for guiding experimental design and for *in silico* drug screening. In fact, testing the pharmacophores identified using the structure above, for their ability to impair aggregation *in vitro* would be an additional test of the accuracy of the structure.

5.4 DISCUSSION.

The goal of this study was to identify the driving forces and the sequence determinants underlying the htt^{NT} mediated aggregation pathway of polyQ containing htt fragments. To this end, we designed a series of mutations within htt^{NT} and assessed their effects on the different stages of polyQ containing htt fragment aggregation. First, we assessed the effects of some of the PTMs in htt^{NT} on the kinetics of aggregation and the morphologies of the final aggregates. Amongst the PTMs surveyed, we did not find any major effects on polyQ containing htt fragments' aggregation though there were subtle effects on the aggregation kinetics which correlated with a change in hydrophobicity. The results of our alanine scan mutagenesis studies

of the htt^{NT} sequence identified the hydrophobic residues in the region between Leu 4-Leu 14 to be the major drivers of aggregation. Mutating any of the hydrophobic residues within this region to alanine substantially impaired aggregation kinetics (Fig 5-5.C) though it did not abrogate aggregation nor alter drastically the morphology of the aggregates. On the other hand, mutating the polar or charged residues did not alter the aggregation kinetics by much except in the case of the K6A mutation which substantially accelerated aggregation (Fig 5-5.A and 5-5.B). While superficially the results described here might suggest that average hydrophobicity is the major driving force of polyQ containing htt fragment aggregation, the sequence-position dependence of the aggregation rates of chemically identical mutations suggests otherwise. Thus peptides M1A and M8A, F11A and F17A and K6A and K9A/K15A while being similar in terms of net hydrophobicity have substantially different aggregation kinetics.

The role of helicity within the htt^{NT} sequence in mediating polyQ containing htt fragment aggregation has received considerable attention. The observation that htt^{NT} retains its helical character in the oligomers and in the final fibrils formed during/after polyQ containing htt fragments' aggregation underscore the importance of helicity in htt^{NT} mediated aggregation. It also provides an explanation for the sequence dependent effect of the hydrophobic residues on polyQ containing htt fragment aggregation based on α-helix amphipathicity. In other words, helicity within htt^{NT} creates a hydrophobic face that promotes interactions between htt^{NT} and subsequent aggregation.

The role of amphipathic helicity in mediating the aggregation of polyQ containing htt fragments was found to be most crucial in the oligomerization stage of the pathway (Fig 5-9). Thus all alanine mutations of hydrophobic residues were observed to destabilize the thermodynamics of oligomer formation. Amongst the other alanine mutants, only K6A showed

any significant effect, stabilizing the formation of helical oligomers (Table 1) consistent with its effects on the aggregation of the $htt^{NT}Q_{37}P_{10}K_2$ peptide. A correlation between the ratios of molar ellipticities at 222nm and 208nm (proxy for helicity) and the $t_{1/2}$ of aggregation in the $htt^{NT}Q_{37}P_{10}K_2$ background, gave a R^2 of 0.8 suggesting that the effects of the alanine mutations on aggregation are driven primarily by their effects on oligomerization.

Our results from the alanine scan mutagenesis studies also make another subtle point regarding the structural differences between oligomers and fibrils. ssNMR studies of final aggregates of polyQ containing htt fragments (136) showed that Leu 14 is typically disordered lying between the helical segment of htt^{NT} from the β-sheet portion of the rest of the peptide. Yet, this residue plays a crucial role in oligomerization as evinced by impairment of helical oligomer formation and the reduced aggregation rates in the $htt^{NT}Q_{37}P_{10}K_2$ peptide. Taken together these results suggest that stochastic nucleation within the oligomers is accompanied by structural re-arrangements within htt^{NT}, similar to the conformational re-arrangement model proposed in other aggregating systems (192) though in this case such re-arrangements presumably follow amyloid nucleation elsewhere within the aggregate.

The major quantitative difference between the aggregation mechanisms of simple polyQ peptides and htt fragment peptides is observed in the concentration dependence of the initial aggregation rates. Here we demonstrated that helicity within htt^{NT} that drives oligomerization underlies this lack of concentration dependence. Thus the helix-breaking M8P mutation that disrupts oligomerization (Appendix A) shows a concentration dependence of initial aggregation kinetics that is more similar to that of a $K_2Q_{37}P_{10}K_2$ peptide than the control $htt^{NT}Q_{37}P_{10}K_2$ peptide. However, the M8P mutant still aggregates though the final aggregates are different in their properties than those formed by WT peptide. For instance, the aggregates seem to be much

smaller in size (Fig 5-11) and exhibit greater susceptibility to protease cleavage and are less stable than WT aggregates (Fig 5-12). In the light of these results, it is tempting to speculate that the greater toxicity observed (29) and the lack of inclusion bodies in cells expressing a M8P version of a pathogenic htt fragment might be linked to the observed alteration of aggregation properties by this mutation.

Overall, the results presented here implicate amphipathic helicity within the htt^{NT} sequence as the primary driving force in aggregation of polyQ containing htt fragments and are consistent with those from our studies with the scrambled analogs of htt fragment peptides (Chapter 3). However, net hydrophobicity might still play a role, albeit a sub-ordinate one, the aggregation of polyQ containing htt fragments. Thus, despite a concentration dependence of initial aggregation that is similar to polyQ peptides, the M8P mutation still aggregates substantially faster than an equivalent concentration of a MF-$Q_{37}P_{10}K_2$ peptide (Fig 5-11.A).

In addition to clarifying the biophysical driving forces underlying htt^{NT} mediated aggregation, the results described here also have significant implications on the role and fate of htt fragments *in vivo*. htt^{NT} is the site of several PTMs and at least some of these mutations seem to enhance the rates of aggregation presumably by promoting oligomerization of htt^{NT}. Thus, in addition to the normal assumption that PTMs affect protein behavior by altering cellular localization, trafficking and/or degradation, our results suggest that at least some of the PTMs might also significantly alter biophysical properties. The results presented here on the effects of some reported PTMs on polyQ containing htt fragment aggregation will thus be crucial to our understanding of the cellular and pathological role of PTMs within htt^{NT}.

We have also used the data from the mutants described here in constructing a preliminary model of the htt^{NT} tetramer which seems to be the fundamental unit of polyQ containing htt

fragment oligomers (100). The structural model described here will not only guide future experiments but can also be used for *in silico* identification of compounds that can destabilize tetramer formation and hence by extension htt^{NT} mediated aggregation. Such compounds would greatly enhance our understanding of the role that aggregation plays in HD pathology (especially the relative importance of the htt^{NT} mediated aggregation pathway) and might have therapeutic implications.

6.0 EFFECT OF SERINE PHOSPHORYLATION ON AGGREGATION OF POLYQ CONTAINING HTT FRAGMENTS.

6.1 OVERVEW.

The phosphorylation of the serine residues at positions 13 and 16 within htt^{NT} was suggested to have a neuroprotective role in tg mice models of HD. We thus assessed the effects of phosphorylation at the serine residues on the aggregation of polyQ containing htt fragments. Our results indicate that phosphorylation of serine residues alters different facets of the aggregation of polyQ containing htt fragments though it does not alter the mechanism of aggregation. Thus, the introduction of negatively charged Ser replacements significantly impaired the assembly of the α-helical translating to impairment of aggregation rates. In addition to impaired aggregation, serine phosphorylation also seems to alter aggregate properties evinced by differences in aggregate morphology and aggregate stabilities. Overall, these results might provide some crucial insights into the current understanding of the role that phosphorylation at serines 13 and 16 plays in HD pathology.

6.2 INTRODUCTION.

The htt^{NT} sequence is the site of several post-translational modifications (Fig 1-1), some of which have been observed to alter aggregation kinetics based on changes in the biophysical properties of the htt^{NT} sequence (Chapter 5). One such modification, phosphorylation of the two serine residues at positions 13 and 16 is particularly relevant primarily because of its ability to completely abrogate disease phenotype in a tg mouse model of HD. Thus, expression of fl-htt in BACHD mice harboring the S13D/S16D mutations was observed to be neuroprotective, preventing the development of neuronal and behavioral deficits as is characteristic with the control mice. More interestingly however, SD mice lacked any detectable aggregates in contrast to the control mice raising the possibility that impairment of aggregation might be a possible mechanism of phosphorylation mediated neuroprotection. While some subsequent studies have suggested that the effects of serine phosphorylation might be mediated, in part at least, through altered cellular localization (193, 194), the S13D/S16D mutation was not observed to appreciably alter cellular localization in tg mice reflective most likely of divergent mechanisms in different HD models. Notwithstanding these observations, the finding that phosphorylation of serine residues can affect aggregation underscores the need for a detailed assessment of this modification on the aggregation of polyQ containing htt fragments. Here, we have assessed the effects of serine phosphorylation on the different stages of the aggregation of polyQ containing htt fragments by using both phosphomimetic Ser-Asp mutations and Ser-phosphoSer mutations.

6.3 RESULTS.

6.3.1 Introduction of negative charges at serines 13 and 16 impairs aggregation rates.

We started by first looking at the effects of the phosphomimetic Ser-Asp mutation on the aggregation kinetics of a $htt^{NT}Q_{37}P_{10}K_2$ (F17W) peptide (Fig 6-.A) since this is the mutation that was used in the studies with tg mice. We found that the mutating both the serine residues to aspartate (●) impairs aggregation kinetics (16).

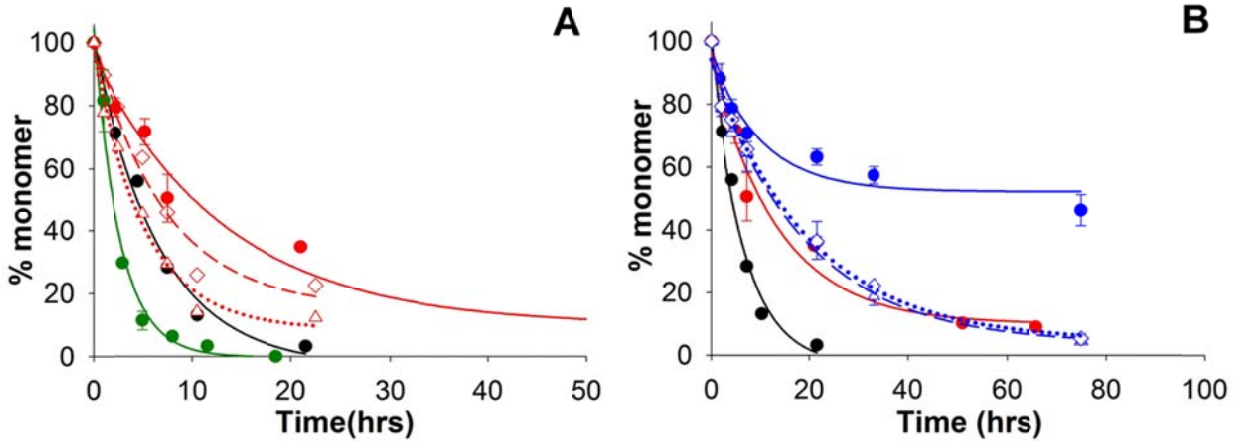

Figure 6-1: Phosphorylation of serine residues impairs aggregation kinetics. (A) Aggregation of $htt^{NT}Q_{37}P_{10}K_2$ peptides in PBSA. WT (●, 20μM), S13A/S16A (●, 30μM), S13/S16D (●, 34μM), S13D(Δ, 32μM) and S16D (◊, 30μM). (B) Aggregation of phosphoserine versions of $htt^{NT}Q_{37}P_{10}K_2$ peptides. WT (●, 20μM), S13D/S16D (●, 34μM), S13pS/S16pS (●, 20μM), S13pS (Δ, 21uM); S16pS (◊ ,20uM).

Thus, the WT peptide aggregates to 50% within 4 hours (●) while the S13D/S16D takes 11 hours (●). As a control we also looked at the aggregation of the S13A/S16A mutant, a negative control for serine phosphorylation. Expectedly, this mutation aggregates faster than the WT control, aggregating to 50% within 2 hours (●) consistent with the slight acceleration observed with the single Ser-Ala mutants in Chapter 5. This acceleration in aggregation rates

probably stems from an increase in hydrophobicity (amphipathicity) upon mutating serine to alanine residues. Next, we looked at the aggregation of each of the single Ser-Asp mutants to determine whether there was position dependence of the aggregation impairing effects of the S13, 16D mutations. We found that while the S13D mutant (Δ) aggregates with almost identical kinetics as the WT, the S16D mutant (◊) is similar to the S13D/S16D mutant in its aggregation suggesting that the serine 16 probably contributes to a greater extent to the kinetic effect of S13D/S16D mutation.

Although the Ser->Asp mutation has proved a remarkably good mimic of phosphorylated serine in a variety of biological settings, we were concerned about whether this is necessarily true for any physicochemical impact on htt aggregation. We therefore investigated the aggregation of htt^{NT} $Q_{37}P_{10}K_2$ (F17W) peptides with phospho-Ser residues built into the peptides at positions 13 and/or 16 during chemical synthesis. We found that the doubly phosphorylated S13pS/S16pS peptide (●) exhibits substantially reduced aggregation compared not only to the WT peptide (●), but also to the S13D/S16D mutant (●) (Fig. 2A). Furthermore, overall aggregation rates of the single phosphoryl-Ser peptides S13pS (Δ) and S16pS (◊) are also slower than the WT rate (●) and similar to S13D/S16D rate (●) indicative perhaps of a link between net-charge and aggregation kinetics.

6.3.2 Serine phosphorylation alters aggregate morphologies.

Having ascertained that substituting the serine residues in htt^{NT} with aspartates or phosphoserines impairs aggregation, we proceeded to examine the morphologies of the final aggregates formed by these mutants. As demonstrated before, the final aggregates of the WT

peptide are fibrillar in nature (Fig 6-2.A). In dramatic contrast, the final aggregates of the S13, 16D mutant are not fibrillar but resemble rather oligomeric/protofibrillar intermediates (C- F).

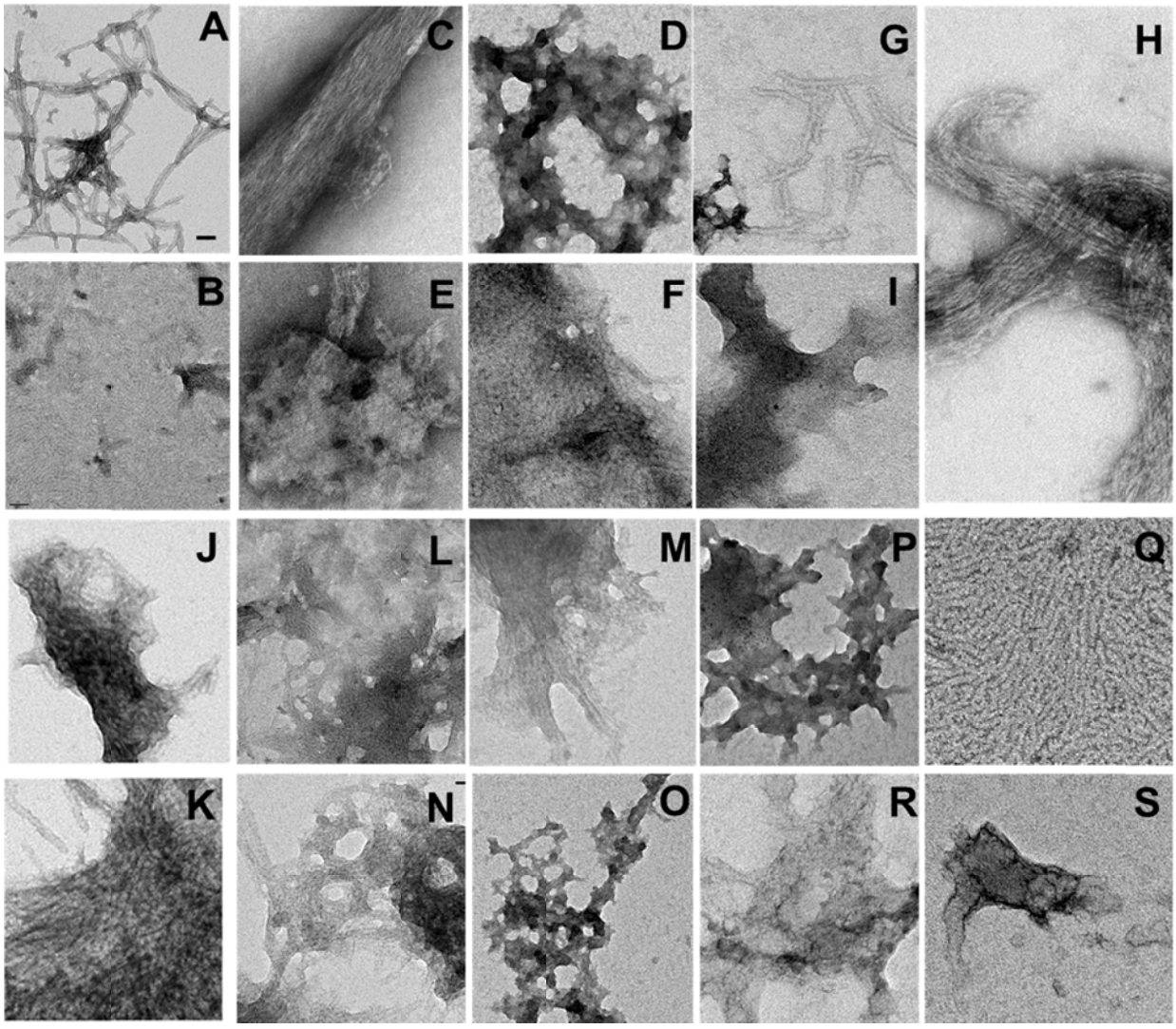

Figure 6-2 Morphologies of aggregates formed by $htt^{NT}Q_{37}P_{10}K_2$ peptides. Aggregates of WT isolated after 47hrs (A) and 1hr (B). Final aggregates of S13D/S16D (after 100 hrs , C-F), S13pS/S16pS (163 hrs, G-I), S13D (30hrs, J), S16D (30hrs, K), S13pS (33hrs, L-M), S16pS (33hrs, N-O) . Also shown are early aggregation intermediates isolated after 1.5 hrs of S13D/S16D (P-O) and S13pS/S16pS (R-S). Scale bar in (A) represents 50nm.

This alteration in final aggregate morphologies was also observed in the case of the S13pS/S16pS mutant (G-I) which, similar to the S13D/S16D mutant, forms aggregates that resemble protofibrillar species with some evidence of altered staining compared to the WT (G). We also looked at the aggregate morphologies of the single Asp and/or phosphoserine mutants and observed mostly protofibrillar species with some evidence for fibrils (16). Overall, these results suggest that the incorporation of negatively charged residues at positions 13 and 16 seems to alter aggregate morphologies considerably.

Next, we looked at the morphologies of aggregates isolated at early time-points of both the S13D/S16D and the S13pS/S16pS mutants to determine whether this difference in aggregate morphologies is also maintained at such early times. We observed that in contrast to the WT which exhibits intermediate aggregates (Fig 6-2.B) with morphologies substantially different from final aggregates (Fig. 6-2.A), early aggregates of peptides with both Ser residues replaced with Asp (Fig. 6-2. P-Q) or phosphoSer (Fig. 6-2.R-S) generally are no different from final aggregates.

Overall, the results from our study of aggregation kinetics and of aggregate morphologies suggest that the mutation of the serine residues to Asp or phosphoSer not only impairs aggregation kinetics but also alters aggregate morphologies. We were thus interested in exploring the mechanisms by which phosphorylation at serines alters aggregation behavior. To this end, we started by looking at the effects of serine phosphorylation on different stages of the aggregation pathway (Fig 1-4.B).

6.3.3 Effect of serine phosphorylation on monomeric ensemble.

Even though polyQ containing htt fragments are disordered in the monomeric state, it is possible that mutating the serine residues to Asp or phosphoSer alters the conformational properties of the monomer. In order to explore this possibility, we started by looking at the CD spectra of the S13D/S16D (Fig 6-3.A,—) and the S13,16p (Fig 6-3.A,—) mutants in a $htt^{NT}Q_{37}P_{10}K_2$ background. Overall, we found that the introduction of negative charges at serines 13 and 16 does not alter the average conformation of the monomer which is still disordered, similar to the WT (Fig 6-3.A, inset).

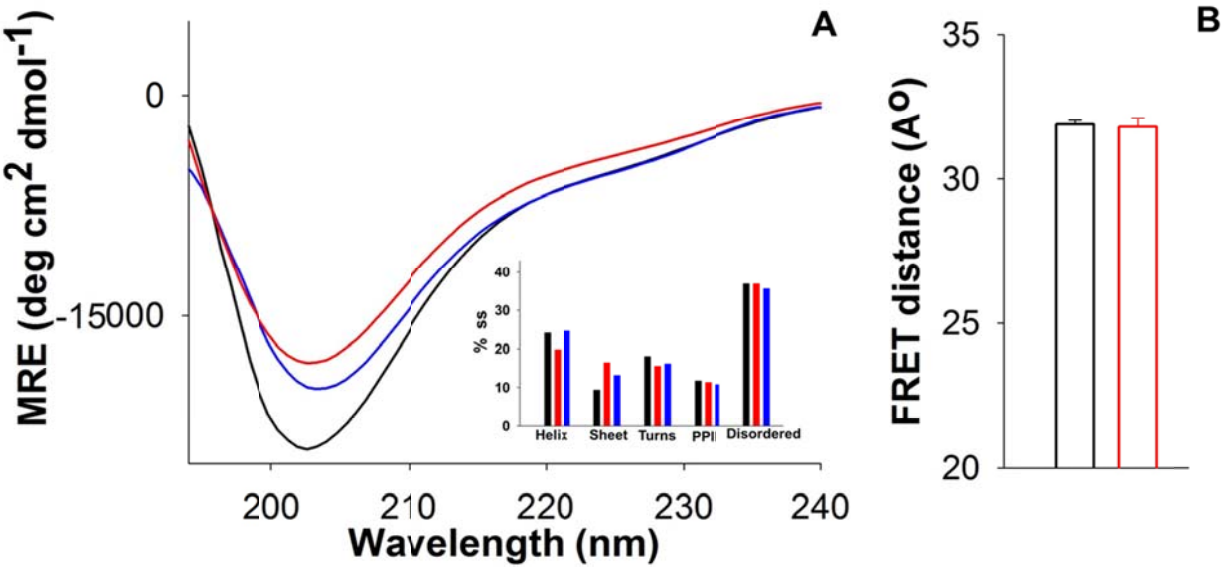

Figure 6-3: Effect of serine phosphorylation on conformation of monomeric ensemble of polyQ containing htt fragments. (A) CD spectra of $htt^{NT}Q_{37}P_{10}K_2$ peptides WT (—), S13D/S16D (—) and S13pS/S16pS (—) at ~ 35 µM in 10mM TRIS, pH 7.4; inset, secondary structure deconvolution of CD spectra. Color scheme is same as above. (B) FRET distance between residues -1 and 17 in $htt^{NT}Q_{37}P_{10}K_2$ background at ~ 15 µM in 20mM PBSA, pH 7.4 for WT (—) and S13D/S16D (—) htt^{NT} versions.

As an additional test of serine phosphorylation on the monomeric ensemble, we also looked at the compactness of the htt^{NT} sequence in these mutants by measuring the FRET distance between residues -1 and 17 in the WT (Fig 6-3.B,—) and the S13D/S16D (Fig 6-3.B,—) mutants in the $htt^{NT}Q_{37}P_{10}K_2$ context. Based on the -1-17 distance in these mutants, the htt^{NT} compactness appears to be similar in both these peptides.

While, it is possible that there are subtle differences between these peptides in their propensities for structural subtypes that constitute the disordered monomeric ensemble, overall these results are consistent with the lack of any appreciable effect of serine phosphorylation on the average conformation of the monomeric ensemble in polyQ containing htt fragments.

6.3.4 Kinetic impairment by serine phosphorylation is mediated at the oligomeric level.

The aggregation enhancing role of htt^{NT} in the aggregation of polyQ containing htt fragments, stems from its ability to form oligomers that can serve as sites for stochastic nucleation (Chapter 4, 5). Since mutation of serines 13 and 16 to either Asp or phosphoSer was observed to reduce the rates of aggregation, we next explored whether serine phosphorylation affects htt^{NT} mediated oligomerization.

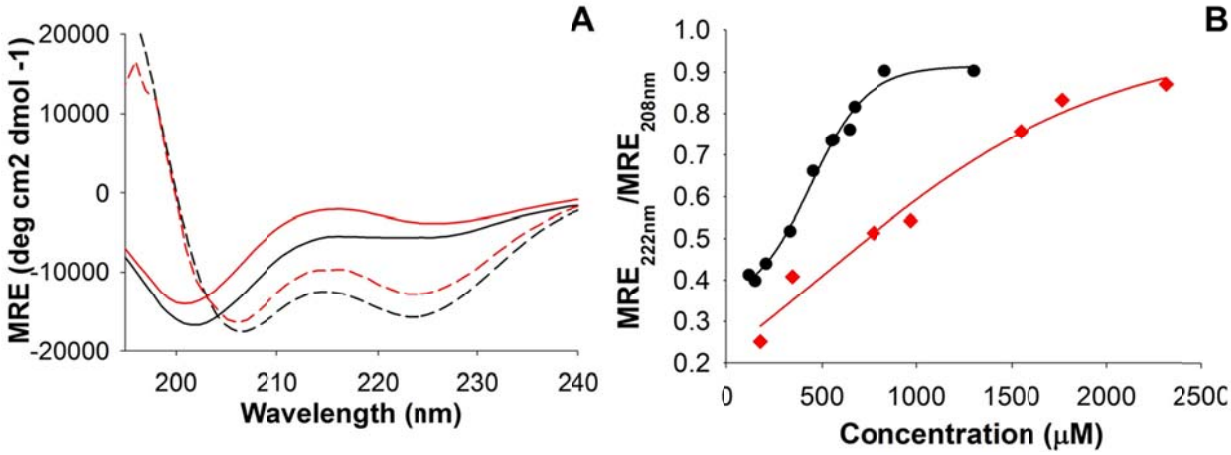

Figure 6-4: Phosphomimetic mutations at serines impair oligomerization. (A) CD spectra of htt^{NT} peptides. WT at ~300μM (▬) and 800μM (---) and S13D/S16D at ~ 1000μM (▬) and 1800μM (---). (B) Concentration dependencies of random-coil to α-helix transition in CD spectra of WT (●) and S13D/S16D (♦).

To investigate this, we started by looking at the concentration dependence of htt^{NT} mediated oligomerization. Thus, the WT htt^{NT} peptide displays a typical random-coil to α-helical spectrum (Fig 6-4.B,−−, ▬) with the mid-point of this concentration dependence ($C_{1/2}$) ~ 400-500μM. The htt^{NT} (S13D/S16D) mutant on the other hand displays a much less co-operative assembly of oligomers with a $C_{1/2}$ of ~ 1mM (Fig 6-4.B). However, at higher concentrations this mutant does display a predominantly α-helical spectrum (---) consistent with its ability to eventually form oligomers.

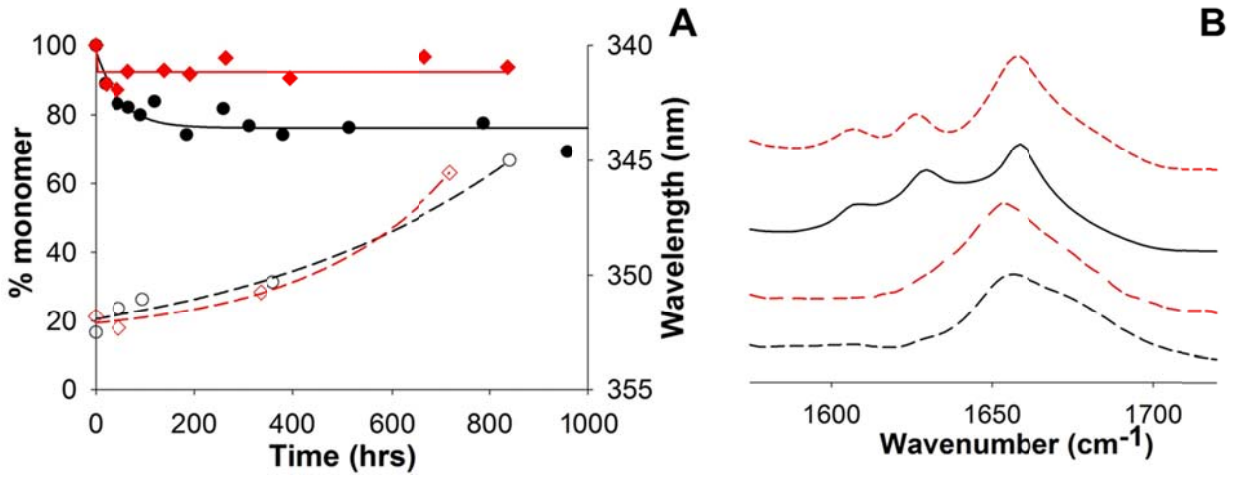

Figure 6-5: Phosphomimetic mutations at serines can still nucleate within oligomers. (A) Aggregation of $htt^{NT}Q_8K_2$ (F17W) peptides WT (●) and S13D/S16D (♦). Also shown are the λ_{emm} of Trp17 in aggregated isolated at different times for the WT (○) and S13D/S16D mutant (◊). (B) FTIR spectra of the aggregates of the $htt^{NT}Q_8K_2$ peptides isolated at different times: WT at 48hrs (---) and 840 hrs (▬); S13D/S16D at 48hrs (---) and 720 hrs (▬).

Consistent with impaired oligomerization in the case of the S13D/S16D mutation, in peptides of the form $htt^{NT}Q_8K_2$, a background that supports very slow htt^{NT} mediated nucleation of polyQ amyloid formation (Chapter 5, (135)), the S13D/S16D mutation greatly diminishes the time-dependent formation of sedimentable oligomeric intermediates (Fig. 6-5. A). Thus, both WT and S13D/S16D initially form oligomers that are rich in α-helix (Fig. 6-5.B) and despite the slower formation of α-helix rich aggregates, the S13D/S16D $htt^{NT}Q_8K_2$ peptide is able to undergo nucleation of β-rich, amyloid-like structure. This is shown by the previously described (135) transition, within the aggregate pool, of the Trp at position 17 from a solvent exposed (λ_{emm} ~351-353nm) to a solvent-excluded (λ_{emm} ~345nm) environment (Fig. 6-5.A) and in development of FTIR bands, including β-sheet (1625-1630 cm-1), characteristic of polyQ amyloid structure (Fig. 6-5.B).

Overall, these studies with shorter polyQ repeat length htt peptides indicate that the kinetic impairment of aggregation resulting from the introduction of negative charges at serine residues is mediated at the oligomeric level. However, oligomers of S13D/S16D, once formed, retain the ability to act as sites of stochastic nucleation.

6.3.5 Mechanistic effects of serine phosphorylation.

Our studies with the short polyQ versions of htt fragments gave us some insights into the effects of serine phosphorylation on the aggregation of polyQ containing htt fragments. However, it is possible that these shorter polyQ repeat peptides do not accurately describe the mechanistic details in play in the aggregation of longer polyQ containing htt fragments. Thus, we proceeded to assess whether the results from these shorter peptides were also true in the case of longer polyQ containing htt fragments. Since, the rapid aggregation kinetics of these peptides makes it challenging to isolate and spectroscopically study aggregation intermediates, we had to utilize other probes to assess the effects of serine phosphorylation on aggregation mechanisms.

First, we looked at the concentration dependence of the initial aggregation kinetics of the S13D/S16D mutant in a $htt^{NT}Q_{37}P_{10}K_2$ background. Thus, as has been described earlier, the WT $htt^{NT}Q_{37}P_{10}K_2$ peptide displays a shallow concentration dependence with a log-log slope of ~1 while simple polyQ peptides lacking the htt^{NT} sequence display slopes of ~3. We found that the slope of an analogous log-log plot for the S13D/S16D mutant of $htt^{NT}Q_{37}P_{10}K_2$ is ~ 1.3 consistent with an htt^{NT}-mediated nucleation mechanism.

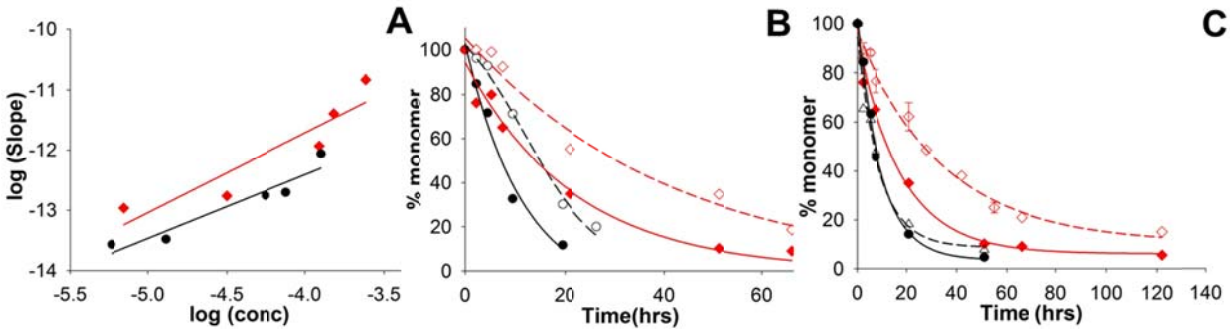

Figure 6-6: Mechanistic consequences of S13D/S16D mutation in htt$^{NT}Q_{37}P_{10}K_2$. (A) Concentration dependence of initial phase of the aggregation reaction of WT (●) and S13D/S16D (♦). (B) Inhibition of aggregation by 1:1 ratio of htt$^{NT}Q_3$ to peptide. WT alone (●, 50uM) and with inhibitor (○,48μM) ; S13D/S16D alone (♦,43μM) and with inhibitor (◊, 68μM). (C) Inhibition of aggregation by ~ 5-fold excess of elongation inhibitor $PGQ_9P^{1,2,3}K_8$ compared to peptide. WT alone (●, 22μM) and with inhibitor (Δ, 26μM); S13D/S16D alone (♦, 43μM) and with inhibitor (◊, 34μM).

The use of peptide-based inhibitors has in the past (Chapter 1, 3) provided us with crucial insights into the mechanism of polyQ containing htt fragments. Thus, the htt^{NT} peptide with few if any attached Gln residues is able to transiently inhibit htt^{NT} mediated amyloid nucleation by co-assembling with polyQ containing htt fragments at the α-helix-rich oligomer stage, thereby reducing the local polyQ concentration in the oligomers and hence the amyloid nucleation efficiency. We assessed the effects of the htt$^{NT}Q_3$ peptide on inhibiting the aggregation of the htt$^{NT}Q_{37}P_{10}K_2$ (S13D/ S16D) mutant. As shown in Fig 6-6.A, htt$^{NT}Q_3$ peptide can inhibit the aggregation of both the WT htt$^{NT}Q_{37}P_{10}K_2$ peptide and the S13D/S16D mutant consistent with the ability of the S13D/S16D mutant to form α-helical oligomers. In addition to htt$^{NT}Q_3$ inhibitor, we also looked at the inhibitory effect of the $PGQ_9P^{1,2,3K8}$ peptide. Such peptides inhibit the elongation of amyloid-like aggregates of simple polyQ, and due to the importance of elongation in the nucleation process, also suppress spontaneous amyloid formation by simple polyQ

peptides (163). Consistent with past results in the lab, we find that $PGQ_9P^{1,2,3}K_8$ gives no detectible inhibition of spontaneous aggregation of WT $htt^{NT}Q_{37}P_{10}K_2$. However, there is a measurable reduction in the aggregation of the S13D/S16D mutant. The meaning of the $PGQ_9P^{1,2,3}K_8$ inhibition of the Ser-modified peptide is not entirely clear, but it does raise the possibility of a defective nucleation/elongation step in the case of the S13D/S16D mutant compared to the WT.

Overall, these mechanistic probes support the view that Ser modifications in htt^{NT} do not alter the fundamental, htt^{NT}-mediated nucleation mechanism of polyQ containing htt N-terminal fragments. The modest reductions in overall aggregation rate observed with the S13D/S16D mutant and reported here for the phosphoryl-Ser peptides (Fig. 6-1), appear to be primarily due to less favorable formation of the α-helix-rich oligomeric intermediates that are the springboard for amyloid nucleation.

6.3.6 Serine phosphorylation does not change the secondary structure of the final fibrils.

The final aggregate morphologies of the S13D/S16D mutant as well as those of the S13pS/S16pS mutant are considerably different from those of the WT (Fig 6-2). One possible explanation for these differences in aggregate morphologies is that the structure of the polyQ containing htt fragment in these aggregates is different. To test this hypothesis, we decided to use ssNMR techniques to look at the secondary structure of the htt^{NT} segment in the $htt^{NT}Q_{37}P_{10}K_2$ (S13D/S16D).

Previously we had reported solid state NMR data on mature amyloid fibrils of $htt^{NT}Q_{30}P_{10}K_2$ peptides that confirmed the expected β-structure in many of the polyQ Gln residues while surprisingly showing that residues 4-11 of the htt^{NT} reside in stable α-helix

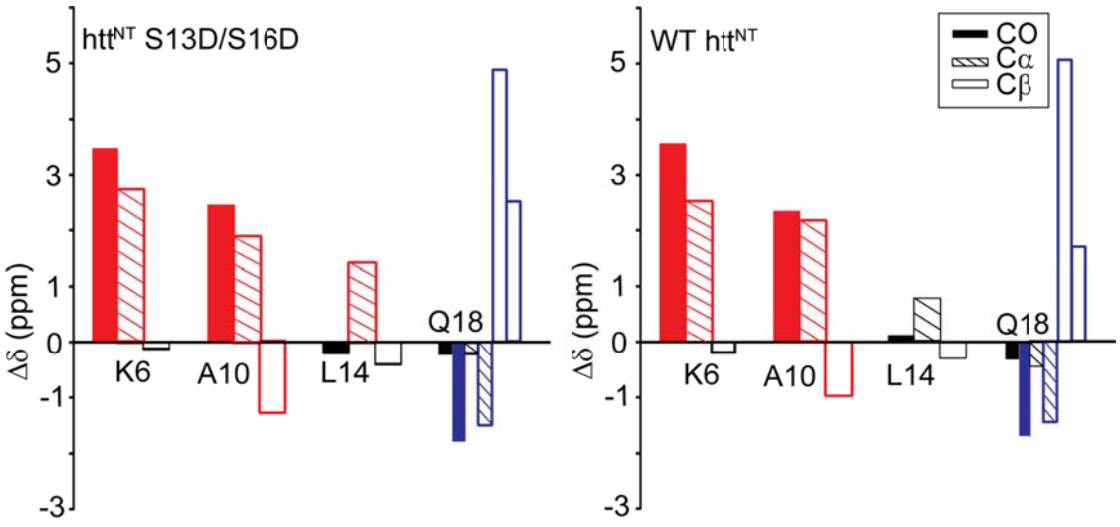

Figure 6-7: ssNMR studies of S13D/S16D mutant. Graphical representation of the ^{13}C chemical shift differences compared to random coil positions (δΔ) for different labeled positions in aggregates from WT and S13D/S16D peptides, with secondary structures inferred from those values. Split bars for Gln18 indicate two environments associated with two conformations, both β.

(136). We carried out a similar analysis on the S13D/S16D mutant with residues Lys6, Ala10, Leu14 and Gln18 labeled. The results (Fig 6-7) show that the S13D/S16D fibrils have a secondary structure that is remarkably similar to that of the WT htt^{NT} peptide. Thus, the Lys6 and Ala10 residues of S13D/S16D exhibit the same kind of strong α-helix as found in the WT peptide aggregates. Likewise, Leu14 exhibits the absence of any strongly favored secondary structure in aggregates of both peptides. Finally, as in the previously reported aggregates with WT htt^{NT}, a specifically-labeled Gln18 is found in two chemically distinct environments, both of which are β-conformations. The S13D/S16D aggregates exhibit an essentially identical split β profile. Thus, in spite of significant differences in EM morphology, the S13D/S16D peptide aggregates are indistinguishable at the level of secondary structure from the WT htt^{NT} aggregates, at least at the labeled residues. This is consistent with the other data in suggesting

that serine phosphorylation does not alter the overall aggregation mechanism of polyQ containing htt fragments.

6.3.7 Serine phosphorylation alters stability of aggregates.

In contrast to these ssNMR results, other tests detect some important differences in aggregate structure and stability introduced by serine modifications. We exposed final aggregates of various $htt^{NT}Q_{37}P_{10}K_2$ peptides to trypsin proteolysis - a sensitive, if low resolution, probe of amyloid structure. We found that mature WT aggregates are relatively stable to cleavage within the htt^{NT} segment, with only about 10% of the peptides being cleaved (Fig. 6-8.A). In contrast, about 30% of the peptides in S13D/S16D aggregates, and nearly 50% of the peptides in S13pS/S16pS aggregates, are cleaved by trypsin exposure under the same conditions. Interestingly, the single phosphoryl-Ser mutants, S13pS and S16pS, are both about 30% cleaved, the same level as the S13D/S16D aggregates. Thus, the sensitivity of these modified Ser aggregates to trypsin cleavage rank very similarly to their relative formation rates (Fig 6-8.A).

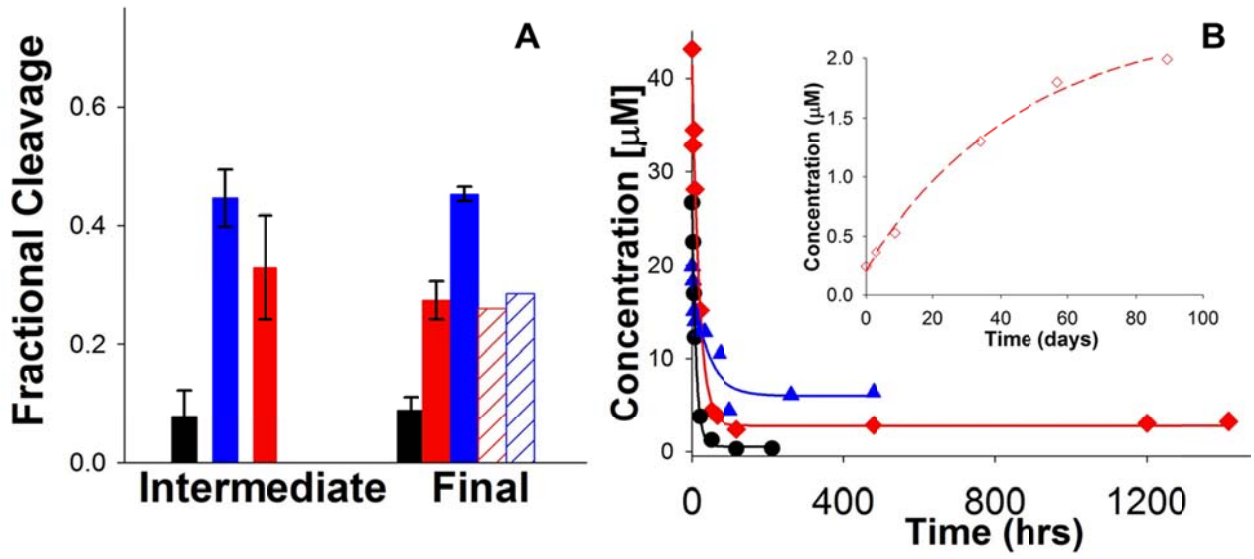

Figure 6-8: Aggregate stabilities of htt^{NT}Q$_{37}$P$_{10}$K$_2$ peptides. (A) Fraction of molecules cleaved within htt^{NT} after exposure to trypsin in various mature aggregates (WT, black; S13pS/S16pS, blue; S13D/S16D, red; S13pS, hatched red S16pS, hatched blue). (C) Sedimentation assays of aggregation kinetics and plateau levels of monomer for WT (●), S13D/S16D (♦) and S13pS/S16pS (▲) peptides in PBSA at 37 ºC. Inset: Dissociation of S13D/S16D aggregates in PBSA at 37 ºC by sedimentation assay.

We also examined the trypsin cleavage sensitivities of the aggregates of some of these peptides isolated relatively early (30-35% completion) in the aggregation reactions. We observed very similar trypsin susceptibilities in these early aggregates as in the mature aggregates (Fig. 6-8.A). The aggregate stabilities suggested by the limited proteolysis experiments are confirmed by a more rigorous measure of stability, the concentration of monomeric peptide remaining when the aggregation reaction reaches equilibrium. This residual monomer concentration, which typically can be reached both in the aggregate association and dissociation directions is essentially the critical concentration, or C_r, for the polymerization reaction, and hence is linked to the thermodynamic favorability of aggregate elongation (29-31). We found a surprisingly dramatic effect of the Ser modifications within htt^{NT} on this measure of aggregate stability.

Thus, the aggregation reaction of a $htt^{NT}Q_{37}P_{10}K_2$ with a WT htt^{NT} sequence reaches equilibrium after about 50 hrs, with no further change up to 200 hrs, for a C_r in the 0.3 μM range (Fig. 6-8.B, -●-). In comparison, the corresponding S13D/S16D peptide aggregation reaction reaches a plateau in monomer concentration after about 100 hrs, with no further change out to 1400 hrs (Fig. 6-8.B, ♦). This plateau is in the 2.5 – 3.0 μM range, almost 10-fold higher (i.e., less stable) than the WT. A similar monomer concentration of 2 μM is reached when S13D/S16D aggregates are diluted and given the opportunity to dissociate to toward equilibrium (Fig. 6-8.B inset), showing the robustness of the measurement as a feature of a dynamic equilibrium. The S13pS/S16pS peptide requires about 200 hrs to reach equilibrium where it indicates a C_r value in the 4.5 – 6.0 μM range (Fig. 5C, ▲). Based on these values, we calculated the aggregation destabilization ($\Delta\Delta G_{ag}$) (31) from placing negative charges at the serines to be ~1.3-1.4 kcal/mol for the S13D/S16D mutation and ~1.7-1.8 kcal/mol for the S13pS/S16pS peptide.

6.4 DISCUSSION.

Protein phosphorylation and de-phosphorylation play an enormous role in cell regulation and cell pathway dysfunction linked to disease. In the context of the htt protein, phosphorylation has been implicated in modulating several cellular processes (16, 36, 195). Particularly, phosphorylation of serines 13 and 16 has been shown to enhance the degradation of htt by the proteasome in cell models (37) and abrogate aggregation of htt in tg HD mice (16). Here, we have aimed to investigate the biophysical basis of serine phosphorylation on the aggregation of htt peptides.

Our studies indicate a significant impact of the replacement of Ser13 and Ser16 with negatively charged groups on the rates of spontaneous aggregation of htt N-terminal fragments. Thus, both the S13D/S16D mutations and the S13pS/S16pS mutations reduce the aggregation rates of $htt^{NT}Q_{37}P_{10}K_2$ peptides considerably with the degree of impairment depending on the net-charge of the peptide.

In principle, there are a number of mechanistic steps that might be targeted by htt^{NT} sequence changes to explain observed aggregation rate reductions; these include monomer conformation, oligomer formation, amyloid nucleation and amyloid elongation. We found that the S13D/S16D mutation does not appreciably affect the ensemble monomeric conformation of the $htt^{NT}Q_{37}P_{10}K_2$ peptides based on CD and FRET results. In contrast, Truant and colleagues described CD experiments showing significant reductions of α-helix in htt^{NT} peptides modified on the Ser residues which they interpreted as evidence for altered monomer conformations (29). The different results may be due to sample disaggregation procedures, peptide sequence background used, or peptide concentrations used. The htt^{NT} Ser modifications do not appear to alter the reliance of these peptides on htt^{NT} mediated oligomer formation as a basis of polyQ amyloid nucleation, nor is there any evidence for a difference in the efficiencies of nucleation and elongation after formation of α-helix-rich oligomers. However, we found that htt^{NT} segments containing the S13D/S16D mutations assemble less readily into these α-helix-rich oligomers (Fig. 6-4.B). Thus, the most likely source of diminished spontaneous aggregation rates is a reduced ability to form the α-helix-rich tetramers and higher aggregates that serve as the species within which polyQ amyloid structure is nucleated (135).

Consistent with the CD results that suggest that a role for htt^{NT} α-helix formation in the amyloid nucleation mechanism is retained in Ser modified peptides, ss NMR shows that central

residues in htt^{NT} exist in α-helix in mature aggregates of Ser modified peptides, as they do in WT. While it might have been expected that negatively substituted residues near the C-terminus of htt^{NT} would impair the ability of the first Gln residues of polyQ to engage in amyloid structure, ss NMR also shows essentially identical β-structure features in $htt^{NT}Q_{37}P_{10}K_2$ aggregates containing either WT or S13D/S16D htt^{NT} segments.

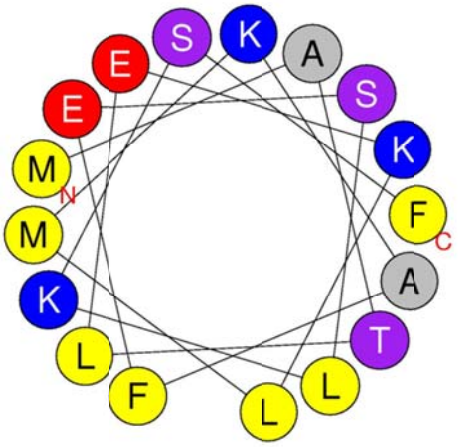

Figure 6-9: Helical wheel representation of htt^{NT}.

In spite of these similarities in secondary structure, amyloid-like aggregates of Ser-modified htt N-terminal fragments exhibit substantial differences from WT aggregates. In EM images, while WT $htt^{NT}Q_{37}P_{10}K_2$ peptides form a uniform network of unbranched fibrils, similar peptides containing negatively charged residues at positions 13 and/or 16 exhibit a heterogeneous mixture of less well-defined structures, some of which resemble intermediates formed during the aggregation of the WT sequence (Fig. 6-2). Since the secondary structures of these aggregates are similar, these morphology differences might reflect an altered ability of the simplest amyloid units to assemble into larger structures. The implied reductions or alterations in quaternary structure in Ser-modified aggregates might help explain the enhance susceptibility of htt^{NT} segments to trypsin (Fig. 6-8.A) and the decreased stabilities of these aggregates (Fig. 6-

8.B). These dramatic effects have strong implications for the ability of the cell to manage aggregation. The Cr values of 2-6 μM for $htt^{NT}Q_{37}P_{10}K_2$ amyloid-like aggregates with Asp or phosphoryl-Ser residues at positions 13 and 16 mean that peptide solutions below these concentrations have no thermodynamic driving force to aggregate at all. Of course the crowded environment might drive C_r values lower, but even so the ~10 fold difference in WT vs. Ser-modified htt fragment stabilities is likely to be maintained and would be expected to reduce the tendency of the mutated peptides to aggregate. The increased susceptibility of htt^{NT} to trypsin in the Ser-modified aggregates suggests a greater accessibility of the htt^{NT} segment to many modifying enzymes. For instance, htt fragments have been shown to be ubiquitinylated at the N-terminus (19) and it would not be surprising if the ubiquitinylating enzymes responsible for flagging misfolded and aggregated proteins for destruction at the proteasome were found to more efficiently modify S13D/S16D and S13pS/S16pS aggregates compared with WT aggregates based on the enhanced htt^{NT} accessibility observed in the trypsin experiments (Fig. 6-8.A).

Mutations of Ser or Thr residues to Asp or Glu residues have long been seen as viable, ribosomally accessible mimics of phosphorylated residues, in spite of the dramatically different sizes and pK_as of carboxylic acid and phosphoric acid moieties. Our results suggest that Asp mutations are also reasonable mimics of the effects of phosphorylation of Ser residues on htt N-terminal fragment aggregation. While the tendency of these acidic groups to have negative effects on β-sheet rich amyloid formation is not surprising, their ability to reduce the formation of htt^{NT} α-helix-rich oligomers is somewhat puzzling. The helical wheel diagram of htt^{NT} (Fig 6-9) shows a strong amphipathic nature, and recent results suggest that the hydrophobic face of this helix plays a major role in oligomer stabilization (R. Mishra and R. Wetzel, Ms. in preparation). However, Ser13 and Ser16 are on the hydrophilic face of the α-helix, which would be then

predicted to be solvent exposed and relatively unfazed by the introduction of negatively charged groups. It is possible that this hydrophilic face is involved in packing of α-helical tetramers into higher order oligomers that might be required for amyloid nucleation.

Many substrates for phosphorylation are intrinsically disordered proteins, and the mechanisms by which phosphorylation imparts cellular effects has a strong protein folding component. Our results suggest a feasible pathway by which protein phosphorylation might impact protein misfolding and aggregation by modulating the long term viability of such aberrant species. The data provide a consistent mechanism to explain the lack of aggregate accumulation, and potentially the lack of toxicity, of S13D/S16D htt in a mouse model of HD.

7.0 EFFECT OF POLYQ EXPANSION ON AGGREGATION OF POLYQ CONTAINING HTT FRAGMENTS.

7.1 OVERVIEW.

Since polyQ expansion is the fundamental trigger in HD pathology, we explore in detail the relationship between polyQ expansion and aggregation of polyQ containing htt fragments. We have looked at the effects of polyQ expansion on aggregation rates, the conformational ensemble in the monomeric state of polyQ containing htt fragments and on the thermodynamics of oligomerization. We did not find any substantial effect of polyQ expansion on the monomeric conformational ensemble. However, our preliminary observations do indicate that polyQ expansion stabilizes oligomerization which might underlie the acceleration of aggregation that is observed. Overall, these results are expected to be crucial in adding to our existing understanding of the role that polyQ expansion plays in aggregation and in guiding future experiments

7.2 INTRODUCTION.

Polyglutamine expansion is the fundamental trigger in Huntington's disease thereby making it one of the ten CAG repeat diseases. While the cellular and pathological manifestations of polyQ

expansion are still not clear, it has been shown to be associated with an increased propensity to aggregate. Thus, peptides with longer polyQ repeat lengths have a greater tendency to aggregate than those with shorter repeats.

7.3 RESULTS.

7.3.1 PolyQ expansion affects aggregation kinetics.

Earlier studies in the lab had shown that the aggregation kinetics of polyQ containing htt fragments is linked to the glutamine repeat length (Fig 7-1.A) (31). Thus, while htt^{NT} hardly aggregates by 15% in 200 hrs (●), $htt^{NT}Q_{37}P_{10}K_2$ aggregates to completion within 10 hrs (♦).

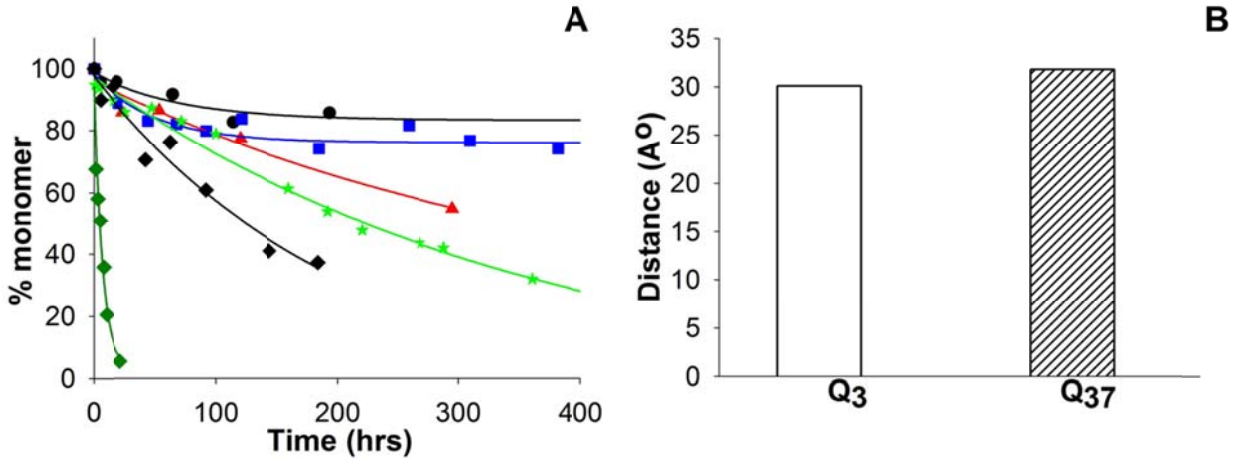

Figure 7-1: PolyQ effects on aggregation and htt^{NT} conformation. (A) Aggregation of htt^{NT} (20μM, ●), $htt^{NT}Q_8K_2$ (90μM, ■), $htt^{NT}Q_{15}P_{10}K_2$ (50μM, ▲), $htt^{NT}Q_{23}P_{10}K_2$ (12μM, ☆), $htt^{NT}Q_{30}P_{10}K_2$ (30μM, ♦) and $htt^{NT}Q_{37}P_{10}K_2$ (20μM, ♦). (B) FRET distance between residues -1 and 17 in a htt^{NT}-Q_3 (open) and $htt^{NT}Q_{37}P_{10}K_2$ background (hatched bar).

Over the next few sections, we highlight some of the preliminary results in our efforts to identify the mechanistic details of such polyQ expansion induced rate enhancement.

7.3.2 polyQ expansion does not alter monomeric conformation.

Earlier FRET based studies in the lab has suggested that expansion of polyQ within htt peptides alters the conformation of the leader htt^{NT} sequence from a compact coil at lower polyQ repeats to an extended coil at higher polyQ repeats. However, a caveat with these studies is that they did not account for any sequence dependent changes in quantum yield of the donor (acceptor). Thus, when these same experiments were performed using a ratiometric FRET (Chapter 3) approach that does not require the donor-only control, there was no substantial difference in the conformation of the htt^{NT} sequence in htt fragments of different polyQ repeat lengths (Fig 7-1 .B) (B.Sahoo *et al*, unpublished results). To explore the polyQ length dependence of monomeric conformational ensemble in greater detail, we decided to use double electron-electron resonance (DEER), an EPR based technique that uses the relaxation of two spin probes to obtain a mutual distance distribution. Thus, we attached the MTSL spin probe to cysteines mutated into the htt^{NT} sequence at positions 1 and 17 in polyQ containing htt fragments with 1, 30 or 37 glutamine repeats. Since the DEER experiments are performed at low temperatures (80K), any aggregation of the samples during sampling is expected to be minimal. Nevertheless, we decided to first ensure that this is actually true, especially in the cases of the peptides with 30 and 37 polyQ repeats.

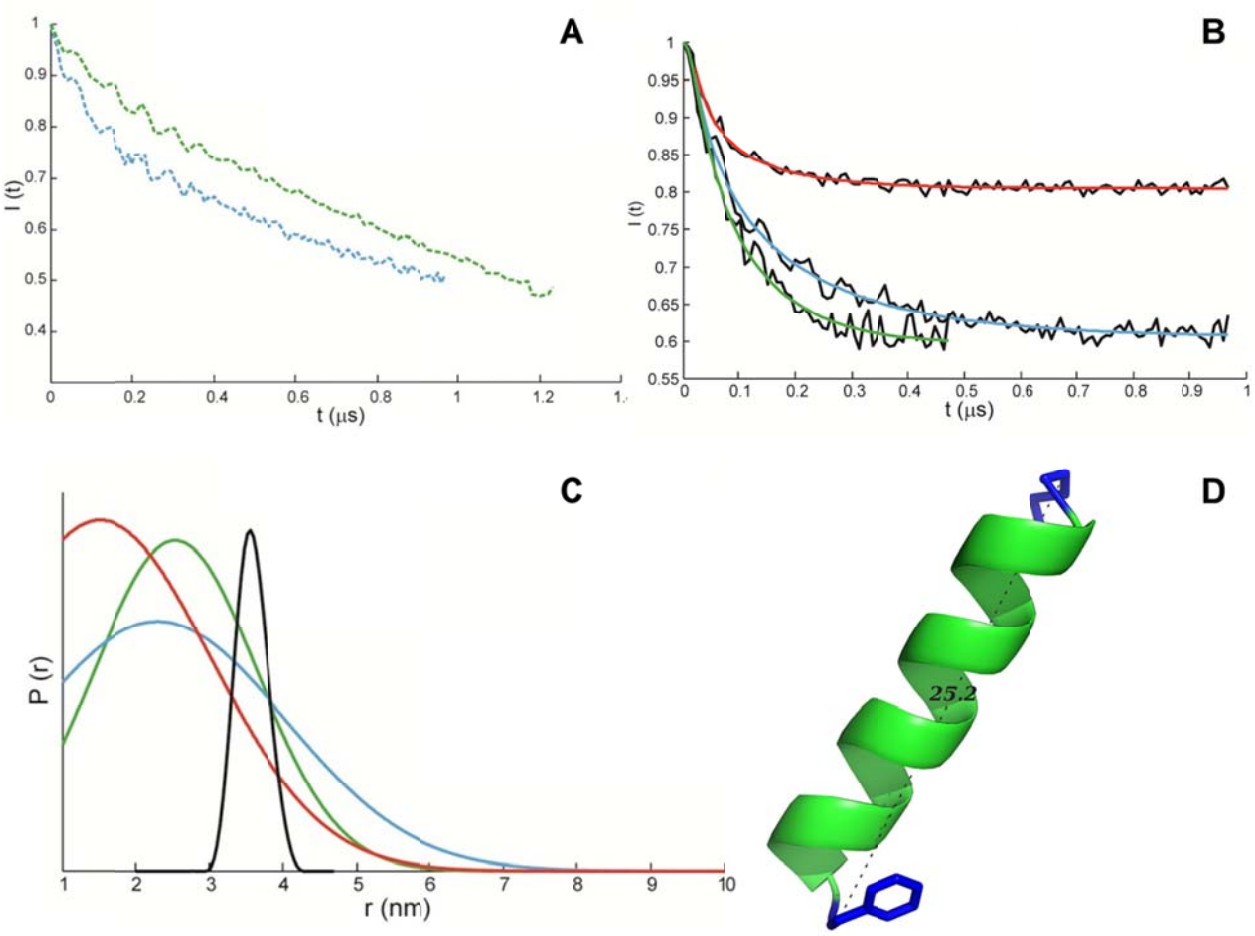

Figure 7-2: EPR studies of polyQ containing htt fragments. (A) Spin-echo decay of $htt^{NT}Q_{30}P_{10}K_2$ (cyan) and $htt^{NT}Q_{37}P_{10}K_2$ (green) singly-labeled with MTSL dye at position 1. (B) Spin-echo decay of $htt^{NT}Q$ (red), $htt^{NT}Q_{30}P_{10}K_2$ (cyan) and $htt^{NT}Q_{37}P_{10}K_2$ (green) doubly-labeled with MTSL dye at positions 1 and 17. (C) 1-17 distance distributions calculated from data shown in B. Color scheme is same as the previous panels. Also shown in black is the distance distribution for a globular protein. (Data from **J**.S and R.M)

DEER experiments with the single spin labeled $htt^{NT}Q_{30}P_{10}K_2$ and $htt^{NT}Q_{37}P_{10}$ K_2 peptides (Fig 7-2.A) didn't show any stable inter-molecular signal as would be expected if these peptides formed ordered assemblies (or tetramers where the spin label distances would be ~20A$^{\circ}$) under these conditions. Having thus established the lack of any stable aggregating species under these experimental conditions, we moved to investigate monomeric conformational ensembles of the

htt^{NT}, $htt^{NT}Q_{30}P_{10}K_2$ and $htt^{NT}Q_{37}P_{10}K_2$ peptides based on the 1-17 distance distribution (Fig 7-2.B,C). Both the $htt^{NT}Q_{30}P_{10}K_2$ (—) and the $htt^{NT}Q_{37}P_{10}K_2$ (—) peptides display a broadened distance distribution with an average distance of ~25A^0 consistent with the notion that in the monomeric state polyQ containing htt fragments are disordered and can transiently sample multiple conformations. Also shown is the distance distribution between labeled residues in a globular protein (—) which is much narrower than observed in the htt fragments. Interestingly, the average distances calculated by this method match the expected distance between the C_β atoms of Met 1 and Phe 17 when htt^{NT} is an α-helical conformation (Fig 7-2.D). Overall, these results are consistent with previously reported CD studies in suggesting that in the monomeric ensemble polyQ containing htt fragments display a heterogeneous conformational ensemble with some hints of helical structure (100).

Unfortunately however, our efforts to look at the intra-molecular distance distribution in $htt^{NT}Q$ under the same conditions (1X PBS) turned out to be futile since under the same conditions, the relaxation rates of the spin labels were too rapid for DEER measurements. However, we were able to collect some data in the presence of 10-15% glycerol that suggest $htt^{NT}Q$ exists in a compact conformation with a 1-17 distance of ~16 A^0. It is not clear whether this calculated distance is representative of the physiological conformation and short of repeating the other experiments in the same conditions as those used in htt^{NT} sample, there is no way of confirming whether there is actually a conformational transition in the htt^{NT} monomeric ensemble with polyQ expansion. Nevertheless, the results from the $htt^{NT}Q_{30}P_{10}K_2$ and $htt^{NT}Q_{37}P_{10}K_2$ peptides suggest that the monomeric ensemble of longer polyQ containing htt fragments is essentially disordered.

We also tried to explore the effect of polyQ expansion on the monomeric conformation of polyQ containing htt fragments by using molecular dynamics simulation in explicit solvent. Specifically, we were looking at any changes in the conformational preferences of htt^{NT} in response to polyQ expansion.

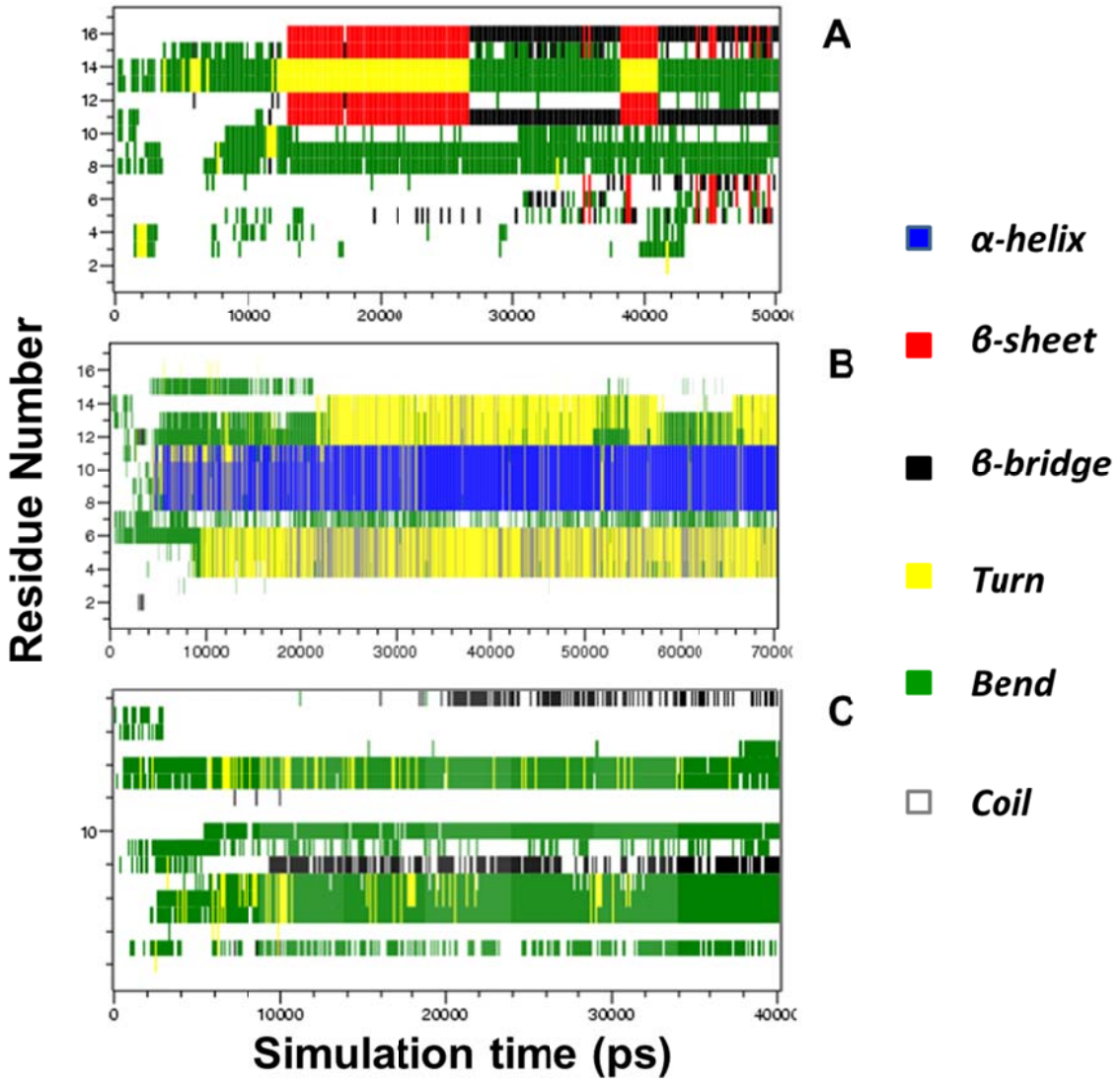

Figure 7-3: MD simulations of monomers of htt fragments. Shown is the evolution in secondary structure for htt^{NT} (A), $htt^{NT}Q_{20}P_{10}K_2$ (B) and $htt^{NT}Q_{37}P_{10}K_2$ (C) during a single-simulation run.

Earlier, Pande and co-workers using replica-exchange based simulation strategies had showed that htt^{NT} adopts helical conformations in aqueous solutions (104). Within the relatively shorter time-scales of these simulations (Fig 7-3), we did not observe any stable secondary structure in htt^{NT} across the three peptides of different polyQ lengths that were studied. The slightly enhanced helicity in htt^{NT} in the $htt^{NT}Q_{20}P_{10}K_2$ is not maintained in the $htt^{NT}Q_{37}P_{10}K_2$ peptide hinting that under these simulation conditions (i.e. not allowing for oligomerization) polyQ expansion does not seem to alter the conformational preferences of htt^{NT}. However, our studies of the aggregation of htt peptides with different polyQ repeat lengths suggest that polyQ expansion does alter initial aggregation rates (Fig 7-1.A, initial 20%). Since the effects do not seem to be mediated at the monomeric level, we next sought to ascertain whether polyQ expansion might affect oligomerization of polyQ containing htt fragments.

7.3.3 polyQ expansion stabilizes oligomerization.

We have shown in earlier chapters that the oligomerization of polyQ containing htt fragments is mediated by htt^{NT}. Thus, CD studies of htt^{NT} identified a concentration dependent transition from random-coil to α-helical spectra indicative most likely of oligomerization, with the mid-point of this transition at ~ 400-500μM. Since polyQ expansion is associated with an acceleration of aggregation rates (Fig 7-1) and given the intricate link between oligomerization and aggregation rates (Chapter 5), we next explored whether polyQ expansion can affect stability of htt^{NT} mediated oligomerization.

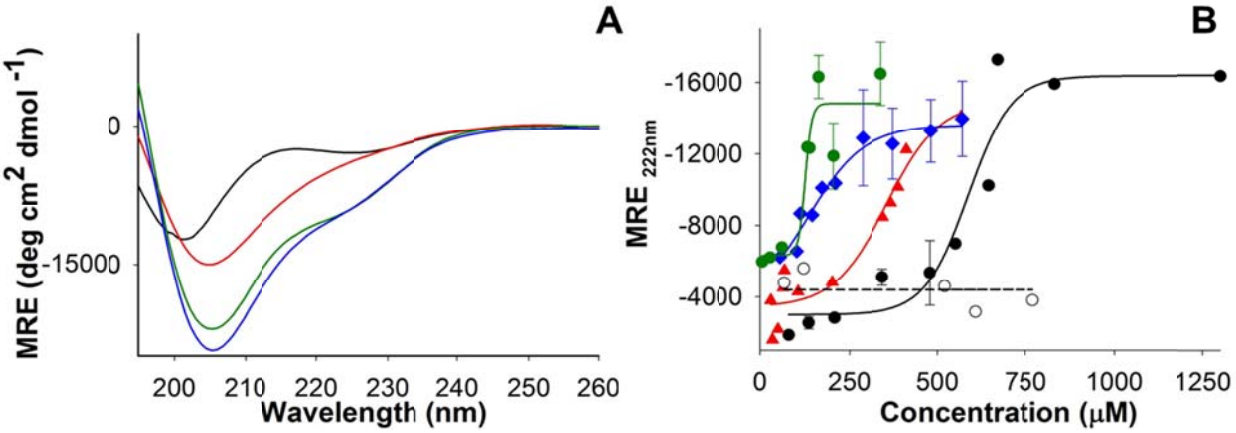

Figure 7-4: CD studies of polyQ containing htt fragments. (A) CD spectra of ~200μM of htt^{NT} (—), $htt^{NT}Q_{15}P_{10}K_2$ (—), $htt^{NT}Q_{25}P_{10}K_2$ (—) and $htt^{NT}Q_{37}P_{10}K_2$ (—). (B) Concentration dependencies of mean residue ellipticities at 222nm for htt^{NT} (●), $htt^{NT}Q_{15}P_{10}K_2$ (▲), $htt^{NT}Q_{25}P_{10}K_2$ (♦) and $htt^{NT}Q_{37}P_{10}K_2$ (●) and $K_2Q_{30}P_6K_2$ (○).

To this end, we decided to look at the concentration dependence of helicity in htt fragments of different polyQ lengths using CD spectroscopy. The presence of polyQ stretches that might remain disordered (based on MW1 binding, (31), Chapter 4) in oligomers was expected to pose complications diluting out helical signal from the htt^{NT} segment in oligomers (Fig 7-4.A, — for example). Therefore, unlike in our previous studies (Chapter 5, 6), we did not use the ratios of the mean residue ellipticity at 222nm and 208nm as proxy for helicity. Instead, we decided to look at the concentration dependence of mean residue ellipticities at 222nm to parse out the random-coil to α-helical conformation. For this approach to work it is important that the MRE_{222nm} signals from polyQ do not change appreciably with concentration.

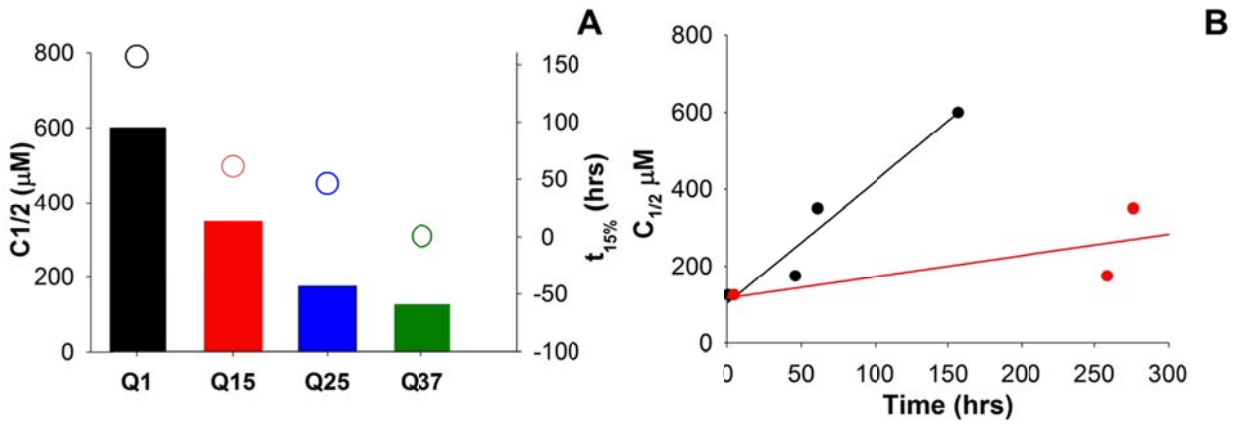

Figure 7-5: polyQ expansion favors oligomerization energetically and kinetically. (A) Mid-points of concentration dependence of helicity in different polyQ containing htt fragments (bars,left axis). Also plotted is the time to 15% aggregation as circles (right axis) of peptides that are similar in sequence to the ones used for CD. (B) Correlation between $C_{1/2}$ and $t_{15\%}$ for these four mutants (—, R^2=0.94) and between $C_{1/2}$ and $t_{1/2}$ (—, R^2=0.5). htt^{NT} was not used in the $t_{1/2}$ correlation.

In our studies with a $K_2Q_{30}P_6K_2$ peptide we indeed did not find much change in the MRE_{222nm} signals with concentration (Fig 7-4.B, ○). Thus, it is likely that the MRE_{222nm} signals at higher concentrations are indicative of helicity within htt^{NT} following oligomerization. We found that as the polyQ repeat length is increased the transition from random-coil to α-helical conformations becomes more favorable at lower concentrations (Fig 7-4.B). This trend is also reflected by the concentration at the mid-point of this transition, $C_{1/2}$ (Fig7-5.A) ranging from 600μM (htt^{NT}-Q) to 125μM for $htt^{NT}Q_{37}P_{10}K_2$. This stabilization of oligomer formation at higher polyQ repeat lengths probably underlies the acceleration of oligomerization with increasing polyQ repeats. Thus, a plot of $C_{1/2}$ of helicity and the time to 15% ($t_{15\%}$) aggregation gave a strong correlation with a R^2 of 0.94. The choice of 15% aggregation as a proxy for oligomerization was dictated by htt^{NT} which was observed to aggregate to 15% (Figure 7-1) and since htt^{NT} forms only oligomers (136), we chose this as a proxy for oligomerization rates. Of

course the time to 15% aggregation is also expected to be modulated by other aggregation events aside from oligomerization (viz. nucleation and elongation).

Next, we wanted to ascertain whether polyQ expansion might also affect other stages of the aggregation pathway independent of its effects on oligomerization. Expectedly, the time to 50% aggregation of any peptide should be modulated by contributions from both oligomerization and other downstream stages of aggregation. Thus, it can be reasoned that if the correlation between the $C_{1/2}$ of helicity for different polyQ length htt peptides and the time to 50% aggregation (that reflects nucleation processes) is comparable to that between $C_{1/2}$ of helicity and the time to 15% aggregation (that reflects, presumably, oligomerization) then the effects of polyQ expansion on aggregation can be explained, in the major part at least, on the basis of its effect on oligomerization. Such an analysis (Fig 7-5.B, —) however gave a poor correlation with a R^2 of 0.5 suggesting that polyQ expansion exhibits independent effects on both oligomer formation and stochastic nucleation efficiency(and/or elongation) in htt fragments . However, one must consider that the sample size in these analyses is too small to conclusively prove this point. Rather, the purpose of this exercise is to set the hypothesis for future studies that aim to delineate the role of polyQ expansion on nucleation and/or elongation efficiencies.

7.4 DISCUSSION.

Polyglutamine expansion is the fundamental molecular event that precipitates HD. While, repeat length expansion has been linked to several cellular processes, the increase in aggregation kinetics *in vitro* and aggregate burden *in vivo* is of particular interest to us. Early studies with simple polyQ peptides showed that aggregation propensities are directly tied to the

size of the polyQ stretch. Subsequently, this polyQ dependence of aggregation was also observed in the aggregation of polyQ containing htt fragments ((31), Fig 7-1). It is possible for the pro-aggregation effects of polyQ expansion to be mediated at any of the different stages of the aggregation pathway i.e by altering the monomeric conformational ensemble, by stabilizing oligomerization, by favoring nucleation within oligomers, by increasing the stabilities of the final fibrils. Here, we have looked at the effects of polyQ expansion on the average monomeric conformation and on htt^{NT} mediated oligomerization.

A case for a conformational transition to a β-rich structure within the monomeric ensemble at higher polyQ repeat lengths has been made based on antibody binding and bulk spectroscopic techniques (96, 99, 108, 131). CD results from our group (31, 100) and those of others (103) do not show the existence of any stable β-sheet conformation in the monomeric ensemble of polyQ containing proteins of any repeat length. The focus of this current work has therefore been to primarily look at the conformation of htt^{NT} in the monomeric ensemble of htt fragments with different polyQ repeats. Earlier, FRET based studies from the lab had shown that with an increase in the polyQ repeat length, the htt^{NT} conformation switches from a compact to an extended state. However, using a more careful FRET approach to measuring the distance between residues at -1 and 17 in the htt^{NT} sequence, we did not notice any major difference in the conformation of the htt^{NT} sequence in htt fragments with 3 or 37 glutamine repeats. As an additional probe of htt^{NT} conformation at different polyQ repeat lengths we also looked at the distance distribution between residues 1 and 17 using EPR based DEER techniques. Consistent with our CD results, htt fragments of different polyQ repeat lengths are essentially disordered in their monomeric ensemble, evinced by the spread of the 1-17 distance distributions. Also, at higher polyQ repeat lengths the average distance is ~25A° as would be expected for the htt^{NT}

sequence in an α-helical conformation consistent with the increase in helical propensities reported for the monomer at higher polyQ repeats (100). While, there was an observed difference in the average 1-17 distance in htt^{NT} and $htt^{NT}Q_{37}P_{10}K_2$ this is most likely due to difference in the measurement conditions. Overall, these results suggest that polyQ expansion does not appreciably alter the monomeric ensemble of htt segments which are still predominantly disordered.

Based on our work detailed in Chapters 4 and 5, the primary role of htt^{NT} in the aggregation of polyQ containing htt fragments is mediated through oligomerization. While oligomerization is believed to be primarily mediated through interactions between htt^{NT}, it is still possible that polyQ expansion can affect htt^{NT} mediated oligomerization. The preliminary results shown here indicate that polyQ expansion stabilizes htt^{NT} mediated oligomer formation based on the reduction in the $C_{1/2}$ of helicity with increasing glutamine repeats. This observation is also consistent with the increase in the rates of oligomerization observed upon increasing polyQ length in htt fragments (100). At this stage, the structural/mechanistic details of polyQ stabilization of oligomers are not clear. It is possible that polyQ stabilizes helicity, a fundamental facet of polyQ containing htt fragments' aggregation. For instance, the crystal structure of a htt exon-1 fragment suggests that the polyQ stretch adjacent to htt^{NT} can adopt a helical sequence (80). However, our results with the htt^{NT}-P-$Q_{37}P_{10}K_2$ peptide (Chapter 5) that aggregates similar to the WT control argue against such stabilization. Alternately, stabilization of these oligomers could also possibly be mediated through inter-molecular interactions between polyQ segments from different monomers within tetramers.

While, we have not yet looked at the effects of polyQ expansion on stochastic nucleation within the oligomers, it is entirely possible (and in fact likely) that there is an intricate link

between the two. In fact, a cursory examination of the aggregation kinetics of htt fragments with different length polyQ repeats suggests this to be the case. Thus, the aggregation of $htt^{NT}Q_{37}P_{10}K_2$ (Fig 7-1, ♦) is substantially faster than $htt^{NT}Q_{23}P_{10}K_2$ (Fig 7-1, ☆) even though these peptides are not substantially different in their oligomerization stabilities (Fig 7-4.B). This observation suggests that the differences in kinetics probably stem from polyQ repeat length effects on the subsequent nucleation event. This would not be surprising given the role of repeat length in nucleation of simple polyQ peptides (121). While the transience of the nucleation event makes it intractable to most bulk biophysical techniques, it is hoped that the use of single-molecule techniques such as fluorescence correlation spectroscopy or total internal reflection based fluorescence microscopy might allow us to investigate this particular hypothesis.

8.0 CONCLUSIONS.

8.1 THESIS CONTRIBUTIONS.

Work from the lab, at the outset of this work, had just highlighted the crucial role that the first seventeen residues of huntingtin (htt^{NT}) play in the aggregation of polyQ containing htt fragments. The major focus of the work presented in this thesis has been to elucidate in detail the mechanistic and structural details of htt^{NT} mediated aggregation.

8.1.1 Amphipathic helicity drives htt^{NT} mediated aggregation

Using a combinatorial approach relying on rationally designed mutations and structural and biochemical techniques we have identified that the adoption of a helical conformation by htt^{NT} is crucial to oligomerization and by extension the aggregation of polyQ containing htt fragments (Chapters 4 and 5). A particularly distinctive feature of the htt^{NT} sequence is the presence of hydrophobic residues that are uniformly distributed throughout the sequence. Our results show that net hydrophobicity cannot solely explain the aggregation enhancing role of htt^{NT}. Rather, it is the ability of htt^{NT} to adopt an amphipathic helical conformation within oligomers that can present a hydrophobic interaction surface that stabilizes oligomers and promotes stochastic nucleation of amyloid structure. However, as the results of our work with the scrambled htt^{NT} sequences (Chapter 4) suggest, in addition to the role that htt^{NT} plays in

mediating initial oligomerization there is some evidence for a secondary role in mediating stochastic nucleation consistent with at least part of this sequence adopting a β-sheet conformation in final aggregates formed by polyQ containing htt fragments.

8.1.2 Delineating the effects of PTMs on htt^{NT} mediated aggregation

In addition to its role in modulating the aggregation of polyQ containing htt fragments, the htt^{NT} sequence is also the site of several post-translational modifications. The results of our studies with some of these modifications suggest that in addition to the cellular roles they can also modulate aggregation of polyQ containing htt fragments. Particularly the phosphorylation of serines 13 and 16 which abrogates HD pathology substantially impairs the aggregation kinetics and aggregate stability highlighting the importance of acknowledging the effect of post-translational modifications on biophysical properties of the target sequence.

8.1.3 Putative htt^{NT} tetrameric structure

Oligomers of polyQ containing htt fragments have been widely cited as being the toxic species in HD pathology though this still remains controversial. A structural insight into the organization of such oligomers is not only crucial for our understanding of their role in HD pathology but also for designing aggregation inhibiting strategies. Here, we have described a preliminary model of the putative htt^{NT} tetrameric structure that is populated during aggregation. While this structure does not account for the role of polyQ segments on oligomer formation, it still provides a theoretical framework for the design of experiments aimed at elucidating structure of these oligomers. In addition, it could also possibly pave the way for *in silico*

screening experiment aimed at identifying inhibitors of oligomerization which might not only have potential therapeutic relevance but also provides us with reagents that can directly test the role of aggregation in disease pathology in cellular or animal models of HD.

8.1.4 Exploring the effect of polyQ expansion on htt^{NT} mediated oligomerization.

While the htt^{NT} sequence is the primary driver in the oligomerization of polyQ containing htt fragments, the polyQ segment does not play an entirely passive role in this process. Thus, at least some portion of the effect of polyQ expansion on the aggregation of htt fragments stems from its ability to stabilize oligomerization (Chapter 7). It is unclear at this stage as to how polyQ expansion structurally stabilizes oligomers and this will remain the focus of future studies.

8.2 FUTURE DIRECTIONS.

Overall, these results have contributed to an emerging picture that unmasks the role of htt^{NT} in the oligomerization stage of the aggregation pathway. Yet, there are several aspects to the aggregation of polyQ containing htt fragments that remain to be ascertained. Thus far we have not been able to get many insights into the process of stochastic nucleation of polyQ amyloid structure that is believed to occur within these oligomers. The transience of this event makes it pretty inaccessible to most, if not all, bulk techniques and the only insights that we have gleaned are based on analyses of events that are linked to this process. However, single-molecule techniques such as TIRFM and FCS-FRET can shed some light on this aspect of the aggregation pathway and particularly the role that polyQ expansion plays in this process. Finally, since the

ultimate goal of these studies is to clarify the role of aggregation in the context of HD pathology, the study of htt aggregation *in vivo* is indispensable. This is one direction that the lab has currently set its focus towards, guided by the results from our *in vitro* studies.

APPENDIX A: SUPPLEMENTARY DATA.

A.1 EFFECT OF HYDROPHOBIC ALA MUTANTS ON HTT^{NT}-Q3 PEPTIDES.

The htt^{NT}-Q3 peptide when incubated for ~1000 hours forms oligomers that can be visualized by EM and pelleted and studied by FTIR (at high starting concentrations). Using the sedimentation assay, we looked at the ability of the M8A, L4A and M8P mutants on the aggregation kinetics and aggregate (oligomer) structure of htt^{NT}-Q3 peptides. We found that all of these mutants hardly aggregate at low concentrations. Even when incubated at high concentrations (~1mM) for ~1000 hrs, these mutants yield very small amount of pelletable oligomers that exhibit predominantly random coil spectra. In contrast, the WT htt^{NT}Q$_3$ peptide forms predominantly helical oligomers.

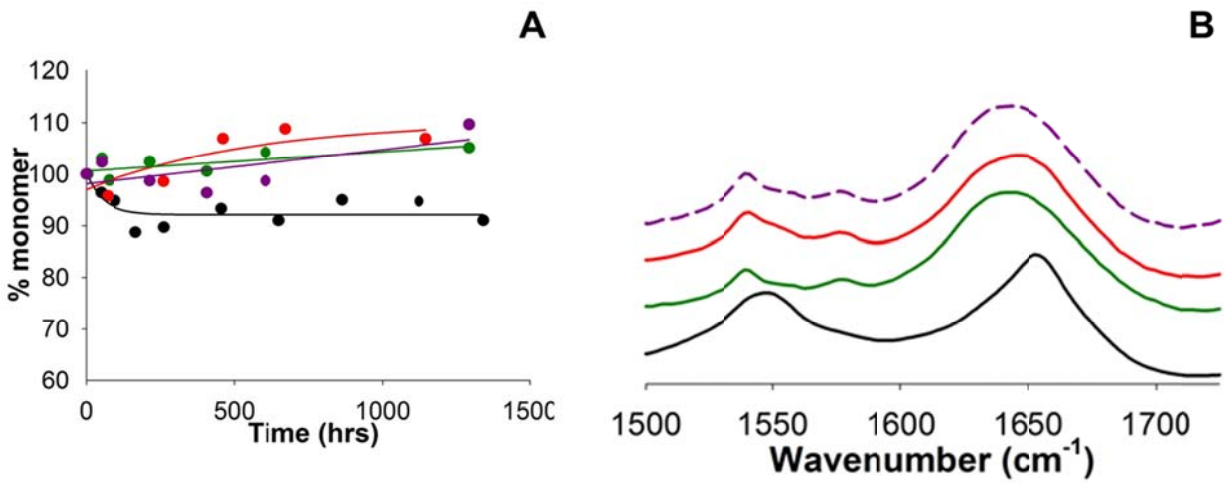

Figure A-1: Role of ampiphilicity in htt^{NT} oligomerization (I) (a) Kinetics of oligomerization of ~10μM-20μM of htt^{NT}-Q_3 peptides WT (●),M8A (●), L4A (●) and M8P (●). (b) FTIR spectra of isolated oligomers of alanine mutants in a htt$^{NT}Q_3$ background. The same coloring scheme is used as in (a). Also shown is the FTIR spectrum of the M8P mutant (---) in the same peptide background. Peptide concentrations were in the millimolar regime.

A.2 STUDIES WITH THE HTT^{NT}-Q3 (K6A) MUTANT.

We had initially designed the htt$^{NT}Q_3$ (K6A) peptide to investigate the effect of this mutation on oligomer kinetics and structure (in analogy to the studies discussed above) since studies with the htt$^{NT}Q_{37}P_{10}K_2$ peptide indicated that this mutation accelerates aggregation kinetics. The peptide aggregates essentially identically to the WT at lower concentrations. Surprisingly however, at high concentrations, this peptide, unlike the WT, was observed to form well defined-fibrils (Fig A-2.C) with an anti-parallel orientation (based on FTIR peaks at 1625cm-1 and 1690 cm-1). These fibrils are formed through a helical intermediate (Fig A-2.B, - - -) however consistent with the increased stabilization of oligomerization observed in this mutant (K6A). Also, a

substantial portion of the final fibrils are in a helical conformation (1653cm-1) which can participate in HD –exchange. (Fig A-2.B,---)

At this stage the mechanism of fibrillation observed in the K6A mutant is not entirely clear. However, the unexpected behavior of this peptide indicated that the simplistic "divide and conquer" strategy for understanding the role of htt^{NT} mutations in oligomer formation is problematic, since altering the sequence context of the mutated htt^{NT} segment appeared to significantly alter it's aggregation properties.

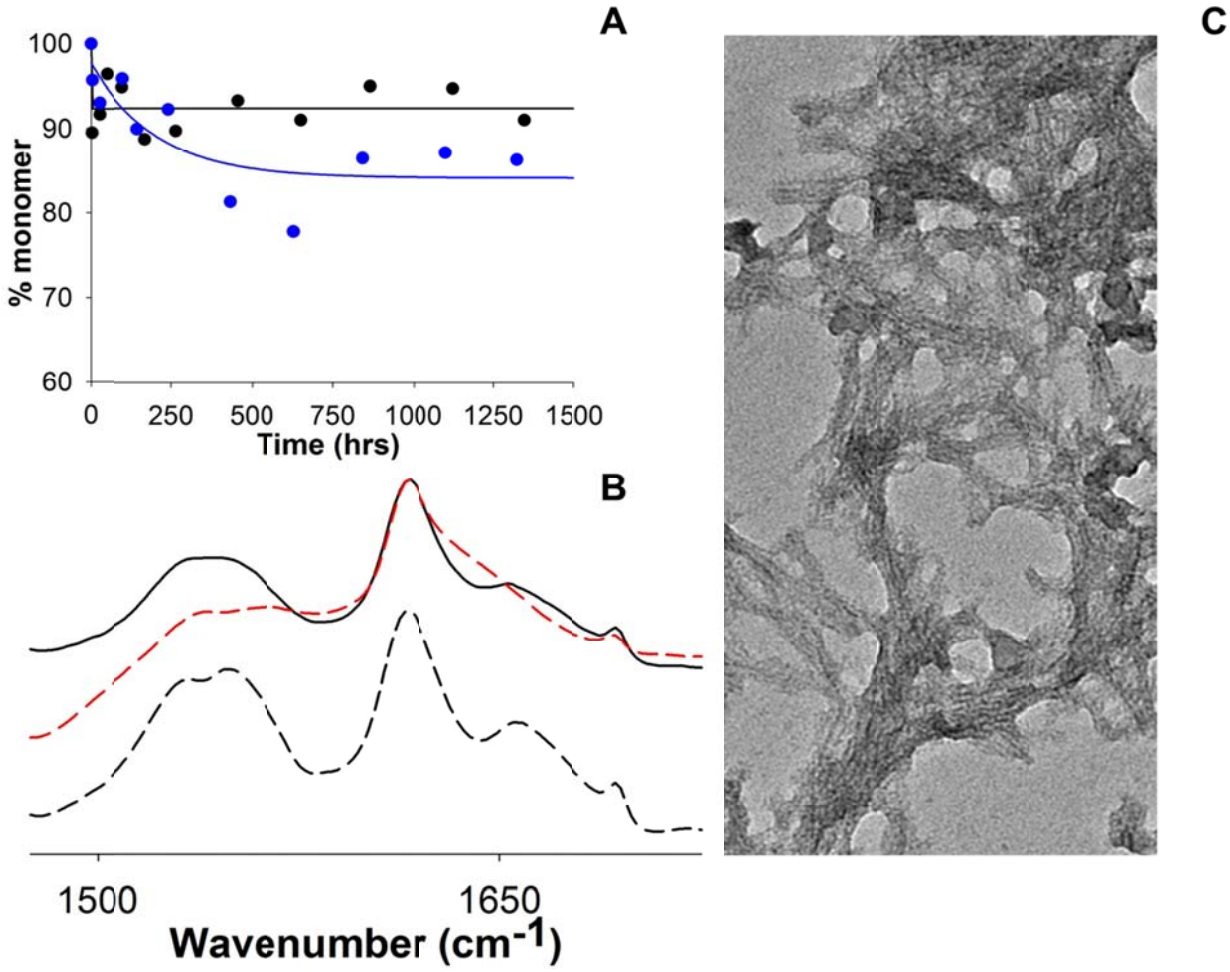

Figure A-2: Effect of K6A mutation on aggregation of $htt^{NT}Q_3$. (A) Aggregation kinetics of ~20-30μM of WT (●) and K6A (●) peptides. (B) FTIR spectra of $htt^{NT}Q_3$(K6A) aggregates isolated after 1 hr (– –), 3500 hrs (▬) and aggregates isolated after 800 hrs that were incubated in D2O for 2hrs (---) .

A.3 CALCULATION OF $C_{1/2}$HELIX FOR ALANINE MUTANTS OF HTTNT PEPTIDES.

In order to compute $C_{1/2}^{helix}$, the MRE_{222nm}/MRE_{208nm} ratios at different concentrations of various mutants were plotted and then fitted with a four-parameter sigmoidal function. The concentration corresponding to the mid-point of this transition was then used to calculate the value of $C_{1/2}^{helix}$.

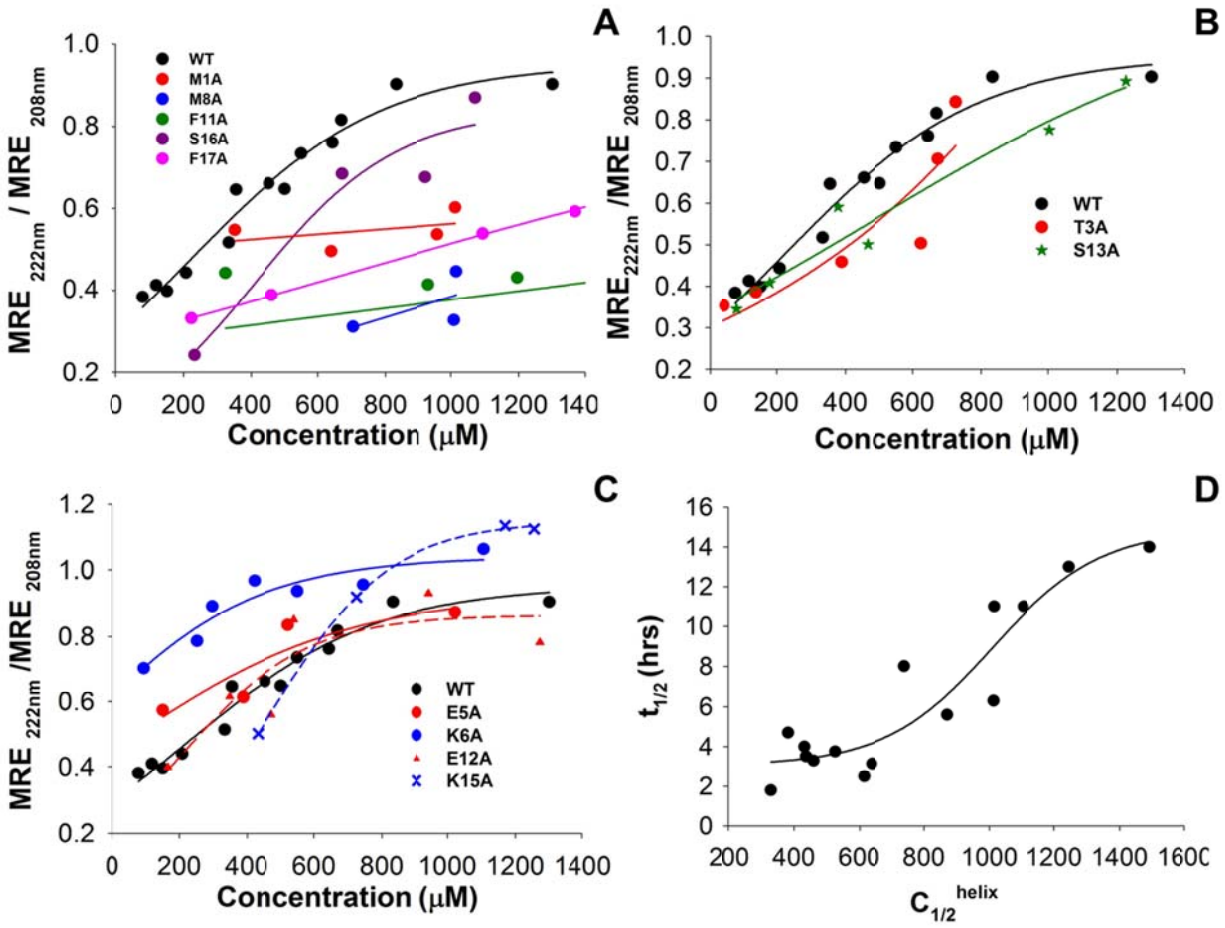

Figure A-3. Stabilities of mutant htt^{NT} oligomerization. (A-C) Dependence of helicity on concentrations for different alanine mutants. (D) Correlation between $t_{1/2}$ of aggregation and $C_{1/2}^{helix}$ for different alanine mutants. (R^2=0.9). The K9A mutant data is not shown.

A.4 STUDIES OF THE M8P MUTATION IN A HTT$^{NT}Q_8K_2$ PEPTIDE.

Since the M8P mutation was observed to reduce the aggregation of polyQ containing htt fragments and abrogate oligomerization in htt^{NT} (Chapter 5) we decided to look at the effect of this mutation on the stochastic nucleation within oligomers by looking at the aggregation of a htt$^{NT}Q_8K_2$ peptide.

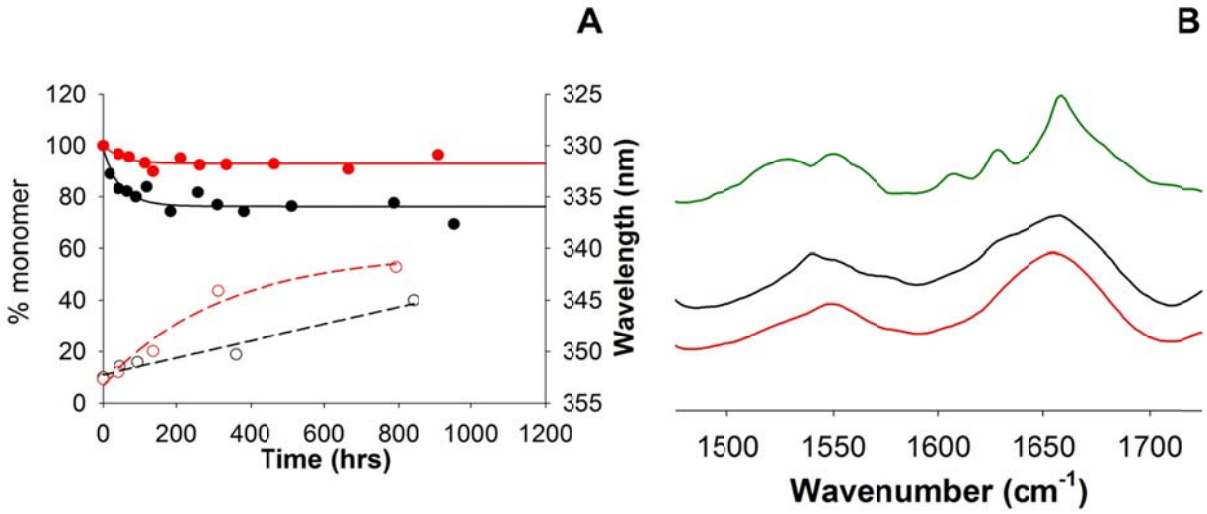

Figure A-4: Aggregation of htt$^{NT}Q_8K_2$ (F17W) peptides. (A) Aggregation of WT (●) and M8P (●) followed by sedimentation assay. Also shown are the peak positions of the maxima in the fluorescence emissions spectra of Trp 17 in aggregates of WT (○) and M8P (○) isolated at different times. (B) FTIR spectra of aggregates of M8P isolated after 1 hr (—), 45 hrs (—) and 312 hrs (—).

Going into these studies, our hypothesis was that the M8P mutation would impair stochastic nucleation. Consistent with this hypothesis, at low concentrations, the M8P mutant (Fig A-4.A,●) aggregates slower than the WT (Fig A-4.A, ●). However at high concentrations, this trend is reversed with the M8P mutant forming pelletable β-sheet rich aggregates (Fig A-2.B,—) considerably faster than the WT based on the burial of the Trp17 (Fig A-4.A, ○ vs ○).

Furthermore, the aggregation of the M8P mutant seems to proceed through α-helical oligomers (Fig A-4.B, —) contrary to our hypothesis. This data is another indication of the risks of the "divide and conquer" approach to analyzing the aggregation behavior of htt fragments.

A.5 STUDIES ON THE S13A/S16A MUTATION.

Summarized here are some of the studies on the S13, 16A mutation. We first looked at the effect of the S13/S16A mutation on the monomeric conformation of a $htt^{NT}Q_{37}P_{10}K_2$ peptide.

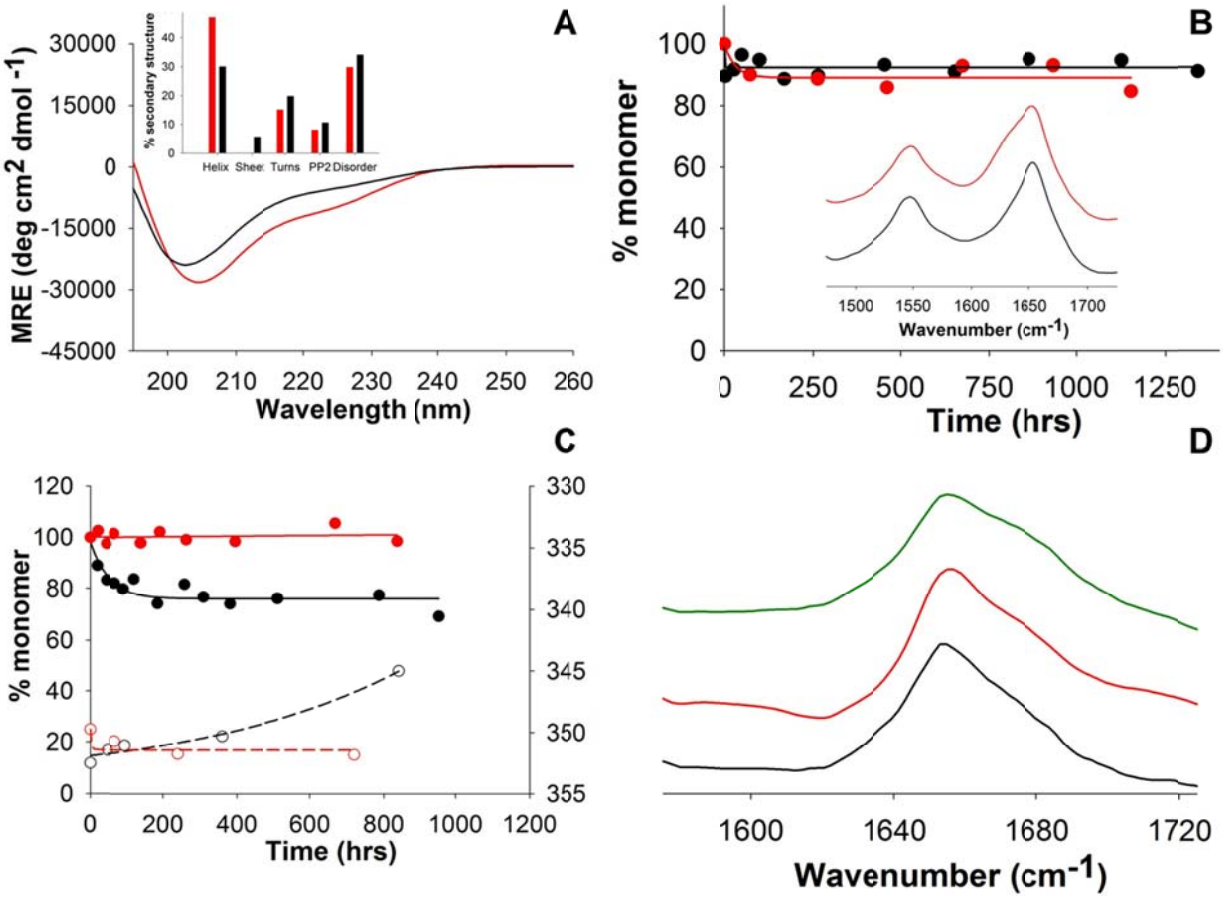

Figure A-5: Effect of S13A/S16A mutation on aggregation of polyQ containing htt fragments. (A) CD spectra of $htt^{NT}Q_{37}P_{10}K_2$ peptides: WT (—) and S13A/S16A (—). Inset shows the deconvolution of these spectra into individual secondary structure components. (B) Aggregation of $htt^{NT}Q_3$ peptides , WT (—) and S13A/S16A (—).

(Inset) FTIR spectra of oligomers isolated from these peptides (Same color scheme). (C) Aggregation of $htt^{NT}Q_8K_2$ (F17W) peptides. WT (●) and S13A/S16A (●) followed by sedimentation assay. Also shown are the peak positions of the maxima in the fluorescence emissions spectra of Trp 17 in aggregates of WT (○) and S13A/S16A (○) isolated at different times. (B) FTIR spectra of aggregates of $htt^{NT}Q_8K_2$ S13A/S16A isolated after 68 hrs (—), 240 hrs (—) and 720 hrs (—).

We found that the monomeric conformation of this mutant showed slightly more helicity than the WT (Fig A-5.A). We also looked at effect of this mutation on the aggregation of the $htt^{NT}Q_3$ peptide. Overall, we found that the WT and the S13A/S16A aggregate with similar kinetics to form predominantly helical oligomers (Fig A-5.B). Next, we explored whether the S13A/S16A mutation affects the stochastic nucleation within oligomers by looking at the aggregation of the $htt^{NT}Q_8K_2$ (S13A/S16A). To our surprise, this peptide did not aggregate appreciably at low concentrations (Fig A-5.C). FTIR spectra of aggregates isolated at high concentrations showed that while the $htt^{NT}Q_8K_2$ (S13A/S16A) forms helical oligomers, stochastic nucleation within these oligomers seems impaired evinced by the lack of β-sheet rich aggregate formation, as observed with the WT peptide (Fig A-5.D). One possible explanation of this result is that the S13A/S16A stabilization of oligomerization interferes with nucleation which is probably associated with at least part of the htt^{NT} sequence (including S16) adopting a β strand conformation. Since in the $htt^{NT}Q_{37}P_{10}K_2$ context the S13A/S16A mutant aggregates substantially more to form amyloid fibrils, it is likely that these counter-intuitive results are a feature of the peptide context used.

A.6 TRYPSIN DIGESTION STUDIES OF SCRAMBLED HTTNTQ30P6K2 PEPTIDES.

The susceptibility of aggregates to cleavage by proteases can provide crucial insights into the underlying structure. Earlier, we had reported that final aggregates formed by htt^{NT} $Q_{30}P_6K_2$ peptides are substantially protected from cleavage by the protease trypsin (which cuts at three lysine residues within the htt^{NT} sequence). We thus decided to look at the susceptibility of the $shtt^{NT}$ sequences to trypsin cleavage in the final aggregates of the $shtt^{NT}Q_{30}P_6K_2$ peptides. The differences in the relative positions of the lysine residues make comparisons across these peptides unfeasible. Nevertheless, we still hoped to glean some information about the degree to which these scrambled htt^{NT} sequences participate in the final aggregate structures.

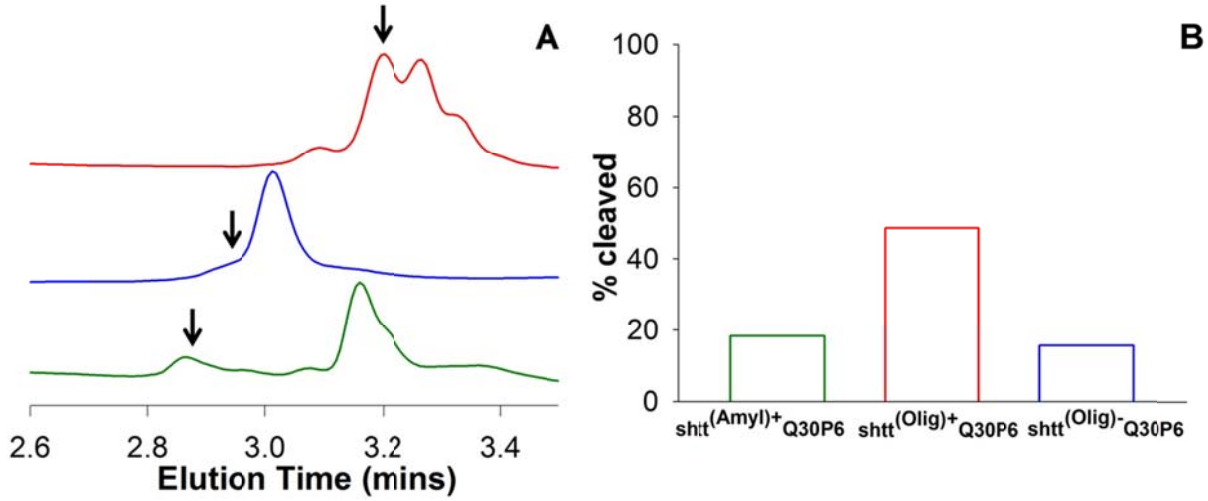

Figure A-6: Trypsin digestion of $shtt^{NT}Q^{30}P^6K^2$ peptides. (A) LC-MS chromatograms of the trypsinization products of final aggregates of $shtt^{(Olig)+}Q_{30}P_6K_2$ (—), $shtt^{(Olig)-}Q_{30}P_6K_2$ (—) and $shtt^{(Amyl)+}Q_{30}P_6K_2$ (—) with arrows showing the position of cleaved fragments in the eluent. (B) Quantification of trypsin cleavage of aggregates calculated based on peak-areas of cleaved and uncleaved fragments (for $shtt^{(Olig)+}Q_{30}P_6K_2$ and $shtt^{(Amyl)+}Q_{30}P_6K_2$ peptides) or normalized relative abundances of cleaved and uncleaved fragments for $shtt^{(Olig)-}Q_{30}P_6K_2$ peptide.

We found that the aggregates formed by all the three peptides showed greater susceptibility to trypsin cleavage than that observed for the final aggregates of polyQ containing htt fragments ((31),Chapter 6). Of the three shtt$^{NT}Q_{30}P_6K_2$ peptides, the shtt$^{(Amyl)+}Q_{30}P_6K_2$ and (Fig A-6.A/B, —) and the shtt$^{(Olig)-}$ $Q_{30}P_6K_2$ (Fig A-6.A/B, —) peptides showed the least susceptibility to trypsin (~20% cleavage).

Also, the major sites of cleavage in both these peptides were in the early portion of the sequence (Table A-1). On the other hand, final aggregates of both the shtt$^{(Olig)+}Q_{30}P_6K_2$ (Fig A-6.A/B, —) peptide were cleaved substantially by trypsin (~50%) with the sites of cleavage located in different regions of the leader shtt^{NT} sequence. Overall, these results indicate that amongst the shtt^{NT} sequences, the shtt$^{(Amyl)+}$ sequence has the highest tendency to be incorporated into fibril structures while the shtt$^{(Olig)+}$ has the least propensity to do so.

Peptide	***Fragment Masses (Cut-site)***	***% abundance***
shtt$^{(Amyl)+}Q_{30}P_6K_2$	6090 (Lys 6)	100
shtt$^{(Olig)+}Q_{30}P_6K_2$	6155 (Lys5)	62
	6027 (Lys 6)	31
	5768 (Lys 8)	7
shtt$^{(Olig)-}Q_{30}P_6K_2$	6310 (Lys 3)	58
	5746 (Lys 8)	42

Table A-1: Fragments obtained after trypsinization of shtt$^{NT}Q_{30}P_6K_2$ aggregates. Masses of cleaved fragments alongwith corresponding cut-sites within the shtt^{NT} sequence. The % abundance of cleaved fragments for any particular peptide were calculated by normalizing the individual relative abundances of these fragments to the sum-total of all relative abundances of the cleaved fragments for that peptide.

BIBLIOGRAPHY

1. A novel gene containing a trinucleotide repeat that is expanded and unstable on Huntington's disease chromosomes. The Huntington's Disease Collaborative Research Group. Cell. 1993;72(6):971-83.

2. DiFiglia M, Sapp E, Chase KO, Davies SW, Bates GP, Vonsattel JP, et al. Aggregation of huntingtin in neuronal intranuclear inclusions and dystrophic neurites in brain. Science. 1997;277(5334):1990-3.

3. Kozlowski P, de Mezer M, Krzyzosiak WJ. Trinucleotide repeats in human genome and exome. Nucleic Acids Res. 2010;38(12):4027-39. PMCID: 2896521.

4. Mirkin SM. Expandable DNA repeats and human disease. Nature. 2007;447(7147):932-40.

5. Wojciechowska M, Krzyzosiak WJ. CAG repeat RNA as an auxiliary toxic agent in polyglutamine disorders. RNA Biol. 2011;8(4):565-71. PMCID: 3225975.

6. Zu T, Gibbens B, Doty NS, Gomes-Pereira M, Huguet A, Stone MD, et al. Non-ATG-initiated translation directed by microsatellite expansions. Proc Natl Acad Sci U S A. 2011;108(1):260-5. PMCID: 3017129.

7. Krzyzosiak WJ, Sobczak K, Wojciechowska M, Fiszer A, Mykowska A, Kozlowski P. Triplet repeat RNA structure and its role as pathogenic agent and therapeutic target. Nucleic Acids Res. 2012;40(1):11-26. PMCID: 3245940.

8. Nasir J, Floresco SB, O'Kusky JR, Diewert VM, Richman JM, Zeisler J, et al. Targeted disruption of the Huntington's disease gene results in embryonic lethality and behavioral and morphological changes in heterozygotes. Cell. 1995;81(5):811-23.

9. Boxall R, Porteous DJ, Thomson PA. DISC1 and Huntington's disease--overlapping pathways of vulnerability to neurological disorder? PLoS One. 2011;6(1):e16263. PMCID: 3027647.

10. Costa MC, Magalhaes P, Guimaraes L, Maciel P, Sequeiros J, Sousa A. The CAG repeat at the Huntington disease gene in the Portuguese population: insights into its dynamics and to the origin of the mutation. J Hum Genet. 2006;51(3):189-95.

11. Barron LH, Warner JP, Porteous M, Holloway S, Simpson S, Davidson R, et al. A study of the Huntington's disease associated trinucleotide repeat in the Scottish population. J Med Genet. 1993;30(12):1003-7. PMCID: 1016632.

12. Tartari M, Gissi C, Lo Sardo V, Zuccato C, Picardi E, Pesole G, et al. Phylogenetic comparison of huntingtin homologues reveals the appearance of a primitive polyQ in sea urchin. Mol Biol Evol. 2008;25(2):330-8.

13. Clabough EB, Zeitlin SO. Deletion of the triplet repeat encoding polyglutamine within the mouse Huntington's disease gene results in subtle behavioral/motor phenotypes in vivo and elevated levels of ATP with cellular senescence in vitro. Hum Mol Genet. 2006;15(4):607-23.

14. Schilling B, Gafni J, Torcassi C, Cong X, Row RH, LaFevre-Bernt MA, et al. Huntingtin phosphorylation sites mapped by mass spectrometry. Modulation of cleavage and toxicity. J Biol Chem. 2006;281(33):23686-97.

15. Matsumoto G, Wada K, Okuno M, Kurosawa M, Nukina N. Serine 403 phosphorylation of p62/SQSTM1 regulates selective autophagic clearance of ubiquitinated proteins. Mol Cell. 2011;44(2):279-89.

16. Gu X, Greiner ER, Mishra R, Kodali R, Osmand A, Finkbeiner S, et al. Serines 13 and 16 are critical determinants of full-length human mutant huntingtin induced disease pathogenesis in HD mice. Neuron. 2009;64(6):828-40. PMCID: 2807408.

17. Aiken CT, Steffan JS, Guerrero CM, Khashwji H, Lukacsovich T, Simmons D, et al. Phosphorylation of threonine 3: implications for Huntingtin aggregation and neurotoxicity. J Biol Chem. 2009;284(43):29427-36. PMCID: 2785575.

18. Cong X, Held JM, DeGiacomo F, Bonner A, Chen JM, Schilling B, et al. Mass spectrometric identification of novel lysine acetylation sites in huntingtin. Mol Cell Proteomics. 2011;10(10):M111 009829. PMCID: 3205870.

19. Steffan JS, Agrawal N, Pallos J, Rockabrand E, Trotman LC, Slepko N, et al. SUMO modification of Huntingtin and Huntington's disease pathology. Science. 2004;304(5667):100-4.

20. Yanai A, Huang K, Kang R, Singaraja RR, Arstikaitis P, Gan L, et al. Palmitoylation of huntingtin by HIP14 is essential for its trafficking and function. Nat Neurosci. 2006;9(6):824-31. PMCID: 2279235.

21. Gafni J, Hermel E, Young JE, Wellington CL, Hayden MR, Ellerby LM. Inhibition of calpain cleavage of huntingtin reduces toxicity: accumulation of calpain/caspase fragments in the nucleus. J Biol Chem. 2004;279(19):20211-20.

22. Kim YJ, Yi Y, Sapp E, Wang Y, Cuiffo B, Kegel KB, et al. Caspase 3-cleaved N-terminal fragments of wild-type and mutant huntingtin are present in normal and

Huntington's disease brains, associate with membranes, and undergo calpain-dependent proteolysis. Proc Natl Acad Sci U S A. 2001;98(22):12784-9. PMCID: 60131.

23. Wellington CL, Ellerby LM, Hackam AS, Margolis RL, Trifiro MA, Singaraja R, et al. Caspase cleavage of gene products associated with triplet expansion disorders generates truncated fragments containing the polyglutamine tract. J Biol Chem. 1998;273(15):9158-67.

24. Wellington CL, Singaraja R, Ellerby L, Savill J, Roy S, Leavitt B, et al. Inhibiting caspase cleavage of huntingtin reduces toxicity and aggregate formation in neuronal and nonneuronal cells. J Biol Chem. 2000;275(26):19831-8.

25. Zhang Y, Leavitt BR, van Raamsdonk JM, Dragatsis I, Goldowitz D, MacDonald ME, et al. Huntingtin inhibits caspase-3 activation. EMBO J. 2006;25(24):5896-906. PMCID: 1698892.

26. Southwell AL, Bugg CW, Kaltenbach LS, Dunn D, Butland S, Weiss A, et al. Perturbation with intrabodies reveals that calpain cleavage is required for degradation of huntingtin exon 1. PLoS One. 2011;6(1):e16676. PMCID: 3031625.

27. Zuccato C, Valenza M, Cattaneo E. Molecular mechanisms and potential therapeutical targets in Huntington's disease. Physiol Rev. 2010;90(3):905-81.

28. Rockabrand E, Slepko N, Pantalone A, Nukala VN, Kazantsev A, Marsh JL, et al. The first 17 amino acids of Huntingtin modulate its sub-cellular localization, aggregation and effects on calcium homeostasis. Hum Mol Genet. 2007;16(1):61-77.

29. Atwal RS, Xia J, Pinchev D, Taylor J, Epand RM, Truant R. Huntingtin has a membrane association signal that can modulate huntingtin aggregation, nuclear entry and toxicity. Hum Mol Genet. 2007;16(21):2600-15.

30. Cornett J, Smith L, Friedman M, Shin JY, Li XJ, Li SH. Context-dependent dysregulation of transcription by mutant huntingtin. J Biol Chem. 2006;281(47):36198-204.

31. Thakur AK, Jayaraman M, Mishra R, Thakur M, Chellgren VM, Byeon IJ, et al. Polyglutamine disruption of the huntingtin exon 1 N terminus triggers a complex aggregation mechanism. Nat Struct Mol Biol. 2009;16(4):380-9. PMCID: 2706102.

32. Duennwald ML, Jagadish S, Muchowski PJ, Lindquist S. Flanking sequences profoundly alter polyglutamine toxicity in yeast. Proc Natl Acad Sci U S A. 2006;103(29):11045-50. PMCID: 1544171.

33. Andrade MA, Bork P. HEAT repeats in the Huntington's disease protein. Nat Genet. 1995;11(2):115-6.

34. Takano H, Gusella JF. The predominantly HEAT-like motif structure of huntingtin and its association and coincident nuclear entry with dorsal, an NF-kB/Rel/dorsal family transcription factor. BMC Neurosci. 2002;3:15. PMCID: 137586.

35. Kalchman MA, Graham RK, Xia G, Koide HB, Hodgson JG, Graham KC, et al. Huntingtin is ubiquitinated and interacts with a specific ubiquitin-conjugating enzyme. J Biol Chem. 1996;271(32):19385-94.

36. Luo S, Vacher C, Davies JE, Rubinsztein DC. Cdk5 phosphorylation of huntingtin reduces its cleavage by caspases: implications for mutant huntingtin toxicity. J Cell Biol. 2005;169(4):647-56. PMCID: 2171695.

37. Thompson LM, Aiken CT, Kaltenbach LS, Agrawal N, Illes K, Khoshnan A, et al. IKK phosphorylates Huntingtin and targets it for degradation by the proteasome and lysosome. J Cell Biol. 2009;187(7):1083-99. PMCID: 2806289.

38. Jeong H, Then F, Melia TJ, Jr., Mazzulli JR, Cui L, Savas JN, et al. Acetylation targets mutant huntingtin to autophagosomes for degradation. Cell. 2009;137(1):60-72. PMCID: 2940108.

39. Li W, Serpell LC, Carter WJ, Rubinsztein DC, Huntington JA. Expression and characterization of full-length human huntingtin, an elongated HEAT repeat protein. J Biol Chem. 2006;281(23):15916-22.

40. Wellington CL, Hayden MR. Of molecular interactions, mice and mechanisms: new insights into Huntington's disease. Curr Opin Neurol. 1997;10(4):291-8.

41. Heng MY, Detloff PJ, Albin RL. Rodent genetic models of Huntington disease. Neurobiol Dis. 2008;32(1):1-9.

42. Hermel E, Gafni J, Propp SS, Leavitt BR, Wellington CL, Young JE, et al. Specific caspase interactions and amplification are involved in selective neuronal vulnerability in Huntington's disease. Cell Death Differ. 2004;11(4):424-38.

43. Lunkes A, Lindenberg KS, Ben-Haiem L, Weber C, Devys D, Landwehrmeyer GB, et al. Proteases acting on mutant huntingtin generate cleaved products that differentially build up cytoplasmic and nuclear inclusions. Mol Cell. 2002;10(2):259-69.

44. Ratovitski T, Chighladze E, Waldron E, Hirschhorn RR, Ross CA. Cysteine proteases bleomycin hydrolase and cathepsin Z mediate N-terminal proteolysis and toxicity of mutant huntingtin. J Biol Chem. 2011;286(14):12578-89. PMCID: 3069459.

45. Kegel KB, Sapp E, Alexander J, Reeves P, Bleckmann D, Sobin L, et al. Huntingtin cleavage product A forms in neurons and is reduced by gamma-secretase inhibitors. Mol Neurodegener. 2010;5:58. PMCID: 3018386.

46. Kim YJ, Sapp E, Cuiffo BG, Sobin L, Yoder J, Kegel KB, et al. Lysosomal proteases are involved in generation of N-terminal huntingtin fragments. Neurobiol Dis. 2006;22(2):346-56.

47. Harjes P, Wanker EE. The hunt for huntingtin function: interaction partners tell many different stories. Trends Biochem Sci. 2003;28(8):425-33.

48. Cha JH. Transcriptional dysregulation in Huntington's disease. Trends Neurosci. 2000;23(9):387-92.

49. Miller JP, Hughes RE. Protein Interactions and Target Discovery in Huntington's Disease. 2011.

50. Dunah AW, Jeong H, Griffin A, Kim YM, Standaert DG, Hersch SM, et al. Sp1 and TAFII130 transcriptional activity disrupted in early Huntington's disease. Science. 2002;296(5576):2238-43.

51. Boutell JM, Thomas P, Neal JW, Weston VJ, Duce J, Harper PS, et al. Aberrant interactions of transcriptional repressor proteins with the Huntington's disease gene product, huntingtin. Hum Mol Genet. 1999;8(9):1647-55.

52. Holbert S, Denghien I, Kiechle T, Rosenblatt A, Wellington C, Hayden MR, et al. The Gln-Ala repeat transcriptional activator CA150 interacts with huntingtin: neuropathologic and genetic evidence for a role in Huntington's disease pathogenesis. Proc Natl Acad Sci U S A. 2001;98(4):1811-6. PMCID: 29339.

53. Steffan JS, Kazantsev A, Spasic-Boskovic O, Greenwald M, Zhu YZ, Gohler H, et al. The Huntington's disease protein interacts with p53 and CREB-binding protein and represses transcription. Proc Natl Acad Sci U S A. 2000;97(12):6763-8. PMCID: 18731.

54. Kegel KB, Meloni AR, Yi Y, Kim YJ, Doyle E, Cuiffo BG, et al. Huntingtin is present in the nucleus, interacts with the transcriptional corepressor C-terminal binding protein, and represses transcription. J Biol Chem. 2002;277(9):7466-76.

55. Faber PW, Barnes GT, Srinidhi J, Chen J, Gusella JF, MacDonald ME. Huntingtin interacts with a family of WW domain proteins. Hum Mol Genet. 1998;7(9):1463-74.

56. Li SH, Cheng AL, Zhou H, Lam S, Rao M, Li H, et al. Interaction of Huntington disease protein with transcriptional activator Sp1. Mol Cell Biol. 2002;22(5):1277-87. PMCID: 134707.

57. Huang CC, Faber PW, Persichetti F, Mittal V, Vonsattel JP, MacDonald ME, et al. Amyloid formation by mutant huntingtin: threshold, progressivity and recruitment of normal polyglutamine proteins. Somat Cell Mol Genet. 1998;24(4):217-33.

58. Zuccato C, Tartari M, Crotti A, Goffredo D, Valenza M, Conti L, et al. Huntingtin interacts with REST/NRSF to modulate the transcription of NRSE-controlled neuronal genes. Nat Genet. 2003;35(1):76-83.

59. Kalchman MA, Koide HB, McCutcheon K, Graham RK, Nichol K, Nishiyama K, et al. HIP1, a human homologue of S. cerevisiae Sla2p, interacts with membrane-associated huntingtin in the brain. Nat Genet. 1997;16(1):44-53.

60. Singaraja RR, Hadano S, Metzler M, Givan S, Wellington CL, Warby S, et al. HIP14, a novel ankyrin domain-containing protein, links huntingtin to intracellular trafficking and endocytosis. Hum Mol Genet. 2002;11(23):2815-28.

61. Modregger J, DiProspero NA, Charles V, Tagle DA, Plomann M. PACSIN 1 interacts with huntingtin and is absent from synaptic varicosities in presymptomatic Huntington's disease brains. Hum Mol Genet. 2002;11(21):2547-58.

62. Sittler A, Walter S, Wedemeyer N, Hasenbank R, Scherzinger E, Eickhoff H, et al. SH3GL3 associates with the Huntingtin exon 1 protein and promotes the formation of polygln-containing protein aggregates. Mol Cell. 1998;2(4):427-36.

63. Li XJ, Li SH, Sharp AH, Nucifora FC, Jr., Schilling G, Lanahan A, et al. A huntingtin-associated protein enriched in brain with implications for pathology. Nature. 1995;378(6555):398-402.

64. Sun Y, Savanenin A, Reddy PH, Liu YF. Polyglutamine-expanded huntingtin promotes sensitization of N-methyl-D-aspartate receptors via post-synaptic density 95. J Biol Chem. 2001;276(27):24713-8.

65. Bao J, Sharp AH, Wagster MV, Becher M, Schilling G, Ross CA, et al. Expansion of polyglutamine repeat in huntingtin leads to abnormal protein interactions involving calmodulin. Proc Natl Acad Sci U S A. 1996;93(10):5037-42. PMCID: 39402.

66. Holbert S, Dedeoglu A, Humbert S, Saudou F, Ferrante RJ, Neri C. Cdc42-interacting protein 4 binds to huntingtin: neuropathologic and biological evidence for a role in Huntington's disease. Proc Natl Acad Sci U S A. 2003;100(5):2712-7. PMCID: 151406.

67. Liu YF, Deth RC, Devys D. SH3 domain-dependent association of huntingtin with epidermal growth factor receptor signaling complexes. J Biol Chem. 1997;272(13):8121-4.

68. Tang TS, Tu H, Chan EY, Maximov A, Wang Z, Wellington CL, et al. Huntingtin and huntingtin-associated protein 1 influence neuronal calcium signaling mediated by inositol-(1,4,5) triphosphate receptor type 1. Neuron. 2003;39(2):227-39. PMCID: 3220623.

69. Zucchelli S, Marcuzzi F, Codrich M, Agostoni E, Vilotti S, Biagioli M, et al. Tumor necrosis factor receptor-associated factor 6 (TRAF6) associates with huntingtin protein and promotes its atypical ubiquitination to enhance aggregate formation. J Biol Chem. 2011;286(28):25108-17. PMCID: 3137084.

70. Liu YF, Dorow D, Marshall J. Activation of MLK2-mediated signaling cascades by polyglutamine-expanded huntingtin. J Biol Chem. 2000;275(25):19035-40.

71. Boutell JM, Wood JD, Harper PS, Jones AL. Huntingtin interacts with cystathionine beta-synthase. Hum Mol Genet. 1998;7(3):371-8.

72. Burke JR, Enghild JJ, Martin ME, Jou YS, Myers RM, Roses AD, et al. Huntingtin and DRPLA proteins selectively interact with the enzyme GAPDH. Nat Med. 1996;2(3):347-50.

73. Subramaniam S, Sixt KM, Barrow R, Snyder SH. Rhes, a striatal specific protein, mediates mutant-huntingtin cytotoxicity. Science. 2009;324(5932):1327-30. PMCID: 2745286.

74. Yang H, Liu C, Zhong Y, Luo S, Monteiro MJ, Fang S. Huntingtin interacts with the cue domain of gp78 and inhibits gp78 binding to ubiquitin and p97/VCP. PLoS One. 2010;5(1):e8905. PMCID: 2811200.

75. Cornett J, Cao F, Wang CE, Ross CA, Bates GP, Li SH, et al. Polyglutamine expansion of huntingtin impairs its nuclear export. Nat Genet. 2005;37(2):198-204.

76. Tam S, Spiess C, Auyeung W, Joachimiak L, Chen B, Poirier MA, et al. The chaperonin TRiC blocks a huntingtin sequence element that promotes the conformational switch to aggregation. Nat Struct Mol Biol. 2009;16(12):1279-85. PMCID: 2788664.

77. Yu H, Chen JK, Feng S, Dalgarno DC, Brauer AW, Schreiber SL. Structural basis for the binding of proline-rich peptides to SH3 domains. Cell. 1994;76(5):933-45.

78. Gerber HP, Seipel K, Georgiev O, Hofferer M, Hug M, Rusconi S, et al. Transcriptional activation modulated by homopolymeric glutamine and proline stretches. Science. 1994;263(5148):808-11.

79. Schaefer MH, Wanker EE, Andrade-Navarro MA. Evolution and function of CAG/polyglutamine repeats in protein-protein interaction networks. Nucleic Acids Res. 2012.

80. Kim MW, Chelliah Y, Kim SW, Otwinowski Z, Bezprozvanny I. Secondary structure of Huntingtin amino-terminal region. Structure. 2009;17(9):1205-12. PMCID: 2863341.

81. Chun W, Lesort M, Tucholski J, Faber PW, MacDonald ME, Ross CA, et al. Tissue transglutaminase selectively modifies proteins associated with truncated mutant huntingtin in intact cells. Neurobiol Dis. 2001;8(3):391-404.

82. Davranche A, Aviolat H, Zeder-Lutz G, Busso D, Altschuh D, Trottier Y, et al. Huntingtin affinity for partners is not changed by polyglutamine length: aggregation itself triggers aberrant interactions. Hum Mol Genet. 2011;20(14):2795-806.

83. Suopanki J, Gotz C, Lutsch G, Schiller J, Harjes P, Herrmann A, et al. Interaction of huntingtin fragments with brain membranes--clues to early dysfunction in Huntington's disease. J Neurochem. 2006;96(3):870-84.

84. Groves MR, Hanlon N, Turowski P, Hemmings BA, Barford D. The structure of the protein phosphatase 2A PR65/A subunit reveals the conformation of its 15 tandemly repeated HEAT motifs. Cell. 1999;96(1):99-110.

85. Palidwor GA, Shcherbinin S, Huska MR, Rasko T, Stelzl U, Arumughan A, et al. Detection of alpha-rod protein repeats using a neural network and application to huntingtin. PLoS Comput Biol. 2009;5(3):e1000304. PMCID: 2647740.

86. Crick SL, Jayaraman M, Frieden C, Wetzel R, Pappu RV. Fluorescence correlation spectroscopy shows that monomeric polyglutamine molecules form collapsed structures in aqueous solutions. Proc Natl Acad Sci U S A. 2006;103(45):16764-9. PMCID: 1629004.

87. Dougan L, Li J, Badilla CL, Berne BJ, Fernandez JM. Single homopolypeptide chains collapse into mechanically rigid conformations. Proc Natl Acad Sci U S A. 2009;106(31):12605-10. PMCID: 2722357.

88. Chen S, Ferrone FA, Wetzel R. Huntington's disease age-of-onset linked to polyglutamine aggregation nucleation. Proc Natl Acad Sci U S A. 2002;99(18):11884-9. PMCID: 129363.

89. Bhattacharyya A, Thakur AK, Chellgren VM, Thiagarajan G, Williams AD, Chellgren BW, et al. Oligoproline effects on polyglutamine conformation and aggregation. J Mol Biol. 2006;355(3):524-35.

90. Chellgren BW, Miller AF, Creamer TP. Evidence for polyproline II helical structure in short polyglutamine tracts. J Mol Biol. 2006;361(2):362-71.

91. Darnell G, Orgel JP, Pahl R, Meredith SC. Flanking polyproline sequences inhibit beta-sheet structure in polyglutamine segments by inducing PPII-like helix structure. J Mol Biol. 2007;374(3):688-704.

92. Bennett MJ, Huey-Tubman KE, Herr AB, West AP, Jr., Ross SA, Bjorkman PJ. A linear lattice model for polyglutamine in CAG-expansion diseases. Proc Natl Acad Sci U S A. 2002;99(18):11634-9. PMCID: 129321.

93. Vitalis A, Wang X, Pappu RV. Quantitative characterization of intrinsic disorder in polyglutamine: insights from analysis based on polymer theories. Biophys J. 2007;93(6):1923-37. PMCID: 1959550.

94. Vitalis A, Wang X, Pappu RV. Atomistic simulations of the effects of polyglutamine chain length and solvent quality on conformational equilibria and spontaneous homodimerization. J Mol Biol. 2008;384(1):279-97. PMCID: 2847503.

95. Dlugosz M, Trylska J. Secondary structures of native and pathogenic huntingtin N-terminal fragments. J Phys Chem B. 2011;115(40):11597-608.

96. Peters-Libeu C, Miller J, Rutenber E, Newhouse Y, Krishnan P, Cheung K, et al. Disease-Associated Polyglutamine Stretches in Monomeric Huntingtin Adopt a Compact Structure. J Mol Biol. 2012.

97. Nagai Y, Inui T, Popiel HA, Fujikake N, Hasegawa K, Urade Y, et al. A toxic monomeric conformer of the polyglutamine protein. Nat Struct Mol Biol. 2007;14(4):332-40.

98. Schaffar G, Breuer P, Boteva R, Behrends C, Tzvetkov N, Strippel N, et al. Cellular toxicity of polyglutamine expansion proteins: mechanism of transcription factor deactivation. Mol Cell. 2004;15(1):95-105.

99. Zhang QC, Yeh TL, Leyva A, Frank LG, Miller J, Kim YE, et al. A compact beta model of huntingtin toxicity. J Biol Chem. 2011;286(10):8188-96. PMCID: 3048705.

100. Jayaraman M, Kodali R, Sahoo B, Thakur AK, Mayasundari A, Mishra R, et al. Slow amyloid nucleation via alpha-helix-rich oligomeric intermediates in short polyglutamine-containing huntingtin fragments. J Mol Biol. 2012;415(5):881-99.

101. Pejchal R, Gach JS, Brunel FM, Cardoso RM, Stanfield RL, Dawson PE, et al. A conformational switch in human immunodeficiency virus gp41 revealed by the structures of overlapping epitopes recognized by neutralizing antibodies. J Virol. 2009;83(17):8451-62. PMCID: 2738203.

102. Dyson HJ, Wright PE. Coupling of folding and binding for unstructured proteins. Curr Opin Struct Biol. 2002;12(1):54-60.

103. Bulone D, Masino L, Thomas DJ, San Biagio PL, Pastore A. The interplay between PolyQ and protein context delays aggregation by forming a reservoir of protofibrils. PLoS One. 2006;1:e111. PMCID: 1762411.

104. Kelley NW, Huang X, Tam S, Spiess C, Frydman J, Pande VS. The predicted structure of the headpiece of the Huntingtin protein and its implications on Huntingtin aggregation. J Mol Biol. 2009;388(5):919-27. PMCID: 2677131.

105. Takahashi Y, Okamoto Y, Popiel HA, Fujikake N, Toda T, Kinjo M, et al. Detection of polyglutamine protein oligomers in cells by fluorescence correlation spectroscopy. J Biol Chem. 2007;282(33):24039-48.

106. Davies SW, Turmaine M, Cozens BA, DiFiglia M, Sharp AH, Ross CA, et al. Formation of neuronal intranuclear inclusions underlies the neurological dysfunction in mice transgenic for the HD mutation. Cell. 1997;90(3):537-48.

107. Becher MW, Kotzuk JA, Sharp AH, Davies SW, Bates GP, Price DL, et al. Intranuclear neuronal inclusions in Huntington's disease and dentatorubral and pallidoluysian atrophy: correlation between the density of inclusions and IT15 CAG triplet repeat length. Neurobiol Dis. 1998;4(6):387-97.

108. Miller J, Arrasate M, Brooks E, Libeu CP, Legleiter J, Hatters D, et al. Identifying polyglutamine protein species in situ that best predict neurodegeneration. Nat Chem Biol. 2011;7(12):925-34. PMCID: 3271120.

109. Sathasivam K, Lane A, Legleiter J, Warley A, Woodman B, Finkbeiner S, et al. Identical oligomeric and fibrillar structures captured from the brains of R6/2 and knock-in mouse models of Huntington's disease. Hum Mol Genet. 2010;19(1):65-78. PMCID: 2792149.

110. Olshina MA, Angley LM, Ramdzan YM, Tang J, Bailey MF, Hill AF, et al. Tracking mutant huntingtin aggregation kinetics in cells reveals three major populations that include an invariant oligomer pool. J Biol Chem. 2010;285(28):21807-16. PMCID: 2898425.

111. Takahashi T, Kikuchi S, Katada S, Nagai Y, Nishizawa M, Onodera O. Soluble polyglutamine oligomers formed prior to inclusion body formation are cytotoxic. Hum Mol Genet. 2008;17(3):345-56.

112. Poirier MA, Li H, Macosko J, Cai S, Amzel M, Ross CA. Huntingtin spheroids and protofibrils as precursors in polyglutamine fibrilization. J Biol Chem. 2002;277(43):41032-7.

113. Scherzinger E, Sittler A, Schweiger K, Heiser V, Lurz R, Hasenbank R, et al. Self-assembly of polyglutamine-containing huntingtin fragments into amyloid-like fibrils: implications for Huntington's disease pathology. Proc Natl Acad Sci U S A. 1999;96(8):4604-9. PMCID: 16379.

114. Ho LW, Brown R, Maxwell M, Wyttenbach A, Rubinsztein DC. Wild type Huntingtin reduces the cellular toxicity of mutant Huntingtin in mammalian cell models of Huntington's disease. J Med Genet. 2001;38(7):450-2. PMCID: 1757193.

115. Yang W, Dunlap JR, Andrews RB, Wetzel R. Aggregated polyglutamine peptides delivered to nuclei are toxic to mammalian cells. Hum Mol Genet. 2002;11(23):2905-17.

116. Hackam AS, Singaraja R, Wellington CL, Metzler M, McCutcheon K, Zhang T, et al. The influence of huntingtin protein size on nuclear localization and cellular toxicity. J Cell Biol. 1998;141(5):1097-105. PMCID: 2137174.

117. Slow EJ, Graham RK, Osmand AP, Devon RS, Lu G, Deng Y, et al. Absence of behavioral abnormalities and neurodegeneration in vivo despite widespread neuronal huntingtin inclusions. Proc Natl Acad Sci U S A. 2005;102(32):11402-7. PMCID: 1183566.

118. Ventruti A, Cuervo AM. Autophagy and neurodegeneration. Curr Neurol Neurosci Rep. 2007;7(5):443-51.

119. Sanchez I, Mahlke C, Yuan J. Pivotal role of oligomerization in expanded polyglutamine neurodegenerative disorders. Nature. 2003;421(6921):373-9.

120. Jayaraman M, Mishra R, Kodali R, Thakur AK, Koharudin LM, Gronenborn AM, et al. Kinetically competing huntingtin aggregation pathways control amyloid polymorphism and properties. Biochemistry. 2012;51(13):2706-16.

121. Kar K, Jayaraman M, Sahoo B, Kodali R, Wetzel R. Critical nucleus size for disease-related polyglutamine aggregation is repeat-length dependent. Nat Struct Mol Biol. 2011;18(3):328-36. PMCID: 3075957.

122. Bhattacharyya AM, Thakur AK, Wetzel R. polyglutamine aggregation nucleation: thermodynamics of a highly unfavorable protein folding reaction. Proc Natl Acad Sci U S A. 2005;102(43):15400-5. PMCID: 1266079.

123. Thakur AK, Wetzel R. Mutational analysis of the structural organization of polyglutamine aggregates. Proc Natl Acad Sci U S A. 2002;99(26):17014-9. PMCID: 139261.

124. Walters RH, Murphy RM. Aggregation kinetics of interrupted polyglutamine peptides. J Mol Biol. 2011;412(3):505-19. PMCID: 3170924.

125. Pfeil W. The problem of the stability globular proteins. Mol Cell Biochem. 1981;40(1):3-28.

126. Marchut AJ, Hall CK. Effects of chain length on the aggregation of model polyglutamine peptides: molecular dynamics simulations. Proteins. 2007;66(1):96-109.

127. Lee CC, Walters RH, Murphy RM. Reconsidering the mechanism of polyglutamine peptide aggregation. Biochemistry. 2007;46(44):12810-20.

128. Demuro A, Mina E, Kayed R, Milton SC, Parker I, Glabe CG. Calcium dysregulation and membrane disruption as a ubiquitous neurotoxic mechanism of soluble amyloid oligomers. J Biol Chem. 2005;280(17):17294-300.

129. Chen S, Berthelier V, Hamilton JB, O'Nuallain B, Wetzel R. Amyloid-like features of polyglutamine aggregates and their assembly kinetics. Biochemistry. 2002;41(23):7391-9.

130. Chen S, Berthelier V, Yang W, Wetzel R. Polyglutamine aggregation behavior in vitro supports a recruitment mechanism of cytotoxicity. J Mol Biol. 2001;311(1):173-82.

131. Nekooki-Machida Y, Kurosawa M, Nukina N, Ito K, Oda T, Tanaka M. Distinct conformations of in vitro and in vivo amyloids of huntingtin-exon1 show different cytotoxicity. Proc Natl Acad Sci U S A. 2009;106(24):9679-84. PMCID: 2689308.

132. Kodali R, Wetzel R. Polymorphism in the intermediates and products of amyloid assembly. Curr Opin Struct Biol. 2007;17(1):48-57.

133. Orr HT, Chung MY, Banfi S, Kwiatkowski TJ, Jr., Servadio A, Beaudet AL, et al. Expansion of an unstable trinucleotide CAG repeat in spinocerebellar ataxia type 1. Nat Genet. 1993;4(3):221-6.

134. Jayaraman M, Kodali R, Wetzel R. The impact of ataxin-1-like histidine insertions on polyglutamine aggregation. Protein Eng Des Sel. 2009;22(8):469-78. PMCID: 2719497.

135. Jayaraman M, Kodali R, Sahoo B, Thakur AK, Mayasundari A, Mishra R, et al. Slow Amyloid Nucleation via alpha-Helix-Rich Oligomeric Intermediates in Short Polyglutamine-Containing Huntingtin Fragments. J Mol Biol. 2011.

136. Sivanandam VN, Jayaraman M, Hoop CL, Kodali R, Wetzel R, van der Wel PC. The aggregation-enhancing huntingtin N-terminus is helical in amyloid fibrils. J Am Chem Soc. 2011;133(12):4558-66. PMCID: 3109494.

137. Tam S, Geller R, Spiess C, Frydman J. The chaperonin TRiC controls polyglutamine aggregation and toxicity through subunit-specific interactions. Nat Cell Biol. 2006;8(10):1155-62. PMCID: 2829982.

138. Mishra R, Jayaraman M, Roland BP, Landrum E, Fullam T, Kodali R, et al. Inhibiting the Nucleation of Amyloid Structure in a Huntingtin Fragment by Targeting alpha-Helix-Rich Oligomeric Intermediates. J Mol Biol. 2011.

139. Wacker JL, Zareie MH, Fong H, Sarikaya M, Muchowski PJ. Hsp70 and Hsp40 attenuate formation of spherical and annular polyglutamine oligomers by partitioning monomer. Nat Struct Mol Biol. 2004;11(12):1215-22.

140. Williamson TE, Vitalis A, Crick SL, Pappu RV. Modulation of polyglutamine conformations and dimer formation by the N-terminus of huntingtin. J Mol Biol. 2010;396(5):1295-309. PMCID: 2832287.

141. Borwankar T, Rothlein C, Zhang G, Techen A, Dosche C, Ignatova Z. Natural osmolytes remodel the aggregation pathway of mutant huntingtin exon 1. Biochemistry. 2011;50(12):2048-60.

142. Sikorski P, Atkins E. New model for crystalline polyglutamine assemblies and their connection with amyloid fibrils. Biomacromolecules. 2005;6(1):425-32.

143. Perutz MF, Finch JT, Berriman J, Lesk A. Amyloid fibers are water-filled nanotubes. Proc Natl Acad Sci U S A. 2002;99(8):5591-5. PMCID: 122814.

144. Stanley CB, Perevozchikova T, Berthelier V. Structural formation of huntingtin exon 1 aggregates probed by small-angle neutron scattering. Biophys J. 2011;100(10):2504-12. PMCID: 3093554.

145. Khare SD, Ding F, Gwanmesia KN, Dokholyan NV. Molecular origin of polyglutamine aggregation in neurodegenerative diseases. PLoS Comput Biol. 2005;1(3):230-5. PMCID: 1193989.

146. Ogawa H, Nakano M, Watanabe H, Starikov EB, Rothstein SM, Tanaka S. Molecular dynamics simulation study on the structural stabilities of polyglutamine peptides. Comput Biol Chem. 2008;32(2):102-10.

147. Stork M, Giese A, Kretzschmar HA, Tavan P. Molecular dynamics simulations indicate a possible role of parallel beta-helices in seeded aggregation of poly-Gln. Biophys J. 2005;88(4):2442-51. PMCID: 1305343.

148. Sharma D, Shinchuk LM, Inouye H, Wetzel R, Kirschner DA. Polyglutamine homopolymers having 8-45 residues form slablike beta-crystallite assemblies. Proteins. 2005;61(2):398-411.

149. Bevivino AE, Loll PJ. An expanded glutamine repeat destabilizes native ataxin-3 structure and mediates formation of parallel beta -fibrils. Proc Natl Acad Sci U S A. 2001;98(21):11955-60. PMCID: 59749.

150. Kajava AV, Baxa U, Wickner RB, Steven AC. A model for Ure2p prion filaments and other amyloids: the parallel superpleated beta-structure. Proc Natl Acad Sci U S A. 2004;101(21):7885-90. PMCID: 419526.

151. Schneider R, Schumacher MC, Mueller H, Nand D, Klaukien V, Heise H, et al. Structural characterization of polyglutamine fibrils by solid-state NMR spectroscopy. J Mol Biol. 2011;412(1):121-36.

152. Heiser V, Engemann S, Brocker W, Dunkel I, Boeddrich A, Waelter S, et al. Identification of benzothiazoles as potential polyglutamine aggregation inhibitors of Huntington's disease by using an automated filter retardation assay. Proc Natl Acad Sci U S A. 2002;99 Suppl 4:16400-6. PMCID: 139900.

153. Hockly E, Tse J, Barker AL, Moolman DL, Beunard JL, Revington AP, et al. Evaluation of the benzothiazole aggregation inhibitors riluzole and PGL-135 as therapeutics for Huntington's disease. Neurobiol Dis. 2006;21(1):228-36.

154. Ehrnhoefer DE, Duennwald M, Markovic P, Wacker JL, Engemann S, Roark M, et al. Green tea (-)-epigallocatechin-gallate modulates early events in huntingtin misfolding and reduces toxicity in Huntington's disease models. Hum Mol Genet. 2006;15(18):2743-51.

155. Rinderspacher A, Cremona ML, Liu Y, Deng SX, Xie Y, Gong G, et al. Potent inhibitors of Huntingtin protein aggregation in a cell-based assay. Bioorg Med Chem Lett. 2009;19(6):1715-7. PMCID: 2710884.

156. Fuentealba RA, Marasa J, Diamond MI, Piwnica-Worms D, Weihl CC. An aggregation sensing reporter identifies leflunomide and teriflunomide as polyglutamine aggregate inhibitors. Hum Mol Genet. 2012;21(3):664-80. PMCID: 3259017.

157. Desai UA, Pallos J, Ma AA, Stockwell BR, Thompson LM, Marsh JL, et al. Biologically active molecules that reduce polyglutamine aggregation and toxicity. Hum Mol Genet. 2006;15(13):2114-24.

158. Nagai Y, Tucker T, Ren H, Kenan DJ, Henderson BS, Keene JD, et al. Inhibition of polyglutamine protein aggregation and cell death by novel peptides identified by phage display screening. J Biol Chem. 2000;275(14):10437-42.

159. Nagai Y, Fujikake N, Ohno K, Higashiyama H, Popiel HA, Rahadian J, et al. Prevention of polyglutamine oligomerization and neurodegeneration by the peptide inhibitor QBP1 in Drosophila. Hum Mol Genet. 2003;12(11):1253-9.

160. Popiel HA, Nagai Y, Fujikake N, Toda T. Protein transduction domain-mediated delivery of QBP1 suppresses polyglutamine-induced neurodegeneration in vivo. Mol Ther. 2007;15(2):303-9.

161. Tomita K, Popiel HA, Nagai Y, Toda T, Yoshimitsu Y, Ohno H, et al. Structure-activity relationship study on polyglutamine binding peptide QBP1. Bioorg Med Chem. 2009;17(3):1259-63.

162. Ren H, Nagai Y, Tucker T, Strittmatter WJ, Burke JR. Amino acid sequence requirements of peptides that inhibit polyglutamine-protein aggregation and cell death. Biochem Biophys Res Commun. 2001;288(3):703-10.

163. Thakur AK, Yang W, Wetzel R. Inhibition of polyglutamine aggregate cytotoxicity by a structure-based elongation inhibitor. FASEB J. 2004;18(7):923-5.

164. Starikov EB, Lehrach H, Wanker EE. Folding of oligoglutamines: a theoretical approach based upon thermodynamics and molecular mechanics. J Biomol Struct Dyn. 1999;17(3):409-27.

165. Lanning JD, Hawk AJ, Derryberry J, Meredith SC. Chaperone-like N-methyl peptide inhibitors of polyglutamine aggregation. Biochemistry. 2010;49(33):7108-18. PMCID: 2965777.

166. Colby DW, Chu Y, Cassady JP, Duennwald M, Zazulak H, Webster JM, et al. Potent inhibition of huntingtin aggregation and cytotoxicity by a disulfide bond-free single-domain intracellular antibody. Proc Natl Acad Sci U S A. 2004;101(51):17616-21. PMCID: 539732.

167. Southwell AL, Khoshnan A, Dunn DE, Bugg CW, Lo DC, Patterson PH. Intrabodies binding the proline-rich domains of mutant huntingtin increase its turnover and reduce neurotoxicity. J Neurosci. 2008;28(36):9013-20. PMCID: 2633448.

168. Li H, Li SH, Cheng AL, Mangiarini L, Bates GP, Li XJ. Ultrastructural localization and progressive formation of neuropil aggregates in Huntington's disease transgenic mice. Hum Mol Genet. 1999;8(7):1227-36.

169. McGowan DP, van Roon-Mom W, Holloway H, Bates GP, Mangiarini L, Cooper GJ, et al. Amyloid-like inclusions in Huntington's disease. Neuroscience. 2000;100(4):677-80.

170. Osmand AP, Berthelier V, Wetzel R. Imaging polyglutamine deposits in brain tissue. Methods Enzymol. 2006;412:106-22.

171. Lajoie P, Snapp EL. Formation and toxicity of soluble polyglutamine oligomers in living cells. PLoS One. 2010;5(12):e15245. PMCID: 3011017.

172. Ossato G, Digman MA, Aiken C, Lukacsovich T, Marsh JL, Gratton E. A two-step path to inclusion formation of huntingtin peptides revealed by number and brightness analysis. Biophys J. 2010;98(12):3078-85. PMCID: 2884247.

173. Mangiarini L, Sathasivam K, Seller M, Cozens B, Harper A, Hetherington C, et al. Exon 1 of the HD gene with an expanded CAG repeat is sufficient to cause a progressive neurological phenotype in transgenic mice. Cell. 1996;87(3):493-506.

174. Landles C, Sathasivam K, Weiss A, Woodman B, Moffitt H, Finkbeiner S, et al. Proteolysis of mutant huntingtin produces an exon 1 fragment that accumulates as an aggregated protein in neuronal nuclei in Huntington disease. J Biol Chem. 2010;285(12):8808-23. PMCID: 2838303.

175. Wetzel R. Physical Chemistry of Polyglutamine: Intriguing Tales of a Monotonous Sequence. J Mol Biol. 2012.

176. Mishra R, Jayaraman M, Roland BP, Landrum E, Fullam T, Kodali R, et al. Inhibiting the nucleation of amyloid structure in a huntingtin fragment by targeting alpha-helix-rich oligomeric intermediates. J Mol Biol. 2012;415(5):900-17. PMCID: 3267848.

177. Gautier R, Douguet D, Antonny B, Drin G. HELIQUEST: a web server to screen sequences with specific alpha-helical properties. Bioinformatics. 2008;24(18):2101-2.

178. Eisenberg D, Weiss RM, Terwilliger TC. The helical hydrophobic moment: a measure of the amphiphilicity of a helix. Nature. 1982;299(5881):371-4.

179. Munoz V, Serrano L. Elucidating the folding problem of helical peptides using empirical parameters. III. Temperature and pH dependence. J Mol Biol. 1995;245(3):297-308.

180. Munoz V, Serrano L. Elucidating the folding problem of helical peptides using empirical parameters. II. Helix macrodipole effects and rational modification of the helical content of natural peptides. J Mol Biol. 1995;245(3):275-96.

181. Munoz V, Serrano L. Elucidating the folding problem of helical peptides using empirical parameters. Nat Struct Biol. 1994;1(6):399-409.

182. Eisenberg D, Weiss RM, Terwilliger TC. The hydrophobic moment detects periodicity in protein hydrophobicity. Proc Natl Acad Sci U S A. 1984;81(1):140-4. PMCID: 344626.

183. Comeau SR, Gatchell DW, Vajda S, Camacho CJ. ClusPro: a fully automated algorithm for protein-protein docking. Nucleic Acids Res. 2004;32(Web Server issue):W96-9. PMCID: 441492.

184. Comeau SR, Gatchell DW, Vajda S, Camacho CJ. ClusPro: an automated docking and discrimination method for the prediction of protein complexes. Bioinformatics. 2004;20(1):45-50.

185. Brooks BR, Bruccoleri RE, Olafson BD, States DJ, Swaminathan S, Karplus M. CHARMM: A program for macromolecular energy, minimization, and dynamics calculations. Journal of Computational Chemistry. 1983;4(2):187-217.

186. Comeau SR, Camacho CJ. Predicting oligomeric assemblies: N-mers a primer. J Struct Biol. 2005;150(3):233-44.

187. Vriend G. WHAT IF: a molecular modeling and drug design program. J Mol Graph. 1990;8(1):52-6, 29.

188. Camacho CJ, Zhang C. FastContact: rapid estimate of contact and binding free energies. Bioinformatics. 2005;21(10):2534-6.

189. Goormaghtigh E, Cabiaux V, Ruysschaert JM. Secondary structure and dosage of soluble and membrane proteins by attenuated total reflection Fourier-transform infrared spectroscopy on hydrated films. Eur J Biochem. 1990;193(2):409-20.

190. LeVine H, 3rd. Quantification of beta-sheet amyloid fibril structures with thioflavin T. Methods Enzymol. 1999;309:274-84.

191. Fiumara F, Fioriti L, Kandel ER, Hendrickson WA. Essential role of coiled coils for aggregation and activity of Q/N-rich prions and PolyQ proteins. Cell. 2010;143(7):1121-35.

192. Serio TR, Cashikar AG, Kowal AS, Sawicki GJ, Moslehi JJ, Serpell L, et al. Nucleated conformational conversion and the replication of conformational information by a prion determinant. Science. 2000;289(5483):1317-21.

193. Atwal RS, Desmond CR, Caron N, Maiuri T, Xia J, Sipione S, et al. Kinase inhibitors modulate huntingtin cell localization and toxicity. Nat Chem Biol. 2011;7(7):453-60.

194. Havel LS, Wang CE, Wade B, Huang B, Li S, Li XJ. Preferential accumulation of N-terminal mutant huntingtin in the nuclei of striatal neurons is regulated by phosphorylation. Hum Mol Genet. 2011;20(7):1424-37. PMCID: 3049362.

195. Zala D, Colin E, Rangone H, Liot G, Humbert S, Saudou F. Phosphorylation of mutant huntingtin at S421 restores anterograde and retrograde transport in neurons. Hum Mol Genet. 2008;17(24):3837-46.